THE UNIVERSITY OF
SYDNEY

The role of Ten-m3 in the development of the mouse thalamostriatal pathway

Heidi Tran

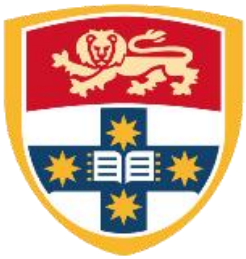

THE UNIVERSITY OF SYDNEY

Department of Physiology

This thesis is submitted in fulfillment of the requirements for the degree of Doctor of Philosophy

2013

Under the supervision of Dr. Catherine Leamey

Table of Contents

Acknowledgements

The years comprising my PhD have indeed been a giant rollercoaster which has been made less arduous by a number of people, whom I'd like to acknowledge here.

Firstly to my supervisor, Dr. Cathy Leamey and co-supervisor Dr. Atomu Sawatari: thank you both for your guidance and encouragement throughout the past few years. Cathy, your amazing eye for detail is to be envied, as is your ability to speed read, and I owe a lot of my progress to you. You also had a wonderful way of making me feel better about my work, even on the worst of days, which was much appreciated. Atomu, your often quirky ideas have always kept me on my feet and your uncanny knowledge of pop culture, although most often went straight over my head, always provided much entertainment. Thank you both for your no-nonsense approaches, with respect to science, my writing and beyond.

Secondly, thank you to the people who made the PhD office a pleasant place to be everyday; Tim and Angela. To Tim, thanks for being a great mentor and for teaching me so much of what I have come to do with ease. Your amazing patience, guidance and encouragement are constant to this day. Thank you for reminding me to be positive and for always making me feel like I can do anything! To Angela; thanks for being a great lab-mate and, in particular for holding a lot of the load towards the end. Thanks also for always willing to lend an ear and a shoulder; yours, and Mark's, kindness have meant a lot. A big thank you, also, to Rajini for your help and friendship throughout the past few years.

To the past PhD students, Sam, Kelly, Hyunchul, and Michael; thanks for your assistance during my earlier years. To the honours/masters students, past and present, thanks for

keeping things interesting. Thanks in particular to Tomasz for helping with programming; and to Peta, Anthony, Nigel and Sam, Tasnim and Tom, for keeping things light and for always being up for ice cream and cake. Thanks also to De Lian and Connie for always being available for a chat and a laugh.

Finally, I'd like to thank my family and friends, without whom this would not have been possible. Thanks to my parents for your neverending support and encouragement, even without really understanding what it is that I've been doing over the past 3-4 years. A big thank you also to my brother Eric for being the bearer of my vents. To my cousins, Lilian and Jeff, thanks for listening and for the streams of advice. And, finally, to my friends; thanks for providing me with fun and laughter outside of my neuroscience bubble.

Declaration

I hereby declare that this submission is my own work and that, to the best of my knowledge, it contains no material previously published or written by another person nor material which to a substantial extent has been accepted for the award of any other degree or diploma, at this or any other institution, except where due acknowledgement is made in the text. Financial support for this work was provided by an Australian Postgraduate Award from the University of Sydney.

Heidi Tran

List of Abbreviations

ACh acetylcholine

AChE acetylcholinesterase

AU arbitrary units

BDA biotinylated dextran amine

BDNF brain-derived neurotrophic factor

BrdU bromodeoxyuridine

BSA bovine serum albumin

cAMP cyclic adenosine monophosphate

CAP c-Cbl-associated protein

ChAT choline acetyltransferase

CM-PF centromedian-parafasicular complex

CNS central nervous system

CTB cholera toxin subunit B

DARPP-32 dopamine- and cAMP-regulated neuronal phosphoprotein

DiI 1,1'-Didodecyl-3,3,3',3'-tetramethylindocarbocyanine perchlorate

dLGN dorsal lateral geniculate nucleus

DL dorsolateral

DM dorsomedial

DV dorsoventral

E embryonic day

EGF epidermal growth factor

EPN entopeduncular nucleus

ECD extracellular domain

FGF8 fibroblast growth factor 8

fr *fasciculus retroflexus*

GABA gamma-aminobutyric acid

GAD glutamate decarboxylase

GPe *globus pallidus* external segment

GPi *globus pallidus* internal segment

ICD intracellular domain

KO knock-out

K-S Kolmogorov-Smirnov test

LGE lateral ganglionic eminence

LP lateral posterior thalamic nucleus

LTS low threshold spiking

Lhx LIM homeobox homeodomain protein

μ-OR μ-opioid receptor

MBD1 methyl-CpG binding domain 1

MGE medial ganglionic eminence

ML mediolateral

MSN medium spiny neuron

NMDA N-methyl-D-aspartate

P postnatal day

PAN phasically active neuron

PB phosphate buffer

PCN precommissural nucleus??

PCR polymerase chain reaction

PF parafascicular nucleus

PNN perineuronal net

PV parvalbumin

RIP regulated intramembrane proteolysis

RT room temperature

RC rostrocaudal

SC superior colliculus

SDS sodium dodecyl sulphate

SH3 SRC homology 3

SNr *substantia nigra pars reticulate*

SNc *substantia nigra pars compacta*

SOM/NPY/NOS somatostatin/ neuropeptide Y/ nitric oxide synthase

STN subthalamic nucleus

TAN tonically active neuron

TEA triethanolamine

TCAP teneurin C-terminal associated peptide

TH tyrosine hydroxylase

tif tagged image files

TMD transmembrane domain

VA/VL ventral-anterior/ventral-lateral thalamic nuclei

VGLUT vesicular glutamate transporter

VL ventrolateral

VM ventromedial

WFA *Wisteria floribunda agglutinin*

WT wild type

Zic1 zinc finger transcription factor 1

Abstract

The striatum is the key input nucleus of the basal ganglia, receiving the majority of inputs from the cortex, thalamus and SN, and is implicated in motor control and learning. Despite the apparent importance of striatal circuits, the mechanisms associated with their development are not well studied. One potential molecular candidate in the formation of striatal circuits is Ten-m3, a member of the teneurin family of transmembrane glycoproteins previously shown to be expressed in interconnected structures of the visual pathway, where it has roles in axon guidance. An overview of the literature relevant to striatal structure, function, connectivity and development, as well as an introduction to the teneurin family of molecules is provided in Chapter 1.

In Chapter 2, potential roles for Ten-m3 in the formation of striatal circuits was investigated in mice by performing an analysis of its expression in the striatum across late embryonic and postnatal development. *In situ* hybrisation showed the first expression of Ten-m3 at embryonic day (E)17 in the striatum, in a pattern of patches/oblique bands and a concurrent high-dorsocaudal to low-ventrorostral gradient, confined to a subregion of the striatal matrix. A survey of afferent/efferent structures of the matrix for Ten-m3 identified the parafasicular nucleus (PF), a thalamic nucleus with specific projections that cluster in the striatal matrix, as an important potential locus of action. *In situ* hybridisation for Ten-m3 in the PF during development similarly revealed the first expression at E17, and corresponding high-dorsal and low-ventral gradients across development, strongly implicating Ten-m3 in the guidance of thalamostriatal axons from the PF.

A functional role for Ten-m3 in striatal circuits was investigated Chapter 3 using anterograde tracer injections in adult wildtype (WT) and Ten-m3 knock-out (KO) mice . Studies in WT adults demonstrated the characteristic patchy distribution of thalamostriatal terminals in the matrix, consistent with that described in other species. In KOs, thalamostriatal terminals exhibit altered topography and cover an expanded area of the matrix. In addition, the characteristic patchy distribution of these terminals is lost in KOs, although they remain confined to the matrix, as in WTs. Despite the overall increase in the area occupied by thalamic terminals, however, there appeared to be a tendency for thalamic axons to avoid the ventrolateral (VL) quadrant of mid-caudal striatum in KOs. Further, retrograde transport of two fluorescent tracers, placed 500 µm apart along the rostrocaudal axis of the striatum, revealed specific reductions to the population of PF cells projecting to the mid-caudal striatum. Interestingly, total area and cell number were reduced at this same striatal level in KOs. In particular, cholinergic interneurons, one of the major striatal targets of PF axons, labeled using immunohistochemistry for choline acetyl-transferase, were reduced in the VL quadrant at this same striatal level. Behaviourally, a footprint analysis revealed reductions in stride length, and a rotorod test showed delayed learning in Ten-m3 KOs.

In Chapter 4, an attempt was made to begin to uncover the mechanisms underlying aspects of the Ten-m3 KO striatal phenotype. To this end, the development of the thalamostriatal projection was investigated. It was found that thalamostriatal projections, labeled with carbocyanine dye in fixed tissue, first invade the striatum at E17, correlating with the first expression of Ten-m3. In the absence of Ten-m3, the number of collaterals were reduced at E17 and, targeting deficits were evident postnatally. A further *in vivo* tracing study at P25-30 indicates an adult-like phenotype. Hence Ten-m3 may have roles in the targeting, collateralisation and refinement of thalamostriatal projections. Investigations into

mechanisms of Ten-m3 used *in situ* hybridisation for Ten-m3 and anterograde tracing to label thalamostriatal projections on adjacent sections to reveal a partial overlap, suggesting that Ten-m3 acts as a direct attractive cue to a subset of these axons. Secondly, previous studies showing reductions in EphA7 in visual structures of Ten-m3 KO mice were observed for the striatum using *in situ* hybridisation and Western blotting, suggesting that Ten-m3 may exert some of its functions through EphA7. Moreover, Ten-m3 and EphA7 show a partially complementary expression, suggesting they may mark distinct matrisomes. Hence, Ten-m3 marks a novel subregion of the matrix that is responsible for the normal guidance and targeting of thalamostriatal axons throughout development.

In Chapter 5, some concluding remarks are made as well as some suggestions for future studies motivated by the current work. This work provides strong evidence of multiple, complex roles for Ten-m3 in regulating striatal connectivity and function. It also provides the first description of normal adult organisation and development of the mouse thalamostriatal pathway.

Chapter 1

The ins and outs of the striatal network

Introduction

The mature nervous system is a highly complex structure. It is comprised of a diversity of specialised cell types arranged into precise, interconnected circuits, which form the basis of an animal's ability to sense and interact with the environment. The mammalian striatum and its associated circuitry is a salient and informative example of this neural intricacy. Since the 1940s (Vogt and Vogt, 1941), the striatum has been the subject of an abundance of studies, which have unveiled key features of its anatomy, function and development. More than anything, however, these studies have revealed the complexity of this structure and its integral role in the control of almost all known behaviour. The striatum is a key component of the basal ganglia circuits, where its position as the major target nucleus for afferents including the cortico-, nigro- and thalamostriatal pathways, forms the basis for highly organised coding of behaviours such as motor control and volition. The roles of striatal pathways are best evidenced by the wide ranging and severe progression of symptoms of patients with disorders of the basal ganglia, such as Parkinson's disease (Jankovic, 2008; Koerts et al., 2009) and Huntington's chorea (Albin et al., 1989; DeLong, 1990).

As for most brain regions, the generation of striatal cells, their compartmentalisation and formation of connections occur in late embryonic and early postnatal development. Over recent years, investigations into the processes mediating these events have begun to focus on cellular and molecular mechanisms. These mechanisms regulate the earliest stages of nervous system development, from neural induction and formation of the neural tube, to regionalisation and differentiation. At slightly later stages, they modulate compartmentalisation, axon guidance and synapse formation. The complex network of cells, their organisation and connections, along with the variety of neurochemicals they express, have made the striatum a difficult structure to unravel developmentally. Hence, although initial descriptions of striatal morphogenesis were first recorded in the 1920s (Johnston, 1923) and early experimental analysis was first performed in the 1970s (Angevine and McConnell, 1974), our knowledge remains limited. We have since gained detailed knowledge regarding a few aspects of striatal development, such as the time-course of cellular events involved in the generation of the striatum and its subsequent compartmentalisation, along with some of the molecular mechanisms underlying the former process. Our knowledge of the temporal development of most afferent pathways and the associated molecular mechanisms, however, as well as the processes which regulate compartmentalisation within the striatum, is still very limited.

It is vital to continue to improve upon our current knowledge, not only to gain a better understanding of how one of the brain's most complicated networks controls complex behaviours, but also to better understand the progression of diseases of the basal ganglia, and in turn, aid the development of potential therapies.

The striatum

The striatum is a major component of the basal ganglia, a group of subcortical structures forming complex connections with the telencephalon and midbrain. Apart from the striatum, it comprises the *globus pallidus* (GP), both external (GPe) and internal (GPi) segments, the latter known as the entopeduncular nucleus (EPN) in rodents; *substantia nigra* (SN), consisting of *pars reticulata* (SNr) and *pars compacta* (SNc) segments; and the subthalamic nucleus (STN). The striatum is the largest structure and sole target of afferent projections to the basal ganglia. These afferents predominantly originate from motor and somatosensory cortex and intralaminar, midline and ventral motor thalamus. The striatum in turn sends efferents to the output nuclei, the GPe and SNr/GPi. In the 'classic' view of basal ganglia circuitry, this occurs in two parallel pathways, known as the direct and indirect pathways, which subsequently provide reciprocal projections back to the cortex to form cortical feedback loops, via ventral motor thalamus. In the direct pathway, the striatum projects to the SNr/GPi, while in the indirect pathway, striatal information is transferred to the GP, which projects to the STN and subsequently the SNr, to direct information back to the cortex via the thalamus (Shink et al., 1996). These circuits are summarised in Figure 1.1. Evidence suggests that these pathways work via opposing mechanisms to balance the amount of excitatory versus inhibitory signals within the circuit. Under resting conditions, the output neurons of the striatum tonically inhibit their targets. During behaviour, corticostriatal input leads to the disinhibition of targets in the direct pathway, but act in the the opposite manner in the indirect pathway to increase inhibition of the thalamus and, hence, the cortex. This results in reduced motor

activity and is believed to be necessary to suppress unwanted movements (Mink and Thach, 1993).

This traditional model of the basal ganglia circuits has been improved upon in recent years. We now know that this is a very simplified description of a complex and intricate network of projections. The following sections will provide a detailed review of the striatum, beginning with the well-established adult phenotype, including cell types, unique patch/matrix organisation and afferent and efferent connections, and their associated functions. This will be followed by a discussion of what is known about the development of the striatum and the molecular mechanisms underlying this.

First, a note on the nomenclature used here. The term 'striatum' is often ambiguously used to describe a group of anatomical structures located deep within the telencephalon. Defined as the 'striate bodies', the term was initially used to reference the striped appearance of the caudate nucleus and putamen in primates, which are traditionally known together as the dorsal striatum or neostriatum, together with the *nucleus accumbens* (Gerfen and Wilson, 1996). Furthermore, the term striatum distinguished these structures from those of the 'corpus striatum', which refers to the striatum and globus pallidus. In today's literature, however, the term striatum is often used interchangeably with neostriatum, to refer to the caudate nucleus and putamen. This is particularly relevant when working with rodents, where, unlike in primates, these structures occur as a single unit. Hence, for the purposes of simplicity, the term striatum will refer only to the caudate nucleus and putamen from here on.

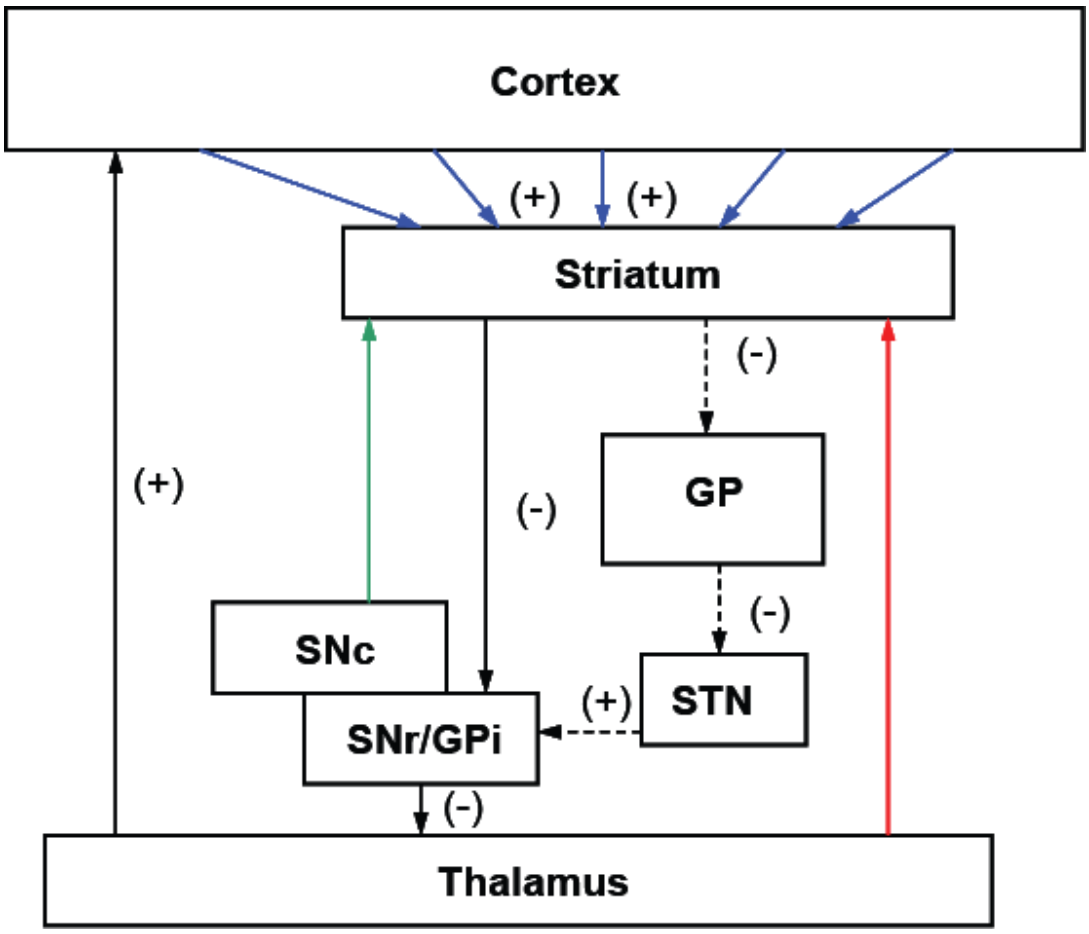

Figure 1.1. A simplfied schematic of the basal ganglia circuitry.

The striatum receives major inputs from all areas of the cerebral cortex (blue arrows), thalamus (red arrow) and SN (green arrow). In the 'classic' view of basal ganglia circuitry, the striatum sends reciprocal projections back to the cortex via the thalamus, along distinct direct (black solid arrows), through the SNr/GPi, and indirect pathways (black dashed arrows), through the GP, STN and SNr/GPi. These pathways work via opposing mechanisms to balance the amount of excitatory (+) versus inhibitory (-) signals such that, during behaviour, excitatory corticostriatal input leads to the disinhibition of targets in the direct pathway but increased inhibition of the thalamus and, hence, the cortex in the indirect pathway.

Adult anatomy

Studies of striatal anatomy have been performed in rats, cats, mice, non-human primates and humans. The major difference between the striatum of rodents compared to cats and primates, as mentioned above, is that the striatum exists as a single structure, as opposed to being physically divided into the caudate nucleus and putamen in the latter group of animals. This physical division of the caudate nucleus and putamen parallels distinct cortical input and, hence, their differential functions, with the former being responsible for sensorimotor coding while the latter is involved in associative processes. Despite being a single unit, the rodent striatum shows similar subdivisions of afferent input and function, albeit in a possibly less organised and specific manner. Further, many other features are transferable between species, for instance, neurochemical markers for striosome and matrix compartments are similar in all species, with the relative area of these compartments having been shown to be highly conserved (Johnston et al., 1990). Some differences, however, have been shown, such as the compartmentalisation of specific cell types (Rice et al., 2011). Hence, the following sections will endeavour to describe striatal organisation as thoroughly as possible, pointing out differences between species where relevant.

Striosome/matrix organisation

Upon observing striatal morphology with a Nissl stain or equivalent, striatal neurons appear to be homogeneously distributed throughout the nucleus. Cytological heterogeneities, nevertheless, have been described. In particular, the best established of

these is the mosaic pattern of two anatomically, chemically and functionally unique compartments, the striosomes (also referred to as patches) and the extra-striosomal matrix. Striosomes have been described as 3-dimensional labyrinths located most prominently in rostral striatum, where they are more numerous medially and sparser dorsolaterally; eventually disappearing at most caudal levels (Graybiel and Ragsdale, 1978). Striosomes also line the lateral border of the striatum, in a region known as the subcallosal streak. On the other hand, the matrix encompasses the remaining, extra-striosomal regions of the striatum. Further heterogeneities have been described within the matrix, with discrete zones similar to striosomes known as ‘matrisomes' formed from the clustering afferent terminals and efferent neurons (Gerfen, 1992; Ragsdale and Graybiel, 1991). The striatal striosome/matrix organisation has predominantly been described in mammals, including rodents (Murrin and Ferrer, 1984; Voorn et al., 1988), cats and primates (Graybiel and Ragsdale, 1978). Heterogeneities have also been reported in the chicken pallium (Heyers et al., 2003) and reptilian telencephalic ventrolateral area and pallidal structures (Brauth et al., 1988; Russchen et al., 1987), suggesting that these compartments may be highly conserved across amniotes.

Striosome and matrix compartments are histochemically distinct, distinguishable by the abundance or paucity of a variety of enzymes, receptors and neurotransmitters. For instance, striosomes are identified by a patchy distribution of opiate receptors in peri- and postnatal animals (Desban et al., 1993; Herkenham and Pert, 1981; van der Kooy, 1984; Lança et al., 1986; Murrin and Ferrer, 1984). Similarly, dopamine, commonly revealed using immunohistochemistry for its major synthetic enzyme, tyrosine hydroxylase (TH),

or dopamine and cAMP regulated phosphoprotein of 32kDA (DARPP-32), is expressed by striosomes in peri- and early postnatal animals, however, it becomes homogeneously distributed after approximately the first week of postnatal development (van der Kooy, 1984; Nisenbaum et al., 1998; Voorn et al., 1988). This change is thought to reflect the development of two distinct waves of dopaminergic projections, the first of which targets striosomes while the second innervates the matrix (Fishell and van der Kooy, 1987). Enkephalin and substance P also mark a subset of striosomes (Graybiel et al., 1981).

A variety of other markers have also been shown to shift expression from marking striosomes to overlapping with the matrix during development. For instance, dense acetylcholinesterase (AChE) activity is observed in patches correlating with striosomes during early postnatal development; in adults, however this switches to overlap with the matrix, avoiding striosomes (Graybiel and Ragsdale, 1978; Murrin and Ferrer, 1984; Ragsdale and Graybiel, 1990). This shift is mirrored by cholinergic interneurons labeled for choline acetyl-transferase (ChAT), which are initially localised to striosomes before moving to predominantly fill the 'intermediate zone' within the striatal matrix in the second postnatal week of development (Van Vulpen and Van Der Kooy, 1996). Similarly, the lectin *Wisteria floribunda agglutinin* (WFA) marks a subset of striosomes in early postnatal mice but later shifts to label perineuronal nets (PNNs) in the matrix of older animals (Lee et al., 2012a; Simonetti et al., 2009). Other markers of the matrix include the calcium-binding protein calbindin and somatostatin (Gerfen, 1984, 1985).

Striosome and matrix compartments are also functionally distinct as a result of their differential afferent and efferent connections. These compartments receive complementary input from different regions of the three major afferent structures, the cortex, SN and thalamus, as summarised in Fig. 1.2. Briefly, the prefrontal and limbic cortical areas preferentially innervate striosomes, while sensorimotor cortices project to the matrix. Further, dopaminergic regions of the SNr primarily project to striosomes, while the SNc innervates the matrix. The heterogeneity of thalamic axons are less well characterised, however, the parafascicular nucleus (PF), a major focus of the current study, provides a very strong projection specifically to the striatal matrix. A detailed description of these afferent connections will be described later.

As mentioned earlier, a third compartment occupies the apparently homogeneous extrastriosomal matrix, known as matriosomes. Matrisomes constitute clusters of corticostriatal afferent terminals (Flaherty and Graybiel, 1993a; Malach and Graybiel, 1986) and output cells of the matrix, grouped according to their targets (Desban et al., 1993; Flaherty and Graybiel, 1993b; Jiménez-Castellanos and Graybiel, 1989; Tai et al., 2013). In addition, afferents from the PF of the thalamus, described in detail later, terminate in clusters in the striatal matrix (Gonzalo, 2002; Herkenham and Pert, 1981), which may constitute a similar or distinct matrisome compartment to those previously described. Hence, matrisomes are predominantly defined by their extrinsic connections, while little is known about their histochemical properties. Recently, Tai et al. (2013) proposed the patchy expression of EphA7, corresponding to striatofugal neurons, as the first molecular marker of matrisomes. Similarly, cadherin-8, is transiently expressed in

patches in the matrix in the first postnatal week, however, the significance of this is currently unknown (Korematsu et al., 1998). Data presented in this thesis suggests that a member of the teneurin family of glycoproteins, Ten-m3, may also mark a novel matrisome compartment.

The unique striatal striosome/matrix/matriosome compartments are believed to constitute a level of organisation analogous to the traditional laminar structure of the cortex. Similar to the development of cortical layers, striatal compartments are comprised of ontogenetically distinct cells (van der Kooy and Fishell, 1987). Unlike the segregation of input and output cells and morphologically different cell types to distinct cortical layers, however, all striatal cell types are distributed throughout both compartments. Moreover, Walker and Graybiel (1993) showed that striatal projection neurons have dendritic fields oriented along a diagonal axis parallel to that of many striosomes and matrisomes. In contrast, the apical dendrites of pyramidal cells in the cortex are oriented at right angles to the cortical layers and are critical for columnar aspects of cortical function. It is proposed that the striatal compartments influence the orientation of dendritic arbors, which may be important in the compartmental organisation of information throughout the striatum (Walker and Graybiel, 1993).

Further, striatal compartments share similarities with other modular multicellular units, such as barrels of the rodent somatosensory cortex, ocular dominance columns of the visual cortex and glomeruli of the olfactory cortex. Like these structures, individual striatal compartments appear to receive converging input from afferent structures to

refine these signals. In contrast to the distinct and regular shapes of barrels, columns and glomeruli, striatal compartments are irregularly shaped; with striosomes described as nearly continuous labyrinths (Graybiel and Ragsdale, 1978). Further, the segregation of inputs is less absolute in the striatum, as described above, and may reflect the more complex integration of non-sensory systems. Hence, striatal compartments may encompass a unique way of segregating and integrating a wide range of functional inputs. This has presumably important functions in balancing inputs for highly organised processing and output for normal function.

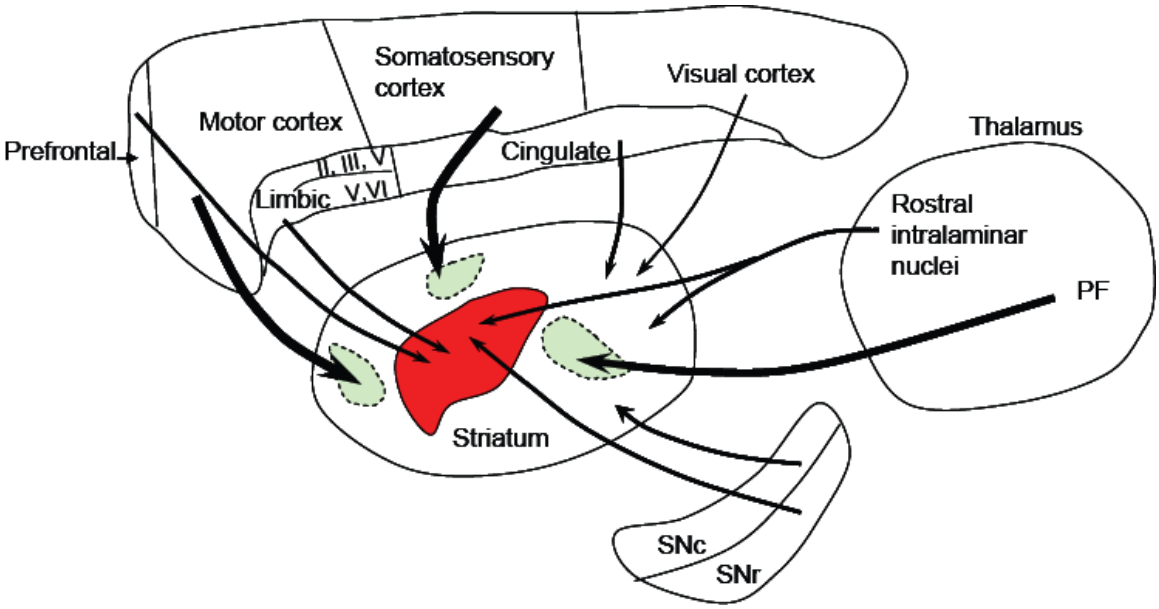

Figure 1.2. A schematic showing striatal afferent projections from the cortex, thalamus and SN, their relative proportions and patterns of heterogeneity within the striatum.

The red and green patches within the striatum represent striosome and matrisome compartments, respectively. The majority of corticostriatal projections originate from the sensorimotor cortices, particularly motor and somatosensory areas, while projections from visual cortex are minimal. These, along with afferents from cingulate cortex predominantly project to the striatal matrix compartment. Sensorimotor terminals cluster to form matrisomes. Prefrontal and limbic cortical areas primarily project to striosomes. Dorsal SNc innervates the matrix while dopaminergic regions of the SNr innervate striosomes. A large portion of thalamostriatal projections originate from the PF, the terminals of which cluster in the matrix. The correlation between thalamic terminal clusters and corticostriatal matrisomes is unclear. Projections from other thalamic nuclei are not well established, however, most regions, such as the rostral intralaminar thalamic nuclei, are believed to project homogenously to the striatum to innvervate both compartments.

Striatal cell types

The rodent striatum is comprised of a number of cell types interspersed by fibres of the internal capsule. The constituent neurons of the striatum are predominantly inhibitory in nature and comprise a single type of projection neuron and a variety of of interneurons. Striatal interneurons are further categorised according to their morphological, chemical and physiological properties, with these features often correlating with one another. These correlations are not absolute, however, with some ambiguities existing, particularly between cellular morphology and physiology. These cell types and their major properties are summarised in Fig. 1.3. The following review of striatal neurons is predominantly based on work from non-primate studies. Although the morphological, neurochemical and physiological properties of these neuronal types and their correlations are mostly transferable between rodents and primates, some differences are present and are noted where appropriate.

The first neuronal type, known as the medium spiny neuron (MSN), is the sole projection neuron of the striatum. MSNs are the most abundant cell type, comprising approximately 95% of the total striatal cell population (Chronister et al., 1976; Kemp, 1968). They utilise gamma-aminobutyric acid (GABA) as their major neurotransmitter and display characteristic phasic firing properties, correlating with the physiologically-defined phasically active neurons (PANs) (Apicella, 2007; Inokawa et al., 2010; Wilson, 1993). These cells are the main targets of extrinsic afferents, including the cortex, thalamus and SN, which predominantly target the distal part of their dendritic arbors (Somogyi et al., 1981; Wu and Parent, 2000), as well as intrinsic connections. They are distributed

throughout both striosome and matrix compartments, with distinct subtypes believed to distinguish direct and indirect basal ganglia pathways. These will be described later.

As evidenced from their name, MSNs are characterised by their medium size (approximately 15 μm diameter soma) and the presence of spines along their dendritic branches. Additionally, evidence suggests that MSNs are morphologically heterogeneous (Kawaguchi et al., 1989; Lee and Sawatari, 2011). All subtypes, however, exhibit collaterals, arising from their dendritic trunks, which arborise profusely in restricted domains, to contact the cell of origin, other local MSNs, or extend longer distances to target more distant MSNs (see Parent and Hazrati, 1995 for a review). In rats, MSN dendrites and axons remain confined to their respective compartments (Kawaguchi et al., 1989), however, they have been shown to cross these boundaries in mice (Lee and Sawatari, 2011), primates (Walker and Graybiel, 1993), cats and ferrets (Bolam et al., 1988), suggesting that MSNs are in contact with cells from both compartments.

As mentioned above, MSNs are the sole output cells of the striatum, and in this context, are often further divided into striatonigral or striatopallidal subtypes, according to their output targets along the direct and indirect basal ganglia pathways, respectively. These subtypes show differential expression of a number of receptors and neurotransmitters. Striatonigral MSNs express D1-dopaminergic and M4-muscarinic acetylcholine (ACh) receptors, along with dynorphin and substance P (Gerfen, 1992; Ince et al., 1997). In contrast, striatopallidal MSNs express D2-dopamine and A2A-purinergic receptors, and enkephalin (Gerfen, 1992; Schiffmann et al., 1991). Recent studies also indicate the

existence of a small subpopulation of MSNs that co-express D1 and D2 receptors in a unique D1-D2 receptor heteromer with dual GABA/glutamate and dynophin/enkephalin phenotype (Perreault et al., 2012). The roles of these neurons have yet to be studied. Direct and indirect pathway MSNs are distributed across striatal compartments (Gerfen, 1992) as well as within individual compartments (see Kawaguchi, 1997 for a review; Wu et al., 2000). Further, striatonigral and striatopallidal MSNs exhibit some differences in physiological properties (see Kreitzer, 2009 for a review). These properties of MSNs suggest an intricate and complex interaction of neurochemicals within this small component of the much larger basal ganglia network.

The remaining striatal neurons are aspiny interneurons which do not project outside the striatum. These are subdivided according to morphology, into (i) large cholinergic interneurons and (ii) medium-sized interneurons, comprising a) parvalbumin-positive (PV+), (b) somatostatin-, neuropeptide Y-, nitric oxide synthase-positive interneurons (SOM/NPY/NOS+) and c) calretinin-positive interneurons. The role of interneurons has traditionally been to connect and relay information between projection neurons. However, despite the majority of the striatal neuron population being comprised of MSNs, increasing evidence suggests that interneurons may play key roles in information processing in the striatum.

Of the four main types of interneurons, the best characterised is the large cholinergic interneuron. For this reason, along with relevance to the current study, these cells will be described in greater detail. Cholinergic interneurons were originally believed to be

projection neurons, however, this theory was rejected following findings that they only comprise 1-2% of the total striatal neuronal population (Kemp and Powell, 1971; Kita and Kitai, 1988). Unlike MSNs, cholinergic interneurons are aspiny and provide the striatum with its highest levels of ACh (Sorimachi and Kataoka, 1975). They possess large (20-50 μm) polygonal or fusiform shaped somata localised to the intermediate zone in the matrix, surrounding striosomes in adults (Van Vulpen and Van Der Kooy, 1996). These somata extend 2-5 very long dendrites, which reach up to 100-200 μm, and branch infrequently but are widespread (Bolam et al., 1984). They also exhibit extensive axonal fields to form a dense plexus of fine axonal branches for innervation (Kemp, 1968, (Bolam et al., 1984). Their dendritic processes, although most dense in the matrix, also extend into striosomes, and thus they are capable of receiving input from both compartments (Graybiel et al., 1986; Kawaguchi, 1997). In humans, cholinergic interneurons show varying spatial distributions, cell volumes and compartmentalisation across the different functional regions of the caudate nucleus and putamen (Bernácer et al., 2007).

Cholinergic interneurons receive strong inputs primarily from the thalamus and to a lesser extent from cortex (Lapper and Bolam, 1992). Synaptic contacts are most prominent on distal dendrites and sparse on the somata and proximal dendrites. Further, they receive input from MSNs and other interneurons via symmetrical synapses (Bolam et al., 1984). Cholinergic interneurons, in turn, form symmetrical synapses onto all parts of MSNs and some PV+ interneurons (Izzo and Bolam, 1988).

Physiologically, cholinergic interneurons are autonomously active (Ding et al., 2010), displaying tonic (3-10/sec), irregular firing patterns, correlating with the physiologically-defined tonically active neurons (TANs). TANs are linked to motor and reward-based learning involving sensory conditioning stimuli. Their activity is highly dependent on behavioural context (Aosaki et al., 1994) and they are proposed to control flexible stimulus-response associations and motivationally driven responses in time, possibly in order to suppress movement controlled by MSNs (Lee et al., 2006). Cholinergic inteneurons/TANs respond to salient stimuli by a pause in their tonic firing pattern (Kimura et al., 1984; Matsumoto et al., 2001). This response has been shown to require thalamic and nigrostriatal dopaminergic input (Aosaki et al., 1994; Ding et al., 2010; Matsumoto et al., 2001) and is believed to serve a 'teaching' role. Similar to dopaminergic neurons, cholinergic interneurons also show changes in activity following the omittance of an expected reward, reflected by a decrease in their tonic firing (Morris et al., 2004). These cells, however, are not exclusively linked to reward-based behaviours, showing different response profiles towards aversive stimuli (see Apicella, 2007 for a review).

In addition, recent evidence suggests that the functions of cholinergic interneurons may be even more complex. Like MSNs, cholinergic interneurons have been shown to express transcripts for glutamate transporters VGLUT1 and VGLUT2 (Danik et al., 2005), as well as VGLUT3 exclusively (Fremeau, 2002; Gras et al., 2002). Further, these cells co-release glutamate and produce postsynaptic responses in MSNs predominantly via N-methyl-D-aspartate (NMDA) receptors (Higley et al., 2011). Interestingly,

VGLUT3 on cholinergic interneurons has been shown to enhance ACh transmission (Gras et al., 2008), which can have wide ranging actions upon direct and indirect pathway MSNs. Hence, cholinergic interneurons may play complex roles in striatal circuitry and behaviour.

The remaining striatal interneurons are GABAergic in nature. These cells have been shown to exert powerful control on MSN activity (Koós and Tepper, 1999) and express VGLUT1 and 2, suggesting that they may also co-release glutamate (Danik et al., 2005). The first of these is the PV+ neurons, which comprise approximately 1% of the striatal cell population. These are medium-sized neurons with a long axon and multiple, dense collaterals within or near their dendritic fields. These cells are slightly larger than MSNs, are spineless and distinctively positive for the calcium-binding protein PV. Their somata are predominantly localised to the matrix while their dendrites extend into both striatal compartments (Gerfen, 1992; Kubota and Kawaguchi, 1993). Further, these neurons are often surrounded by PNNs, extracellular matrix structures with roles in axon guidance and synapse strengthening (Bicknese et al., 1994). Their appearance is associated with the closing of the critical period in the visual cortex (Hensch, 2005) and are postulated to play a similar role in the striatum (Lee et al., 2012a; Simonetti et al., 2009).

PV+ neurons receive a high volume of afferent input from the cortex and much sparser projections from the thalamus (Bennett and Bolam, 1994). They also receive inhibitory input locally from other PV+ and cholinergic interneurons. There is, however, no evidence of a reciprocal PV+ to cholinergic interneuron innervation (Chang and Kita,

1992). Studies indicate that single afferent fibers form multiple synaptic contacts onto PV+ interneurons (Ramanathan et al., 2002). These interneurons subsequently target MSNs, such that a single PV+ cell contacts between 135-541 MSNs (Chang and Kita, 1992; Koós and Tepper, 1999), suggesting high levels of control over their activity. Specifically, activation of a single PV+ cell has been shown to simultaneously block or delay MSN activity (Koós and Tepper, 1999) and is believed to provide feed-forward modulation (Bennett and Bolam, 1994). Physiologically, PV+ neurons produce continuous, high-frequency firing, and are often referred to as 'fast-spiking' cells (Kita, 1993). Enhanced PV+ cell spiking occurs from de-sychronised cortical activity, which leads to a dramatic reduction in MSN activity (Mallet et al., 2005).

The second type of medium-sized interneuron is the SOM/NPY/NOS+ interneuron. These small spineless neurons have short processes and are very few in number (Gerfen and Wilson, 1996; Kemp, 1968). They have fewer dendritic branches that are less ramified, less dense and have longer axonal arborisations compared to PV+ cells (see Kawaguchi, 1997 for a review), with extensive local arborisations. SOM/NPY/NOS+ somata occupy both striosome and matrix compartments, however, their fibers are primarily localised to the matrix (Gerfen, 1985). It has been suggested that these cells may be the physical link between striosome and matrix compartments.

SOM/NPY/NOS+ cells receive inputs from cortical and thalamic afferents and contact MSNs (Sidibé and Smith, 1999). In rats, however, these interneurons have been found to receive input from the cortex but not the thalamus (Kachidian et al., 1996).

Physiologically, they are known as low-threshold spiking cells, with low firing rates and plateau thresholds. They also contain glutamate decarboxylase (GAD)-67, suggesting that they may also release GABA, and express D5-dopamine and M1 and M2-muscarinic receptors (see Kawaguchi, 1997 for a review).

The last group of medium-sized interneurons is the calretinin-positive neurons. These show similar firing patterns to low-threshold spiking neurons, however, they have not been classified physiologically (Tepper and Bolam, 2004). These cells may be a second class of low-threshold spiking neurons that differ in that they do not receive thalamic input (Sidibé and Smith, 1999).

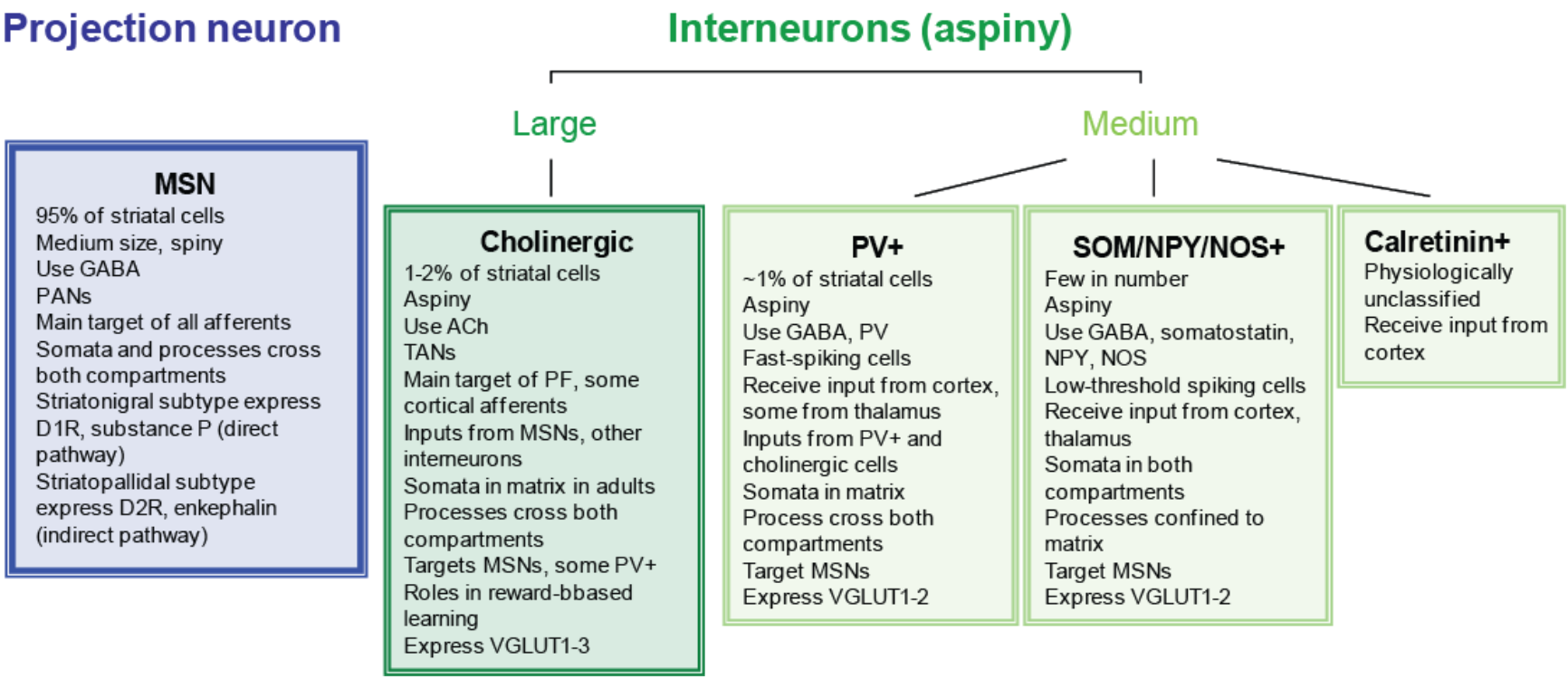

Figure 1.3. A summary of the striatal neuron types and their properties.

The striatal neuronal population comprises one type of projection neuron and four types of interneurons. These are categorised by their distinct morphology, neurochemical and physiological properties.

Connections

As mentioned earlier, the striatum is the key input nucleus of the basal ganglia, where it plays an important role in organising and integrating inputs and subsequently coding appropriate responses. The striatum receives projections from three main afferent structures: the cortex, thalamus and SN. These inputs originate from all regions of the cortex, a number of thalamic nuclei and both components of the SN, which are highly organised throughout every component of the basal ganglia circuitry. In particular, afferents are arranged in a general topographical fashion to reflect the spatial organisation of their origins (Kitai et al., 1976). Further, they are concurrently integrated into the complex, heterogeneous structure of the striatum, with afferent terminals predominantly innervating one striatal compartment over the other (Fig. 1.2). It is important to note that these organisational features are complex, and not always absolute, as evidenced below.

Corticostriatal projections

The striatum receives its largest source of afferent input from the cerebral cortex. All regions of the cortex provide projections to the striatum in the form of excitatory glutamatergic inputs. These terminals express VGLUT1 and mostly form symmetric synapses onto dendritic spines of MSNs (Raju et al., 2006; Spencer, 1976). Cortical axons project bilaterally to the striatum with ipsilateral predominance (Berendse et al., 1992; Carman et al., 1965; McGeorge and Faull, 1989). These projections are generally topographically and heterogeneously arranged across striatal compartments and oriented along the longitudinal axis (McGeorge and Faull, 1989). Functionally, corticostriatal projections are believed to modulate cholinergic activity trans-synaptically, through

activation of MSNs (Anderson et al., 1993; Bolam et al., 1986). Alternatively, they may directly target cholinergic interneurons via non-NMDA receptors through which stimulation is short lived (Consolo et al., 1996a).

Corticostriatal fibers are organised to represent their cortical origin in terms of areal proportion, topography and function. For instance, lesion studies indicate that the rostral half of the cortex, particularly motor and somatosensory areas, are the most highly represented cortical regions within the striatum. This is in contrast to caudal cortical areas, which project more sparsely to the striatum, as is represented in Fig. 1.2. Thus, the extensive sensorimotor projections received by the striatum are believed to be responsible for its primary role in the control of voluntary movement. Furthermore, the innervation of striatal regions by limbic and prefrontal cortical areas implicate the striatum with a role in controlling higher order cognitive activities involving reward and the planning and initiation of movements (Schultz and Romo, 1988; Kimura et al., 1992; Miller and Cohen, 2001; Lauwereyns et al., 2002). Hence, corticostriatal afferents impart functionality to the striatum.

As mentioned above, corticostriatal afferents are topographically organised within the striatum. Early descriptions of these inputs described a 'point to point' transfer of cortical topography (Kemp and Powell, 1970). Due to the complex organisation of these afferents into striatal compartments and the apparent subdivision of the rodent striatum into associative, sensorimotor and limbic regions (described later), more recent studies indicate a more general topography (Veening et al., 1980). Furthermore, there is

evidence that afferents from different cortical regions converge onto single cells in the striatum (Ramanathan et al., 2002). Nevertheless, tracing and lesion studies in monkeys and rats demonstrate a functional topography along the rostrocaudal (RC) axis, where frontal cortex projects to rostral striatum, occipital cortex to caudal striatum and temporal cortex to ventral striatum (Kemp and Powell, 1970; Webster, 1965). Corticostriatal projections are also topographically arranged along the mediolateral (ML) axis, with more lateral cortical regions projecting to progressively more lateral areas of the striatum.

In addition, non-adjacent cortical areas also project to adjacent striatal regions (Selemon and Goldman-Rakic, 1985). This has led to proposed subdivisions of the striatum into three functional regions: i) associative, ii) sensorimotor and iii) limbic areas, across the dorsoventral (DV) and ML axes. These subdivisions differ between rodents and primates due to the structural differences between the species. Associative striatum predominantly receives afferents from frontal, temporal and parietal cortex. In primates, these cortical areas target pre-commisural putamen and the entire caudate nucleus. This region is equivalent to the dorsomedial (DM) striatum in rodents and is linked to the control of goal-directed behaviour, such as the initial learning and acquisition of procedural learning tasks. Sensorimotor striatum receives afferents from primary motor and somatosensory cortex. These cortical areas target the dorsolateral (DL) post-commissural putamen and DL rim of the caudate in primates, and the DL striatum in rodents (Flaherty and Graybiel, 1993a; Ramanathan et al., 2002). Sensorimotor striatum is responsible for the control of habitual sensorimotor activities following the initial task learning (Yin, 2004; Yin and Knowlton, 2006; Yin et al., 2009). Lastly, limbic striatum receives inputs from limbic,

paralimbic cortex, along with the hippocampus and amygdala, which is represented by the ventral regions of the caudate and putamen and the *nucleus accumbens* in primates and rodents. Hence, cortical information converges and is integrated and transferred into strict functional modalities within the striatum.

Furthermore, the topographical and functionally distinct arrangement of corticostriatal terminals is superimposed upon the heterogeneous striosome and matrix compartments. These distinct projections are summarised in Fig. 1.2. Corticostriatal projections are believed to impart distinct functions upon striatal compartments, as they largely receive input from differing cortical regions. Striosomes receive bilateral corticostriatal afferents from prefrontal and limbic areas (Gerfen, 1984) and are distributed across the extent of the striatum, proposedly to allow for interactions with motor/sensory-innervated areas of the matrix (Donoghue and Herkenham, 1986). Further, tracing studies indicate differential compartmentalisation of afferents from superficial versus deep cortical layers of prelimbic and orbital cortex of rats, with deep layers of prelimbic cortex predominantly innervating striosomes, while superficial regions primarily project to the matrix compartment (Gerfen, 1989; Schilman et al., 2008). Similarly, in macaques, only some regions of prefrontal cortex have been shown to innervate striosomes (Eblen and Graybiel, 1995).

In contrast, the matrix receives mostly sensorimotor cortical input, including bilateral afferents from motor and cingulate cortices and ipsilateral projections from somatosensory and visual cortical areas (Donoghue and Herkenham, 1986). In cats and

primates, a large number of these terminate in distinct matrisomes (Goldman and Nauta, 1977; Malach and Graybiel, 1986). Interestingly, many matrisomes innervated by prefrontal cortex are paired with nearby striosomes (Eblen and Graybiel, 1995). Further, afferents from somatosensory cortex are spatially separated as well as interdigitated (Malach and Graybiel, 1986) such that distinct inputs from motor and sensory cortex representing the same body parts innervate the same ipsilateral matrisomes, and which overlap or interdigitate with those receiving the corresponding contralateral projection (Flaherty and Graybiel, 1993a). It is proposed that this apparent alternating contralateral and ipsilateral representation is reminiscent of alternating ocular dominance columns in the visual cortex (Flaherty and Graybiel, 1993a). Furthermore, somatosensory neurons that are organised in columnar groups project to the striatum to terminate in distinct laminae, forming a lattice-like grid of cortical input, with some evidence of interdigitation and overlap (Brown et al., 1998). In addition, labeled matrisomes also intermingle with striosomes and matrisomes receiving differing inputs. Hence, the striatal compartmentalisation, as was suggested by Ragsdale and Graybiel (1990), may act to 'reorder' corticostriatal inputs such that they can be reorganised into different combinations. This organisation, therefore, appears to be a more complex but potentially more sophisticated version of the cortical laminar structure.

Nigrostriatal projections

The nigrostriatal projections form one of the major feedback loops of the basal ganglia circuits. Originating from both the SNc and SNr (Gerfen et al., 1987), these loops also provide the major source of dopaminergic innervation to the striatum. Nigrostriatal

afferents project bilaterally to form symmetric synapses with MSN spines. Nigrostriatal axons, like all afferent projections, are arranged in a topographical and compartment-specific manner. The lateral and caudal regions of the dorsal dopaminergic SNc project to the matrix compartment of the striatum, while afferents from ventral regions of caudal, predominantly dopaminergic, SNr project densely to striosomes located in DM striatum. These distinct projections are also summarised in Fig. 1.2. Similarly, in primates, clusters of cells located in rostral and dorsal SNc project to the caudate nucleus, while those located in caudal and ventral regions project to the putamen (Parent et al., 1983). Interestingly, the same innervation pattern is described for striatonigral neurons (Gerfen, 1985; Jiménez-Castellanos and Graybiel, 1989). These distinct innervation patterns form the basis of the distribution of dopamine within striosomes early in development (see development of nigrostriatal projections).

Dopaminergic nigrostriatal terminals act to modulate the activity of afferent inputs and intrinsic projections in the striatum. These projections converge onto MSNs that also receive cortico- and thalamostriatal inputs (Graybiel et al., 1981; Kocsis et al., 1977; Moss and Bolam, 2008) and are believed to regulate the response of MSNs to these afferents, along with their GABAergic activity through the activation of D1- and D2-receptors (see Gerfen and Surmeier, 2011 for a review). Further, dopamine has important roles in gating striatal cholinergic response activity to salient stimuli (Aosaki et al., 1994) presumably via direct contact with these interneurons (Kubota et al., 1987). Moreover, dopamine has been shown to directly inhibit the activity of subsets of corticostriatal terminals via D2 receptors (Bamford et al., 2004). Despite suggestions that these

terminals may co-release glutamate to help convey rapid reward-related signals, Moss *et al*. (2011) showed that, unlike cortico- and thalamostriatal axons, nigrostriatal axons do not express VGLUTs which are required for glutamatergic transmission (Fremeau, 2002; Fremeau et al., 2001).

Thalamostriatal projections

The discovery of direct thalamostriatal projections has enhanced the level of complexity of the traditionally described basal ganglia loops (see Galvan and Smith, 2011 for a review). The thalamus was traditionally viewed as a relay station for directing afferents from the basal ganglia output nuclei back to the cortex (Albin et al., 1989). The presence of direct thalamostriatal projections were first proposed in the 1940s (Vogt and Vogt, 1941) and were subsequently confirmed using degeneration and tracing studies in rodents (Powell and Cowan, 1954) and primates (Cowan and Powell, 1956). Further, a reciprocal striatothalamic projection has been described in rats, however, appears to be a transient projection during development which is not described in the adult (Hattori et al., 1990).

Thalamostriatal projections make up the second largest source of afferents to the striatum, after corticostriatal input, and originate from multiple thalamic nuclei (Deschênes et al., 1995; Mengual et al., 1999; Smith et al., 2004, 2009). Of these, the largest source originates from the caudal intralaminar group, consisting of the PF, central-medial, paracentral, central-lateral and subparafascicular nuclei. In addition, midline thalamic nuclei, such as paraventricular; and relay nuclei, including ventral motor thalamus, such as ventral-anterior/ventral-lateral (VA/VL); along with the posterior

group, including the lateral-posterior nucleus, which also form important thalamostriatal projections (Barroso-Chinea et al., 2007, 2008; Castle et al., 2005; Deschênes et al., 1995; Groenewegen and Berendse, 1994). Thalamic projections as a whole, are topographically organised such that medially located paraventricular nucleus predominantly projects to medial striatal regions, while the more laterally located PF and the lateral-posterior group project to progressively more lateral regions of the striatum (Beckstead, 1984; Berendse and Groenewegen, 1990; Ragsdale and Graybiel, 1991). Moreover, these projections are also heterogeneous, with medially located thalamic nuclei generally innervating striosomes, while those more laterally positioned primarily project to the matrix (Ragsdale and Graybiel, 1991).

Afferent projections from within individual thalamic nuclei are also topographically organised. For instance, the intralaminar nuclei project to the head of the caudate nucleus in a ML and RC topography in primates (Cowan and Powell, 1956). In addition, midline thalamic nuclei project predominantly to ventral, but also dorsal striatum (see Smith et al., 2004 for a review). Further, VA/VL nuclei terminate broadly along the RC extent of the caudate and putamen, in a functionally topographic fashion. These projections are also heterogeneous, however, their correlation with striatal compartments is currently unclear (McFarland and Haber, 2001). Thalamostriatal projections from the VA/VL nuclei are believed to be responsible for regulating motor cortical input to the striatum (McFarland and Haber, 2001).

The most well characterised and largest single source of thalamostriatal projections originates from the PF, the rodent homologue of the centromedian-parafascicular (CM-PF) complex in primates. Hence, the majority of anatomical and functional data on thalamostriatal projections has been derived from studies on these projections. Further, thalamostriatal projections from the rodent PF constitute a major focus of the current study, and, therefore, will be described here in detail.

In rodents, the PF encloses a bundle of fibres known as the *fasciculus retroflexus* (fr), which roughly divides the PF into medial and lateral regions. The lateral portion of the rodent PF is believed to be the equivalent of the primate CM nucleus (Smith et al., 2004). The PF not only provides a massive projection to the striatum but also receives substantial, topographically organised input from other basal ganglia nuclei, including the GP and SNr (François et al., 1988). Moreover, distinct functional 'sensorimotor' and 'associative' loops are believed to exist, linking the CM-putamen-GPi and PF-caudate-SNr circuits, respectively (Sidibé et al., 2002). The PF also projects to all other basal ganglia nuclei (Tandé et al., 2006).

Thalamostriatal axons from the PF project ipsilaterally and innervate the striatum in a topographical manner (Vercelli et al., 2003). Terminals are topographically arranged along the RC axis, where rostral regions of the PF innervate rostral striatum and caudal PF projects to caudal striatum. Furthermore, these projections show a DV and ML topography, with DL PF innervating dorsal striatum, VL PF projecting to lateral striatum and medial regions of the PF filling up medial striatum (Berendse and Groenewegen,

1990; Elena Erro et al., 2002; Lanciego et al., 2004). In primates, axons from the PF predominantly innervate the caudate nucleus while the CM projects to the putamen (Parent et al., 1983; Smith and Parent, 1986), with dorsally located cells targeting dorsal, while lateral CM innervates lateral putamen (François et al., 1991).

Importantly, these profuse projections specifically innervate the striatal matrix compartment, largely avoiding striosomes (Deschênes et al., 1996a; Herkenham and Pert, 1981; Sadikot et al., 1992a; Xu et al., 1991). Within the matrix, axon terminals are arranged into numerous clusters that appear as diagonal or oblique bands of highly varicose axons (Gonzalo, 2002; Parent and Parent, 2005a). Single cell tracing studies suggest that multiple clusters of terminals arise from collaterals originating from single PF neurons (Deschênes et al., 1996a). This is similarly observed in primates (Parent and Parent, 2005a), where the clustering of terminals is predominantly observed in the caudate nucleus from fibers originating from the CM, whereas those from the PF predominantly terminate in a diffuse manner (Sadikot et al., 1992a). Reconstruction of patches of terminals in 3-dimensions indicate similarities with striosome 'labyrinths' (Desban et al., 1989), with patches consisting of a small number of long oblique streaks in transverse, almost sagittal sections, which appear as roughly parallel layers linked by bridges and separated by regions devoid of terminals (François et al., 1991; Parent and Parent, 2005a).

Single PF neurons have also been shown to send collateral branches to more than one brain structure, including the EPN and STN, reticular thalamic nucleus, GP and sparse

terminals to the cortex in rats (Deschênes et al., 1996a). Similar collateralisation of CM-PF neurons has been observed in primates, where they densely innervate the striatum and only sparsely innervate the cortex (Parent and Parent, 2005a). Findings from other groups, however, indicate separate thalamic innervation of the striatum and cortex (Féger et al., 1994; Sadikot et al., 1992b). In the cat, double-labeling studies show that the PF contains neurons that innervate both the striatum and cortex, whereas CM neurons show preference for one site over the other (Royce, 1983). Hence, perhaps the level of collateralisation and multi-nuclear innervation observed in single cell tracing studies is not a feature of all PF neurons. Nevertheless, thalamic axons from the PF project more densely to the striatum than the cortex.

Thalamostriatal terminals originating from the PF predominantly form asymmetric synapses onto MSNs and cholinergic interneurons (Lacey et al., 2007; Lapper and Bolam, 1992; Sadikot et al., 1992a; Xu et al., 1991). In primates, they have also been described to contact PV+ and SOM/NPY/NOS+ interneurons (Rudkin and Sadikot, 1999; Sidibé and Smith, 1999), however, in rodents they show a very sparse innervation of PV+ cells and have not been shown to form synapses with SOM/NPY/NOS+ cells (see Smith et al., 2009 for a review). At the ultrastructural level, PF terminals form both axospinous and axodendritic synapses with striatal MSNs (Dubé et al., 1988; Lacey et al., 2007; Sadikot et al., 1992a) and express the glutamate transporter VGLUT2. In addition, thalamostriatal axons originating from the VA/VL nuclei also express VGLUT1 (Fremeau et al., 2001; Kaneko et al., 2002). The innervation of striatal cells by thalamic afferents is important for the survival of these neurons and the normal levels of a number

of neurochemicals (Nieoullon and Kerkerian-Le Goff, 1992; Nieoullon et al., 1985; Samuel et al., 1990). Importantly, the terminal fields of thalamostriatal afferents overlap with cells of the direct and indirect pathways, suggesting dual influence on these circuits (Castle et al., 2005; Gonzalo, 2002).

The functional characteristics of thalamostriatal projections are still poorly understood. Recent studies suggest that they are well positioned to play an intricate role within basal ganglia circuits. It has been proposed that thalamostriatal projections preferentially innervate indirect pathway MSNs projecting to the GPe (Dubé et al., 1988; Sidibé and Smith, 1996), although they may also innervate direct pathway MSNs (Gonzalo, 2002). In addition, they directly innervate cholinergic interneurons via NMDA receptors (Consolo et al., 1996a). It has been proposed that substance P-containing terminals of the indirect pathway are in contact with cholinergic interneurons to cause depolarisation and facilitate ACh release via NK1 receptors. This is thought to regulate the tonic effect of dopamine on ACh release or to provide a link between direct and indirect pathways within the striatum (Anderson et al., 1993; Arenas et al., 1991; Bolam et al., 1986). Lesioning of the PF has been shown to prevent increases in activity within the STN and basal ganglia output nuclei, similar to that produced in midbrain dopaminergic lesions (Bacci et al., 2004).

The function of thalamostriatal projections is also best characterised for those originating from the PF. Behavioural studies using animals following PF lesions suggest that the thalamostriatal pathway may have roles in the formation of stimulus-response

associations. In rodents, active avoidance tasks suggest that PF lesions do not affect acquisition, but do increase the rate of extinction (Bohus and de Wied, 1967; Quiroz-Padilla et al., 2007). Similar deficits are observed in operant conditioning tasks (Tikhonravov, 1998). Further, deficits are observed in the accuracy and timing of responses to a visual cue-dependent discrimination task, while only deficits in accuracy were observed if lesions were produced following prior training, suggesting roles for the PF in relaying information about stimulus-response associations (Kato et al., 2011). Similarly, no differences in acquisition are observed in goal-directed tasks in rats, however, performance drops when action-outcome contingencies are changed in animals lacking an intact thalamostriatal pathway. These rats also perform poorly in extinction tests and reversal learning paradigms (Bradfield et al., 2013). Specifically, lesioned animals exhibit more perseverative errors but no differences in regressive errors, suggesting that this circuit has roles in maintaining newly learned strategies (Ragozzino, 2004; Thompson and Yang, 1982; Thompson et al., 1981).

These deficits are largely consistent with primate and human studies, which have implicated the PF in roles of attention and arousal. The CM-PF complex is activated in the transition to alert, attentive states in positron emission tomography (PET) and MRI studies in humans (Hulme et al., 2010; Kinomura et al., 1996). Further, inactivation of the CM-PF affects sensory cue-directed attentional orienting on the contralateral side (Minamimoto and Kimura, 2002). The redirection of attentional behaviour is often associated with a simultaneous suppression of motor activity, which is believed to rely on thalamic input to shift action selection signals originating from the cortex.

Mechanistically, this is believed to be a direct effect of thalamic input to cholinergic interneurons via presynaptic muscarinic receptors on corticostriatal terminals, and not direct inputs to MSNs or other striatal terminals (Barral et al., 1999; Ding et al., 2010; Ebihara et al., 2013). This may be reflected in the reduction of cholinergic activity, as measured by p-Ser240-244-S6rp-immunoreactivity, but not MSNs following PF lesions (Bertran-Gonzalez et al., 2012; Bradfield et al., 2013). Further, thalamostriatal projections typically induce the characteristic burst-pause activity in cholinergic interneurons in response to sensory stimuli (Smith et al., 2009). Ding et al (2010) used slice preparations preserving cortico- and thalamostriatal connections to show that upon stimulation of thalamic axons, the initial burst response triggers a transient, presynaptic suppression of cortical input to all MSN subtypes. In turn, striatopallidal MSNs showed prolonged responsiveness lasting approximately the length of the interneuron 'pause' to presumably control motor suppression (Ding et al., 2010).

Further, the loss of the cholinergic burst-pause response occurs following inactivation of thalamic innervation from the CM-PF complex. This results in a concurrent reduction in behavioural response to stimuli associated with reward, suggesting the PF provides information about salient events (Matsumoto et al., 2001). In addition, dopaminergic connections also influence the burst-pause response of cholinergic interneurons (Aosaki et al., 1994). Interestingly, Bradfield *et al*. (2013) showed that the behavioural and anatomical deficits observed following PF inactivation are a function of the connections between the PF and the posterior-DM striatum and not due to connections with the anterior-DM striatum.

The PF also has roles in non-spatial memory. Rats with PF lesions show deficits in spontaneous object recognition tasks (Castiblanco-Piñeros et al., 2011). In addition, animals also show delays in socially transmitted food preference tasks (Quirozpadilla et al., 2006). Further, no changes to motor skill learning, as measured by performance on an accelerating rotorod, which is known to be dependent on dorsal striatum function, has been noted (Kato et al., 2011).

Other striatal afferents

As mentioned above, apart from the three major sources of afferent input, the striatum also receives projections from a number of other structures. For instance, limbic areas such as the hippocampus project strongly to the *nucleus accumbens*, but also to the most medial, ventral, rostral and caudal regions of the striatum. Further, ventral subiculum innervates ventral and caudal striatum, while dorsal subiculum projects to rostral striatum (Groenewegen et al., 1987). The striatum also receives a large serotonergic input from contralateral midbrain raphe nuclei; a small to moderate innervation from the pulvinar, and a small input from amygdala, as well as scattered input from ventral tegmental area and locus coeruleus (Parent et al., 1983; Veening et al., 1980). The subparafascicular nucleus, which is closely related to the PF in topography and cytology, also projects to the striatum (Sadikot et al., 1992b).

Striatal efferents

Striatal efferents are also topographically and heterogeneously organised within the striatum and their targets. Efferents to the SN are predominantly located within striosomes, while those projecting to the GP are primarily localised to the matrix, with some evidence of intermixing. Within the matrix, efferent cells are further compartmentalised, showing heterogeneities similar to matrisomes (Jiménez-Castellanos and Graybiel, 1989). As mentioned previously, striatonigral and nigrostriatal projections have reciprocal links to corresponding striatal regions (Gerfen, 1985; Jiménez-Castellanos and Graybiel, 1989). This is not observed for striatopallidal and pallidostriatal axons (Jiménez-Castellanos and Graybiel, 1989). Striatonigral projections are topographically organised, with a conserved ML distribution and inverted DV organisation, while RC distribution is less organised (Gerfen, 1985).

Within the basal ganglia, there is a high level of convergence. For instance, striatal and STN axons converge onto single pallidal cells, but while striatal axons innervate pallidal dendrites, subthalamic axons synapse with cell somata (Hazrati and Parent, 1992). In contrast, these brain structures traverse the GP at right angles to one another. Similar to the striatum, band-like termination patterns are observed in the GP (Hazrati and Parent, 1992). Further, striatopallidal efferents are also compartmentalised.

As evidenced by the studies discussed above, the striatum plays a major role in organising, integrating, processing, responding and transmitting outputs in response to sensory, motor and limbic cortical inputs using its intrinsic network of striatal neurons

and extrinsic input from thalamo- and nigrostriatal afferents via a variety of neurochemicals. This very complex organisation reflects the equally complex roles associated with the striatum in motor control, motivation and learning and memory. Hence, it is critical for striatal connections to form normally during development. The development of the striatum and its major afferent connections, including what is known of the underlying mechanisms involved, are described in the next section.

Development

Striatal development

The striatum, along with the pallidum, develops from the ventricular or ganglionic eminences, transient germinal epithelial swellings into the lateral ventricle. These structures are divided into distinct medial and lateral subdivisions by a sulcus running along the RC axis (Smart and Sturrock, 1979), and are hence referred to as the medial ganglionic eminence (MGE) and lateral ganglionic eminence (LGE), respectively. The LGE is located rostral, dorsal and lateral of the MGE (Fentress et al., 1981). The MGE develops first, appearing at embryonic day (E)11 in mice, with the LGE observed a day later (Smart and Sturrock, 1979). The sulcus dividing the MGE and LGE disappears by E15 and the ganglionic eminences flatten against the wall of the lateral ventricles and disappear by the end of gestation, at approximately E19 in mice (Smart and Sturrock, 1979). In humans, the ganglionic eminences disappear by the first year (Encha-Razavi and Sonigo, 2003).

Newly postmitotic neurons of the LGE and MGE cells migrate along different routes to form the striatum along several spatiotemporal gradients (Wichterle et al., 2001). The time course of these events has been described for rats and mice, with approximately 2-3 days difference in embryonic dates, associated with the slightly longer gestational period of the former species. As the majority of studies have been performed in rats, the dates below are quoted for this species, unless otherwise stated, and a summary of the major

developmental events is illustrated in Fig. 1.4. The striatal primordium is first distinguishable at approximately E12 (Angevine and McConnell, 1974; Sturrock, 1980), being located lateral to the subependymal layer between the two halves of the ganglionic eminences. At these early stages, a small number of neuroblasts are observed, predominantly in caudal regions of the primordium, compared to rostral, where they are restricted to the lateral edge of the nucleus (Angevine and McConnell, 1974; Sturrock, 1980). Early-born neurons, between E12-16, are most numerous in the lateral half of the striatal primordium, while neurons born in the middle period (E14-16), when neuroblast differentiation peaks, are evenly scattered. Late-born neurons, born between E18-22, are mostly located to the medial half of the primordium (Angevine and McConnell, 1974; Bayer, 1984; Smart and Sturrock, 1979). This developmental gradient has also been observed in monkeys (Brand and Rakic, 1979). In addition, there is some evidence of a superficial to deep developmental gradient, however, this appears to flip at rostral versus caudal levels of the striatum (Bayer, 1984). These developmental gradients are also observed in other aspects of striatal development, such as striosome/matrix formation and afferent innervation, which will be described later.

Neuronal differentiation is no longer observed at P1, with subsequent increases in striatal volume proposed to be attributed to neuropil and myelin formation (Smart and Sturrock, 1979). Synapse-like structures are first observed at E14, when fibre bundles comprising the internal capsule also become prominent. Axodendritic synapses are observed by P5 and internal capsule fibers become myelinated by P10 (Sturrock, 1980). In humans, the striatum appears in the 6th week of gestation (O'Rahilly and Muller, 1994).

Development of striatal neurons

There is some evidence to suggest that cells within the ventricular and subventricular zones may be committed to a striatal phenotype by the time the LGE and MGE are delineated (Magrassi et al., 1998). This is important as the LGE and MGE provide distinct, but overlapping sources of striatal neurons (Olsson et al., 1998). A large proportion of striatal neurons are born in the LGE, including all MSNs, PV+ and a large proportion of SOM/NYP/NOS+ interneurons (Jain et al., 2001; Olsson et al., 1995, 1998). In contrast, the MGE has been shown to be an important source of cholinergic interneurons and some SOM/NPY/NOS+ cells. Migration patterns may also differ between cell types, with evidence suggesting that interneurons mostly migrate from the MGE in a tangential fashion (Marin et al., 2000). It is now believed that cells from the MGE which migrate radially generally become projection neurons while those migrating tangentially predominantly become interneurons of the striatum and cortex (see Marín et al., 2001 for a review).

A large number of LGE progenitors are specified towards striatal projection neuronal fate at the beginning of neurogenesis. These are not irreversibly specified, however, as environmental cues and cell autonomous factors appear to influence differentiation (Olsson et al., 1998). Projection neurons are generated only from the LGE between E12.5-E15.5 (Olsson et al., 1998) and express DARPP-32 (Anderson et al., 1997). Interneurons such as PV+ and some SOM/NPY/NOS+ cells are also generated in the LGE. PV+ cells are born postnatally, first seen at P9 in lateral striatum, and increase in number to fill more medial regions (Schlösser et al., 1999). These cells do not show full

molecular or morphological maturation until the second-fourth postnatal weeks, a critical period in striatal development, which also encompasses the major period for corticostriatal synaptogenesis (Hattori and McGeer, 1973) and MSN morphological and physiological maturation (Lee and Sawatari, 2011; Tepper et al., 1998). In contrast, SOM/NPY/NOS+ interneurons are generated between E15-16 and show no developmental gradient (Semba et al., 1988). Similarly, calretinin+ cells, are born embryonically, being present in the striatum by birth, where they increase in number to peak at P5 before declining across the following 2 weeks. These cells show a transient medial to lateral gradient of development (Schlösser et al., 1999).

Cholinergic interneurons solely originate from the MGE. These are the earliest born cells in the striatum, generated between E12-17 (Phelps et al., 1989; Semba and Fibiger, 1988; Semba et al., 1988). Like the majority of striatal neurons, cholinergic interneurons mature along a lateral to medial and caudal to rostral gradient in the first and second postnatal week of development (Schlösser et al., 1999; Semba and Fibiger, 1988). Their distibution with respect to compartments changes from preferentially overlapping with striosomes prior to P7 to the intermediate zone within the matrix, surrounding striosomes. Counts suggest that this change in distribution is due to a delayed turning on of ChAT by cholinergic cells in the matrix, possibly combined with cell death in striosomes and possibly some migration of cells between striosome and matrix (Van Vulpen and Van Der Kooy, 1996), however, it is unclear which of these processes dominates.

Molecular mechanisms of striatal neuronal development

Striatal neurons show wide ranging differences in temporal development, neurochemical expression and morphology. It is not well established when or how these cells become specified and differentiated into their respective subtypes. There is some evidence that cortical neurons may be committed to a specific phenotype around the time they cease mitosis (Floeter and Jones, 1985). Some striatal neurons arising from the LGE are believed to be specified towards an MSN fate due to their expression of DARPP-32 (Anderson et al., 1997). Hence, intrinsic molecular mechanisms must be recruited for this process. Specification of developing neurons appears to be highly dependent on the combinatorial expression of a number of developmental genes (Olsson et al., 1998). In the interest of space and relevance to the current study, only a brief account of some of these genes will be described in this section. For a more comprehensive review, see Marin *et al.* (2000) and Evans *et al.* (2012).

Studies are currently more plentiful for some cell types over others, in particular, the development of interneurons are best described. An important family of genes in the development of interneurons is the Nkx family of homeodomain transcription factors. Marin et al. (2000) showed that approximately 10% of cells express Nkx2.1, which is required for the specification of developing interneurons. Striatal cholinergic, calretinin and PV+ cells maintain expression of Nkx2.1 into adulthood, while SOM/NPY/NOS+ cells downregulate Nkx2.1 as they leave the neuroepithelium. The latter group of cells do not develop in Nkx2.1 mutants (Marin et al., 2000). Further, a number of other genes have been implicated in the development of cholinergic interneurons. MGE cells

expressing the homeobox gene Gbx2 give rise to almost all striatal cholinergic interneurons (Chen et al., 2010; Marin et al., 2000). In addition, the homeodomain protein LIM homeobox 7 (Lhx7) is required for maintaining the morphological and molecular characteristics of striatal cholinergic interneurons. The absence of Lhx7 leads to a depletion of cholinergic interneurons and expression of markers such as ChAT, with a respecificiation of these cells into Lhx6 expressing GABAergic interneurons (Lopes et al., 2012). MGE cells that express Lhx6 differentially mature to become GABAergic interneurons expressing substance P and PV (Marin et al., 2000).

An important group of genes in the development of both striatal projection neurons and interneurons is the Dlx family of homeodomain transcription factors, which are expressed in overlapping patterns in ventral telecephalon (Anderson et al., 1997). Dlx1/2 and Dlx5/6 are expressed in the ventricular and subventricular zones of the LGE. Dlx1/2 play the most dramatic roles in striatal development, with Dlx1/2 double mutants showing ectopic accumulation of late-born, but not early-born cells, in the proliferative zones. With a proportion of these being Nkx2.1-positive, Dlx1/2 appears to have a role in the normal development of the striatal proliferative zones and differentiation of late born striatal MSNs and interneurons (Anderson et al., 1997). Moreover, the transcription factor COUP TF1-interacting protein 2 (Ctip2) is implicated in the differentiation of MSNs, with a dramatic reduction in MSN markers, such as DARPP-32, observed in the absence of Ctip2 (Arlotta et al., 2008). Further, Mash1, a basic helix-loop-helix transcription factor, expressed in the proliferative zones of the LGE and MGE, is responsible for the development of Nkx2.1-positive striatal neurons, particularly

cholinergic, and calretinin, or early-born interneurons. Hence, it is believed that Dlx1/2 and Mash1 regulate the balance between early- and late-born neuronal differentiation within the striatum (Marin et al., 2000).

Development of striatal compartments

Compartmentalisation, described as the embryonic fating of cells to result in spatially contiguous regions in the adult (Krushel and van der Kooy, 1993), is an important developmental feature of the brain, as well as entire organisms. The brain is compartmentalised in early development, into its major subdivisions, the telen-, dien-, mesencephalons. Such developmental compartmentalisation further occurs within individual brain regions, with the best established being the laminar structure of the cortex, which is divided into deep (V and VI) and superficial (comprising layers I-III and granular layer IV) layers. Compartmentalisation is also evident in the striatum, in the form of striosome/matrix/matriosome compartments. The significance of compartmentalisation within the striatum is only just coming to light. The development of birth dating techniques has advanced our knowledge of the time course of the cellular development of these compartments, revealing that, similar to cortical layers, they are ontogenic units. Further studies have revealed the intrinsic and extrinsic mechanisms associated with the formation of these compartments, suggesting that both factors play important roles. These are described below.

Compartmentalisation of striatal cells is determined by birth date. The use of pulse injections of [^{3}H]-thymidine and/or bromodeoxyuridine (BrdU), which label mitotically

active cells (Messier and Leblond, 1960; Miller and Nowakowski, 1988), combined with a suitable striosome marker, have shown that cells destined for the striosome compartment are born during an earlier period of striatal neurogenesis than matrix neurons (Graybiel and Hickey, 1982). In rats, striosome cells are generated around E13-E15, while matrix neurons are formed at E18-E20 (van der Kooy and Fishell, 1987; Song and Harlan, 1994). In cats, cells generated between E24-30 make up striosomes and cluster in non-medial regions of the striatum, with the medial striatum virtually devoid of AChE and TH expression at early ages (Graybiel and Hickey, 1982). The apparent lateral to medial gradient of striosome development is also observed in rats, where striosome neurons first aggregate in lateral striatum (Krushel et al., 1995), and gradually fill up more medial regions, where some of the youngest striatal neurons are located (Graybiel and Hickey, 1982). Concurrently, matrix cells spread out to concentrate primarily in medial striatum and avoid extreme VL striatum, primarily occupied by the first striosome patches (Krushel et al., 1995; Song and Harlan, 1994). These data confirm that the aggregation of striosome neurons occurs in a similar spatiotemporal gradient to striatal neurogenesis (Bayer, 1984).

Intrinsic mechanisms

The formation of striosome versus matrix compartments appears to stem from differences in the intrinsic ability of early and later-born neurons to cluster. Krushel *et al.* (1993) performed a series of studies using *in vivo* labeled [^{3}H]-thymidine early-born cells and BrdU-labeled late-born cells that were subsequently dissociated into suspension cultures. They found that early-born cells from both brain regions aggregated whilst late-born cells

were dispersed and distributed towards the periphery of the reaggregates (Krushel and van der Kooy, 1993; Krushel et al., 1993, 1995). *In vivo*, early-born neurons intermix with late-born neurons at E20 in rats, where their spatial domains overlap (Krushel and van der Kooy, 1993; Song and Harlan, 1994; Krushel et al., 1995; Snyder-Keller et al., 2001). This suggests that early- and late-born cells show an initial mutual attraction, during which the physical properties that lead to their segregation into their not yet established. Approximately two days later, however, these cells are segregated to form mature striosome and matrix compartments.

The molecular mechanisms associated with the development of compartments are still poorly understood, though some candidates, which also regulate the differential development of early- versus late-born striatal neurons, have been suggested. For instance, Mash 1, which is required for the development of early born MSNs, and Dlx1/2, which regulates the fate of late-born neurons, have been implicated, as the respective groups of neurons fail to form in the absence of these genes (Anderson et al., 1997). Further, reaggregation cultures showing the coaggregation of cortical and striatal cells suggests that the ontogenetic properties of early- versus late-born cells may be conserved between the striatum and cortex. Hence, mechanisms associated with the development of cortical layers may be transferable to the development of striatal compartments. For instance, Reelin has been shown to have important roles in the normal organisation of the laminar structure of the cortex (see Rakic and Caviness, 1995 for a review) and has also been shown to be expressed in striosomes in the striatum (Nishikawa et al., 1999), however, its role here has yet to be investigated.

The first and only molecular candidate thus far to be shown to have a direct role in the formation of striatal compartments is EphA4. EphA4 is a member of the Eph family of receptor tyrosine kinases, which have well established roles in axon guidance in a range of brain systems, where interactions between the receptor and their respective ligands primarily results in the repulsion of axonal processes expressing the ligand. Passante et al (2008) showed that disruption to Eph/ephrin signaling *in situ* leads to a disrupted sorting of cells within striosome and matrix compartments. More specifically, EphA4, expressed in matrix cells, and its ligand ephrinA5, expressed in striosomes, appear to control the normal segregation of striosome and matrix compartments, as EphA4/ephrinA5 mutants show a uniform distribution of matrix neurons, with little segregation from striosomes. The actions of EphA4 appear to be confined to matrix neurons, however, as striosomes appeared normal in these mutants, suggesting that it is unlikely that EphA4-espressing late-born neurons influence the clustering of these cells. It may be possible, however, that the repellant nature of Eph/ephrin signaling has roles in the segregation of striosome clusters from matrix cells, described further below.

Extrinsic mechanisms

In addition to intrinsic adhesive mechanisms, it is likely that the formation of striatal compartments is influenced by extrinsic factors. There are currently two main groups of extrinsic factors that have been proposed to influence striosome clustering. The first is the physical migration of new matrix cells into the striatum, which is believed to be sufficient to cause early-born neurons to physically cluster. This theory is supported by

observations of an initial intermixing of early- and late-born cells prior to clustering *in vivo* (Fishell and van der Kooy, 1987; Krushel et al., 1995; Song and Harlan, 1994), suggesting that early born cells may not be able to aggregate in the absence of late-born matrix cells. In addition, Song and Harlan (1994) showed that the distance between early-formed clusters is greater at progressively later stages of development, when matrix neurons occupy the striatum. This suggests that the invasion of matrix cells may force early-born neurons to cluster and become separated from other similarly-isochronic groups of cells. Hence, late-born cells may express molecular cues that induce adhesive properties within early-born cells and/or cues that repel isochronically dissimilar cells to result in the clustering of this latter population but not the former. The repulsive properties of Eph/ephrins, such as EphA4 expressed in matrix neurons described above, may be important candidates for controlling striosome/matrix segregation.

The second extrinsic mechanism involves the influence of afferent projections from the cortex, thalamus and SN. Striatal transplant experiments show that in the absence of extrinsic factors, the striosome compartment occurs as a single large patch, and their markers are expressed at lower than normal levels (Johnston et al., 1987). Interestingly, organotypic culture experiments where striatal slices were removed prior to compartment formation *in vivo* showed normal striosome/matrix organisation in 6% of cultures (Snyder-Keller et al., 2001), suggesting that some intrinsic mechanisms are present to instruct compartment formation. Co-culturing striatal slices with ventral mesencephalon enhanced patch formation, with approximately one third of cultures showing the

striosome/matrix organisation (Snyder-Keller et al., 2001) indicating that extrinsic input from dopaminergic afferents further help to instruct patch formation.

The mutual attraction between cortical and striatal neurons in dissocation-reaggregate experiments (Krushel and van der Kooy, 1993; Krushel et al., 1993) suggests that corticostriatal afferents may influence striatal compartmentalisation. This may be further supported by the organisation of projections between isochronically similar cortical layers and striatal compartments: that is, early-born deep layer cortical cells specifically project to striosomes also comprising early-born cells (Gerfen, 1989). Decortication, however, does not disrupt striosome/matrix organisation (Lança et al., 1986). Similarly, co-culturing striatal slices with those from the cortex, as well as the thalamus, does not affect compartment formation (Snyder-Keller et al., 2001). Hence, corticostriatal and thalamostriatal afferents do not appear to be important extrinsic factors in striatal compartmentalisation.

Dopaminergic afferents from the SN, as noted briefly above, have also been of particular interest due to the extensive spatial overlap between the genesis of striosome neurons and the development of dopaminergic fibers (Moon Edley and Herkenham, 1984). The blockade of dopamine with haloperidol, however, did not block or delay striosome formation (van der Kooy and Fishell, 1992; Moon Edley and Herkenham, 1984). Interestingly, severing or lesioning nigrostriatal connections in the first postnatal week results in more than 50% reduced striatal volume and μ-opioid receptor (μ-OR) binding (Moon Edley and Herkenham, 1984). In addition, surviving striosome neurons are no longer clustered, but instead are diffusely distributed (van der Kooy, 1996), suggesting

that early projections from the SN are required for the survival and clustering of striatal neurons into striosomes. Intriguingly, Fishell and van der Kooy (1991) showed that early born cells comprising striosomes with reciprocal afferent projections to the SN are preferentially spared during the cell death phase of development in the striatum. The striatal cell death phase occurs by the end of the first postnatal week, where approximately 25% of striatal neurons undergo cell death in the rat (Fentress et al., 1981). In addition, a small number of early-born matrix neurons that also have striatonigral projections are, likewise, spared, while those without projections undergo cell death. Hence, reciprocal nigrostriatal and striatonigral projections may play important roles in the survival of neurons and the clustering of striosome cells.

Development of afferent striatal connections

The development of proper connections is essential for normal function, with aberrant axonal connectivity having been linked to a variety of human genetic disorders (Engle, 2010). A number of processes must be tightly controlled for the proper formation of connections, including elongation, axon guidance, axon branching, terminal arborisation and patterning, and subsequently, axon pruning. Each of these processes can be further broken down into multiple steps, for which different molecular cues, as well as activity-dependent mechanisms, have been shown to be responsible. Examples of the latter include the balance of output activity within the direct and indirect pathways, which is believed to regulate excitatory innervation of the striatum during development; and glutamatergic stimulation or release, which is sufficient to drive spinogenesis in the developing striatum (Kozorovitskiy et al., 2012). Molecular candidates implicated in the

formation of striatal afferent connections are limited. A small number of candidates have been described for the guidance of nigrostriatal/striatonigral and thalamostriatal projections, while those for the cortiocostriatal pathway are believed to overlap with callosal and corticofugal projections (Sohur et al., 2012). The following section will describe the temporal development of these major afferent connections and the molecular candidates implicated in their connectivity, where available. Some reference is made to the thalamocortical and corticothalamic projection, which may provide insight into the mechanisms associated with the thalamostriatal and corticostriatal pathways.

Development of corticostriatal pathways

The development of corticostriatal fibers takes place during embryonic ages and extends into postnatal stages. Corticostriatal neurons are observed as early as E10.5 in mice, peaking between E12.5 and E14.5, similar to callosal projection neurons (Sohur et al., 2012). Cortical axons are observed in the internal capsule as single, non-collateralised and unfasciculated axon trunks between E12-17. The subsequent collateralisation and targeting of these projections have been described to occur at different time points by different groups. For instance, Sheth et al. (1998) described collateralisation to occur at E18, whereas these branches were not observed until P3-4 by Sohur et al. in mice (2012). It is likely that this discrepancy reflects differences in the cortical areas examined by the two groups, as Sheth et al. (1998) also report a second group of finer axon trunks entering the striatum, intermingled with the initial group within the internal capsule after E18. Nevertheless, terminal arborisations fill the entire striatum by P7. Similar temporal development is observed in cats, where retrogradely labeled cells are observed in cortical

layers III, V and some in VI at P7 (Fisher et al., 1983); and rats (Iñiguez et al., 1990). In mice, the number and spatial distribution of corticostriatal projections increases until at least the end of the second postnatal week. In particular, axon terminals are patterned into clusters and rows from birth, for prelimbic cortical projections (Nisenbaum *et al.*, 1998), to P14, for motor cortical afferents (Christensen *et al.*, 1999). Development of corticostriatal innervation of the striatal matrix has been shown to peak in the second postnatal week, and development continues into the third postnatal week, at which time corticostriatal projections are adult-like (Christensen et al., 1999; Iñiguez et al., 1990).

Studies on the molecular mechanisms associated with the formation of corticostriatal projections are currently based on those shown for other cortical projections. Corticostriatal projections are believed to be an anatomical 'hybrid' of callosal and corticofugal projection neurons, due to their dual projections outside the cortex (to the striatum) and the contralateral hemisphere (Sohur et al., 2012). This is somewhat reflected in their molecular character, with their expression of Satb2, a chromatin binding protein required for the differentiation of callosal projection neurons, and Lmo4, a LIM domain-containing protein expressed by both callosal and corticofugal neurons (Sohur et al., 2012). Additionally, corticostriatal and corticofugal projections traverse the internal capsule to their final destinations (O'Leary and Koester, 1993), and hence, may share similar guidance mechanisms associated with the initial stages of their trajectory. Pioneer neurons and fibers are proposed to serve as a scaffold to guide corticofugal axons by connecting three intermediate developmental targets (or decision regions), the ganglionic eminence, subplate and thalamic reticular nucleus, to form a guidance axis

(Deng and Elberger, 2003). Corticofugal axons are presumably guided by chemoattractants, such as Netrin-1, which is released as a diffusible molecule from the internal capsule and/or ganglionic eminence (Richards et al., 1997) along this axis. It is possible that corticostriatal and corticofugal axons are initially one and the same, and are guided to the internal capsule by molecular cues such as Netrin-1, before corticostriatal collateral branches form and are guided into the striatum, while corticofugal axons continue onto their other targets. The molecular cues responsible for this, however, have yet to be established.

Development of nigrostriatal projections

The developmental events of the nigrostriatal pathway are the best established out of the three major striatal afferent pathways. It is the earliest source of dopamine to the striatum and, hence, is studied using TH localisation. In prenatal rodents, mesencephalic cells extend fibers after E12.5, at the same time as some of the first striatal neurons are migrating into the striatal primordium, to reach the developing striatum by E13.5-14. (Specht et al., 1981). Prenatal formation of nigrostriatal connections is also observed in cats (Fisher et al., 1983). These fibres traverse the internal capsule to initially terminate in a uniform manner in the striatum, gradually filling up VL to DL and finally medial regions, between E18-21 (Specht *et al.*, 1981; Voorn *et al.*, 1988). Clustering of nigrostriatal terminals is first observed along the lateral border of the striataum at E20, and then along the RC extent, and into medial striatum by E21, being complete by P7 (Voorn et al., 1988). After P7, dopaminergic terminals become diffuse, with patches

disappearing first medially until only those along the lateral border are detected in adults (Voorn et al., 1988).

Evidence suggests that striatal cells that receive nigrostriatal axons correspond to the same population of cells which project to the SN. These also appear to develop along similar timelines. The first striatonigral cells are observed in VL striatum at E17 in rats. These cells are initially homogeneously distributed between E18-19, with many already showing striatonigral projections, before clustering into patches between E20-P4. At E20, most striatal cells have become postmitotic, migrating to the striatum where they form separate striosome patches, with striatonigral connections, and matrix cells, which project to the SN postnatally (Fishell and van der Kooy, 1987). This overlap of striatonigral and nigral dopaminergic fibers occurs between E20-P5 in rats (Fishell and van der Kooy, 1987).

It appears that dopamine in the striatum undergoes two separate patterns of homogeneity during development, moving from homogeneous to patchy between E19-20, and then patchy to homogeneous between P2-6 in rats (Fishell and van der Kooy, 1987). This is believed to result from two distinct waves of striatonigral projections and the corresponding change in distribution of dopaminergic fibers contacting these cells. The first transition occurs from homogeneously distributed striosome cells innervating the SN between E17-19, and the second occurring when newly migrated matrix cells send axons to the SN in early postnatal ages. This theory is supported by the increase in retrogradely-labeled matrix cells observed from the SN at P3 (Fishell and van der Kooy,

1987). Further, this is presumably accompanied by a similarly timed nigrostriatal projection to these matrix neurons, as peak nigrostriatal innervation of the striatal matrix has been shown to occur in the 2nd postnatal week (Christensen et al., 1999).

The molecular mechanisms governing the development of nigrostriatal/striatonigral pathways is, likewise, the best described of the three systems. In particular, a number of Eph/ephrin molecules have been shown to be responsible for their formation. For instance, blocking EphA/ephrinA signaling *in vivo* leads to a 30-40% reduction in SN volume and 40-50% reduction of nigrostriatal dopaminergic neurons (Sieber et al., 2004). More specifically, EphA5 is expressed by a proportion of mesencephalic dopaminergic cells, and its ligand, ephrinA5, has a graded expression in the ventral telecephalon and striosome patches during development (Deschamps et al., 2010; Janis et al., 1999; Passante et al., 2008). EphA5 repels ephrinA5-positive projections *in vitro* and is believed to control the guidance of nigrostriatal projections using these mechanisms (Deschamps et al., 2009, 2010). Recently, interactions between ephrinA5 in the SN and GP and EphA7 in patches in the striatal matrix have also been described (Tai et al., 2013). EphA7-positive axons project to a confined region in VM GP, and innervate rostral and caudal margins of SN, avoiding dopaminergic neurons.

Expression studies strongly implicate Eph/ephrin molecules in the development of the nigrostriatal projection. For instance, dopamine levels have been shown to regulate EphB1 expression in the cortex and striatum, with declining EphB1 levels mirroring dopamine levels after SN lesions, and dramatic increases from cocaine treatment leading

to increased dopamine levels (Halladay et al., 2000). EphB1 and ephrinB2 are expressed in a complementary pattern in midbrain dopamine neurons and the striatum (Passante et al., 2008; Yue et al., 1999). In addition, ephrinB2 inhibits neurite growth, suggesting that it may act in concert with its receptor EphB1, to guide nigrostriatal axons via these mechanisms. Further, ephrinB2 induces cell death in the SN, and, hence, may be involved in cell survival of mistargeted connections (Yue et al., 1999).

Development of thalamostriatal projections

The development of thalamostriatal projections is currently not well characterised. It has only been investigated in rats (Srivastava, 1999; Vercelli et al., 2003), and briefly described in opposums (Martin et al., 1989) and cats, where the pathway is observed by birth and proposed to form prenatally, some time between the formation of the nigrostriatal and corticostriatal projections (Fisher et al., 1983). Indeed, in rats, tracer injections performed predominantly postnatally, show a small number of thalamostriatal somata in the PF at E19/20 (Vercelli et al., 2003). A more comprehensive study described in a PhD thesis by Srivastava (1999) in pre- and postnatal rats, indicates that fibres from the PF are first observed to terminate in rostral striatum at E19. By E20, arborisation of axon collaterals is evident and thalamostriatal fibers continue to fill up the striatum. Patterning of these terminals is evident as early as E19.5, with short varicose fibres described to terminate in a 'patchy' fashion within the striatum, which develops into postnatal ages.

At birth, anterograde fibers are observed running rostrally and radiating into the entire striatum. At this stage, thalamostriatal axons are thin with frequent varicosities and growth cones, which decrease with age (Srivastava, 1999; Vercelli et al., 2003). Furthermore, a lighter covering of fine varicose fibers is often interrupted by regions of scant labeling from long, non-arborising fibres, which correspond to striosomes (Srivastava, 1999). Hence, the characteristic heterogeneous patterning of thalamostriatal terminals and their compartmentalisation occurs early in development in rats. At this age, thalamostriatal fibers are densest laterally, with some also projecting dorsal, lateral and medially, to enter the corpus callosum and the cingulate cortex (Vercelli et al., 2003).

Only a small number of molecular candidates have been implicated in the development of thalamostriatal projections. The first, semaphorin3E, a traditional axon repulsive cue, is highly expressed in thalamostriatal projection neurons, and its receptor plexinD1 is selectively expressed in direct pathway MSNs in the striatum. Deletion of plexinD1 or semaphorin3E leads to changes in glutamatergic synapses in the direct but not indirect pathway MSNs, including increased dendritic complexity, synapse number and strengthened thalamostriatal innervations (Ding et al., 2011). This suggests that semphorin3E/plexinD1 may be working in addition to other guidance cues to regulate thalamostriatal connections to direct pathway MSNs. Along similar lines, Cerebellin1, a secreted glycoprotein, is highly expressed in the PF. Cerebellin1-positive processes form axodendritic synapes with MSNs and the deletion of this gene leads to increased spine

density and increased axospinous MSN synapses (Kusnoor et al., 2010), suggesting that it may be involved in the regulation of thalamostriatal synapses onto MSNs.

Some thalamostriatal axons show dual innervation of the striatum and cortex (Deschênes et al., 1996a; Parent and Parent, 2005a), suggesting they may share guidance cues with thalamocortical axons. Thalamostriatal axons pass through and send collaterals into the reticular thalamic nucleus, one of the three decision points along which pioneer neurons are proposed to form a guidance axis for developing corticothalamic and thalamocortical axons (Deng and Elberger, 2003; Deschênes et al., 1996a). This 'corridor', extending through the internal capsule, which has been shown to secrete Netrin-1 (Richards et al., 1997), expresses Islet-1 and requires Pax6 for the normal routing of corticothalamic axons (Simpson et al., 2009). Further, there is evidence of a transient striatothalamic projection in early postnatal rats (Hattori et al., 1990), which may also function to guide thalamostriatal axons during development.

Another family of molecules that are potential candidates for a role in the targeting and patterning of the thalamostriatal projection is the teneurins. These molecules display functional roles in cell-cell contact and axon guidance in a number of neural pathways (see Young and Leamey, 2009 for a review). Interestingly, one of the family members, Ten-m3, is expressed in a patchy pattern in the developing striatum and is also present in the PF (Leamey et al., 2007a, current data), providing strong evidence for a potential role in the development of this pathway. Since Ten-m3 is the focus of this thesis, the following section will provide a detailed review of the teneurin family of molecules.

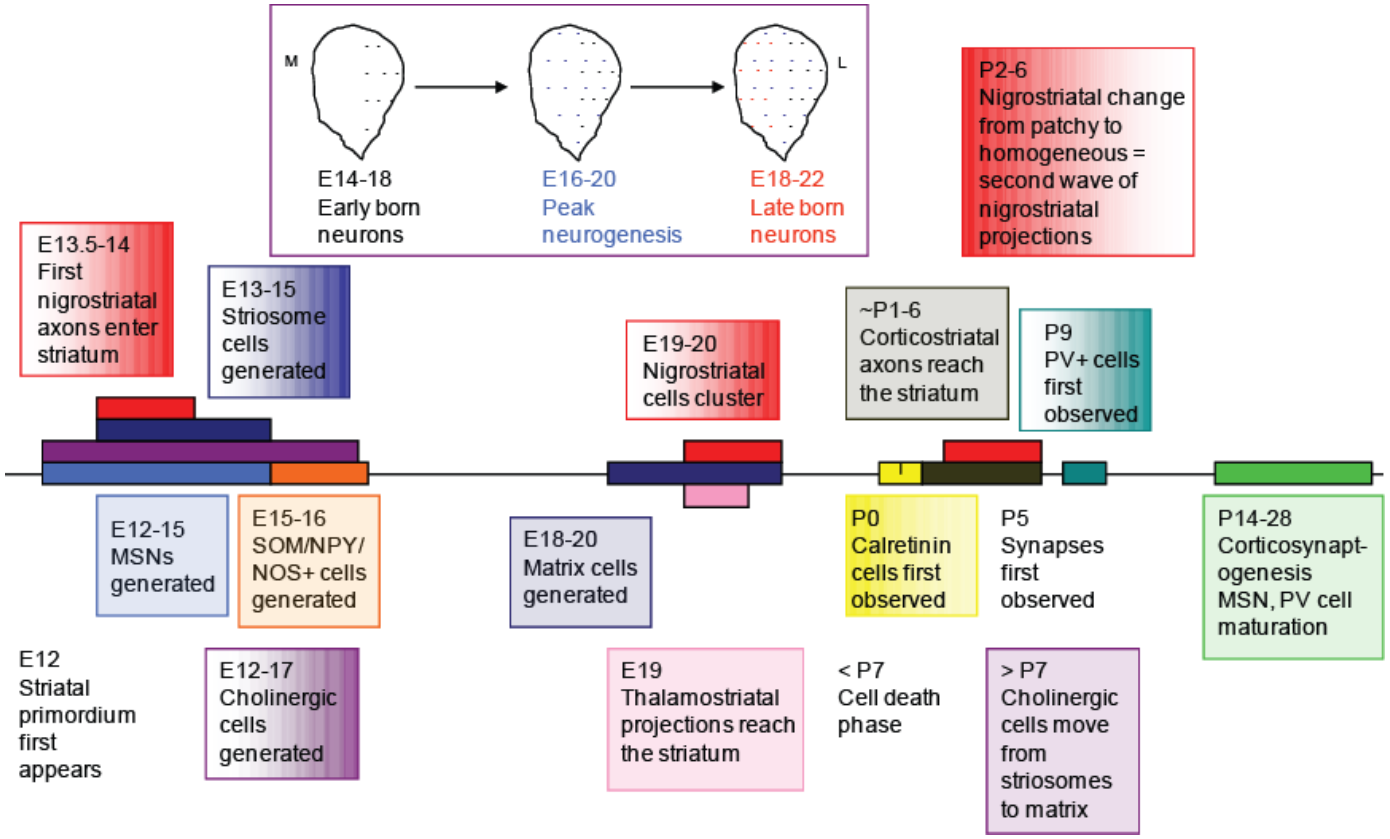

Figure 1.4. Timeline of the major developmental events in the striatum

The ages provided are based on the data from rats. A number of these develop along a lateral-medial gradient, as indicated by the graded colour of the enclosed box. Some also develop along a caudal-rostral gradient, such as cholinergic neuron development, which are not indicated.
M is medial, L is lateral. For gradients, lateral is to the right.

Teneurins

Teneurins, also known as Ten-m/*Odz*, are a family of highly conserved transmembrane proteins. Ten-m was initially discovered, along with a second member, Ten-a, in a search for homologues of the extracellular matrix molecule tenascin in *Drosophila* (Baumgartner et al., 1994; Levine et al., 1994). Teneurin homologues have since been identified and studied in other invertebrates, such as *C.elegans* (Drabikowski et al., 2005; Trzebiatowska et al., 2008), and developing vertebrates, particularly zebrafish (Mieda et al., 1999), chicken (Li et al., 2006; Rubin et al., 1999, 2002) and mice (Oohashi et al., 1999; Zhou et al., 2003; Ben-Zur et al., 2000). Four orthologues of the *Drosophila* Ten-m/*Odz*, known as teneurin-1-4 or Ten-m1-4, are found in mice, with 56-70% overall similarity observed between paralogues (Oohashi et al., 1999). They are all highly expressed in the central nervous system (CNS) where they have been shown to have important roles in cell adhesion, fasciculation and axon guidance. For relevance to the current project, the history and phylogeny of teneurins will not be detailed, but are described elsewhere (see Tucker and Chiquet-Ehrismann, 2006 for a review). Instead, the following sections will outline the structure, expression and functions of the mouse teneurins.

Structure

Teneurins are large, type II transmembrane proteins of approximately 300 kDa (Rubin et al., 1999). The basic organisation of the teneurin structure is highly conserved in bilateria (Tucker et al., 2012). The protein structure of teneurins is approximately 2800

amino acids in length and comprises an intracellular domain (ICD), a short hydrophobic transmembrane domain (TMD) and a large C-terminal extracellular domain (ECD). The ICD is located at the N-terminal and comprises conserved putative tyrosine phosphorylation sites, two EF-hand-like calcium binding motifs and two polyproline domains, the latter reflecting potential SRC homology (SH)-3 binding sites, which in Ten-m1 has been shown to be required for specific protein interactions (Nunes et al., 2005). Interestingly, many studies have reported the cleavage and subsequent translocation of this intracellular domain (Bagutti, 2003; Kenzelmann et al., 2008; Nunes et al., 2005). This may be instructed by the proposed presence of an amino acid sequence containing arginin-lysine-arginine-lysine at position 62-65 from the N-terminal, which has been shown to act as a nuclear localisation signal to direct proteins to the nucleus (Kenzelmann et al., 2008).

Distal to the ICD is the TMD, which comprises approximately 30 hydrophobic residues. The following ECD contains a linker domain immediately adjacent to the TMD, a highly conserved epidermal growth factor (EGF) domain, and a more distal globular domain (Feng et al., 2002; Oohashi et al., 1999). The EGF domain is the most highly conserved sequence between paralogues, showing 70% similarity in amino acid sequence within EGF repeats (Ben-Zur et al., 2000) and is also similar to that of transmembrane protein families like notch and the extracellular-matrix molecule tenascin (Baumgartner et al., 1994). It comprises eight consecutive repeats, with the second and fifth repeats containing conserved free cysteine residues which are believed to facilitate dimer formation through disulphide bonds (Oohashi et al., 1999). Evidence suggests that

teneurins often exist as homo- or heterodimers formed by these disulphide bonds (Feng et al., 2002). The large globular domain contains 17 conserved cysteine residues believed to facilitate protein folding. This is followed by a number of NHL (NCL-1, HT2A and Lin-41) repeats, which show high levels of N-linked glycosylation and have recently been shown to facilitate homophilic interactions (Beckmann et al., 2013; Feng et al., 2002; Oohashi et al., 1999; Rubin et al., 2002). Further distal are a series of 26 tyrosine-rich tyrosine-aspartate (YD)-repeats similar to those encoded by the rearrangement hot spot (rhs) core of *E.coli* (Minet and Chiquet-Ehrismann, 2000) and have been shown to bind heparin (Minet et al., 1999). Additionally, the far end of the C-terminal contains a sequence of approximately 40-50 amino acids distal to a conserved putative furin cleavage site, with structural homology and bioactive properties similar to corticotrophin releasing factor. This region, known as the teneurin C-terminal associated peptide (TCAP) (Qian et al., 2004) is highly conserved (Wang et al., 2005) and synthetic peptides cloned from this sequence have been shown to have bioactive actions *in vitro* and *in vivo*. These will be described later. In general, however, no other gene families show structural similarity to the ECD of teneurins, which has made predictions of their functions difficult.

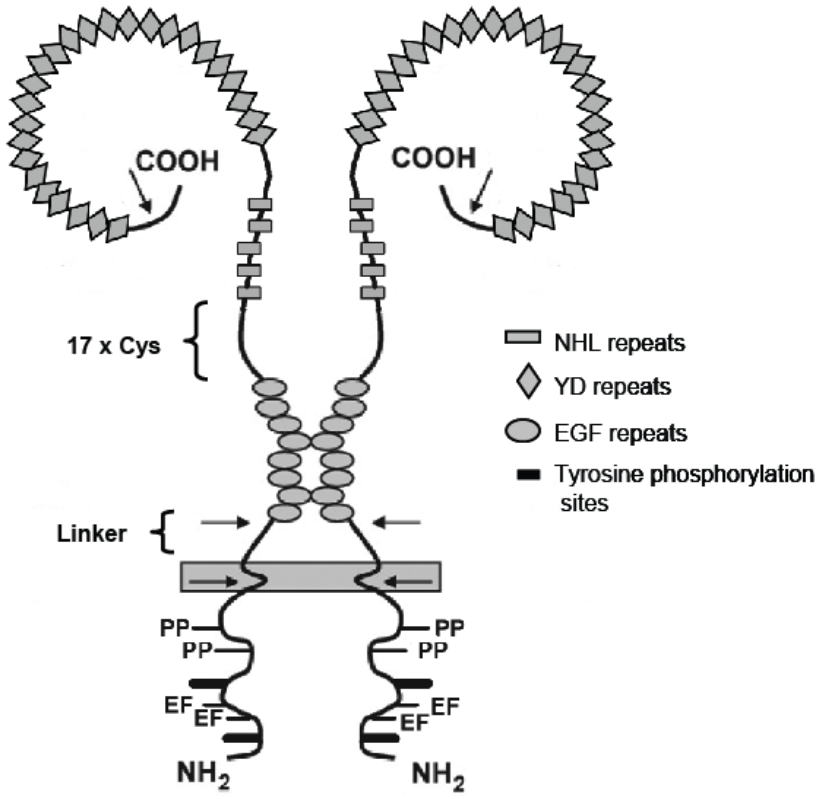

Figure 1.5. Hypothesised structure of a teneurin dimer.

A type II transmembrane protein, the teneurin molecule consists of an intracellular domain at the N-terminal, a short hydrophobic transmembrane domain and a large globular extracellular domain at the C-terminal. The intracellular domain comprises conserved putative tyrosine phosphorylation sites (black bars), two EF-hand-like calcium binding motifs (EF) and polyproline domains (PP). The extracellular domain contains a linker domain, 8 highly conserved epidermal growth factor (EGF) repeats, the 2nd and 5th of which facilitate dimer formation through disulphide bonds. The large globular domain contains 17 conserved cysteines (Cys), followed by a number of NHL repeats recently shown to facilitate homophilic interactions. Further distal are a series of 26 tyrosine-rich YD repeats, followed by a sequence of approximately 40-50 amino acids known as the teneurin C-terminal associated peptide (TCAP), which has bioactive properties. There are three major proposed cleavage sites (arrows), suggesting distinct functions for cleaved intracellular, extracellular and TCAP segments.
Figure adapted from Young and Leamey (2009).

Teneurin expression during development

Teneurins have been shown to be expressed in a number of neural and non-neural structures throughout development. Interestingly, these molecules are expressed in interconnected structures and functionally relevant gradients (Tucker et al., 2007; Young and Leamey, 2009) to suggest important roles in neural connectivity, which will be detailed in the next section.

Teneurins are expressed from early development. Both Ten-m3 and Ten-m4 are expressed in the neural plate at E7.5 in mice, the earliest stage of nervous system development, with Ten-m3 also strongly expressed in the notochord (Zhou et al., 2003). Interestingly, Minet et al. (1999) found no evidence of Ten-m1 or Ten-m2 in the ventricular zone, suggesting they are expressed by postmitotic neurons that are about to form new connections. Subsequently, these paralogues are increasingly expressed in the developing telencephalon, diencephalon and midbrain, throughout prenatal development. Expression levels are generally highest during early postnatal periods, and while expression levels can drop considerably, remain evident into adulthood, where all four paralogues are still expressed in the cortex, thalamus, hippocampus and cerebellum (Zhou et al., 2003).

Interestingly, teneurins are often expressed in complementary patterns within neural structures and in interconnected structures of neural pathways. The majority of studies to date have focused on the expression of teneurins within interconnected structures of the developing visual system. In chicken, Ten-m1 and Ten-m2 are expressed at all levels of

the visual pathway: in retina, telecephalon, optic tectum and diencephalon; in a complementary fashion evident from early development (Kenzelmann et al., 2008; Rubin et al., 1999, 2002). In particular, they exhibit complementary expression patterns, with Ten-m1 predominantly expressed throughout the developing tectofugal system, while Ten-m2 expression is observed throughout the thalamofugal pathway (Kenzelmann et al., 2008; Rubin et al., 2002). Further complementary patterns between Ten-m1 and Ten-m2 are observed in the olfactory bulb, auditory nuclei and cerebellum (Kenzelmann et al., 2008). The temporal expression of these genes correlates with periods of target recognition and synaptogenesis, from E9 in chick, suggesting a role for these molecules in axonal guidance (Rubin et al., 2002).

Similarly, in mice, Ten-m2-4 are also expressed in all visual structures (see Young and Leamey, 2009 for a review). Ten-m2 and Ten-m4 are expressed uniformly (Young, 2011; Young et al., 2013), while Ten-m3 is expressed in gradients in the retina, dorsal lateral geniculate nucleus (dLGN), superior colliculus (SC) and visual cortex, such that expression is highest in topographically connected regions (Dharmaratne et al., 2012; Leamey et al., 2007a, 2007b). A similar pattern of expression is observed in wallaby (Carr et al., 2013). These expression patterns suggest potentially complementary roles for Ten-m2-4 in neural connectivity in mammals.

Teneurin expression is also found in interconnected structures of a number of other pathways. For instance, Ten-m1 expression is found within the olfactory pathways, hippocampal and piriform projections, as well as auditory and cerebellar pathways

(Kenzelmann et al., 2008). Further, Ten-m3 and Ten-m4 are expressed in complementary patterns in the developing forebrain and midbrain of zebrafish, as well as along the RC and DV axis of the spinal cord (Mieda et al., 1999). Moreover, all four paralogues are observed in interconnected thalamocortical/ corticothalamic pathways (Li et al., 2006). Interestingly, Ten-m3 may be expressed within the rodent striatum (Leamey et al., 2007a), as well as corresponding afferent regions of the cortex and thalamus (Allen Brain Atlas). Intriguingly, Ten-m3 expression within the striatum is patchy, reminiscent of the patchy nature of the intrinsic organisation of the nucleus. The correlation between Ten-m3 expression pattern and the striosome/ matrix compartments, as well as matrisome subregions within the striatum is currently unclear. This correlation may provide important insights to the potential roles for Ten-m3 within the striatum and will be a primary focus of the current study.

As mentioned above, teneurins are also expressed in a number of non-neural tissues. Ten-m is expressed in alternating segments of the fly embryo (Baumgartner et al., 1994). Ten-m1 of *C.elegans* is expressed in gonadal somatic cells and muscles (Drabikowski et al., 2005). Ten-m3 and Ten-m4 are expressed in rhombomeres in zebrafish (Mieda et al., 1999), and in chicken, Ten-m2 and Ten-m4 are expressed in the important organising centres of limb development (Kenzelmann-Broz et al., 2010; Tucker et al., 2001), suggesting roles in the development of a number of tissue types.

Teneurin function

In vitro and *in vivo* studies have provided insight into roles inferred by expression patterns for teneurins. Ten-m2 and Ten-m3 have been shown to promote homophilic cell adhesion, with transfection studies revealing significant cell aggregation at the location of the protein on the cell's surface (Leamey et al., 2007a; Rubin et al., 2002). Further, antibodies against the ECD of Ten-m1 in *C.elegans* is localised to cell-cell contact sites (Drabikowski et al., 2005). Ten-m1 and Ten-m2 promote neurite outgrowth *in vitro*, with Ten-m2 overexpression yielding a specific increase in filopodia number and enlarged growth cones. These changes are believed to result from accumulation of actin as a direct result of Ten-m2 overexpression, suggesting it may interact with the actin cytoskeleon (Minet et al., 1999; Rubin et al., 1999, 2002). Further, prolonged overexpression of Ten-m3 *in vivo* leads to an almost three-fold increase in neurite number and their fasciculation (Leamey et al., 2007a). Similarly, Ten-m1 has roles in fasciculation, with knock-down of Ten-m1 expression leading to defasciculation of neurons (Drabikowski et al., 2005; Trzebiatowska et al., 2008). Moreover, Ten-m4 expression in the early chick embryo is limited to bundles of axons in the optic fiber layer of the nasal retina, suggesting that it may, likewise, be necessary for their fasciculation (Kenzelmann-Broz et al., 2010). All of these processes are essential for appropriate formation of neuronal projections during development (Rubin *et al.*, 1999).

There is strong evidence implicating teneurins in regulating the connectivity of various neural pathways. The visual pathway is the best established locus for these roles. For instance, the expression patterns, as well as their *in vitro* functions suggest that Ten-m1

and Ten-m2 are involved in establishing the tectofugal and thalamofugal projections, respectively (Rubin et al., 2002). Further, immunostaining in chick retina suggests that Ten-m4 may be involved in establishing connections for mapping the visual field (Kenzelmann-Broz et al., 2010). Further, in the first *in vivo* investigation of teneurin function, Leamey et al. (2007b) showed that the corresponding graded expression of Ten-m3 in all interconnected structures of the visual pathway is important for the normal development of these connections. Ten-m3 knock-out (KO) mice exhibit altered topography of ipsilateral projections within the retinogeniculate pathway (Leamey et al., 2007b). These aberrant connections are carried through into primary visual cortex, where an expanded ipsilateral projection is interdigitated with contralateral inputs to form apparent eye dominance columns, which are not normally present in rodents (Merlin et al., 2012). These mice exhibit deficits in normal binocular vision, which is reflected by a functional suppression of activity in primary visual cortex after binocular stimulation (Leamey et al., 2007b; Merlin et al., 2012). Further, investigations into the development of the retinocollicular pathway showed that ipsilateral axons exhibit targeting errors along two-dimensions and form additional ectopically located terminals zones within the SC (Dharmaratne et al., 2012). These changes are summarised in Fig. 1.6. Hence, Ten-m3 has important roles in the guidance of the ipsilateral visual pathway of mice.

Moreover, Ten-m2 and Ten-m4 have recently been shown to have complementary roles within the visual system (Young, 2011; Young et al., 2013). Ten-m2 KO mice show deficits in regions of the ipsilateral pathway associated with ventral retina, with consequent deficits in visual discrimination tasks associated with the dorsal visual field.

These changes are believed to be linked to a physiologically reduced binocular zone in primary visual cortex resulting from diminished ipsilateral drive (Young et al., 2013). In contrast, Ten-m4 KOs exhibit an expansion of the ipsilateral projection to dorsotemporal retina (Young, 2011). Hence, teneurins appear to have distinct but overlapping, and potentially complementary roles in the visual system of mice.

Recently, the role for teneurins in axonal path finding has been extended to the development of other neural systems. For instance, in the olfactory system of *Drosophila*, Ten-m and Ten-a are expressed in distinct but overlapping subsets of projection neurons and olfactory receptor neuron pairs, where homophilic interactions are responsible for the specific one-to-one connection with olfactory glomeruli (Hong et al., 2012). Ten-a and Ten-m are also expressed in pre- and postsynaptic regions of the *Drosophila* neuromuscular junction, respectively, where they are involved in the normal routing of motor neuron axons. Ten-m and Ten-a are believed to form a complex and organise various features of the cytoskeleton, potentially via indirect interactions with the actin cytoskeleton through Filamin (Zheng et al., 2011) to control normal synapse development (Mosca et al., 2012). Moreover, Ten-m2 has been shown to act as a ligand to latrophilin1, a G protein coupled receptor involved in the control of presynaptic calcium and neurotransmission. *In vitro*, presynaptic latrophilin1 and postsynaptic Ten-m2 interact via the extracellular domain, to induce calcium signals in presynaptic boutons (Silva et al., 2011). Hence, teneurins may have roles in the precise guidance and targeting of neural projections, as well as their final synaptic connections.

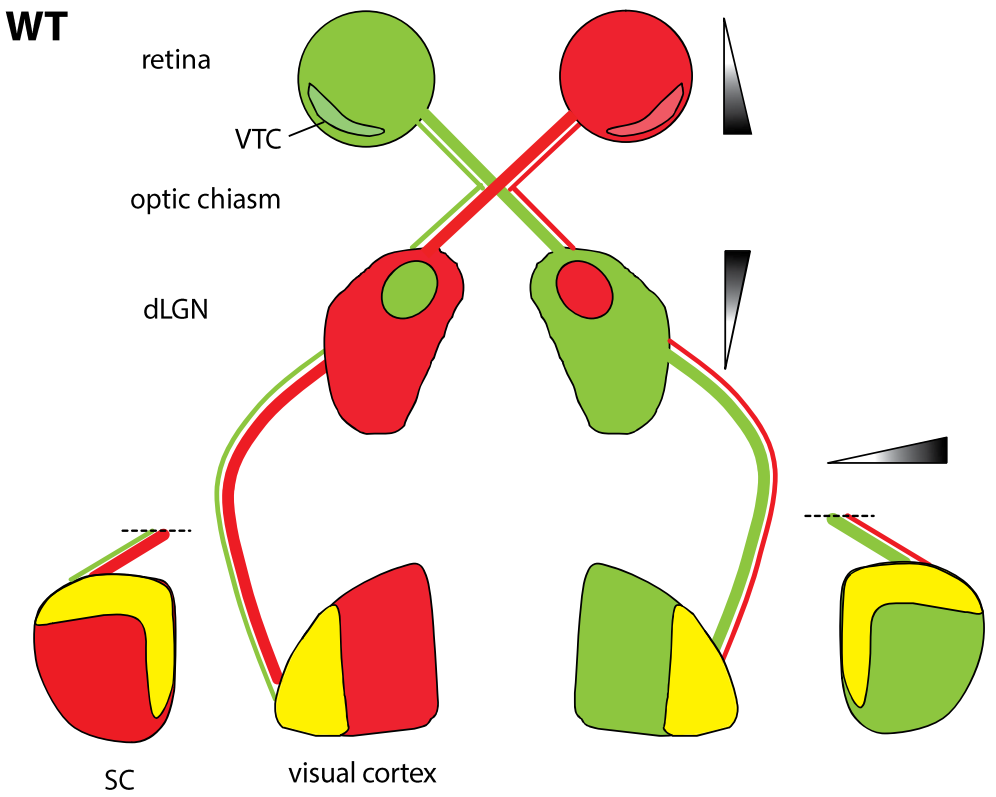
WT
retina
VTC
optic chiasm
dLGN
SC
visual cortex

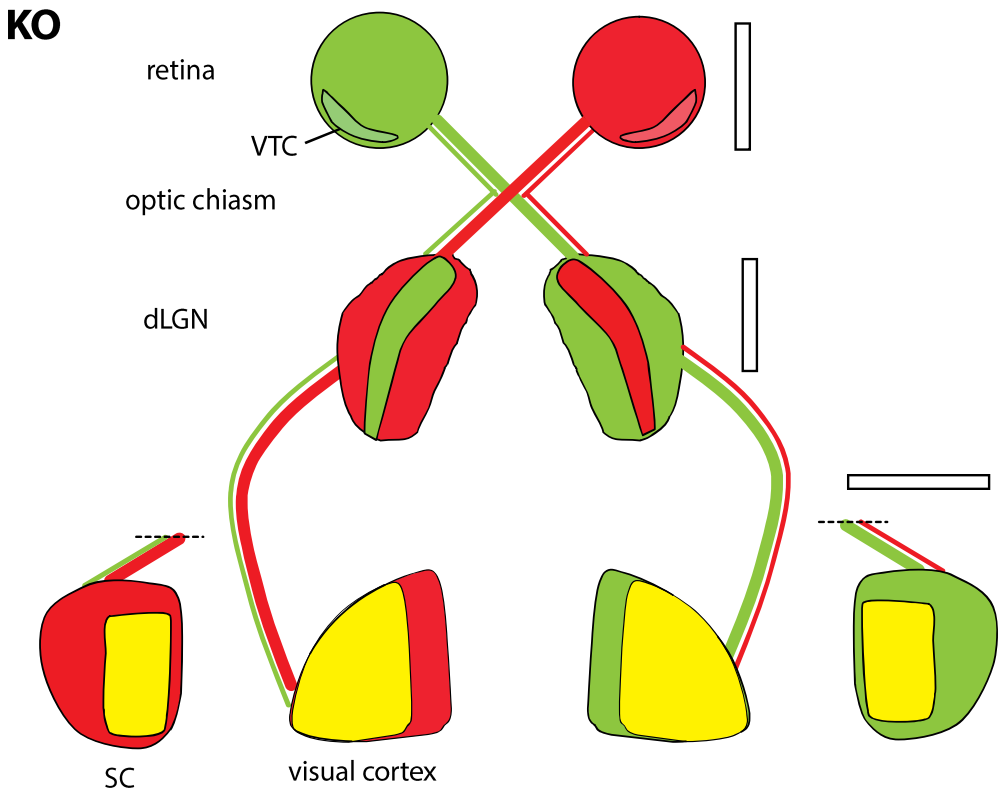
KO
retina
VTC
optic chiasm
dLGN
SC
visual cortex

Figure 1.6. A schematic of the normal visual pathway and the changes observed in Ten-m3 KO mice.

In WT mice, Ten-m3 is expressed in corresponding gradients in the retina, dLGN, visual cortex and SC. All retinal fibers traverse the optic tract to meet at the optic chiasm, where the majority of fibers cross to the contralateral side and a small proportion are repeled to target ipsilateral structures. Ipsilateral fibers primarily originate from the ventral temporal crescent (VTC) in the retina. Fibers within the optic nerve subsequently target the dLGN in the thalamus, where ipsilateral axons terminate in a distinct patch at the DM border, while contralateral fibers occupy the remainder of the nucleus. This organisation is transferred to the visual cortex, where ipsilateral projections occupy a small area in lateral regions, while contralateral fibers occupy all of the visual cortex. A separate retinal projection innervates the SC in the midbrain. Likewise, ipsilateral axons are segregated, predominantly occupying a medial and rostral strip of the SC, while contralateral fibers terminate across the entire nucleus. These specific projections occur in a topographically precise manner, along the gradients of Ten-m3 expression.

In KO mice, the absence of Ten-m3 from all visual structures leads to profound anatomical deficits at all levels of the visual pathway. These changes are observed only in the ipsilateral projections. In the dLGN, ipsilateral fibers are no longer confined to a DM patch, but rather, expand along the entire dorsomedial-ventrolateral axis of the nucleus. This mismapping is transferred to the visual cortex, where ipsilateral axons are expanded medially, and the SC, where they exhibit targeting errors along two-dimensions and form additional ectopically caudally-located terminals zones. Consequent deficits in normal binocular vision, reflected by a functional suppression of activity in primary visual cortex after binocular stimulation is observed in Ten-m3 KO mice.

Diagram based on work by Leamey *et al.*(2007b), Merlin *et al.* (2012) and Dharmaratne *et al.* (2012).

Mechanisms

It has long been proposed that teneurins undergo homophilic interactions to form the basis of a number of functions, including cell adhesion and fasciculation. A recent study showed that this occurs via the NHL domain within the ECD. This domain is selective for homophilic, but not heterophilic, NHL domains on adjacent cells for interaction (Beckmann et al., 2013), indicating that teneurins preferentially form homophilic interactions. These are believed to be strengthened by the presence of the ICD due to its anchorage to the actomyosin cytoskeleton and is sufficient to inhibit axon outgrowth (Beckmann et al., 2013).

Additionally, a number of studies have suggested that homophilic interactions between adjacent cells may lead to a number of downstream events. For instance, it is has been shown that homophilic interactions of the ECD lead to the cleavage of the ICD and its subsequent translocation to the nucleus (Bagutti, 2003). This theory is supported by *in vitro* and *in vivo* studies showing that antibodies against the ICD of Ten-m1 and Ten-m2 are localised to cell nuclei (Bagutti, 2003; Drabikowski et al., 2005; Kenzelmann et al., 2008; Nunes et al., 2005). It is proposed that this cleavage occurs within the TMD and may involve a second cleavage of the ICD in some cells as a result of a nuclear localisation signal amino acid sequence (Kenzelmann et al., 2008). This process is highly reminiscent of a process known as regulated intramembrane proteolysis (RIP) (Bagutti, 2003), which is proposed as the mechanism by which the ICD of teneurins may be cleaved (Brown et al., 2000).

Furthermore, the cleaved ICD has been shown to interact differentially with nuclear proteins to affect gene transcription. For instance, the cleaved ICD of Ten-m2 interacts with the zinc finger transcription factor (Zic1) (Bagutti, 2003) and that of Ten-m1 translocates to the cell membrane to interact with c-Cbl-associated protein (CAP)/ponsin complex, an adaptor protein containing SH3 domains. This results in its translocation into the nucleus to facilitate interactions with the transcriptional repressor methyl-CpG binding domain protein (MBD1) (Nunes et al., 2005). Interestingly, altered levels of a number of guidance genes, such as upregulation of EphB1 and Zic 4 and downregulation of EphA7 in visual structures of Ten-m3 KO mice suggest similar mechanisms for this paralogue (Glendining, 2011).

Further, teneurins have been proposed to be downstream targets of a number of genes. For instance, Ten-m2 expression in developing limbs in chicken is strikingly similar to that of fibroblast growth factor (FGF)-8 in chicken limb buds, the expression of which can induce Ten-m2 expression *in vitro* and *in situ*. Hence, Ten-m2 may be downstream of FGF8 (Tucker et al., 2001). In the cortex, Emx2 and Pax6 are expressed in complementary expression gradients along the RC axis and function to specify area patterning. Further, Emx2 KOs show a downregulation, flattening and caudal shifting of the expression patterns of all mouse teneurins (Li et al., 2006). Moreover, human TEN-M1 has been shown to be a direct target of EMX2 (Beckmann et al., 2011), suggesting that teneurins may also be downstream targets of EMX2.

In addition to the ICD, recent studies suggest that the TCAP sequence may also be cleaved to act as a bioactive peptide. TCAP sequences are possessed by all teneurins and, although their processing *in vivo* has not currently been shown, they are flanked by cleavage signals, suggesting a number of possibilities (Lovejoy et al., 2006). Like corticotrophin releasing factor, TCAP is involved in proliferation and neuronal morphology. Synthetic peptides of TCAP-1 and -3 can increase cyclic-adenosine monophosphate (cAMP) and proliferation of immortalised hypothalamic cells (Al Chawaf et al., 2007a; Qian et al., 2004; Wang et al., 2005). Moreover, TCAP-3 has been shown to alter Ten-m1 expression *in vitro*, with differing concentrations of TCAP-3 leading to a corresponding dramatic changes to Ten-m1 levels (Qian et al., 2004). Injections of synthetic TCAP-1 into the basolateral nucleus of the amygdala results in long term increases in the acoustic startle response test in low-anxiety rats and reduced responses in high anxiety rats (Wang et al., 2005). This has been proposed to result from changes in neurite outgrowth, as treatment of immortalised cells with TCAP-1 showed significant increases in α-actinin-4 and β-tubulin expression and dramatic increase in levels of β-actin. Analysis of primary hippocampal cells showed TCAP-1 treatment induces increases in the number of dendritic arborisations and large fasciculated β-tubulin+ axons (Al Chawaf et al., 2007a). The internalisation of synthetic TCAP has been shown to reduce brain-derived neurotrophic factor (BDNF) levels *in vitro* (Ng et al., 2012).

Human disorders

Teneurins have been implicated in a number of human disorders. The TEN-M1 gene is localized to the Xq25 chromosomal locus, a region mapping many X-linked mental retardation syndromes and non-specific mental retardation (Minet and Chiquet-Ehrismann, 2000). In addition, variants of TEN-M4 have been implicated in bipolar disorder (Craddock and Sklar, 2013). Moreover, a number of teneurins have been implicated in cancer. For instance, levels of a portion of the TEN-M 4 gene, known as miR-708, is reduced in renal carcinoma cells and has been shown to suppress tumor growth *in vitro* and tumor regression in mice (see Ziegler et al., 2012 for a review). Further, the TEN-M3 gene is mutated in chromothripsis, or the local shredding of chromosomes, often associated with some neuroblastomas - childhood tumours of the peripheral sympathetic nervous system (Molenaar et al., 2012). Additionally, reduced TEN-M2 levels are found in patients exhibiting various tumors and premalignant lesions, including the majority of malignant mesothelioma cell lines, breast hyperplastic enlarged lobular units, the earliest precursors to breast cancer, and hepatitis-B virus insertional mutagenesis in liver (see Ziegler et al., 2012 for a review). These findings are in agreement with those showing that Ten-m in *Drosophila* is required for normal proliferation and survival of multiple retinal cell types (Kinel-Tahan et al., 2007). Hence, altered expression or mutagenesis of these genes potentially leads to abnormal proliferation and survival of unwanted cell growth to result in malignant tumours.

Overview of thesis

Although Ten-m3 expression has been shown to be present in numerous brain regions of developing mice, its presence within the striatum has yet to be characterised. Notably, the spatial relationship between the apparently 'patchy' Ten-m3 expression and the striatal compartments is currently unknown. Moreover, it is possible that previous roles in cell adhesion and axon guidance described for Ten-m3, along with the mechanisms by which it acts, such as altering transcription of guidance genes, may also be applicable to the formation of striatal connections during development. Hence, the present study endeavours to investigate each of these in turn.

In Chapter 2, the expression patterns of Ten-m3 will be characterised. Ten-m3 expression within the striatum will be described across a number of embryonic and early postnatal age points, using *in situ* hybridisation. Furthermore, the spatial relationship between Ten-m3 expression and striatal compartments will be investigated in order to localise the 'patchy' Ten-m3 expression to the striosome, matrix or matrisome compartment. The important finding that Ten-m3 is localised to potentially novel matrisome patches motivated a survey of Ten-m3 expression within afferent and efferent structures of the striatal matrix. From this, the PF is identified as an important locus, and Ten-m3 expression described for this structure at the same neonatal age points as for the striatum. Very similar temporal and corresponding patterns of expression within the striatum and PF provide a strong foundation for a potential role for Ten-m3 in the guidance and targeting of thalamostriatal axons from the PF.

In Chapter 3, the potential for Ten-m3 in a role in the normal targeting of thalamostriatal axons from the PF will be investigated by comparing anterograde tracing patterns in adult WT and KO mice. Anterograde tracer injections made into the lateral portion of the PF of both genotypes show increased spread but mostly avoided the ventrolateral (VL) segment of mid-caudal striatum in the absence of Ten-m3. Most notably the normal patchy pattern of thalamstriatal terminals is lost in Ten-m3 KOs. Further, dual labeling of thalamostriatal terminals and striosomes show no changes to the compartmentalisation of these terminals. Dual focal retrograde tracing experiments using two different fluorescent tracers along the RC axis, show intriguing changes specifically to PF cells projecting to mid-caudal striatum, and suggest aberrant targeting of thalamostriatal axons in the absence of Ten-m3. Further, immunohistochemistry for ChAT to investigate cholinergic interneurons, one of the major postsynaptic targets of thalamostriatal axons, show a reduction in the VL quadrant of mid-caudal striatum in Ten-m3 KO mice. Likewise, analysis of striatal area and cell number are reduced at this striatal level, suggesting intriguing region-specific actions for Ten-m3. Finally, behavioural studies indicate slight changes in gait, using a footprint analysis, and delayed motor learning on accelerating rotorod tasks in Ten-m3 KO mice.

Chapter 4 will attempt to elucidate the mechanisms by which Ten-m3 is working to control the normal targeting and patterning of thalamostriatal projections. This projection will again be traced, however, this time at various embryonic and postnatal age points. Firstly, however, the normal development of this projection is determined in WT mice. Comparisons between genotypes indicate an initial delay in the formation of

thalamostriatal collaterals and interesting spatiotemporal changes in terminal distribution in KOs during development, including the loss of their patchy appearance. Overlaying adjacent sections for terminal label from the PF and those revealing Ten-m3 expression show a substantial, though partial overlap, suggesting that Ten-m3 may act as an attractive guidance cue for a subset of thalamostriatal axons. Moreoever, analysis of EphA7 as a potential downstream candidate using *in situ* hybridisation reveals a partially complementary relationship with Ten-m3, and reduced expression intensities of EphA7 in Ten-m3 KO striatum. Further, Western blot analysis for levels of EphA7 in the striatum suggest that, like in the visual system, Ten-m3 may be exerting some of its actions by altering expression of this guidance cue.

Together these experiments provide the first *in vivo* study investigating roles for Ten-m3 in the development of striatal circuits. The unique expression of Ten-m3 may mark a novel matrisome compartment that substantially overlaps with clustered thalamostriatal terminals originating from the PF. Further, this expression is responsible for the normal targeting and patterning of these projections. Hence, this study presents Ten-m3 as a novel candidate for the guidance of thalamostriatal axons from the PF.

Chapter 2

Ten-m3 expression in the striatum and PF

Introduction

The striatum, or caudate/putamen, is a major subcortical structure with complex intrinsic organisation and circuitry, implicated in a plethora of important roles including motor control, goal-directed learning and motivation (see Gerfen, 1992 for a review)). Despite a superficially homogeneous distribution of striatal neurons, these cells are organised into a heterogeneous pattern of striosome (patch) and matrix compartments, which show differential expression of neurochemical markers. For instance, TH and μ-OR are highly expressed in striosome patches, while calbindin and EphA4 are localised to matrix cells (Graybiel, 1990; Passante et al., 2008). Moreover, the matrix compartment displays further heterogeneities, with patches called matrisomes associated with the clustering of afferent and efferent projections (Giménez-Amaya and Graybiel, 1991; Herkenham and Pert, 1981). Potential molecular markers of matrisomes have only recently come to light (Tai et al., 2013). The significance of the striatal compartments, however, largely remains a mystery.

As the key input nucleus of the basal ganglia circuits, the striatum receives and processes a plethora of afferent information, particularly from the cortex, thalamus and SN. It, in turn, sends reciprocal efferents to the GP and SNr, and back to the cortex, via the thalamus (Gerfen and Wilson, 1996), forming the direct and indirect basal ganglia loops. These major striatal afferent and efferent connections are further compartmentalised according to striosome, matrix and matrisome compartments (Gerfen, 1992). In particular, prelimbic cortex and caudal SNr project to striosomes, while sensory and motor cortex, along with the PF thalamic nucleus project to distinct matrisomes (Donoghue and Herkenham, 1986; Herkenham and Pert, 1981). Although recent studies have begun to investigate the specific patterning of striatal connectivity (Richards et al., 2007; Tai et al., 2013), the molecular mechanisms underlying this intriguing organisation of projections are currently not well characterised.

A previous study noted the presence of Ten-m3, a member of the teneurin family of glycoproteins, in the striatum in a striking pattern of patches during development (Leamey et al., 2007a), but this was not characterised in detail. Other work has shown that Ten-m3 is expressed in topographically corresponding gradients throughout the visual pathway of mice (Leamey et al., 2007b). Ten-m3 KO mice show dramatic mapping deficits in the ipsilateral retinogeniculate, and developing retinocollicular projections, with concomitant disruptions to binocular vision (Dharmaratne et al., 2012; Leamey et al., 2007b). Hence, the intriguing patchy expression of Ten-m3 within the striatum suggests that it may play similarly important roles in striatal connectivity.

The aim of the current study is to investigate the expression patterns of Ten-m3 in the developing striatum, particularly with respect to the intrinsic organisation of this structure. This data, together with information regarding the connectivity patterns of the striatal compartments (reviewed in Chapter 1), will be used to provide important clues as to the potential afferent and efferent striatal pathway(s) in which Ten-m3 may play important roles. It was discovered that Ten-m3-positive patches are localised to a subregion of the striatal matrix. This led to a survey for Ten-m3 expression in afferents and targets of the matrix and the subsequent identification of the PF and its projection to the striatum as a possible locus of action. In support of this, characterisation of Ten-m3 expression showed corresponding temporal and spatial expression patterns of Ten-m3 in the striatum and PF. These findings support the hypothesis that Ten-m3 may play a role in the guidance of axons from the PF to the striatum.

Methods

The expression of Ten-m3 within the striatum was visualised using *in situ* hybridisation at number developmental time-points, namely E15, E17, P3 and P10. The unique expression pattern of Ten-m3 in the striatum was most striking at P3. Hence, further analysis was performed at this time-point to determine the existence of an expression gradient for Ten-m3 and the spatial relationship between Ten-m3 and striosomes in the striatum. This was accomplished by comparing Ten-m3 *in situ* hybridisation expression with immunohistochemistry for TH to mark striosomes. Further, since previous studies in the visual pathway showed that correlated Ten-m3 expression patterns may characterise afferent and efferent structures, a survey was carried out across the brain to identify Ten-m3 expression in structures that provide/receive projections to/from the striatum. The PF was identified as a potentially important candidate locus, and hence, Ten-m3 expression was further characterised in this structure.

Animals and tissue collection

In situ hybridisation experiments were performed on C57/Bl6, and expression patterns confirmed in Ten-m3 WT mice, maintained on a C57/Bl6xSv129 background. For details of the generation of the Ten-m3 mouse strain, refer to Chapter 3. All data presented in this chapter are obtained from C57/Bl6. Littermates were used where possible. All protocols were approved by the Animal Ethics Committee of the University of Sydney and conformed to NHMRC guidelines.

In situ hybridisation and immunohistochemical procedures were performed on fresh frozen tissue. Mice were euthanised with an overdose (<100mg/kg) of sodium pentobarbitone (Lethabarb), injected intraperitoneal. Brains were quickly removed and instantly frozen in 2-methylbutane (Sigma-Aldrich) on dry ice, and stored at -80°C until required. Tissue to be sectioned was embedded in Tissue-Tek (OCT compound; ProSci Tech) and sectioned at 15 µm, coronally or sagittally, using a cryostat. Sections spanning the striatum and PF were collected onto Superfrost Plus slides in 6 contiguous sets per animal, and stored at -80°C until required.

In situ hybridisation

Riboprobe synthesis

The initial stages of the probe synthesis protocol were described and performed previously (Leamey et al., 2007b). Briefly, one set of primers for both sense and antisense probes (Table 2.1) were designed against a 200 base pair region of the Ten-m3 gene and the target sequence amplified using polymerase chain reaction (PCR). This sequence was ligated into a pGEM-T Easy vector (Promega), transformed into DH-5α competent cells (Invitrogen), and cultured on LB agar plates containing 20 mg/mL ampicillin (Gibco) overnight at 37ºC. Colonies were screened for the inserted plasmid using PCR, and positive clones extracted using a Miniprep kit (Qiagen), and the resulting DNA was sequenced (Australian genomics research facility, University of Queensland, Australia). Once insert orientation was confirmed, DNA was extracted for sense and

antisense sequences using a Maxiprep kit (Qiagen) and aliquots stored at -20ºC until required for probe synthesis.

Extracted DNA was subsequently linearised using restriction enzymes Not1 (Promega), for the sense sequence, and EcoR1 (Promega), for antisense DNA, for 2 hours at 37ºC. Linearised DNA was then purified by phenol:chloroform extraction and ethanol precipitation, before resuspending in 10 mM Tris-HCl and quantifying on a Nanodrop spectrophotometer. Sense and antisense probes were subsequently synthesised using an *in vitro* transcription reaction, where 1 µg of linearised DNA was incubated with 40 units of T7 (Promega), for sense probes, or T3 RNA polymerase (Promega), for antisense probes, for 1 hr at 37ºC. The DNA template was removed by reacting with 1 unit of RQ1 DNase (Promega) for 30 min at 37ºC and the enzyme subsequently deactivated by heating with RQ1 DNase Stop solution (Promega) at 65ºC for 15 min. Riboprobes were purified using Micro BioSpin columns (Biorad), eluted in 10 mM Tris HCl and quantified by gel electrophoresis by comparison of band intensities with a low molecular mass ladder (Invitrogen). Probes were stored at -80ºC until required.

Table 2.1. Primer sequences for generation of Ten-m3 *in situ* hybridisation probes.

Gene	**Accession number**	**Primer sequence (5'-3')**
Odz3 (Drosophila)	NM_023456	Forward: TGACATCTCTGGCAAAGTCG Reverse: TTACCCGGCCCATATTATCA

Pretreatment and hybridisation washes

Pretreatment and hybridisation reactions were performed using RNase-free conditions. All glassware was baked at 180ºC overnight prior to use, and all solutions made using autoclaved MilliQ-filtered water. Filter paper, magnetic stir bars and parafilm were sterilised under ultraviolet light for approximately 20 min prior to use. Pretreatment and hybridisation washes were performed in glass coplin jars. All reactions were performed at room temperature (RT) and all washes in 0.1 M phosphate buffer (PB) for 2 min unless otherwise stated.

Fresh frozen sections were thawed for 30 min and then fixed in 4% (w/v) paraformaldehyde in 0.1 M PB for 15 min. Cells were permeabilised by incubation in 0.08 µg/mL proteinase K (Sigma-Aldrich; in 10 mM Tris-HCl, pH 8.0, and 1 mM EDTA), at 37ºC for 30 min. Sections were post-fixed in 4% paraformaldehyde for 15 min and washed before being treated with 0.2 M HCl (Sigma) for 10 min. Following a wash, sections were pre-incubated in 0.1 M triethanolamine (TEA) for 2 min, before treating with 0.25% (v/v) acetic anhydride in TEA for 10 min. Sections were washed and then dehydrated in 70%, 80%, 90% and 2 x 100% ethanol solutions for 2 min each, followed by a final dehydration in 100% chloroform for 10 min.

Digoxigenin-labeled antisense or sense control riboprobes were added to pre-warmed hybridisation buffer at a final concentration of 150 ng/mL. The hybridisation buffer consisted of 50% (v/v) formamide, 10 mM Tris-HCl (pH 8.0), 400 µg/mL tRNA, 1X

Denhardt's solution, 600 mM sodium chloride (NaCl), 0.25% (w/v) sodium dodecyl sulphate (SDS), 1 mM ethylenediaminetetraacetic acid (EDTA) and 10% (w/v) Dextran sulphate. Riboprobes were denatured by heating at 85ºC before placing on ice for 5 min and adding to sections. Slides were covered with parafilm to create a temporary coverslip and hybridised in a humidified chamber with 50% (v/v) formamide at 55ºC for 18 hours.

Hybridised sections were washed in 5X saline sodium citrate (SSC) buffer for 1 min to remove parafilm and then again for 30 min, before washing for 2 x 30 min in 2X SSC at 55ºC. Sections were washed in a solution of 10 mM Tris-HCl (pH 7.6), 500 mM NaCl and 1 mM EDTA (TNE) for 10 min at 37ºC, and then treated with 12.5 µg/mL RNase A in TNE for 30 min at 37ºC. Sections were subsequently washed in TNE at 37ºC for 10 min and then 2 x 30 min in 2X SSC followed by 0.2X SSC at 55ºC.

Labeled riboprobes were visualised using an alkaline phosphatase catalysed reaction with a bromochloro-indolyl phosphate (BCIP; Roche) and nitroblue tetrazolium (NBT; Roche) substrate solution. First, sections were washed in wash buffer containing 100 mM Tris HCl (pH 7.5) and 150 mM NaCl for 10 min and then again for 2 x 5 min each. Using Pap pens (Liquid blocker super pap pens; ProSciTech), circles were drawn around sections to create a hydrophobic barrier to ensure that solutions in subsequent incubation steps were confined to the encircled section. Care was taken to minimise drying of the tissue during this process. Sections were then incubated in a blocking solution of 2% bovine serum albumin (BSA; Roche) and 0.1% Triton-X 100 in wash buffer for 1 hr at RT, followed by alkaline phosphatase-conjugated anti-digoxigenin antibody (Roche; 1:1500) in 1% BSA,

0.1% Triton-X 100 in wash buffer overnight at 4ºC. Sections were washed 2 x 10 min in wash buffer, then once in developing buffer containing 100mM Tris HCl (pH 9.5) and 100 mM NaCl for 10 min. Sections were subsequently reacted with 5 uL/mL NBT and 3.75 uL/mL BCIP in developing buffer for 3-7 days at RT in the dark, with reaction solution replaced every 24-48 hours. Once signal had developed, sections were washed in MilliQ water for 10 min and permanently mounted with Clearmount CC (Sigma) followed by coverslipping with entellan (ProSciTech).

TH immunostaining

Staining for TH was performed on sections immediately adjacent to those used for *in situ* hybridisation for Ten-m3. Control experiments, consisting of no primary and no secondary forms, were performed for initial trials to confirm signal specificity. Once established, controls were not carried out, particularly as it was important that multiple sets of adjacent sections were available for these studies.

All solutions and washes were made in 0.3% TritonX-100 in 0.1 M PB unless stated otherwise. Fresh frozen sections were thawed, fixed in 4% paraformaldehyde for 30 min, and washed 3 x 5 min. Hydrophobic circles were drawn around sections (Pap pen; Pro Sci Tech) and non-specific binding was blocked by incubating sections in 4% normal rabbit serum (NRS; Vector Labs). Sections were then incubated in sheep polyclonal anti-TH antibody (Abcam; 1:500 in 2% NRS) overnight at 4°C. Sections were subsequently rinsed 3 x 10 min and then incubated in donkey anti-sheep secondary antibody conjugated to Alexa Fluor 488 (Invitrogen; 1:200 in 2% NRS) for 2 hours at RT. Excess

antibody was washed off in 2 x 5 min washes in 0.1 M PB, and sections were counterstained and mounted with 50% glycerol in 0.1 M PBS with DAPI.

Imaging and analysis

All images were taken using the Zeiss Deconvolution Microscope (Bosch Advanced Microscopy facility, University of Sydney) using the AxioCam HR camera. Images of Ten-m3 expression were taken using transmitted light, while the fluorescence filters for DAPI (λ = 360 nm) and Alexa Fluor-488 (λ = 488) were used to image TH reactivity. Images were exported as merged tagged image files (tif) using ZEN 2011 and AxioVision Rel. 4.7 software. Subsequently, the photomerge function in Adobe Photoshop CS3 was used to merge images of the same section. Each image was then flattened, and fluorescence images divided into its constituent channels ready for overlaying.

For overlaying, Alexa Fluor-488 channel images were warped using IR-tweak (www.sci.utah.edu) to control for differences in tissue shrinkage and other morphological changes resulting from tissue processing. Landmarks, such as the striatal border and anterior commissure, were used in the warping and subsequently in the overlaying of TH-labeled and Ten-m3-labeled images. Processed images were converted to RGB images in ImageJ, and pseudocoloured red for Ten-m3 and green for TH. Images were subsequently overlayed using the linear dodge function in Adobe Photoshop CS3.

Gradient analysis

A potential graded expression of Ten-m3 was analysed in P3-labeled tissue. For coronal sections, two images (one from each hemisphere) from three animals (a total of six sections) were chosen for analysis. For sagittal sections, two images from each of three hemispheres through the striatum of two animals (a total of six sections) were analysed. Images were inverted and rotated in ImageJ such to orient the striatum or PF horizontally. A rectangular box of 1.17 (arbitrary units; AU) height for the striatum and 0.65 AU for the PF; and varying widths (in accordance to the dorsal and ventral boundaries of the structures) was drawn across the midline. A plot profile of the pixel intensities within the rectangular box was obtained and the coordinates binned using Microsoft Excel to produce averaged pixel intensities in 10% intervals across the DV and RC axes of the striatum and the DV axis of the PF.

Analysis of the compartmentalisation of Ten-m3

The differential localisation of Ten-m3 to the matrix versus striosome compartment was analysed in Fiji (Image J, NIH) using the striosome and Ten-m3 channels from overlayed images. The perimeter of the striatum and individual striosomes were traced using the polygon tool. The striatum contour was applied to the Ten-m3 image, background subtracted and the image thresholded automatically using Tai's 'moments' method. The striosome contours were applied to the thresholded Ten-m3 image and the area of these contours, along with the area covered by pixels within the striatum and individual striosome contours, measured. The area of the matrix was calculated by subtracting the

total area occupied by striosomes from the area of the striatum. Likewise, the matrix area occupied by Ten-m3 was calculated by subtracting the area of Ten-m3 in striosomes from the total area occupied by Ten-m3 in the striatum. The density of Ten-m3 per striatal area was compared between striosome and matrix compartments.

Results

Ten-m3 expression in the striatum during development

In order to determine whether Ten-m3 may have potential roles in striatal circuits, i*n situ* hybridisation was used to characterise the expression patterns of Ten-m3 in the striatum during development.

E15

At E15, the LGE and MGE were still distinguishable in coronal sections through the rostral forebrain as protrusions into the lateral ventricle (LV) (Fig 2.1A, C). The MGE was clearly separated from the LGE by a sulcus, and was much smaller, approximately half the size of the LGE. Ten-m3 expression in the LGE was sparse, while a band of Ten-m3-positive cells could be observed in the superficial layer of the MGE, presumably corresponding to the ventricular zone (Fig. 2.1A, arrowheads). The ventricular zone while dense, was largely devoid of Ten-m3 label in the sense control (Fig. 2.1C) suggesting that this was specific staining. The striatal primordium appeared at more caudal levels (Fig. 2.1B; dashed line), emerging VL to the ventricular zone. Ten-m3 expression in the striatal primordium was sparse to absent (Fig. 2.1B), as it was in the sense control (Fig. 2.1C).

E17

The striatum was well developed and easily identifiable by E17 (Fig. 2.1D-F). Ten-m3 expression was observed at all RC levels of the developing striatum (Fig. 2.1D-E). At rostral levels (Fig. 2.1D), Ten-m3 was highly expressed around the medial and dorsal edge of the striatum, forming a dark border lining the edge of the nucleus (Fig. 2.1D, arrowheads). Expression was most intense in dorsal regions and decreased ventrally. In the middle of the nucleus, expression was patchy, with small islands of Ten-m3-positive cells scattered between cells showing low expression (Fig. 2.1D, arrows). Expression was generally similar more caudally (Fig. 2.1E), although patches appeared slightly larger and better defined. At this level, Ten-m3 expression was, likewise, highest in cells at the dorsal edge of the nucleus (Fig. 2.1E; arrowheads). Further, Ten-m3-positive cells located at the lateral edge of the striatum formed large patches separated by more sparsely labeled regions. Large and more distinct patches were also obvious in more ventral and medial parts of the nucleus (Fig. 2.1E; arrows). No staining was present in the sense control (Fig. 2.1F, dashed line).

P3

A more mature patterning of Ten-m3 expression was observed in the striatum at P3 (Fig. 2.1G-I, dashed line). In rostral sections, Ten-m3 expression lined the border of the striatum in bands (Fig. 2.1G, arrowheads). Similarly, bands of Ten-m3-positive cells, oriented along the DM-VL axis and parallel to the dorsal and lateral borders of the nucleus, were evident ventral of the border (Fig. 2.1G, arrow). These bands were separated by large areas of low Ten-m3 expression. Ventrally, Ten-m3 expression was

more disorganised and 'patch-like'. As at earlier ages, expression was higher in dorsal, and lower in ventral striatum. Caudally, Ten-m3 expression was generally higher compared to rostral levels, however, a similar overall pattern of expression was observed (Fig. 2.1H). Expression was highest at the medial and lateral borders of the nucleus, which were lined by patches of Ten-m3 (Fig. 2.1H, arrowheads). Bands of label, similar to those seen at rostral levels, were oriented along the DM-VL axis throughout the middle of the nucleus (Fig. 2.1I, arrow), however, they appeared more disjointed than in rostral regions. No staining was observed in the sense control (Fig. 2.1I).

P10

At P10, the intensity of Ten-m3-positive signal in the striatum (Fig. 2.1 J-L) appeared generally lower than that observed at P3. The patterns of expression were, nevertheless, similar. In rostral sections (Fig. 2.1J), distinct Ten-m3-positive bands, approximately parallel to the dorsal and lateral border of the striatum (Fig. 2.1J, arrows), were separated by bands of cells showing low Ten-m3 expression. Ten-m3 expression was highest in dorsal and medial patches and lowest in ventral and lateral areas of the nucleus. At caudal levels (Fig. 2.1K), Ten-m3 expression appeared less organised. A band of Ten-m3-positive cells was still observed along the lateral border (Fig. 2.1K, arrow). Intriguingly, the location of this band appeared to complement that observed at rostral levels (Fig. 2.1J). Distribution of Ten-m3 expression in the middle of the nucleus appeared less organised, and predominantly seen in patches. Expression of Ten-m3 was highest in mid-dorsal striatum, and sparse in ventral regions. Ten-m3 expression was absent in the sense control (Fig. 2.1L).

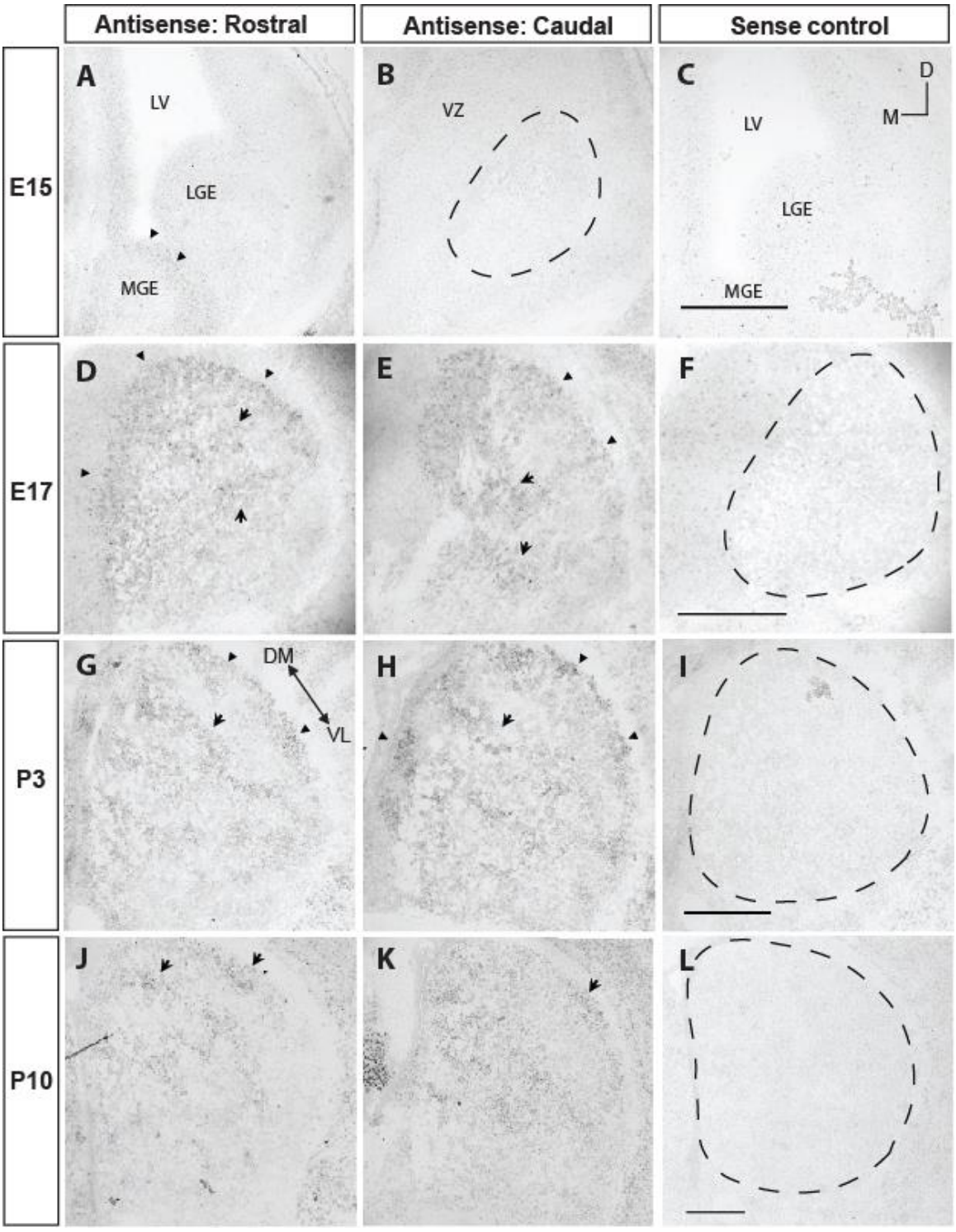
Antisense: Rostral
Antisense: Caudal
Sense control
E15
E17
P3
P10
A
LV
LGE
MGE
B
VZ
C
D
M
LV
LGE
MGE
D
E
F
G
DM
VL
H
I
J
K
L

Figure 2.1. *In situ* hybridisation for Ten-m3 in the striatum across development.
(A-C) Coronal sections through the forebrain showing Ten-m3 expression at E15. (A) In rostral sections, the LGE and MGE were distinguishable abutting the lateral ventricle (LV). A band of Ten-m3 expression was present in the ventricular zone of the MGE (arrowheads). (C) The striatal primordium was evident in caudal sections (dashed line), lateral to the ventricular zone (VZ). Ten-m3 expression was scant in the striatum at this age. (C) The sense control (near/adjacent to section shown in A) was devoid of staining.
(D-F) As for (A-C) at E17. (D) At rostral levels, Ten-m3-positive cells formed a dark border lining the edge of the nucleus (arrowheads). Expression was most intense in dorsal striatum, decreasing ventrally. In the middle of the nucleus, Ten-m3-positive cells formed small patches (arrows) scattered between areas scant of expression. (E) Ten-m3 expression was similar in more caudal sections. Similar to rostral striatum, Ten-m3 expression was most intense in dorsal striatum, with strongly labeled patches of cells lining the dorsal and lateral edge of the nucleus (arrowheads). Ventrally, larger and more distinct patches were obvious, particularly medially (arrows). (F) The sense control (striatal borders indicated by dashed line) was devoid ofstaining.
(G-I) As for (A-C) at P3. (G) In rostral sections, bands of intense Ten-m3 expression lined the border of the striatum (arrowheads). A second band of Ten-m3 was located ventral to this (arrow). These parallel oblique bands were oriented along the DM-VL axis, parallel to the dorsal and lateral borders of the nucleus, and were separated by large areas of greatly reduced Ten-m3 expression. Ventrally, Ten-m3 expression was more disorganised and 'patch-like'. Overall, Ten-m3 expression appeared higher in dorsal and lower in ventral striatum. (H) At caudal levels, Ten-m3 expression was generally higher than at rostral levels. Ten-m3-positive cells were similarly organised into bands (arrow), and were particularly intense at the medial and lateral striatal borders (arrowheads). (I) No staining was observed in the sense control (striatal borders indicated by dashed line).
(J-L) As for (A-C) at P10. (J) In rostral sections, Ten-m3 bands (arrow) were organised similar to those seen at P3. Expression was likewise highest dorsally and lowest ventrally. (K) At caudal levels, a band of Ten-m3-positive cells lined the lateral border (arrow) with more patches of expression distributed randomly throughout the striatum. Expression remained highest in mid-dorsal striatum, and sparse in ventral regions. (L) Staining was absent from the sense control (striatal borders indicated by dashed line).
Scale bar in C applies to A and B. Scale bar in F applies to D and E. Scale bar in I applies to G and H. Scale bar in L applies to J and K. For all images, scale bars represent 500 μm. D is dorsal, M is medial, DM is dorsomedial, VL is ventrolateral.

Ten-m3 expression in the sagittal plane

The developmental time course of Ten-m3 expression revealed differing levels and patterning of gene expression with time. The most intense expression was observed at P3, where the patterning of Ten-m3 into oblique bands was also most striking. In order to gain more information about the distribution of Ten-m3 expression, this was further investigated in the sagittal plane at P3 (Fig. 2.2).

The pattern of bands observed in coronal sections was similarly observed in lateral (Fig. 2.2A), middle (Fig. 2.2B) and medial (Fig. 2.2C) sections in the sagittal plane. Laterally, this pattern appeared less organised (Fig. 2.2A), with large Ten-m3-positive patches interspersed with areas of low expression. These patches were most intense in the caudodorsal region of the striatum. In middle sections (Fig. 2.2B), a band of intensely-labeled Ten-m3-positive cells lined the caudodorsal edge of the striatum (Fig. 2.2B, arrowheads). This band was often broken, and thus appeared as patches at the edge of the nucleus. Smaller patches were distributed throughout the rest of the striatum (Fig. 2.2B, arrows), being more numerous and intense in the dorsal and caudal halves and fading off in ventral and rostral regions. Ten-m3-positive patches were smaller in medial sections (Fig. 2.2C, arrows) and appeared to constitute larger bands that were interrupted by fibers of the internal capsule. These were oriented parallel to the striatal border and particularly striking in the most medial sections, where the expression became lattice-like in appearance. A single, apparently continuous, thin band of Ten-m3 lined the caudal and dorsal-rostral edge of the striatum (Fig. 2.2C, arrowheads). Ten- m3 expression was absent in the sense control (Fig. 2.2D, striatal border indicated by dashed line).

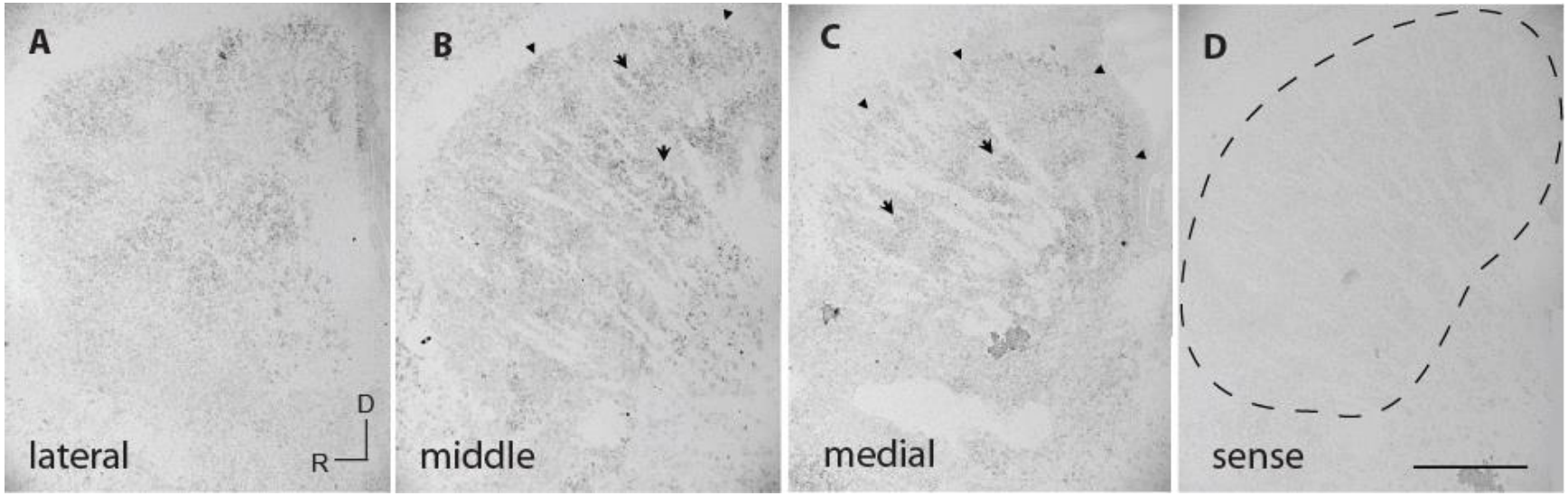

Figure 2.2. *In situ* hybridisation for Ten-m3 in the sagittal plane, at P3.

(A) In lateral striatum, large Ten-m3-positive patches were distributed throughout the nucleus, being most intense in the caudodorsal edge.

(B) In the middle of the striatum, a band of Ten-m3-positive cells similarly lined the caudal and dorsal edge of the striatum (arrowheads). Smaller patches of Ten-m3 were distributed throughout the remainder of the striatum (arrows). These were more numerous and intense in the dorsal and caudal halves and faded off in ventral and rostral regions.

(C) In medial sections, a single, apparently continuous, thin band of Ten-m3-positive cells lined the caudal and dorsal-to-rostral edge of the striatum (arrowheads). Patches of Ten-m3 were small (arrows) and appeared to constitute larger bands of Ten-m3-positive cells that were interrupted by fibers of the internal capsule. These were oriented parallel to the striatal border.

(D) The sense control showed the striatum (borders indicated by dashed line) devoid of staining.

The scale bar in D applies to A- C. Scale bar represents 500 µm. For all images, D is dorsal, R is rostral.

Ten-m3 is localised to a subregion of the matrix compartment

The patchy pattern of Ten-m3 in the striatum was reminiscent of the unique organisation of striatal cells into striosome and matrisome patches of the matrix compartment. Hence, it was of interest to investigate the relationship between Ten-m3 and the striatal compartments (Fig. 2.3). Here, *in situ* hybridisation for Ten-m3 and immunohistochemistry for TH to mark striosomes were performed on adjacent sections at P3, in coronal (Fig. 2.3A-C) and sagittal planes (Fig. 2.3D-F). Ten-m3, as described above, was expressed in patches in coronal (Fig. 2.3 A) and sagittal sections (Fig. 2.3D), being particularly intense in dorsal striatum. In adjacent sections, TH marked striosomes as patches of cells distributed throughout the striatum. In coronal sections, striosomes were most numerous in lateral, and scant in medial striatum (Fig. 2.3B). In the sagittal plane, striosomes were distributed throughout most of the striatum, with the exception of the most caudal regions (Fig. 2.3E). The overlayed images (Fig. 2.3C, F) showed a complementary pattern between Ten-m3 and TH. That is, bands of high Ten-m3 expression overlapped with areas expressing low levels of TH (Fig. 2.3A-F, arrows). Conversely, regions lowest in Ten-m3 expression overlapped with areas highly labeled for TH (Fig. 2.3A-F, arrowheads). Areas of low Ten-m3 expression were, however, also found in the matrix compartment (Fig. 2.3A-F, *). Quantitatively, the density of Ten-m3-positive pixels per striatal area was significantly higher in the striatal matrix compared to striosomes (striosome: 0.020 ± 0.004 (mean (AU) ± SEM), n = 4; matrix: 0.16 ± 0.03, n = 4, p = 0.01, t-test). Hence, Ten-m3 appears to be expressed in a subregion of the matrix, suggesting that it may mark a novel matrisome compartment.

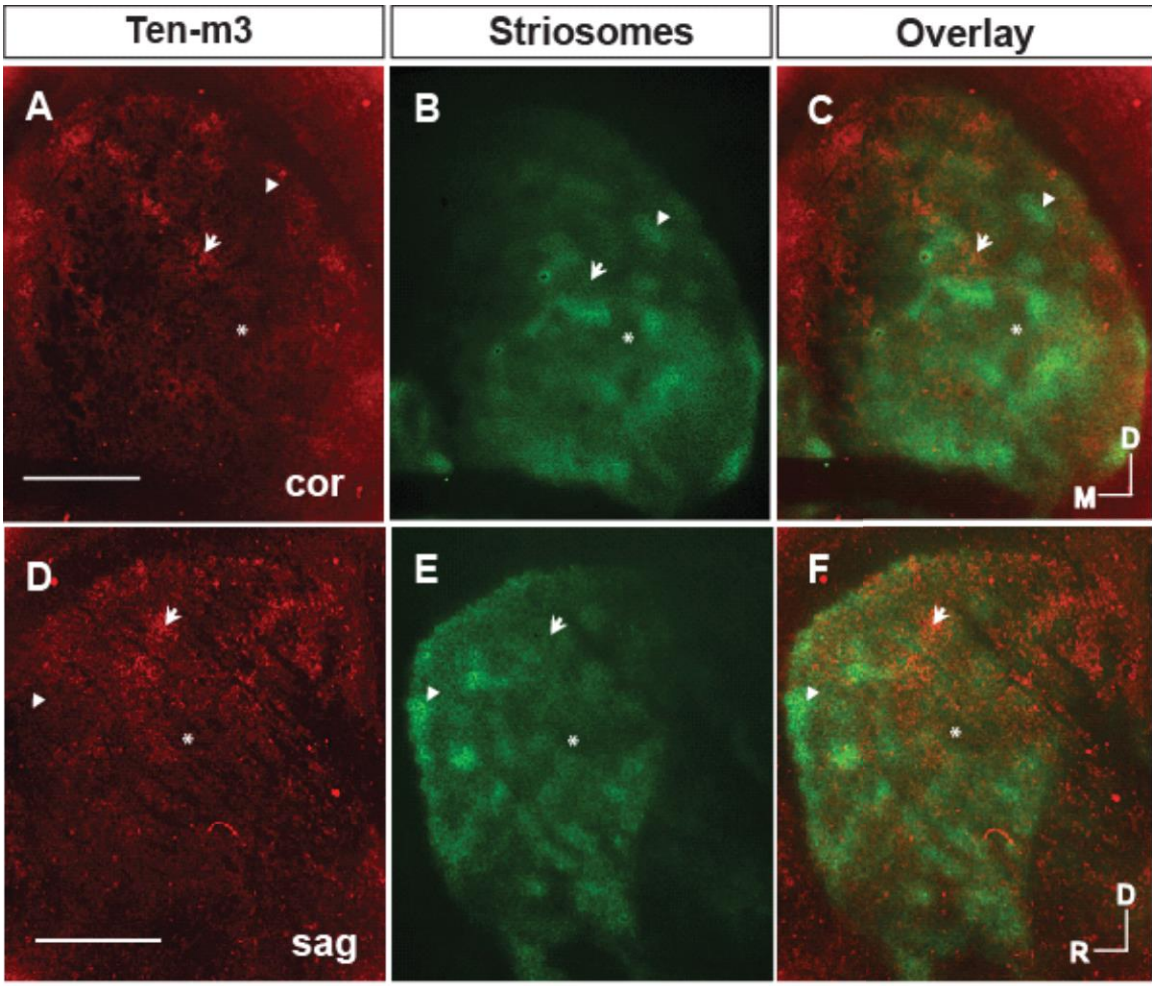
Ten-m3
Striosomes
Overlay
A
B
C
cor
D
M
D
E
F
sag
D
R

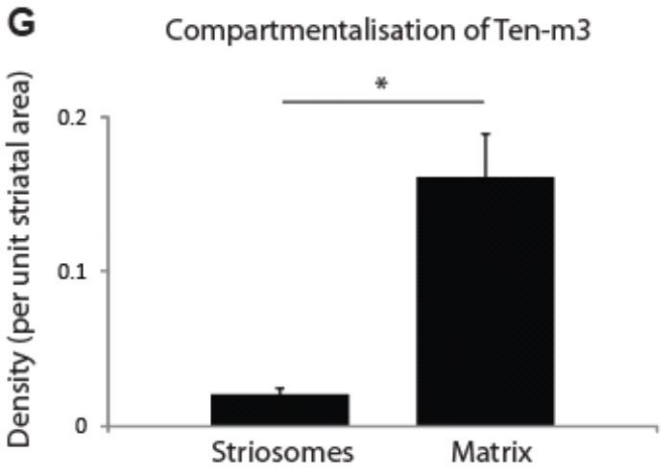
G
Compartmentalisation of Ten-m3
*
Density (per unit striatal area)
0.2
0.1
0
Striosomes
Matrix

Figure 2.3. Ten-m3 is localised to a subregion of the striatal matrix compartment.
(A-C) Comparison of Ten-m3 and TH in adjacent coronal sections through P3 striatum. (A) *In situ* hybridisation for Ten-m3 (red), revealed patches of expression throughout the striatum, being particularly intense in dorsal regions. (B) Immunohistochemistry for TH (green) showed striosome patches predominantly in lateral striatum and scant in medial regions. (C) The resulting overlayed image showed bands of high Ten-m3 expression overlapping with areas of low TH (arrow). Conversely, regions lowest in Ten-m3 expression overlapped with areas showing high levels of TH (arrowhead). Additionally, areas of low Ten-m3 expression were similarly found in the matrix compartment (*).
(D-F) Comparison of Ten-m3 and TH in adjacent sagittal sections through P3 striatum. (D) *In situ* hybridisation for Ten-m3 (red), revealed patches of expression throughout the striatum, likewise, being particularly intense in dorsal, and caudal regions. (E) Immunohistochemistry for TH (green) showed striosome patches throughout the majority of the striatum with the exception of the most caudal regions. (F) The resulting overlayed image showed bands of high Ten-m3 expression overlapping with areas of low TH label (arrow). Conversely, regions lowest in Ten-m3 expression overlapped with areas highly labeled by TH (arrowhead). Areas of low Ten-m3 expression were similarly found in the matrix compartment (*).
(G) Quantitatively, the density of Ten-m3-positive pixels per striatal area was significantly higher in the striatal matrix compared to striosomes (striosomes: 0.020 ± 0.004 (mean (AU) ± SEM), n = 4; matrix: 0.16 ± 0.03, n = 4, p = 0.01, t-test). Hence, Ten-m3 is expressed in a subregion of the matrix, and may mark a novel matrisome compartment.
The scale bar in A applies to B and C. Scale bar in D applies to E and F. Scale bars represent 500 µm. D is dorsal, M is medial, R is rostral. For A-C, dorsal is up, medial is left. For D-F, dorsal is up, rostral is left.

Survey identifies the PF as an important locus of action for Ten-m3

The above results indicate that Ten-m3 is expressed in an intricate pattern of patches in the striatal matrix during development. Previous studies in the visual system found that that correlated Ten-m3 expression in afferent and target structures was indicative of a role in regulating their connectivity (Dharmaratne et al., 2012; Leamey et al., 2007b). Based on this premise, a survey was performed to determine the striatal circuit in which Ten-m3 may play a regulatory role. Hence, afferent and efferent structures of the striatal matrix were surveyed for Ten-m3 expression, and the PF was identified as a potentially important locus for the actions of Ten-m3.

In situ hybridisation for Ten-m3 identified expression at all RC levels of the PF at P3 (Fig. 2.4). At the most rostral levels, the PF (Fig. 2.4A, dashed line) was small and located dorsally in the thalamus, enclosing the fr. Here, Ten-m3 was expressed in all regions surrounding the fr. Approximately 90 µm caudal of this level, the PF became its characteristic round shape (Fig. 2.4, dashed line), and was shifted slightly ventrally. Ten-m3 was expressed throughout the entire nucleus, showing highest expression in dorsal regions. This expression pattern was consistent into the caudal PF (Fig. 2.4 C, D, dashed line). Staining was absent in sense controls at all RC levels (Fig. 2.4 A'-D'). Hence, consistent with previous reports (Leamey et al., 2007b), the high-dorsal to low-ventral gradient of expression in the dLGN was also visible in the PF (Fig 2.4A-C).

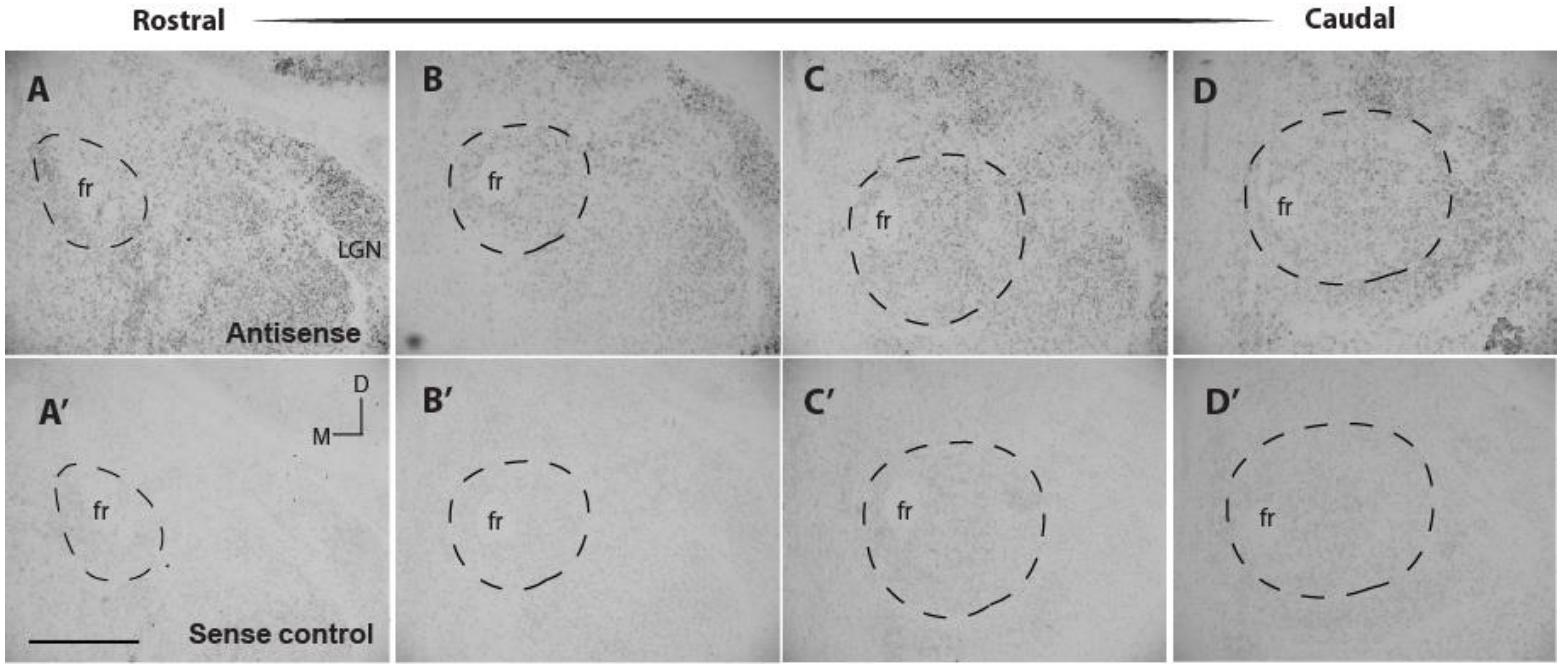

Figure 2.4. Survey of Ten-m3 identifies expression in the PF at P3.

(A-D) *In situ* hybridisation for Ten-m3 identified expression in a RC series of coronal sections through the PF (border indicated by dashed line) at approximately 90 µm intervals, at P3. (A) At the most rostral levels, Ten-m3 was expressed in all regions surrounding the fr. (B-D) Slightly caudal to (A), the PF took on its characteristic round shape and Ten-m3 was expressed throughout the entire nucleus, where it was highest dorsally (B). In the mid region of the PF, Ten-m3 was similarly expressed highest dorsally (C). This expression pattern was consistent into the caudal part of the PF (D).

(A'-D') Staining was absent in sense controls at all RC levels.

Scale bar in A' applies to A-D, B'-D'. Scale bar represents 500 µm. D is dorsal, M is medial.

Ten-m3 expression in the PF during development

In order to investigate potential temporal and spatial similarities of Ten-m3 expression between the interconnected structures, this was subsequently characterised in the PF throughout the same developmental time points analysed for the striatum

E15

The presumptive PF at E15 was small and the borders non-distinct, with only its association with the fr enabling it to be identified. The fr appeared as white circles just lateral to the midline, at the level at which the third ventricle opened laterally (Fig. 2.5A, A'). The borders of the PF, however, could not be distinguished, and, hence, the location of the nucleus is indicated by an arrow in Fig. 2.5A and A'. Ten-m3 expression was sparse, appearing as a band of labeled cells predominantly ventral to the fr (Fig. 2.5A). It is unclear whether this band of Ten-m3-positive cells belongs to the PF or are merely cells migrating from the ventricular zone to more lateral areas of the thalamus. Dense Ten-m3 expression was also observed in the ventricular zone, medial to the PF. This expression was not observed in the sense control (Fig. 2.5A').

E17

At E17, the fr was larger however the borders of the PF were still difficult to define, and, hence, the location of the nucleus is indicated by an arrow in Fig. 2.5B and B'. Ten-m3 was more highly expressed in the PF at this age point (Fig. 2.5B). In particular, its expression was observed in cells immediately surrounding the fr and in the DL quadrant,

and was less prominent in the ventral part of the PF. Additionally, Ten-m3 expression was observed throughout a number of other thalamic structures, including the developing precommisural nucleus (PCN) and dLGN on the DL edge of the thalamus. There was no such signal observed in the sense control (Fig. 2.5B').

P3

At P3, Ten-m3 expression in the thalamus was more specific and distinct (Fig. 2.5C) compared to that at E17. The borders of the PF were more defined (Fig. 2.5C, C', dashed line), and Ten-m3 expression covered the entire nucleus, being particularly prominent around the medial side of the fr and in the DL quadrant. Label in the ventral part of the nucleus was lower, suggesting the presence of a dorsal to ventral gradient of expression. There was also still evidence of Ten-m3 expression in the pretectal nucleus dorsal of the PF. The sense control showed no equivalent signal at this age point (Fig. 2.5C').

P10

At P10, Ten-m3 expression in the PF (Fig. 2.5D, dashed line) was more distinct compared to earlier ages. In the PF, Ten-m3 expression appeared higher than that at P3, covering the entire nucleus, as at previous ages. Expression at this age point was higher in dorsal versus ventral regions of the PF. Staining was absent in the sense control (Fig. 2.5D').

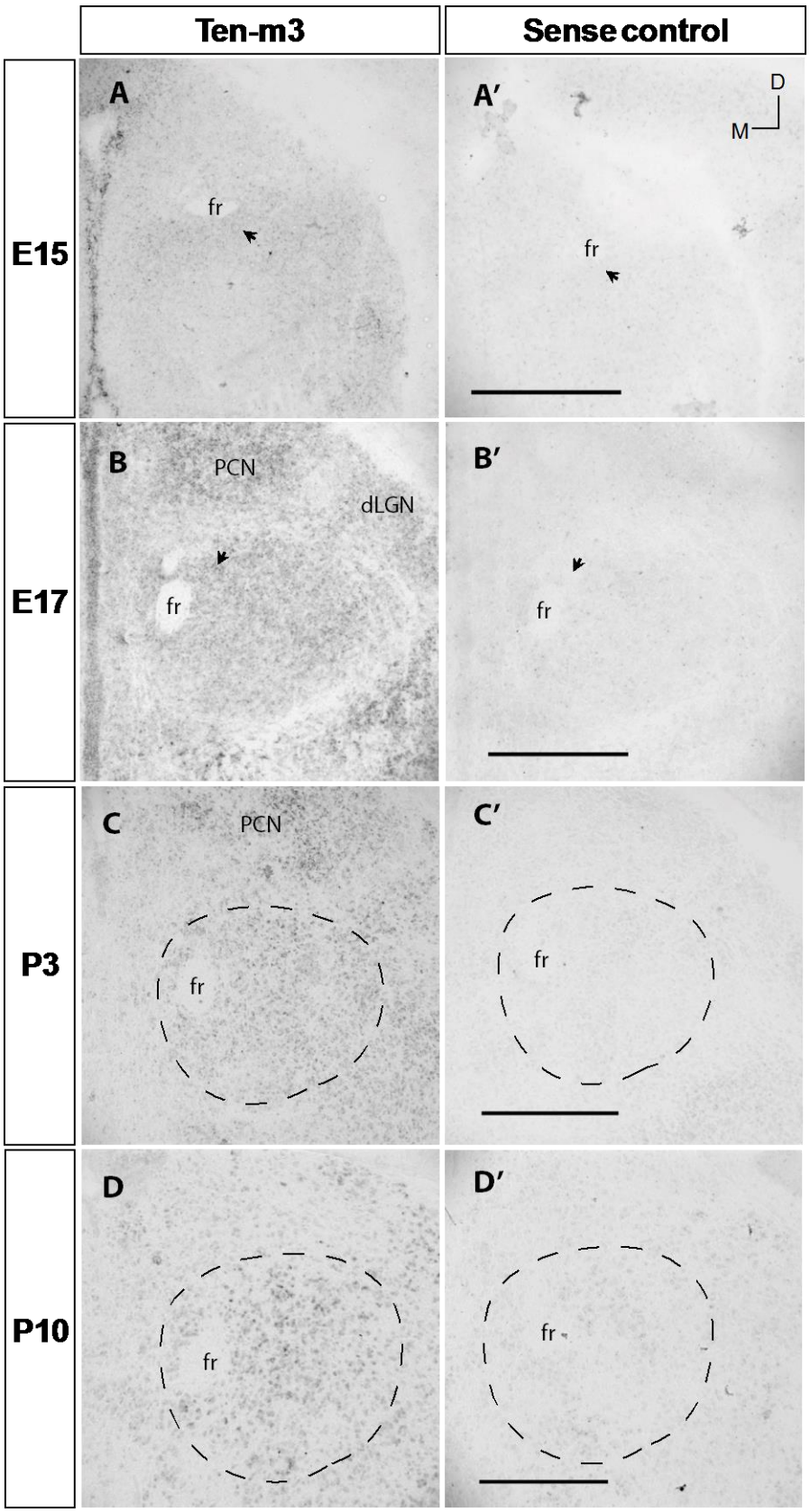
Ten-m3
Sense control
E15
E17
P3
P10
A
A′
B
B′
C
C′
D
D′
fr
PCN
dLGN
D
M

Figure 2.5. *In situ* hybridisation for Ten-m3 in the PF during development.
(A) A coronal section through the thalamus showing Ten-m3 expression at E15. A band of Ten-m3-positive cells was observed directly ventral to the fr, in the presumptive PF (location indicated by the arrow). It is unclear whether these are PF cells or cells migrating from the ventricular zone to more lateral areas of the thalamus. The ventricular zone, medial to the PF, also showed dense Ten-m3 expression.
(B) As for (A) at E17. The borders of the PF were still difficult to define (location indicated by the arrow). Ten-m3 was highly expressed, particularly in cells immediately surrounding the fr and in the approximate DL quadrant of the nucleus. Ten-m3 expression was lower in ventral PF. Ten-m3 was also present in the developing precommissural nucleus (PCN) and dLGN.
(C) As for (A) at P3. Ten-m3 expression was less diffuse and covered the entire PF (dashed line), being most prominent dorsally. Similar to E17, Ten-m3 expression in the ventral PF was lower, suggesting the presence of a dorsal to ventral gradient. Expression was still obvious in the PCN.
(D) As for (A) at P10. Expression of Ten-m3 in the PF (dashed line) appeared higher than that at P3. It was more evidently higher in lateral PF compared to medial regions, and remained higher in dorsal versus ventral regions of the PF.
(A'-D') Staining was absent from sense controls at (A') E15, (B') E17, (C') P3 and (D') P10.
The scale bar in A' applies to A. Scale bar in B' applies to B. Scale bar in C' applies to C. Scale bar in D' applies to D. Scale bars represent 500 μm. D is dorsal, M is medial.

Ten-m3 is expressed in corresponding gradients in the striatum and PF

The above expression studies in both coronal and sagittal sections through the striatum and coronal sections through the PF, indicated differential levels of Ten-m3 across some of the axes of these structures. Hence, striatal sections were analysed for the presence of a graded expression along the DV (in coronal sections) and RC axes (in sagittal sections). Pixel analysis showed a linear high-dorsal to low-ventral gradient in the striatum (Fig. 2.6A). Along the RC axis, Ten-m3 expression showed a linear high-caudal to low-rostral gradient (Fig. 2.6B). This gradient was less steep than that observed along the DV axis. This suggests the presence of an overall high-dorsocaudal to low-ventrorostral gradient. Image analysis was also performed on coronal sections through the PF to show a high-dorsal to low-ventral gradient of Ten-m3, similar to that observed along the same axis in the striatum (Fig. 2.6C).

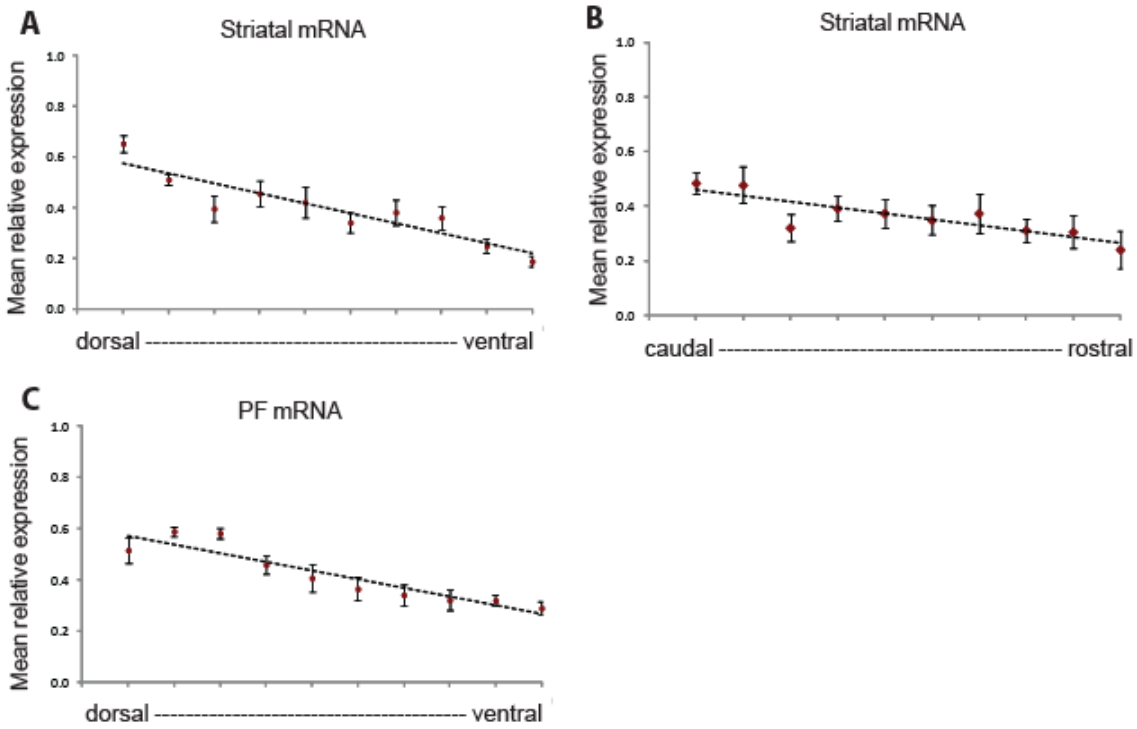

Figure 2.6. Ten-m3 is expressed in corresponding gradients in the striatum and PF.
(A-B) Gradient analysis of Ten-m3 expression in the striatum. (A) In coronal sections, Ten-m3 expression was highest at the most dorsal, and lowest in ventral regions of the striatum. (B) In sagittal sections, Ten-m3 was expressed highest in caudal and lowest in rostral striatal regions. This caudal to rostral gradient was shallower than that observed along the DV axis. Together, these suggest the presence of a high-dorsocaudal to low-ventrorostral gradient.
(C) Gradient analysis in the PF showed Ten-m3 expression was highest dorsally and lowest ventrally, with a similar gradient to that observed in (A).

Discussion

Summary of results

This study constitutes the first investigation into the expression patterns of Ten-m3 in the striatum and its afferent structure the PF, with the aim of inferring potential roles for the gene in this circuit. Firstly, analysis of Ten-m3 expression across four developmental time points, E15, E17, P3 and P10, showed that Ten-m3 is first expressed in the striatum on or just before E17, where it continues to be expressed until at least P10. Distribution of Ten-m3 expression was patchy from E17, and matured into oblique bands of labeled cells oriented approximately parallel to the striatal border, along the DM-VL axis, at postnatal age points. The maturation of this expression pattern was evident with time, but also within single age points, with Ten-m3 patches appearing more 'mature' at caudal regions compared to those more rostrally. This pattern of expression was most striking and the level of expression highest at P3, which was utilised for further analysis. In sagittal sections, Ten-m3 was also expressed in patches and bands, once again oriented approximately parallel to the dorsorostral border of the nucleus. Further analysis showed Ten-m3-positive bands/patches localised to a subregion of the striatal matrix. Hence, we propose that Ten-m3 may mark a novel matrisome compartment. A survey of Ten-m3 expression in afferent/efferent striatal structures identified the PF, which provides a major projection specifically to the striatal matrix (Gonzalo, 2002; Herkenham and Pert, 1981) as a potential important locus of action. A developmental time course of expression subsequently showed a similar temporal and spatial organisation of Ten-m3 expression in the PF, with expression particularly strong in the dorsal portions of the nucleus. Image analysis confirmed the presence of a correspondingly high-

dorsal to low-ventral expression gradient in both the striatum and PF, and a high-caudal to low-rostral gradient in the striatum at P3.

Technical considerations

In situ hybridisation experiments were performed on tissue obtained from C57/Bl6 and Ten-m3 WT mice on a C57/Bl6xSv129 background. Although there was some variability in intensity levels of Ten-m3 both within and between strains, this parameter was not analysed. Importantly, early experiments indicated that the distribution patterns of Ten-m3 were very similar in tissue from both strains of mice. Hence, expression studies were performed on both strains interchangeably.

In order to determine the spatial relationship between Ten-m3and striatal compartments, a comparison of *in situ* hybridisation for Ten-m3 and immunohistochemistry for TH in adjacent sections was performed by overlaying images in Photoshop. An attempt was previously made (Tran, 2009) to perform dual *in situ* hybridisation and immunohistochemistry on the same sections, however, to no avail. Further, dual immunohistochemistry experiments were impossible as several commercial Ten-m3 antibodies were trialled, also with no success. For a period, efforts were focused on producing a Ten-m3 antibody, however, due to the student's inexperience with bacterial cloning and a range of other factors, this task proved too extensive. Hence, efforts were focused on overlaying images of *in situ* hybridisation-labeled Ten-m3 and immunohistochemically-labeled TH. These were performed on sections that were exactly adjacent to one another, to enhance the accuracy of the resulting overlay. Further, IR-tweak (http://www.sci.utah.edu) was used to 'warp' images according to landmarks visible in both images, such as the striatal border, anterior commissure and blood vessels. This step was necessary as individual sections underwent differing degrees of tissue

shrinkage and stretching as a result of mounting and various steps within distinct *in situ* hybridisation and immunohistochemistry protocols. Hence, all precautions were taken to ensure that images were aligned as well as possible for the most accurate overlay. While an overlay of adjacent sections can never be perfect, given the typical size of striosomes (from 150 µm diameter) compared the thickness of cryostat sections used here (15 µm) and alignment methods used, this approach allowed a sufficient level of accuracy to determine the relationship between Ten-m3 expression and striatal compartments. Importantly, a consistent relationship was observed in all examples analysed suggesting the efficacy of this approach.

Ten-m3 expression in the striatum

As mentioned earlier, although Ten-m3 has been observed in the striatum (Leamey et al., 2007a; Li et al., 2006), the current study provides the first in depth investigation into the unique patterning of Ten-m3 expression. These experiments suggest that Ten-m3 expression first occurs in the striatal primordium between E15 and E17. The unique patchy distribution of Ten-m3 was evident by E17. It is unclear from the current data, however, whether this pattern occurred from the very first appearance of Ten-m3 or whether it developed with time. The development of the patchy expression into distinct oblique bands in early postnatal ages suggests that this pattern does mature with age, and that Ten-m3 may be first expressed slightly earlier than E17. Hence, it would of interest to characterise Ten-m3 expression at E16. Additionally, there appeared to be differential maturation of the 'patchy' distribution of Ten-m3 in caudal versus rostral sections at individual time points, with patches of expression generally appearing more 'mature' at caudal levels. This suggests the presence of a developmental gradient of Ten-m3 expression along the RC axis of the striatum, which is consistent with development studies (Angevine, 1970; Bayer, 1984; Sturrock, 1980) suggesting the existence of a caudal-to-rostral spatiotemporal developmental gradient in

striatum. Therefore, the development of the patchy Ten-m3 expression may highlight the migration of striatal cells across time and space within the striatum.

One of the first questions motivated by the identification of the presence of Ten-m3 in the striatum was, what is the spatial relationship between Ten-m3 and striatal compartments? The expression of Ten-m3 in patches of cells suggested a potential spatial overlap with striosome patches. Hence, the localisation of Ten-m3 to the matrix compartment was unexpected. Nevertheless, this is not the first reported case of patches within the matrix. These patches, known as matrisomes (Graybiel, 1990), have been described as a 'collage of discontinuous modules' within the matrix (Tai et al., 2013). Unlike the more established striosome and matrix compartments, however, until very recently, matrisomes had only been identified by the clustering of afferents from the cortex (Malach and Graybiel, 1986) or efferent neurons projecting to the GP and SN (Desban et al., 1989; Giménez-Amaya and Graybiel, 1991; Jiménez-Castellanos and Graybiel, 1989) with no molecular markers of matrisomes known. In the last few months, however, Tai et al. (2013) reported that the patchy expression of the tyrosine kinase receptor EphA7 within the striatal matrix may mark a novel matrisome compartment. Hence, we propose that clusters of Ten-m3-positive cells may also constitute either the same or possibly a novel matrisome compartment. The pattern of 'discontinuous bands..diagonally oriented ..along a dorsomedial and ventrolateral axis' reported by Tai et al. closely resembles the pattern of Ten-m3 expression in the striatum reported here. Further, comparison of Ten-m3 and EphA7 *in situ* hybridisation expression patterns (Chapter 4) suggests that these genes mark distinct regions of the matrix, suggesting that their expression does indeed represent distinct matrisome compartments. This will be taken up further in Chapter 4. Additionally, Tai et al. suggest that EphA7-positive efferents project to specific areas of the GP and SN and, hence, contribute to both the direct and

indirect pathways. This may complement other findings made in this thesis that Ten-m3 is involved in the guidance of thalamostriatal projections from the PF (see Chapter 3). Hence, the only molecular markers of matrisomes discovered to date are both axonal guidance cues, consistent with the initial discovery of matrisomes in association with afferent and efferent striatal projections.

The patchy expression of Ten-m3 in the striatum in the current study is the first description of such patterning for this family of transmembrane glycoproteins. Previously, Ten-m3 has only been observed in a continuously graded pattern in visual structures (Dharmaratne et al., 2012; Leamey et al., 2007b). Further, other teneurin paralogues, Ten-m2 and Ten-m4, have a uniform distribution in these structures (Young, 2011; Young et al., 2013). Within the striatum, Ten-m1, 2 and 4 also appear to display a generally homogeneous pattern of expression across development (Allen Bran Atlas). These have yet to be a fully characterised, however, and a more comprehensive study is required to confirm this.

Despite this, the patchy pattern of Ten-m3 expression resembles that of many other genes expressed in the striatum. Apart from established markers of the striosome compartment, such as TH, μ-OR and DARPP-32 (Desban et al., 1989; Graybiel, 1984; Lança et al., 1986; Murrin and Ferrer, 1984), a number of axon guidance molecules have recently been shown to be expressed in this pattern. For instance, members of the family of Eph receptors and ephrin ligands, including ephrinA2, 3, 5, EphA7 (Janis et al., 1999; Passante et al., 2008; Tai et al., 2013), and EphB1 (Richards et al., 2007) are expressed in patches in the striatum, although with the exception of EphA7, the potential significance of these distributions are yet to be fully characterised. As noted above, EphA7 was recently shown to define a novel matrisome compartment where it is believed to govern striatofugal connections with the GP and SN (Tai

et al., 2013). Similarly, TH-marked striosomes are believed to result from terminals originating from the SN in early development (Olson et al., 1972). Hence, the unique patches of molecules, not only of matrisomes, as mentioned above, but also markers of striosomes, may be so patterned as to reflect the clustering of afferent and efferent striatal projections. This theory is further strengthened by the observation that these expression patterns change across development, possibly as connections change and mature, such as that observed in the distribution of TH and the dispersion of striatonigral projections in later developmental ages (Olson et al., 1972).

The patches of Ten-m3 expression are superimposed upon a high-dorsal to low-ventral gradient in the striatum. This graded pattern of expression for Ten-m3 is consistent with that shown in all visual structures, including the retina, dLGN, visual cortex and SC (Dharmaratne et al., 2012; Leamey et al., 2007b). Further, all teneurins have been shown to be expressed in gradients in the developing cortex (Li et al., 2006). Graded patterns of expression have long been associated with the precise targeting of projections and the formation of topographic maps during development (Sperry, 1963). Multiple pieces of evidence across the past few decades have provided strong support for this theory. A number of well established axon guidance molecules, such as the Eph/ephrins, show graded expression patterns and corresponding deficits in axon targeting in the absence of these genes (see McLaughlin and O'Leary, 2005 for a review). Importantly, the graded expression of Ten-m3 in the mouse visual system, for instance, has been shown to be significant for the mapping of retinogeniculate and retinocollicular projections (Dharmaratne et al., 2012; Leamey et al., 2007b). The corresponding high-dorsal to low-ventral gradients in the striatum and PF, and the high-caudal to low-rostral pattern of Ten-m3 expression in the striatum correlate with the general topography of thalamostriatal projections along the RC and DV axes (Lanciego et al.,

2004). This provides strong implications for the role of Ten-m3 in the striatum, in particular, suggesting roles in the normal topography of thalamostriatal projections originating from the PF.

Thus, the patterns of expression shown in the current study strongly suggest that Ten-m3 may be involved in the control of afferent and/or efferent connections to and/or from the striatum. In particular, the demonstration that Ten-m3 expression is largely confined to the matrix suggests that these afferent/efferent structures will be linked to the striatal matrix. In a survey of potential afferent and efferent structures, including SN and cortex, Ten-m3 was observed in the PF. This is a potentially significant finding as it has been well established that the PF provides a strong and very specific projection to the matrix compartment (Herkenham and Pert, 1981). Further, these projections terminate in clusters within the striatal matrix (Gonzalo, 2002), reminiscent of the patchy pattern of Ten-m3 expression in this compartment. There are currently no molecular candidates implicated in the formation of the clustering of PF terminals within the striatal matrix. Hence, Ten-m3 may be the first molecular candidate proposed to control the guidance and patterning of thalamostriatal axons from the PF. Further evidence for this comes from the corresponding temporal patterns of Ten-m3 expression in the striatum and PF, with axons from the PF first reaching the striatum at approximately E17 in mice (Chapter 4), at the same time as the first expression of Ten-m3 was observed in these structures. Additionally, as mentioned above, the expression of Ten-m3 in corresponding high-dorsal to low-ventral gradients in the striatum and PF correlates with the topography of PF terminals within the striatum (Lanciego et al., 2004). Hence, the expression patterns of Ten-m3 provides strong evidence that it may be involved in the guidance of thalamostriatal projections. This possibility will be examined in the next chapter.

Chapter 3

Ten-m3 mediates thalamostriatal connectivity

Introduction

In early models of basal ganglia circuits, the thalamus was viewed as a relay station for directing afferents from the output nuclei, SNr and GP, back to S1 and M1 cortex. These relay nuclei predominantly referred to the VA/VL thalamic subdivisions (see Albin et al., 1989 for a review). The proposed existence of direct thalamic afferent projections to the striatum in the 1940s (Vogt and Vogt, 1941), have since been shown anatomically to comprise the second largest source of input to the striatum, after cortical afferents (Cowan and Powell, 1956; Powell and Cowan, 1954). These projections are glutamatergic and originate from multiple thalamic nuclei, the largest and most well-established of which arise from the PF nucleus.

Thalamostriatal projections have been examined in rats (Gonzalo, 2002; Lanciego et al., 2004; Veening et al., 1980; Vercelli et al., 2003), monkeys (Parent and Parent, 2005b), cats (Herkenham and Pert, 1981), and to a small extent, in mice (Ellender et al., 2013). Axons from the PF project ipsilaterally to all areas of the striatum with a generally conserved RC and ML topographic correspondence between the thalamus and striatum.

These projections are also compartment specific, terminating in the striatal matrix (Herkenham and Pert, 1981; Sadikot et al., 1992b; Xu et al., 1991), where they are arranged into numerous patches (Deschênes et al., 1996b; Gonzalo, 2002; Parent and Parent, 2005b). Single cell tracing experiments (Deschênes et al., 1996b; Parent and Parent, 2005b) indicate that this occurs at the single cell level, where axon collaterals biruficate to terminate in a number of clusters throughout the striatum. These terminals predominantly synapse onto MSNs and cholinergic interneurons, and to a smaller extent, PV-positive interneurons (see Smith et al., 2004 for a review).

In contrast to the well established anatomical organisation of thalamostriatal projections their functions are less well characterised. The striatum, itself, has been studied extensively, particularly in disease states such as Parkinson's disease and Huntington's chorea (see Albin et al., 1989 for a review), along with rodent studies, implicating it in a plethora of roles, including motor control, associative and motor learning and motivation (see Gerfen and Wilson, 1996 for a review). The functions of the thalamostriatal pathway have only more recently come to light. As a major component of the ascending activating system, the PF has been implicated in roles in alertness and attention (Kinomura et al., 1996; Minamimoto and Kimura, 2002). Early lesion studies in rats suggested a role for the PF in the extinction of learned avoidance conditioning tasks (Bohus and de Wied, 1967) and learned sets in reversal learning tasks (Thompson et al., 1981). In humans, MRI and PET experiments indicate activation of the CM-PF, the primate equivalent of the rodent PF, in tasks requiring subjects to direct attention to salient visual stimuli (Hulme et al., 2010) and to switch to an attentional state (Kinomura

et al., 1996). Similarly, inactivation studies in non-human primates suggest that the CM-PF provides the striatum with information about salient sensory stimuli (Matsumoto et al., 2001) and attentional orienting (Minamimoto and Kimura, 2002). More specifically, Minamimoto and Kimura (2009) suggest that the CM-PF acts to reset the pre-biasing function of the striatum to aid in the selection and execution of appropriate actions to unexpected events. Paradigms to test and measure attention are less well established for rodents. Many studies, similar to the early studies performed by Thompson et al. (1981), utilise goal-oriented paradigms involving various mazes to test the animals ability to associate a particular action with a reward (Bradfield et al., 2013; Ragozzino, 2004).

Interestingly, even less is known about the mechanisms involved in the formation of striatal circuits. Over recent years, however, some molecular candidates have been investigated. Of note are studies on the family of Eph receptors and ephrin ligands, a number of which have recently been shown to be present in the striatum and its afferent/efferent structures. Specifically, the complementary expression patterns of EphB1 and its ligand, ephrinB2, have roles in the development of the nigrostriatal pathway (Halladay et al., 2000; Richards et al., 2007; Yue et al., 1999). Moreover, ephrinB3 is specifically associated with the mesostriatal dopamine projection (Sun et al., 2010). Most recently, the patchy expression of EphA7 in the striatal matrix and ephrinA5 in the SN was shown to be required for the accurate guidance of striatofugal neurons to specific subregions of the SN and GP (Tai et al., 2013) and the subsequent maturation of motor skills (Sheleg et al., 2013). In the thalamostriatal pathway, cerebellin-1-expressing thalamostriatal axons from the PF influence spine density and hence, the number of

synapses formed onto striatal MSNs (Kusnoor et al., 2010). Furthermore, semaphorin 3E and its receptor Plexin-D1 are proposed to control the degree and arrangement of thalamostriatal synapses to direct-pathway MSNs (Ding et al., 2011).

The current study will be the first to characterise the mouse thalamostriatal pathway, with the main aim of investigating the impact of Ten-m3 deletion on this pathway in adults. As shown in Chapter 2, Ten-m3 is expressed in the striatum in a patchy pattern, which is reminiscent of the clustered distribution of thalamostriatal terminals originating from the PF. Furthermore, Ten-m3 is expressed in the PF during development, where its graded expression along the DV axis corresponds to that in the striatum. These data provide strong support for a potential role for this gene, previously shown to have axon guidance roles in the visual system (Dharmaratne et al., 2012; Leamey et al., 2007b), in the development of the thalamostriatal pathway. This will be investigated by performing anterograde and retrograde labeling of the thalamostriatal pathway in adult wild type (WT) and Ten-m3 KO mice. Further, the overall structure of the striatum and PF will be examined. Moreover, potential behavioural deficits associated with changes in the thalamostriatal pathway in KO mice will be investigated using tests of motor function/coordination and motor learning.

Methods

All procedures were performed on pigmented WT (Ten-m3$^{+/+}$) and Ten-m3 KO (Ten-m3$^{-/-}$) mice, and were approved by the Animal Ethics Committee of the University of Sydney and conformed to NHMRC guidelines.

Generation of Ten-m3$^{-/-}$ mice and genotyping

Ten-m3 animals were originally obtained from Professor Reinhard Fassler's laboratory in Munich. Details of the generation of Ten-m3 KO mice were described previously (Leamey et al., 2007b). Briefly, exon 4 of the transmembrane segment of the Ten-m3 gene was disrupted with a neomycin gene. This targeting vector was electroporated into R1 embryonic stem cells and these injected into C57/Bl6 blastocysts. The resulting chimeras were crossed with C57/Bl6 mice to produce WT, heterozygous (Ten-m3$^{+/-}$) and KO mice. Mice were subsequently crossed with Sv129 mice and maintained on this crossed background to enhance survival of KO animals. Hence, progeny are of varied pigment. Breeding was performed between homozygous or heterozygous Ten-m3 animals, and experiments were performed on pigmented WT and KO mice. Littermates were used where possible.

Genotyping was performed with the assistance of Rajini Nagarajah (research assistant, Leamey laboratory) prior to the commencement of experiments. Genotyping was performed from toe/tail biopsy. Briefly, tissue was agitated in lysis buffer containing 50 mM potassium chloride, 10 mM Tris-HCl pH 9.0, and 0.1% Triton X-100, at 500 rpm at

95ºC overnight. PCR was performed on this genomic DNA using primers to the Ten-m3 sequence: F_ACGACGCCACTGTTCAGTAC, R_TGGTTCAACACCACCTTCAC, and a third primer directed at the neomycin sequence: R_GATTAGATAAATGCCTGCTC. Genotype was determined using agarose gel electrophoresis, with WTs showing a band at 320bp, Ten-m3 KOs a band at 450bp, and heterozygotes showing both.

Anterograde tracing

These experiments were initially commenced as part of the student's Bachelor of Science (Advanced)(Honours) degree. The work was significantly expanded as part of her PhD candidature, however, a subset of the tracing data presented here was also included in her Honours thesis (Tran, 2009).

Anterograde tracing was performed on WT and KO adult mice. Mice were anaesthetised with 2-4% isofluorane in oxygen and their heads positioned and stabilised in a rodent stereotax (Model # 922, Kopf instruments, USA) using nose and ear clamps. The hair on the crown was removed, the area sterilised and an incision made to expose the bregmal and lamboidal sutures. The location of the PF was determined using stereotaxic coordinates (Paxinos and Franklin, 2001), to be approximately 2.25 mm caudal of bregma, 0.85 mm lateral of the midline, and 3.2 mm deep, at a standard distance of 4 mm between bregmal and lamboidal sutures. Since this distance varied considerably in KOs, ratiometric calculations were performed on the coordinates for all dimensions except depth, which was kept constant, for these animals. The calculations were as follows:

$$\text{Position caudal of bregma} = \frac{2.25 \times (\text{bregma-lambda})}{4}$$

$$\text{Position lateral of midline} = \frac{0.85 \times (\text{bregma-lambda})}{4}$$

A craniectomy was performed using a dental drill (Micro-torque) and tweezers to remove the immediately surrounding skull and dura. Unilateral injections of 10% biotinylated dextran amine (BDA; Molecular Probes; in distilled water) were made into the left hemisphere using borosilicate glass micropipettes connected to a picopump pressure injector (Model #PV830, WPI, USA). Following the surgery, the scalp was sutured, the animal allowed to recover and a survival period of 7 days was allowed for dye transport.

Following the recovery period, mice were anaesthetised using 4% isofluorane in oxygen and then euthanised with an intraperitoneal injection of an overdose of sodium pentobarbitone (Lethabarb). Animals were then transcardially perfused with 12-15 mL 0.9% saline, followed by 4% (w/v) paraformaldehyde in 0.1 M PB. Brains were dissected and postfixed in the same fixative overnight at 4°C. The tissue was washed in 0.1 M PB and then submerged in a gelatin-albumin mixture for 10 min prior to embedding in gelatin-albumin hardened with a few drops of 25% gluteraldehyde. Coronal sections of 60 µm thickness were collected using a vibratome (1000 Plus Sectioning System) and organised into alternate series' for subsequent reactions.

One series of sections was processed for the BDA injection sites and the resulting thalamostriatal terminal label using an avidin-biotin complex (ABC)-diaminobenzidine

(DAB) reaction. Sections were washed 3 x 5 min in 0.1 M PB and then quenched in a 45% ethanol and 0.3% hydrogen peroxide in 0.1 M PB for 30 min. Sections were rewashed 3 x 5 min in 0.1 M PB before incubating in ABC (Vectastain ABC kit, Vector Labs; 1% in 0.1 % TritonX-100, 0.1 M PB) for 1 hr at RT or overnight at 4ºC. Sections were washed 3 x 10 min in 0.3 % TritonX-100 in 0.1 M PB and then reacted with a solution of DAB and 0.06% hydrogen peroxide in 0.1 M PB for 20-30 min. Sections were washed 2 x 10 min in 0.1 M PB and then mounted onto gelatinised glass slides in a gelatin and 0.1 M PB solution. Slides were left to dry overnight and then dehydrated in 70%, 95% and 2 x 100% ethanol solutions for 1 min each, followed by clearing in histolene for 5 and then 10 min. Slides were coverslipped with entellan (ProSciTech).

Double labeling for anterograde terminals and μ-OR

A representative group of sections through the striatum from the second series of sections were double labeled for thalamostriatal terminals and μ-OR to examine the compartmentalisation of these projections. These sections were chosen from rostral striatum, where striosomes are most numerous (Graybiel and Ragsdale, 1978). Sections were washed, quenched and incubated in ABC as above. After incubation in ABC, sections were washed 3 x 10 min in 0.3% TritonX-100 and then reacted with fluorescein reagent (Perkin Elmer TSA kit; 1 in 50 in amplification reagent) for 3 min to reveal thalamostriatal terminals. Sections were then washed and blocked with 4% normal goat serum (NGS) in 0.3% TritonX-100 for 30 min at RT. Sections were incubated in a solution of rabbit polyclonal anti-μ-OR antibody (Abcam; 1:2000 in 2% NGS, 0.3% TritonX-100. 0.1 M PB) overnight at 4ºC. After washing, sections were incubated in

goat anti-rabbit secondary antibody conjugated to Alexa Fluor-594 (Invitrogen;1:200 in 4% NGS, 0.3% TritonX-100, 0.1 M PB) for 2 hours at RT. Sections were washed 2 x 5 min in 0.1 M PB and mounted onto glass slides and subsequently coverslipped and counterstained with 50% glycerol in 0.1 M PB with DAPI. Control experiments, consisting of no primary and no secondary forms, were performed for initial trials to confirm signal specificity.

Nissl staining

The remaining sections of this second set were Nissl stained to reveal neural structure. Sections were mounted onto gelatinised glass slides and allowed to dry overnight before dehydrating in 70%, 95% and 2 x 100% ethanol solutions for 1 min each, clearing in histolene for 5 and then 10 min and subsequently rehydrating across the same series of ethanol solutions. Slides were then rinsed in distilled water and stained with 0.025% thionin for 2 min, re-rinsed and any excess thionin removed in 70% ethanol. Sections were then dehydrated in 95% and 2 x 100% ethanol solutions for 1 min each and cleared in histolene for 5 and 10 min before coverslipping with entellan (ProSciTech).

Imaging and analysis

DAB labeled sections were imaged using transmitted light microscopy on the Nikon Eclipse e800 (Bosch Advanced Microscopy facility, University of Sydney). Images were taken for Nissl and DAB-reacted sections using Leica Application Suit 3.1.0 software. All sections that were taken as multiple images were merged using the reposition only or

interactive layout modes in the photomerge function of Adobe Photoshop CS3 to form a composite image. Sections that were double labeled for BDA and μ-OR with fluorescence were imaged on the Zeiss deconvolution microscope using filters for DAPI (λ = 360 nm) to view cell nuclei, Texas Red (λ = 594) to visualise striosomes, and Alexa Fluor 488 (λ = 488) to reveal thalamostriatal terminals. Images were taken using the AxioCam HR camera and exported using AxioVision Rel. 4.7 software.

A representative section well labeled for BDA and μ-OR, that is, from rostral striatum, was chosen from all successfully BDA injected brains (WT: n = 8, KO: n = 8) for analysis using Image J. First, a semi-quantitiative analysis was performed to assess possible changes in the patchy pattern of thalamic terminals between genotypes. The perimeter of the striatum was traced and any obvious artefacts, such as bubbles through the section, and edge effects produced from photomerging were coloured in using the paintbrush tool, before proceeding. Grayscale images of BDA label were converted to binary images using the 'make binary' function, and the resulting product used to produce a surface plot. A neutral assessor, who was blind to genotype, was asked to rank the surface plots from the most heterogeneous (ie with the most numerous high peaks and troughs) to most homogeneous (ie. smoothest surface). The results were analysed using a Mann-Whitney test in Matlab (Mathworks).

The same images were subsequently used to trace the perimeter of labeled terminals within the borders of the striatum. This area was analysed using a paired t-test, where statistical significance was defined by $p < 0.05$. Further, these binary images were

processed for analysis in R to create a heat map of the average distribution of terminals from all WT and KO cases. For this, pixels outside of the striatal contour were cleared, and a box was drawn to contain this contour using the 'to bounding box' function to ensure that all images would give the same dimension matrices in R. Images were cropped, and the xy coordinates of black pixels obtained using ImageJ. These coordinates were used to produce 100 x 100 matrices in R, and these matrices subsequently averaged across all WT and KO cases and a representative heat map produced for each genotype. Graphs plotting the distribution of label along the ML axis was generated by summing pixels across the y axis in the averaged matrices. These distributions were analysed using a Kolmogorov-Smirnov (K-S) test.

Retrograde tracing in adult mice

Retrograde tracing studies were performed on WT and KO adult mice to further investigate changes in the thalamostriatal pathway in the absence of Ten-m3. Here, 2 injections of cholera toxin subunit-B (CTB) conjugated to different fluorophores (Alexa Fluor 488 and 594) were injected into distinct sites, separated by 500 µm along the RC axis of the striatum. These surgeries were performed as for BDA tracer injections. The location of injection sites for WT animals was determined from Paxinos and Franklin (2001). Initial experiments using these coordinates in KOs resulted in an obvious caudal positioning of the injection sites compared to WTs. Hence, coordinates were empirically recalculated for KOs. These are summarised in Table 3.1. Unilateral injections of 1% CTB (Invitrogen) were made into the left hemisphere using a picopump pressure injector (Model #PV830, WPI, USA), as described previously. A survival period of 5 days was

allowed for dye transport before animals were euthanised with sodium pentobarbital, perfused with 4% paraformaldehyde and brains sectioned on a vibratome, as described above. Sections were collected onto glass slides and immediately imaged on the Zeiss Deconvolution Microscope using filters for DAPI (λ = 360 nm), Texas Red (λ = 594) and Alexa Fluor 488 (λ = 488) to reveal injection sites in the striatum and retrogradely labeled cells in the PF.

Image analysis was performed using ImageJ. For injection sites, a single image from the centre of the main bolus of the injections was selected from each animal for analysis (WT: n = 6, KO: n = 6). The perimeter of the striatum and the green and red injection bolus were traced, and the areas of these contours measured. Distances between green and red injection sites to the rostral striatal pole were determined using the 'to bounding box' function to bound the striatum, and green and red contours. The centroid function was used to determine the centre of green and red contours and the distance between these centres was also measured. For the PF, 4 consecutive sections through the ML extent of the lateral PF were chosen for analysis. A Nissl stain was performed on sections through the PF after imaging, to aid in identification of the borders of the PF. The perimeter of the PF was traced using DAPI and Nissl images for reference. Green and red cells were counted and contours drawn around these populations and the overlapping area. The area occupied by green and red cells and area of overlap was summed across the 4 sections. These areas, volumes and total cell counts were compared between genotypes using a t-test.

Table 3.1. Stereotaxic coordinates used for retrograde injections into the striatum.

	WT		KO	
	Alexa Fluor 488	Alexa Fluor 594	Alexa Fluor 488	Alexa Fluor 594
Rostral-caudal (from bregma)	+0.5 mm	0 mm	+0.9 mm	+0.4 mm
Lateral of midline	2.2 mm			
Depth	2.5 mm			

Striatum and PF area and cell counts

Nissl-stained coronal sections through the striatum and PF were used to determine potential changes in the number of cells between genotypes using the Leica stereology microscope (Advanced Microscopy Facility, University of Sydney). For the PF, 1-2 sections through rostral and mid-caudal levels of the structure, from 3 animals, totalling 5 distinct images, were analysed for each genotype. For the striatum, 1 section from the left and right hemispheres through separate commissural and caudal striatal levels from 3 animals were analysed where possible. Hence, for commissural sections, cell counts were performed in a total of 6 images for KOs and 4 for WTs. For caudal sections, a total of 5 images were analysed each, for KOs and WTs. Cells were counted using the optical fractionator method in the Leica Stereo Investigator software and data was collated in Microsoft Excel and analysed using a t-test.

ChAT immunohistochemistry

Distribution of cholinergic interneurons in the striatum was investigated in adult WT and KO animals using immunohistochemistry for ChAT. Animals were euthanised, perfused, postfixed, embedded in gelatin-albumin and sectioned coronally, as described above. Sections were washed 3 x 10 min in 0.3% TritonX-100 in 0.1 M PB. All subsequent washes and solutions were performed and made in 0.3% TritonX-100 in 0.1 M PB unless stated otherwise. Sections were then blocked with 4% NRS for 1 hour at RT, washed 3 x 10 min and then incubated in goat anti-ChAT IgG (Millipore; 1:500 in 4% NRS) overnight at 4°C. Sections were washed 3 x 10 min and subsequently incubated in rabbit anti-goat-Alexa Fluor-594 secondary antibody (Invitrogen; in 4% NRS) for 2 hr at RT. Finally, sections were washed 2 x 5 min in 0.1 M PB and mounted and coverslipped with 50% glycerol in 0.1 M PB with DAPI. Control experiments, consisting of no primary and no secondary forms, were performed for initial trials to confirm signal specificity. Images were taken on the Zeiss Deconvolution Microscope using filters for DAPI (λ = 360 nm) and Texas Red (λ = 594). In Image J, the perimeter of the striatum was traced and ChAT-positive cells counted/marked using the point tool. The centroid tool was used to determine the centre of the striatal contour and straight lines drawn at appropriate X and Y coordinates to mark the ML and DV axes. Areas of each quadrant (DM, DL, ventromedial (VM), VL) were measured. The coordinates of ChAT-positive cells were obtained and exported to Microsoft Excel where the data was filtered to determine the number of cells in each quadrant of the striatum. These values were compared between genotypes using a repeated measures ANOVA.

Footprint analysis

The gait of 7 x WTs and 7 x KOs was investigated using a footprint analysis as described previously (Lee et al., 2012b). Hind paws were painted with Vaseline and animals allowed to walk down a narrow path lined with white paper. Graphite powder was used to reveal the footprints. Using the third proximal interphalangeal joint as a reference, stride length, defined as the distance between the third proximal interphalangeal joint of each left or right pad separately, and step width, defined as the normal distance from the third proximal interphalangeal joint of one pad to the line connecting two pads on the contralateral side (see Fig. 3.9A) were measured. These distances were compared between genotypes using a repeated measures ANOVA.

Rotorod

A rotorod (IITC) was used to determine potential deficits in motor learning in Ten-m3 KO mice. A total of 11 x WT and 14 x KOs were tested. On day 1, mice were habituated on a static 7 cm diameter rod for 3 min. Mice that fell off during this period were simply placed back onto the rod. Animals were subsequently tested for time spent on the rod (latency) as it accelerated from 4-40 rpm across a maximum of 180 s. Trials consisted of 5 sessions per day, for 5 consecutive days, as initial studies indicated that KO performance improved to a level convergent with WTs after this period. Habituation was repeated for 1 min, every day prior to testing, and mice were removed and lanes cleaned between sessions. Data was analysed by comparing latencies between genotypes using a repeated measures ANOVA.

Results

Anterograde BDA tracing in adult mice

Expression studies (Chapter 2) indicated topographically corresponding gradients of Ten-m3 in the striatum and PF during development, suggesting potential roles for Ten-m3 in the targeting of thalamostriatal axons from the PF. Hence, anterograde tracing studies were performed to determine potential changes to the distribution of thalamostriatal terminals originating from the PF in Ten-m3 KO mice, compared to WT controls. These were performed in adults, when the anatomical characteristics of this projection, such as the patchy distribution of terminals within the striatal matrix, are well established in normal rodents (Gonzalo, 2002; Smith et al., 2009).

BDA injections were made into the PF of WT and KO mice, with those from 8 x WT and 8 x KOs successfully targeting the PF, and therefore included for analysis. Injections were aimed into the lateral portion of the nucleus, with respect to the fr, as this provided the largest cross-sectional area for which to aim. While these successfully targeted the lateral PF in all cases analysed (Fig. 3.1A, D), the extent of label and their location within the lateral PF varied somewhat between individual animals. Further, in 1 x WT and 2 x KO cases, some of the injected tracer also spilled into the medial part of the PF (Fig. 3.2A, D). Importantly, the average proportion of PF cross-sectional area filled with BDA tracer was not significantly different between genotypes ($p = 0.91$, t-test; see Fig. 3.5E).

Tracer injections into the PF produced anterograde terminal label in the striatum of both WT and KO animals (Fig. 3.1). In all cases, thalamostriatal terminals spanned most of the RC extent of the striatum and were strictly ipsilateral; no evidence of terminal label was observed in the contralateral striatum. The distribution of striatal label varied between subjects, and appeared to be dependent on the location of the tracer in the PF. In WTs, injections localised to the entire lateral PF (Fig. 3.1A) resulted in terminal label in the dorsal and lateral portions of rostral (pre-commissural) (Fig. 3.1B), and mid-caudal striatum (Fig. 3.1C). Dense patches of terminals were often distributed amongst areas of finer label (Fig. 3.1C; arrows), with areas completely devoid of terminals also evident within otherwise labeled regions (Fig. 3.1B, C; arrowheads). When tracer was localised only to the DL portion of the PF, terminals were located in dorsal striatum, whereas injections into VL PF resulted in terminals in lateral striatum (data not shown).

This overall topography was largely conserved in KOs (Fig. 3.1D-F), however, some differences were also evident. Injections into the entire lateral portion of the PF (Fig. 3.1D) also resulted in terminal label in the dorsal and lateral regions of rostral striatum (Fig. 3.1E). A large proportion of the label, however, was observed in more medial regions than the equivalent WT case (compare Fig. 3.1B and E). Generally, the distribution of label appeared to be more widespread in KOs compared to WTs following similar injections. At more caudal levels (Fig. 3.1F), terminals were seen in lateral striatum. Interestingly, in 3 of the 4 KO cases where dense terminal label was present in the vicinity of the VL quadrant in mid-caudal striatum, the label appeared to stop abruptly, almost as if at a border, as shown in the case in Fig. 3.1F. This was not the case

in similar sections from WTs, where if label was intense near this region it also invaded the mid-caudal VL area (3 out of 3 cases), as seen in Fig. 3.1C. In addition, terminals were more diffuse and homogeneously distributed in KOs compared to WTs, which had a patchier appearance. Similar to WTs, however, small areas completely devoid of terminal label were also evident in KOs (Fig. 3.1E, arrowhead).

In cases where tracer spilled into cells medial of the fr (Fig. 3.2A, D), the topography of striatal terminals was more evidently different between genotypes. In WTs, terminals were localised to dorsal and the medial two-thirds of rostral striatum (Fig. 3.2B). This was similar in caudal regions, although the focus of terminal label was more ventral compared to rostral striatum (Fig. 3.2C). Here, there was again evidence of patches of dense terminal label (Fig. 3.2B, C; arrows), areas with sparser label as well as regions completely devoid of terminals (Fig. 3.2B; arrowhead). In KOs, these injections produced terminal label that filled much of rostral (Fig. 3.2E) and caudal striatum (Fig. 3.2F). Rostrally, terminals were distributed throughout most of the striatum with the exception of the far dorsal and medial areas. Similarly, in more caudal regions, thalamic terminals covered the majority of the striatum except for the VL quadrant, as noted above. Likewise, terminals were more homogeneously distributed with little evidence of patches of label, and covered a larger area compared to WTs. Similar to WTs, however, small regions devoid of terminal label were similarly observed at all levels through the striatum (Fig. 3.2E, F; arrowheads).

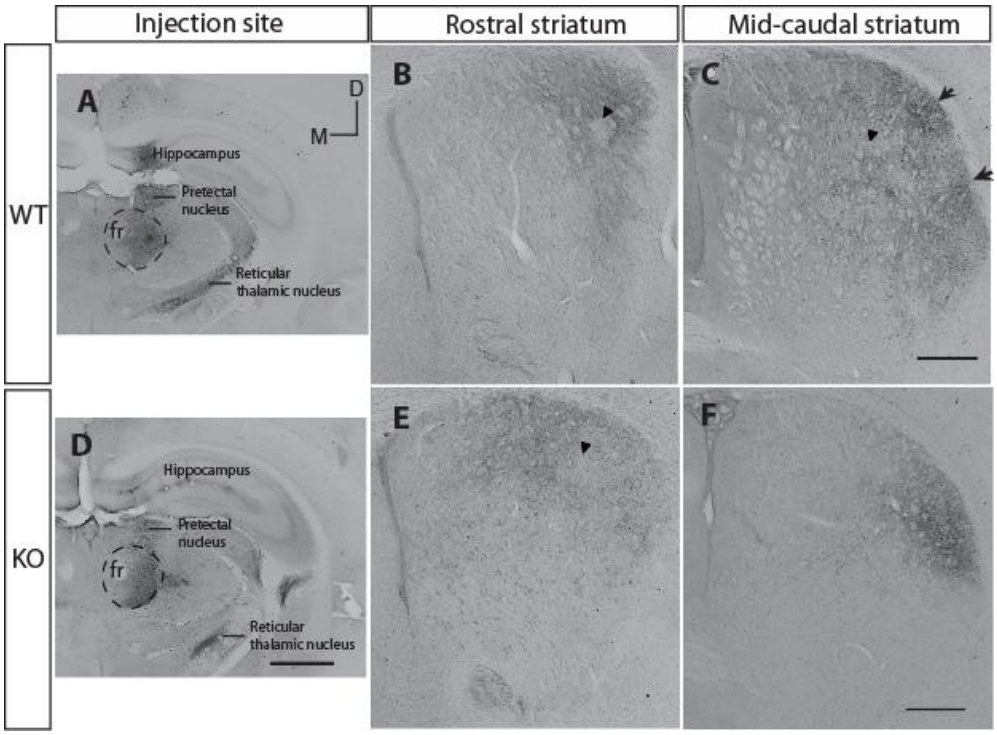

Figure 3.1. Anterograde BDA injections filling lateral PF in adult mice.

(A) A coronal section showing BDA injection into lateral PF (dashed line) in WT. Tracer was observed in the pretectal nucleus and hippocampus along the injection tract. Anterograde and retrograde label was observed in the reticular thalamic nucleus.

(B-C) Rostral (pre-commissural) and mid-caudal coronal sections through ipsilateral striatum showing terminal label resulting from injection in (A). (B) In rostral striatum, terminals were located in dorsal to lateral regions, where 'holes' within the labeled area were evident (arrowhead). (C) In mid-caudal striatum, terminals covered medial and VL regions. Terminals were often distributed in patches (arrows) amongst areas of sparser label. Areas devoid of terminals were also evident (arrowhead).

(D) An equivalent injection site to (A) in KO. As in (A), tracer spread to the pretectal nucleus along the injection tract and label was observed in the reticular thalamic nucleus.

(E-F) As for (B-C) showing terminal label resulting from injection in (D). (E) Rostrally, terminals were found in dorsal striatum where they were distributed more medially than in WTs. Like in WTs, areas devoid of terminal label were evident (arrowhead). (F) In mid-caudal sections, terminals were seen in lateral striatum but avoided the VL area. Terminal label was generally more diffuse and homogeneously distributed compared to WTs.

Scale bar in D applies to A. Scale bar in C applies to B. Scale bar in F applies to E. Scale bar in D indicates 1 mm. Scale bars in C and F indicates 500 μm. D is dorsal, M is medial.

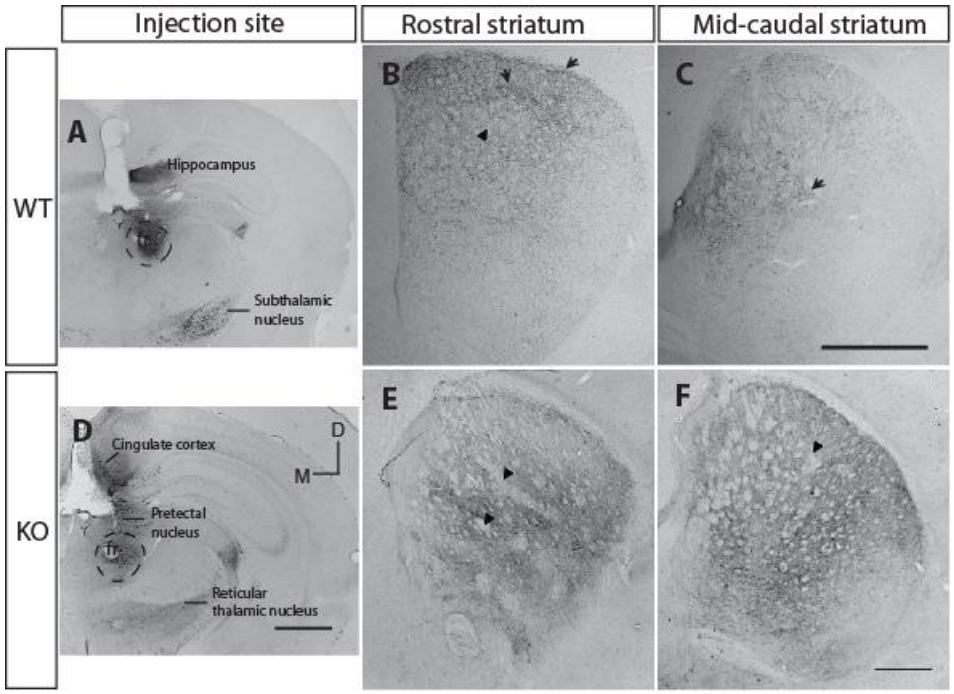

Figure 3.2. Anterograde BDA injection spilling into medial PF in adult mice.

(A) A coronal section showing BDA injection lateral to the fr, however, also spilling into medial regions of the PF (dashed line) in WT. BDA also spread to medial hippocampus along the injection tract. Anterograde and retrograde label was observed in the subthalamic nucleus.

(B-C) Rostral (pre-commissural) and mid-caudal coronal sections through ipsilateral striatum showing terminal label resulting from the injection in (A). (B) Rostrally, terminals were localised to dorsal and the medial two thirds of the striatum. Again, dense (arrows) and sparser patches of terminals were observed, as were 'holes' (arrowhead) within the labeled region. (C) In mid-caudal striatum, terminals were located medially, with patches of dense terminals (arrows) evident.

(D) An equivalent injection site to (A) in KO. BDA also spread to the pretectal nucleus and cingulate cortex along the injection tract. Anterograde and retrograde label was observed in the reticular thalamic nucleus.

(E-F) As for (B-C) from the injection in (D). (E) Rostrally, terminals were distributed throughout mid-lateral striatum. Regions devoid of terminal label were also evident (arrowhead). (F) Caudally, terminals covered the majority of the striatum with the exception of the VL segment. Terminals were more homogeneously distributed than in WTs, although small regions devoid of terminal label were also evident (arrowhead).

Scale bar in D applies to A. Scale bar in C applies to B. Scale bar in F applies to E. Scale bar in D indicates 1 mm. Scale bars in C and F indicates 500 μm. D is dorsal, M is medial.

Dual labeling for striatal terminals and μ-OR for striosomes was used to determine the compartmentalisation of thalamostriatal terminals in WTs (Fig. 3.3 A-C) and KOs (Fig. 3.3 D-F) in rostral striatum, as striosomes are most prominent here (Graybiel and Ragsdale, 1978). Images of striatal terminals revealed 'holes' within otherwise labeled regions in WTs (Fig. 3.3A, arrowhead) and KOs (Fig. 3.3D, arrowhead), as noted above. Striosome patches were distributed throughout the striatum in WTs (Fig. 3.3B) and KOs (Fig. 3.3E), being most prominent in rostral and dorsal striatum, and fading off more caudally. The distribution of, and total area occupied by striosomes was similar between genotypes (Tran, 2009). Merged images (Fig. 3.3C, F) showed terminals forming tight boundaries around striosomes, in both WTs (Fig. 3.3A-C, arrowheads) and KOs (Fig. 3.3D-F, arrowheads). Hence, thalamic terminals target the matrix in KOs, as in WTs.

As mentioned above, thalamostriatal terminals appeared to be distributed differently within the matrix in WTs compared to KOs. In WTs, terminals (Fig. 3.4A, green) formed dense clusters (Fig. 3.4A, arrows) within the striatal matrix which were interspersed by patches containing sparser label and regions completely devoid of terminals, with the latter corresponding to striosomes (Fig. 3.4A, red). In KOs, this patchy pattern was less obvious, with terminals generally distributed in a diffuse, more homogeneous fashion (Fig. 3.4B, green), with the notable exception of striosomes (Fig. 3.4B, red) where no label was seen. At lower power, terminals were dense near the focus of the labeled region in KOs, seen as the most brightly labeled area in Fig 3.3D, E (*), and, within the matrix, declined fairly uniformly away from this region. This was in contrast to that in WTs, where multiple densely labeled patches were seen (Fig. 3.3A, C, arrows).

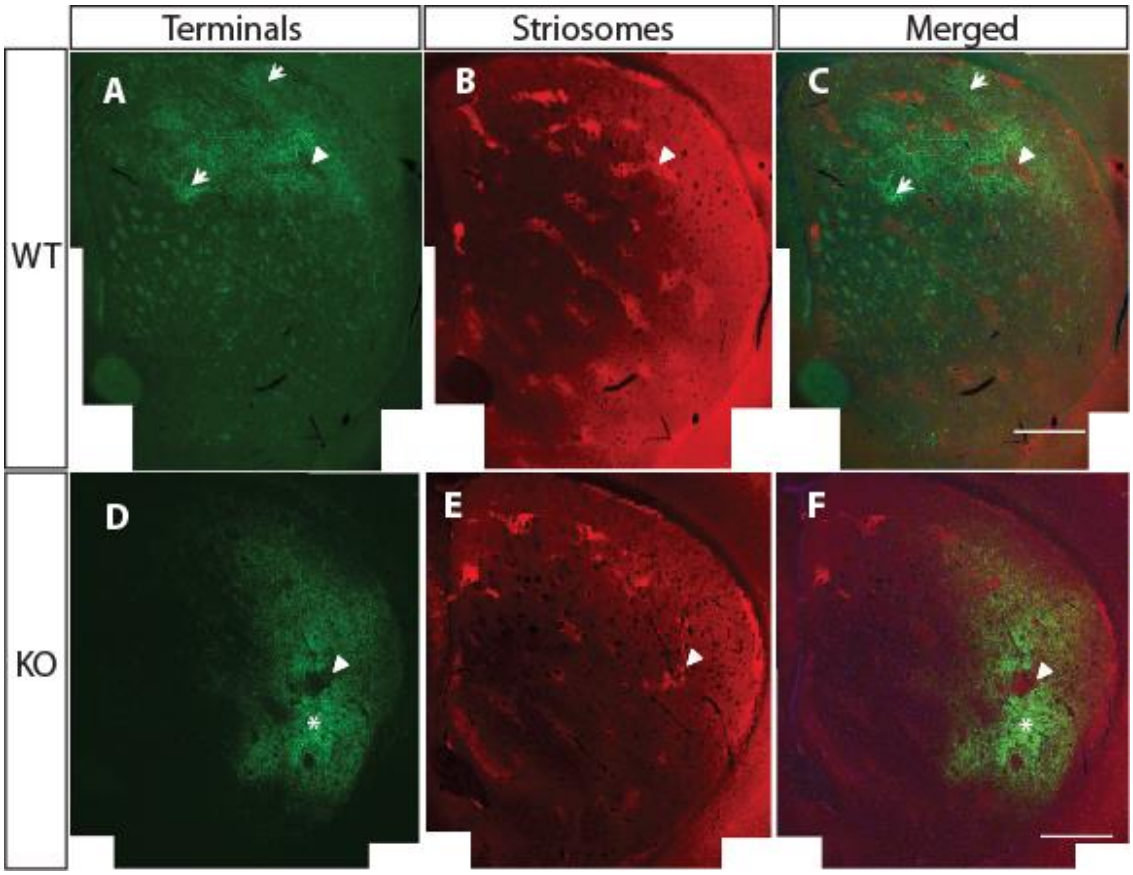

Figure 3.3. Compartmentalisation of thalamostriatal terminals.

Coronal sections through rostral striatum showing dual labeling for striatal terminals (green) and μ-OR, labeling striosomes (red).

(A-C) In WTs, regions completely devoid of thalamostriatal terminals (A, arrowhead) correlated with striosomes (B, arrowhead), the boundaries of which were tightly surrounded by terminals (C). Hence, thalamic terminals were localised to the matrix compartment. Within the matrix, terminals had a patchy appearance, with areas of dense (arrows) and sparse label.

(D-F) Similarly, in KOs, regions completely devoid of thalamostriatal terminals were also evident (D, arrowhead). These correlated with striosomes (E, arrowhead), such that terminals surrounded striosomes in the merged image (C, arrowhead). Hence, thalamostriatal terminals remained localised to the matrix compartment in KOs. Within the matrix, thalamic terminals were distributed more homogeneously, being dense near the focus of the labeled region (*) and declining uniformly away from this area, with little evidence of the multiple dense patches seen in WTs.

Scale bar in C applies to A and B. Scale bar in F applies to D and E. Scale bars indicate 500 μm. For all images, dorsal is up, medial is left.

A semi-quantitative analysis was performed to confirm the difference observed in the degree of 'patchiness' of thalamostriatal terminals. For this, surface plots were created using ImageJ to depict the intensity of label across 2-dimensions for individual WT (Fig. 3.4C) and KO cases (Fig 3.4D). Here, peaks represented intensity of label and distribution of peaks varied according to the spread of terminals across the DV and ML axes. In WTs, the distribution of peaks was often more widespread and formed multiple clusters across the 2-dimensions (Fig. 3.4C), representing the highly patchy organisation of terminals in these animals. In KOs, fewer clusters of peaks were observed, giving rise to a smoother appearance in the surface plots (Fig. 3.4D) compared to WTs, corresponding to the more homogeneous distribution of terminals in these animals. Surface plots were ranked by an assessor who was not involved in the experiments and who was blind to genotype, from the most heterogeneous (ie. the 'peakiest') to the most homogeneous (ie. smoothest), in terms of the number and distribution of peaks. Statistical analysis on this ranking revealed a significant difference between the patterning of thalamostriatal terminals between genotypes ($p = 0.002$, Mann-Whitney test).

Table 3.2. Ranking of surface plots representative of the'patchiness' of thalamostriatal terminals in WT and KO mice.

	"peakiest" ----------> smoothest																
Rank	1	2	3	4	5	6	7	8	9	10	11	12	13	14	15	16	17
Genoptype	WT	WT	WT	WT	WT	WT	WT	KO	KO	WT	WT	KO	KO	KO	KO	KO	KO

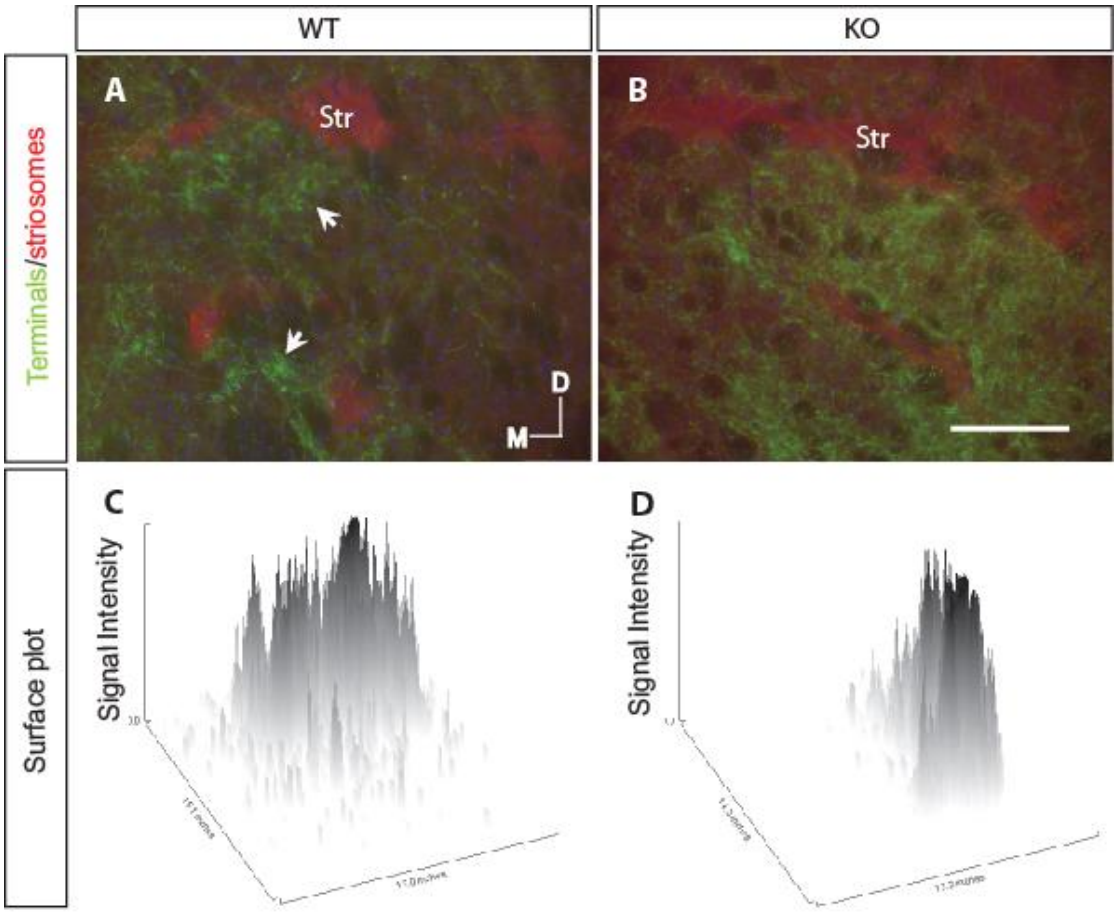

Figure. 3.4. The characteristic patchy pattern of thalamostriatal terminals is abolished in Ten-m3 KO mice.

(A) High power image of the patterning of thalamostriatal terminals (green) around striosomes (Str, red) in WT. These terminals, confined to the striatal matrix, were patchy, forming dense clusters (arrows) surrounded by more faintly labeled terminals.

(B) High power image of the patterning of thalamostriatal terminals (green) around striosomes (Str, red) in KOs. Terminals remained confined to the matrix, however, where they were more homogeneously distributed in the matrix.

(C-D) Surface plots representing thalamostriatal terminals. Peaks represent intensity of label and distribution of peaks varied according to the spread of terminals across the DV and ML axes. (C) In WTs, the distribution of peaks was often more wide spread and formed multiple clusters across the 2-dimensions, reflecting the patchy organisation of terminals in these animals. (D) In KOs, fewer clusters of peaks were observed, resulting in a smoother plot, to represent the more homogeneous distribution of thalamostriatal terminals in these animals.

Scale bar in B applies to A. Scale bar indicates 200 μm. For A and B, D is dorsal, M is medial.

In addition to the apparent loss of targeting specificity, thalamostriatal terminals appeared to cover a larger area of the striatal matrix in KOs compared to WTs. To analyse this, the same images from rostral striatum used to generate surface plots were averaged to produce a single representative heat map showing the distribution of thalamostriatal terminals for WTs (Fig. 3.5A) and KOs (Fig. 3.5B). In WTs, terminals were predominantly localised to dorsal and lateral striatum, while those in KOs extended considerably into medial striatum. Analysis of the average number of pixels across the ML axis of the striatum (Fig. 3.5C) indicated a significant shift in terminal label in KOs compared to WTs ($p < 0.001$, K-S test). Further, statistical analysis indicated that thalamostriatal terminals covered a significantly larger area of the striatum in KOs compared to WTs (Fig. 3.5 D, *; WT: 32.07 ± 5.27 (mean (AU) ± SEM), n = 8; KO: 52.43 ± 6.49 (mean ± SEM), n=8; $p = 0.03$, t-test). This difference arose from similar injection sizes between genotypes (Fig. 3.5 E; $p = 0.91$, t-test), indicating that differences in terminal area between WT and KOs were the result of genotypic differences.

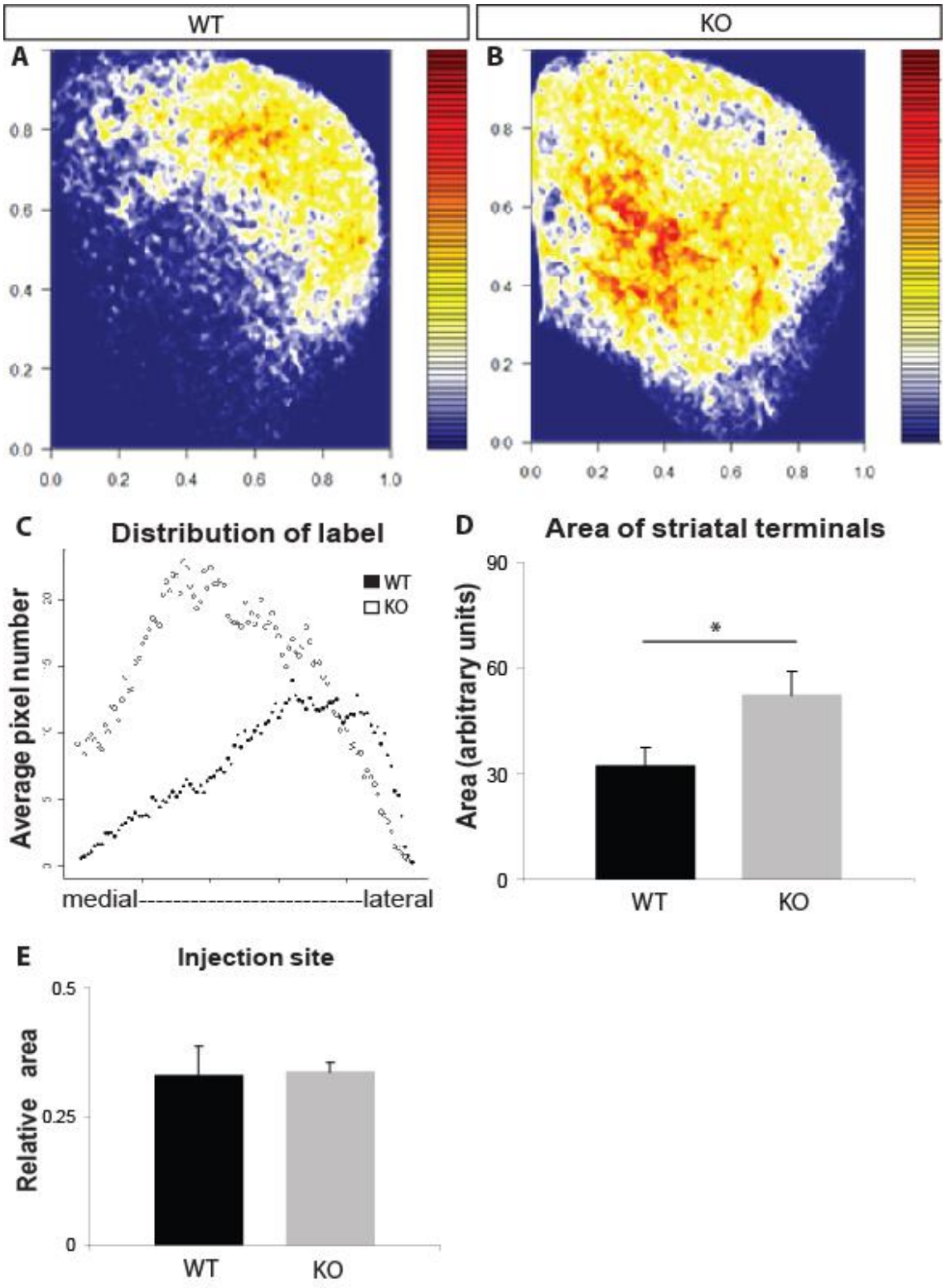
WT
KO
A
B
0.0
0.2
0.4
0.6
0.8
1.0
C
Distribution of label
Average pixel number
WT
KO
medial----------lateral
D
Area of striatal terminals
Area (arbitrary units)
90
60
30
0
*
WT
KO
E
Injection site
Relative area
0.5
0.25
0
WT
KO

Figure 3.5. Thalamostriatal terminals cover a larger area of the striatal matrix in Ten-m3 KOs.

(A-B) Heat maps representing the average distribution of thalamostriatal terminals in rostral striatum. (A) In WTs, terminals were predominantly focused in dorsal and lateral striatum, with some extending medially. (B) In KOs, terminals covered the entire striatum, with the majority of label focused in mid striatum, extending considerably more medially than WT cases.

(C) The average number of pixels across the ML axis of the striatum in WT (closed circles) and KO (open circles). There was a significant shift in the distribution of thalamostriatal terminals between genotypes ($p < 0.001$, K-S test).

(D) Terminals occupied a significantly larger area of the striatum in KOs compared to WTs (WT: 32.07 ± 5.27 (mean (AU) ± SEM), n = 8; KO: 52.43 ± 6.49 (mean ± SEM), n=8; $p = 0.03$, t-test.).

(E) The proportion of the PF filled with BDA tracer was similar between genotypes (WT: 0.33 ± 0.06 (mean ± SEM), n = 8; KO: 0.334 ± 0.02 (mean ± SEM), n=8; $p = 0.91$, t-test).

Values in graphs indicate mean ± SEM

Dual retrograde CTB tracer injections

Retrograde tracing experiments were performed to further investigate changes in the thalamostriatal pathway in Ten-m3 KO mice. Dual focal injections of CTB, conjugated to Alexa Fluor-488 (green; injected into rostral striatum) and Alexa Fluor-594 (red; injected 500 μm caudal to the rostral injection site) were made into the striatum and the subsequent subpopulations of retrogradely labeled green and red PF cells examined. Only cases where the focal injections were well separated and not overlapping, and where transport of the tracer had occurred, were considered for analysis.

In WTs, distinct focal injections into the striatum (Fig. 3.6A, inset) produced correspondingly distinct populations of cells in the PF (Fig. 3.6A, dashed line). Cells projecting to rostral striatum were predominantly located in rostral PF (Fig. 3.5A, green cells), while cells projecting to mid-caudal striatum were localised mostly to the caudal PF (Fig. 3.5A, red cells). This was particularly evident in the most lateral and medial sections where fewer labeled cells were observed. Both subpopulations of retrogradely labeled cells were, nevertheless, predominantly distributed along the majority of the RC axis of the PF, leading to the existence of an overlap region in the centre of the nucleus. In no cases were double-labeled PF cells observed, ie. all labeled cells were either green or red.

In KOs, distinct injections into the striatum (Fig. 3.6B, inset), like in WTs, produced distinct populations of retrogradely labeled cells in the PF (Fig. 3.6B, dashed line). Close inspection, however, revealed specific and intriguing changes. In the majority of cases,

the location of each subpopulation of retrogradely labeled cells appeared to be altered compared to that observed in WTs. Cells projecting to rostral striatum (Fig. 3.6B, green cells) were predominantly localised to the caudal two-thirds of the PF in KOs. Conversely, cells projecting to mid-caudal striatum (Fig. 3.6B, red cells) were predominantly focused in the rostral two-thirds of the PF. Hence, the location of the distinct subpopulations of labeled PF cells often appeared reversed along the RC axis in KOs compared to that observed in WTs. In some cases, this difference was less dramatic such that the two cell populations were intermingled in the middle of the PF. The overlap area occupied by green and red cells, however, was not evidently larger in KOs compared to WTs. Similarly, there was no evidence of double-labeled (ie. yellow) cells in this region in KOs.

Quantitative analysis was performed to determine potential differences in a number of parameters between genotypes. The volume over which green and red-labeled PF cells were distributed and their volume of overlap were analysed (Fig. 3.6C), as were the number of cells within the green and red subpopulations (Fig. 3.6E). The average volume occupied by green cells was similar between genotypes (Fig. 3.6C; $p = 0.75$, t-test). In contrast, the mean volume occupied by red cells was significantly smaller in KOs compared to WTs (Fig. 3.6C, *; WT: 17.44 ± 1.49 (mean (AU) ± SEM), $n = 6$; KO: 13.14 ± 0.88 (mean ± SEM), $n = 6$; $p = 0.037$, t-test). Comparison of the area occupied by the red cell population at five levels across the ML axis of the PF in sagittal sections, showed that these cells occupied a reduced area at each level along this axis, compared to WTs. This area, however, was only significantly reduced in medial striatal sections (Fig.

3.6D, *; WT: 4.17 ± 0.50 (mean (AU) ± SEM), n = 6; KO: 2.32 ± 0.36 (mean ± SEM), n = 6, p = 0.02, t-test), and showed a trend towards a reduction in sections through the middle of the nucleus (p = 0.07, t-test). The area occupied by green cells was not significantly altered at any level along the ML axis (data not shown). Further, although the volume occupied by the overlap of green and red cells was, likewise, reduced in KOs compared to WTs, this reduction was not significantly different between genotypes (Fig. 3.6C; p = 0.22, t-test).

Cell counts showed that the average number of retrogradely-labeled green and red cells was not significantly reduced in KOs compared to WTs (Fig. 3.6E; green: $F(1,10) = 0.32$, $p = 0.58$; red: $F(1,10) = 1.19$, $p = 0.30$, repeated measures ANOVA). Comparison of the number of red cells at five levels across the ML axis of the PF, however, showed that the number of red cells dropped off dramatically in medial sections, with those at the most medial levels showing a trend to being significantly reduced (p = 0.058, t-test). The number of green cells was not significantly altered at any level across the PF (data not shown). In addition, the area and number of separate green versus red cell subpopulations was not significantly different within genotypes (Fig. 3.6C, E; WT: $F(1,10) = 0.27$, $p = 0.62$; KO: $F(1,10) = 1.13$, $p = 0.31$, repeated measures ANOVA). It is particularly intriguing that the red tracer injections, which targeted mid-caudal striatum, approached or reached statistical significance across a range of parameters analysed, whereas the green injections which targeted rostral striatum did not.

To ensure that the above changes were not a result of differences in the injections, these sites were analysed for area (Fig. 3.6G) and location, with respect to the rostral pole of

the striatum and to each other (Fig. 3.6H). The area as a proportion of total striatal area for green and red injection sites were not significantly different between genotypes (Fig. 3.6G; green: $p = 0.70$; red: $p = 0.99$; t-test). Further, there was no significant difference in the area of the green versus red injection sites as a proportion of the total striatal area within both genotypes (Fig. 3.6G; WT: $p = 0.79$; KO: $p = 0.37$, t-test). The location of the respective injection sites was an important parameter to measure, as qualitative analysis suggested that the location of retrogradely labeled PF cells may be altered. The distance of the centre of the green and red injections to the rostral pole of the striatum were not different between genotypes (Fig. 3.6H; green: $p = 0.34$; red: $p = 0.39$, t-test). Additionally, the distance between green and red injection site centers was not significantly different (Fig. 3.6H; $p = 1.00$, t-test). These data suggest that the changes observed in the targeting of thalamostriatal projections were due to genotypic differences.

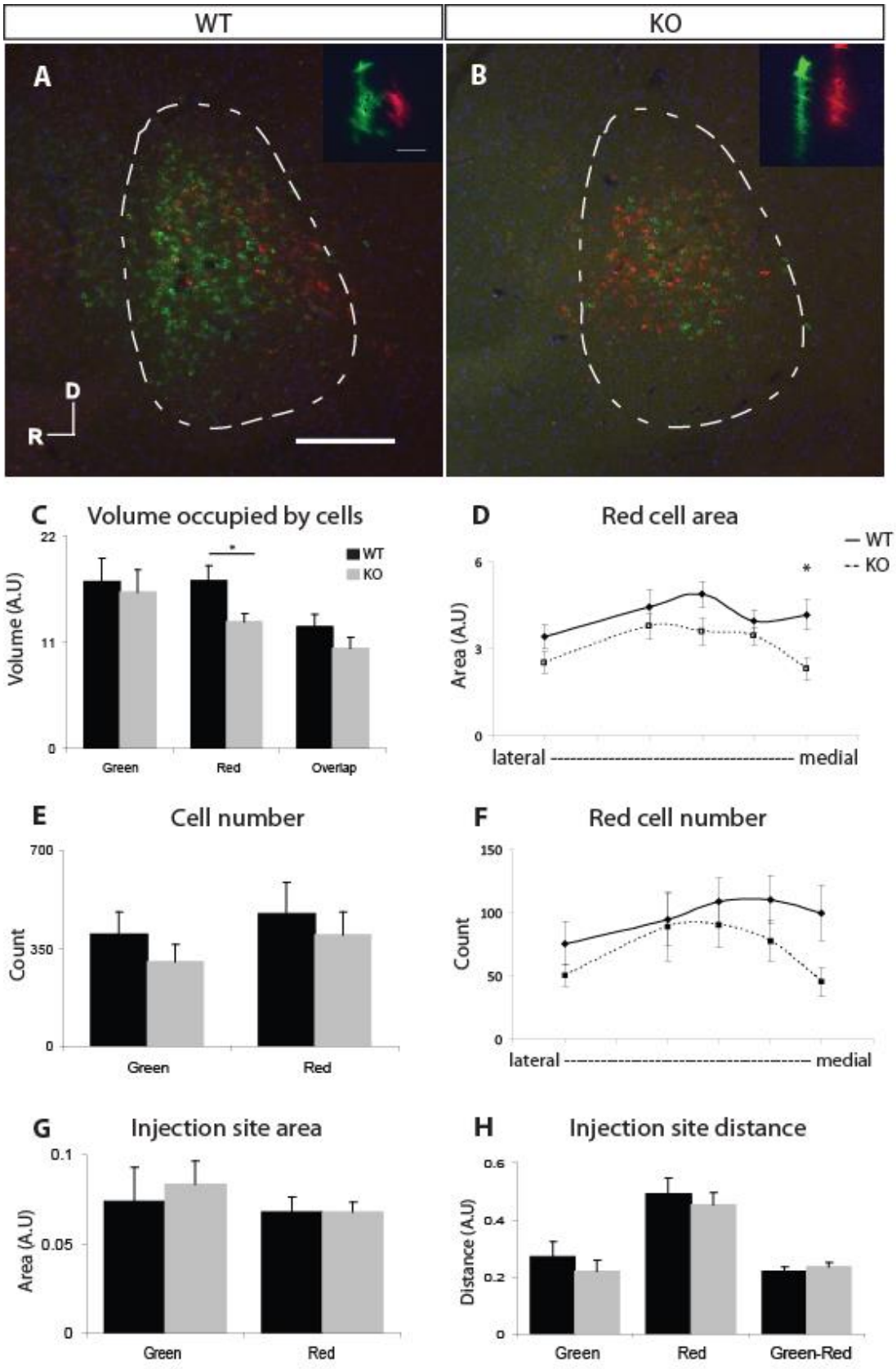
WT
KO
A
B
D
R
C
Volume occupied by cells
Volume (A.U)
22
11
0
WT
KO
*
Green
Red
Overlap
D
Red cell area
— WT
-- KO
Area (A.U)
6
3
0
*
lateral
medial
E
Cell number
Count
700
350
0
Green
Red
F
Red cell number
Count
150
100
50
0
lateral
medial
G
Injection site area
Area (A.U)
0.1
0.05
0
Green
Red
H
Injection site distance
Distance (A.U)
0.6
0.4
0.2
0
Green
Red
Green-Red

Figure 3.6. Dual retrograde CTB injections into the striatum

(A-B) Sagittal sections showing retrogradely-labeled cells in the PF resulting from dual injections of CTB-488 and CTB-594 into rostral and caudal striatum, respectively (insets). (A) In WTs, distinct green and red cell populations were labeled in the PF (dashed line). Cells projecting to rostral striatum were predominantly in rostral (green), while cells projecting to caudal striatum were localised mostly to caudal PF (red). An overlap region in the centre of the PF was occupied by both subpopulations. No double-labeled (yellow) cells were observed. (B) In KOs, distinct populations of green and red cells were also observed in the PF (dashed line). The location of these, however, appeared to be reversed compared to WT. Cells projecting to rostral striatum (green) were predominantly localised to the caudal two-thirds, while cells projecting to caudal striatum (red) were predominantly focused in the rostral two-thirds of the PF. The overlap area was not evidently larger and did not contain double-labeled (yellow) cells, as in WTs.

(C) Volume occupied by green and red cells and the region of overlap. The average volume occupied by green cells was similar between genotypes, while that of red cells was significantly smaller in KOs compared to WTs (WT: 17.44 ± 1.49 (mean (AU) ± SEM), n = 6; KO: 13.14 ± 0.88, n = 6; p = 0.037, t-test). The volume of overlap was not significantly different.

(D) Area occupied by red cells across the ML axis. Area increased from lateral to middle and then dropped off in medial PF. Area was smaller in KOs at each level along this axis, but only significantly reduced in medial striatal sections (*; WT: 4.17 ± 0.50 (mean (AU) ± SEM), n = 6; KO: 2.32 ± 0.36 (mean (AU) ± SEM), n = 6, p = 0.02, t-test). Area also showed a trend towards a reduction in middle sections (p = 0.07, t-test).

(E) The average number of green and red-labeled cells. Both subpopulations were reduced in KOs, but not significantly so, compared to WTs.

(F) Number of red cells across the ML PF axis. Red cells increased from lateral to middle, and dropped off in medial PF in both genotypes. The number of cells showed a trend towards a reduction in KOs in the most medial section, compared to WTs (p = 0.058, t-test).

(G-H) Injection site analysis. (G) The area of injection sites as a proportion of total striatal area for green and red sites were not significantly different between genotypes (green: p = 0.34; red: p = 0.39, t-test), or within genotypes (WT: p = 0.79; KO: p = 0.37, t-test). (H) The location of green and red injection sites with respect to the rostral pole of the striatum and to each other was, likewise, similar between genotypes.

Scale bar in A applies to B. Scale bar in A inset applies to B inset. Scale bar in A represents 200 μm. Scale bar in A inset represents 500 μm. D is dorsal, R is rostral. Values in graphs indicate mean ± SEM

Striatal cholinergic interneurons

Striatal cholinergic interneurons are a major postsynaptic target of thalamostriatal axons from the PF and can be readily labeled using immunohistochemistry for ChAT (Lapper and Bolam, 1992). Hence, preliminary experiments examined potential changes in the distribution of these cells in adult Ten-m3 KOs, compared to WT controls. Cholinergic interneurons were large and distinct, and distributed throughout the RC extent of the striatum in WT (Fig. 3.7A-C) and KO mice (Fig. 3.7 D-F). In coronal sections, these cells were distributed homogeneously in WT striatum, at rostral (Fig. 3.7A), commissural (Fig. 3.7B) and caudal regions (Fig. 3.7C). In KOs, the distribution of cholinergic interneurons, like WTs, appeared to be mostly homogeneous in rostral regions (Fig. 3.7D). More caudally, at the level of the anterior commissure, however, the distribution of cells appeared normal except in the VL quadrant, where cholinergic interneurons were often few in number (Fig. 3.7E, arrow). At caudal levels of the striatum, cholinergic interneurons were still sparse in the VL region of the striatum (Fig. 3.7F, arrow), however, not to the degree observed at the commissural level.

Quantitative analysis examined the number of cholinergic interneurons located within quadrants of the striatum at different RC levels. The total number of cholinergic interneurons in the striatum (Fig. 3.7G) increased from rostral to commissural levels and decreased at the most caudal levels for both genotypes. Although the number of cells was generally lower in KOs, this was most evident in middle sections, where cholinergic interneurons were significantly reduced in KOs compared to WTs (Fig. 3.7G, *; WT: 276.33 ± 8.71 (mean ± SEM), n = 3; KO: 236 ± 5.64 (mean ± SEM), n = 4; $F(1.4) =$

14.13, p = 0.013, repeated measures ANOVA). These changes were further examined in individual quadrants of the striatum. At the level of the anterior commissure, the number of cholinergic interneurons was generally lower in KOs, but was only significantly reduced in the VL quadrant (Fig. 3.7H, *; WT: 88.83 ± 4.78 (mean ± SEM), n = 3; KO: 62 ± 4.19 (mean ± SEM), n = 4; F(1,4) = 14.22, p = 0.013, repeated measures ANOVA). The number of cells in the DL quadrant also showed a trend towards a reduction in KOs (F(1,4) = 6.33, p = 0.053, repeated measures ANOVA). Non-significant trends towards a reduction were, likewise, only observed in the VL quadrant in KOs at rostral (F(1,4) = 4.12, p = 0.098, repeated measures ANOVA) and caudal striatal levels (F(1,4) = 5.44, p = 0.067, repeated measures ANOVA). A significant reduction was also observed in the VL quadrant at the most caudal level analysed (WT: 61.5 ± 4.18 (mean ± SEM), n = 3; KO: 40.75 ± 4.83 (mean ± SEM), n = 4, F(1,4) = 10.10, p = 0.025, repeated measures ANOVA).

The density of cholinergic interneurons was also analysed in each striatal quadrant to investigate a potential skewing of the population. At the level of the anterior commissure, the density of cholinergic cells was similar in all quadrants except the VL, where it was significantly reduced in KOs (Fig. 3.7I, *; WT: 2.33 ± 0.12 (mean (per unit area) ± SEM), n = 3; KO: 1.8 ± 0.11 (mean ± SEM), n = 4, F(4) = 7.74, p = 0.04, repeated measures ANOVA). No differences in density were observed between genotypes in rostral and caudal sections (data not shown).

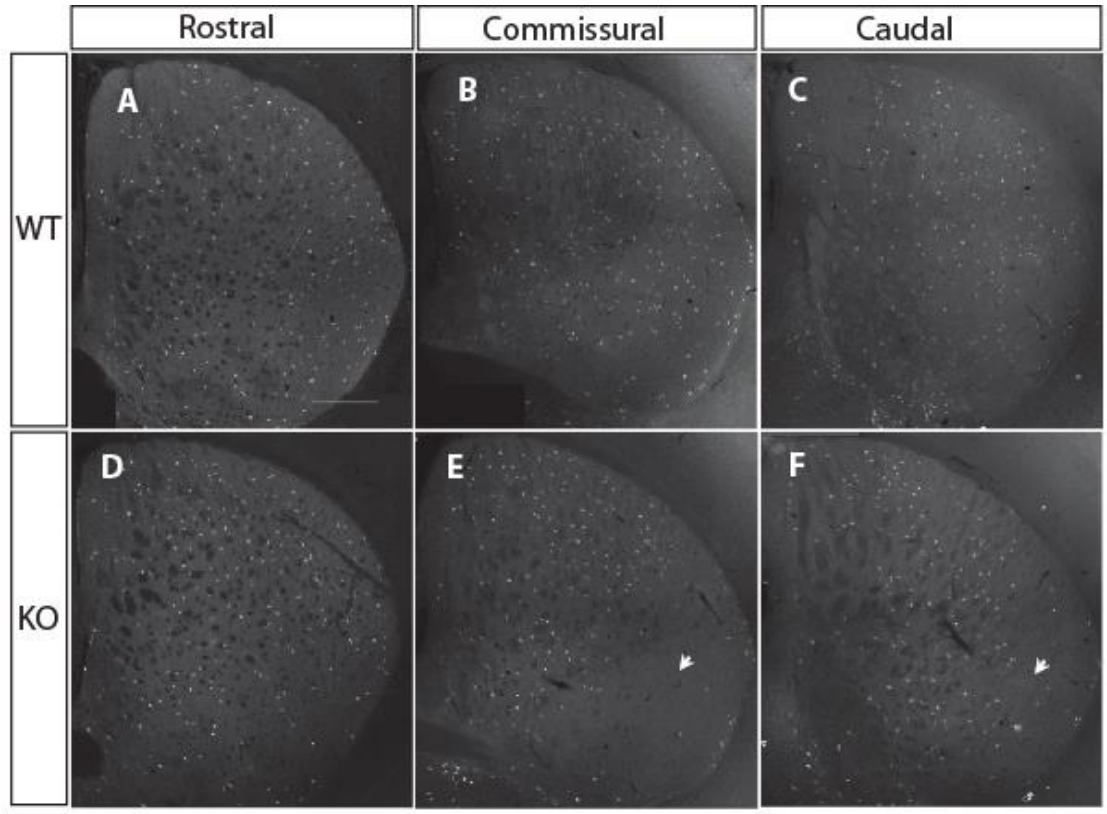
Rostral
Commissural
Caudal
WT
KO
A
B
C
D
E
F

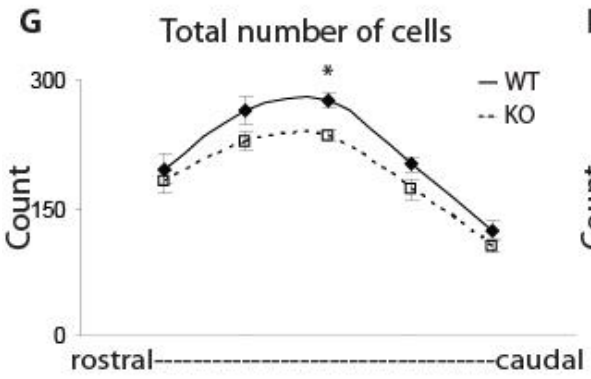
G
Total number of cells
300
150
0
Count
WT
KO
*
rostral----------caudal

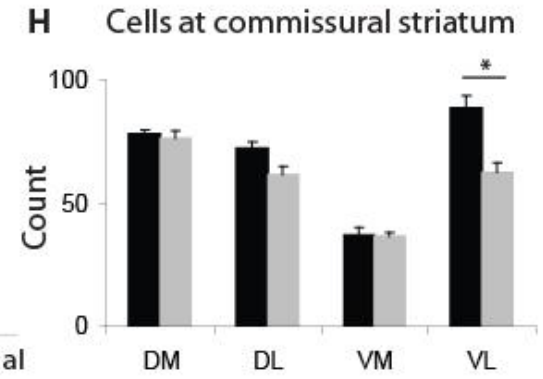
H
Cells at commissural striatum
100
50
0
Count
*
DM
DL
VM
VL

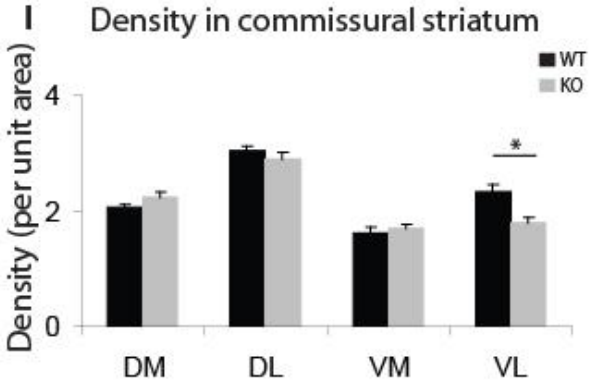
I
Density in commissural striatum
Density (per unit area)
4
2
0
WT
KO
*
DM
DL
VM
VL

Figure 3.7. Striatal cholinergic interneurons

(A-C) Coronal sections through WT striatum showing the distribution of cholinergic interneurons labeled with immunohistochemistry to ChAT. (A) In rostral striatum, these cells were distributed homogeneously. Similar distribution was observed at the level of the anterior commissure (B) and caudal regions (C).

(D-F) Coronal sections through KO striatum showed altered distribution of cholinergic interneurons. (D) In rostral striatum, these cells were homogeneously distributed, as in WTs. (E) At the commissural level, cholinergic interneurons were similarly homogeneous except for a the VL quadrant, where these cells were sparse (arrow). (F) At caudal levels, cholinergic interneurons were still sparse in the VL region of the striatum (arrow), however, not to the degree observed at the commissural level.

(G) The total number of cholinergic interneurons across the RC axis of the striatum increased from rostral to commissural levels and decreased at the most caudal levels for both genotypes. The number of cells was generally lower in KOs but was only significantly reduced at the level of the commissure (*; WT: 276.33 ± 8.71 (mean ± SEM), n = 3; KO: 236 ± 5.64 (mean ± SEM), n = 4; p = 0.013, repeated measures ANOVA).

(H) The number of cholinergic interneurons in each striatal quadrant at the level of the anterior commissure. These cells were reduced in KOs in all quadrants, however, was only significantly reduced in the VL quadrant (*, WT: 88.83 ± 4.78 (mean ± SEM), n = 3; KO: 62.44 ±3.72 (mean ± SEM), n = 4; p = 0.013, repeated measures ANOVA). The number of cells in the DL quadrant also showed a trend towards a reduction in KOs (p = 0.053, repeated measures ANOVA).

(I) The density of cholinergic interneurons in each striatal quadrant at the level of the anterior commissure. Density was similar in all quadrants except the VL, where it was significantly reduced in KOs (*, WT: 2.33 ± 0.12, n = 3; KO: 1.8 ± 0.11, n = 4, F(4) = 7.74, p = 0.04, repeated measures ANOVA).

Values in graphs indicate mean ± SEM

Striatal and PF structure

The area and cell number comprising the striatum and PF were examined to investigate whether observed changes in anterograde and retrograde tracing experiments, and cholinergic interneuron number and distribution, may result from potential changes within these structures. While there was a slight decrease in the mean area of the PF in KOs (Fig. 3.8A), this reduction was not significant ($p = 0.28$, t-test). Moreover, the number of cells comprising the PF was similar between genotypes (Fig. 3.8B; $p = 0.92$, t-test). For the striatum, area was measured across the RC axis (Fig. 3.8C). Total striatal area increased from rostral to commissural levels and reduced into caudal levels for both genotypes. Striatal area was generally smaller in KOs, however, a significant reduction was only observed at commissural (Fig. 3.8C, *; WT: 122.37 ± 2.87 (mean (AU) ± SEM), n = 3; KO: 110.49 ± 1.12 (mean ± SEM), n = 4; $F(1,4) = 10.97$, $p = 0.021$, repeated measures ANOVA) and caudal levels in KOs (Fig. 3.8C, *; WT: 111.91 ± 2.67 (mean (AU) ± SEM), n = 3; KO: 97.56 ± 2.38 (mean ± SEM), n = 4, $F(1,4) = 9.67$, $p = 0.02$, repeated measures ANOVA). The number of striatal cells at commissural levels (Fig 3.8D) was similar between genotypes ($p = 0.46$, t-test). In contrast, at caudal levels (Fig. 3.8E), the number of striatal cells was significantly reduced in KOs compared to WTs (Fig. 3.8E, *; WT: $1.08 \times 10^6 \pm 4.02 \times 10^4$ (mean ± SEM), n = 3; KO: $0.8 \times 10^6 \pm 5.42 \times 10^4$ (mean ± SEM), n = 3; $p = 0.04$, t-test). These changes in striatal structure in mid-caudal levels correlate with changes observed in anterograde and retrograde tracing data and cholinergic interneuron distribution in Ten-m3 KO animals, suggesting region specific roles for the gene in the striatum (see Discussion).

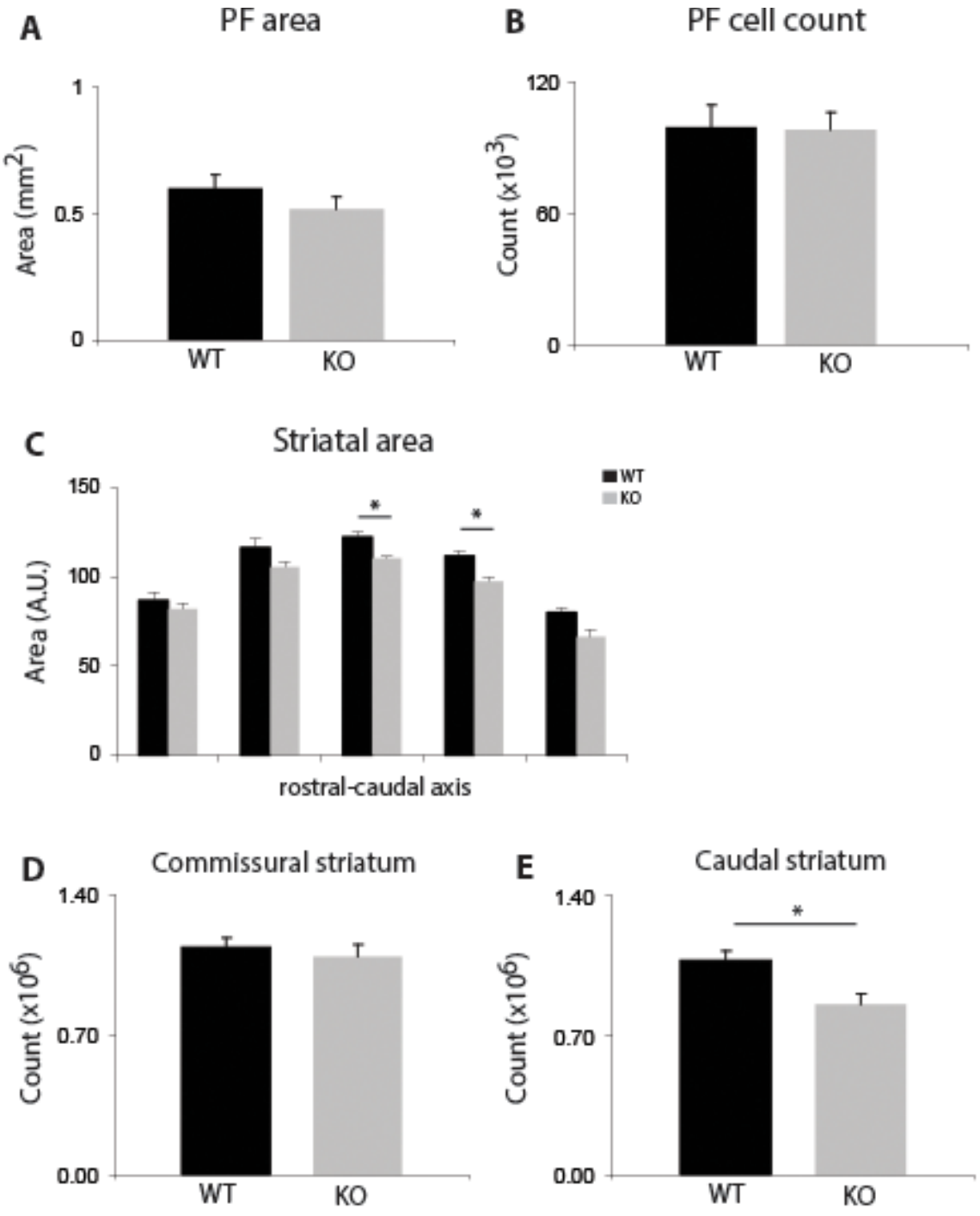
A
PF area
Area (mm2)
1
0.5
0
WT
KO
B
PF cell count
Count (x103)
120
60
0
WT
KO
C
Striatal area
Area (A.U.)
150
100
50
0
WT
KO
*
*
rostral-caudal axis
D
Commissural striatum
Count (x106)
1.40
0.70
0.00
WT
KO
E
Caudal striatum
Count (x106)
1.40
0.70
0.00
*
WT
KO

Figure 3.8. Striatum and PF structure

(A-B) The area and cell number comprising the PF of WTs (black bar) and KOs (grey bar). (A) The area of the PF was slightly smaller in KOs, however, this reduction was not significantly different between genotypes. (B) The number of cells comprising the PF was also similar between genotypes.

(C) Striatal area across the RC axis. Striatal area increased from rostral to middle sections and then decreased into caudal regions in WTs (solid black line) and KOs (dashed line). Area was slightly smaller in KOs across all levels. This reduction was only significant at commissural (*; WT: 122.37 ± 2.87 (mean (AU) ± SEM), n = 3; KO: 110.49 ± 1.12 (mean (AU) ± SEM), n = 4; $F(1,4) = 10.97$, $p = 0.021$, repeated measures ANOVA) and caudal levels of the striatum (*; WT: 111.91 ± 2.67 (mean (AU) ± SEM), n = 3; KO: 97.56 ± 2.38 (mean (AU) ± SEM), n = 4, $F(1,4) = 9.67$, $p = 0.02$, repeated measures ANOVA).

(D) The number of striatal cells was similar between genotypes at the level of the anterior commissure ($p = 0.46$, t-test).

(E) In contrast, at caudal levels, the number of striatal cells was significantly reduced in KOs compared to WTs (WT: $1.08 \times 10^6 \pm 4.02 \times 10^4$ (mean ± SEM), n = 3; KO: $0.8 \times 10^6 \pm 5.42 \times 10^4$ (mean ± SEM), n = 3; $p = 0.04$, t-test).

Values in graphs indicate mean ± SEM.

Behaviour

The anatomical differences observed in the distribution of thalamostriatal projections and cholinergic interneurons in Ten-m3 KO mice may have behavioural consequences. Although the thalamostriatal pathway is implicated in complex goal-directed learning paradigms, due to the significant sensory deficits present in Ten-m3 KO mice (Leamey et al., 2007b), which could confound interpretation as well as a number of other issues (see Discussion), the changes in this pathway were examined using simpler behaviours. Specifically, well established protocols for striatal function were used, including footprint analysis to test gait and gross motor function, and an accelerating rotorod paradigm, to test motor learning in Ten-m3 KO mice.

Footprint analysis

Gait and potential deficits in motor function in Ten-m3 KO, compared to WT mice, were examined using a footprint analysis. Footprints were analysed for stride length (Fig. 3.9A, solid line), and width (Fig. 3.9A, dashed line), using the third proximal interphalangeal joint as a reference. Only prints where 6-8 pads were approximately parallel were chosen for analysis. WT mice showed stereotypical patterns of walking, with left and right pads leading in turn (Fig. 3.9B). This was also mostly true for KOs (Fig. 3.9C, pads 3-8), although some animals exhibited a hopping action, predominantly at the beginning or end of their movement, where left and right pads were at approximately similar positions (Fig. 3.9 C; pads 2 and 3). Analysis of stride length showed that KOs exhibited a significantly shorter stride than their WT counterparts (Fig. 3.8D;*; WT: 5.31 ± 0.12 mm (mean ± SEM), n = 7; KO: 4.64 ± 0.12 (mean ± SEM), n =

7; $F(1,) = 8.50$, $p = 0.013$, repeated measures ANOVA). In contrast, step width was not significantly different ($n = 6$, $F(1,12) = 0.40$, $p = 0.54$, repeated measures ANOVA). To gain an insight into the variability of the differences observed in KOs, variance in both stride length and width were further examined (Fig. 3.9E). Variance in stride was very similar between genotypes ($n = 7$, $F(1,10) = 0.001$, $p = 0.98$, repeated measures ANOVA). KOs showed a larger variance in the width of their step, however, this was not significantly different to that of WTs ($n = 7$, $F(1,10) = 0.64$, $p = 0.44$, repeated measures ANOVA).

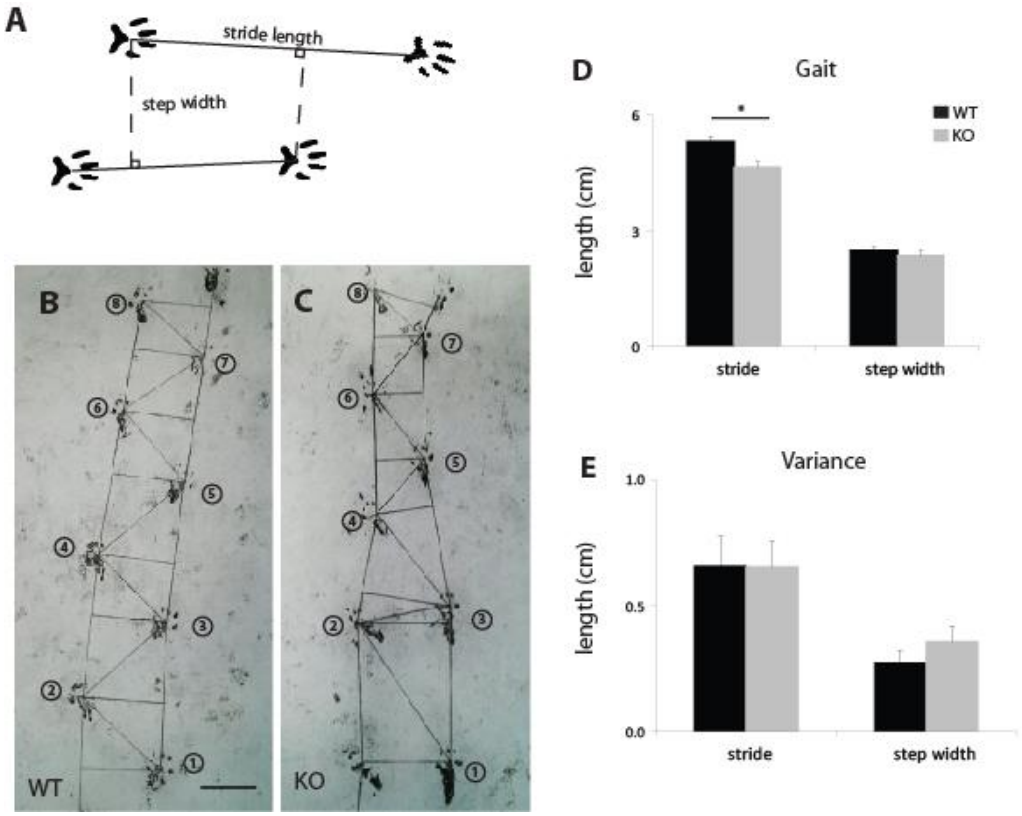

Figure 3.9. Motor function/coordination using footprint analysis.

(A) Footprints were analysed for stride length, defined as the distance between the third proximal interphalangeal joint of each left or right pad separately (solid line), and width, defined as the normal distance from the third proximal interphalangeal joint of one pad to the line connecting two pads on the contralateral side (dashed line).

(B-C) Representative footprints where 8 pads (1-8) were analysed. (B) WT mice showed stereotypical patterns of walking, with left and right pads leading in turn, and in a parallel manner. (C) In KOs, the stereotypical walking patterns were also observed (pads 3-8). However, some animals also exhibited a hopping action, where left and right pads were at approximately similar positions (pads 2-3).

(D) KOs exhibited a significantly shorter stride than their WT counterparts (*; WT: 5.31 ± 0.12 mm (mean ± SEM), n = 7; KO: 4.64 ± 0.12 (mean ± SEM), n = 7; p = 0.013, repeated measures ANOVA). In contrast, step width was very similar between genotypes.

(E) Variance of stride length was very similar between genotypes.

The scale bar in B applies to C. Scale bar represents 2 cm. Values in graphs indicate mean ± SEM

Rotorod

In addition to motor function, the striatum has previously been implicated in motor learning (Beutler et al., 2011; Dang et al., 2006; Yin et al., 2009). Although elimination of the thalamostriatal pathway originating from the PF has previously been shown to have no affect on rotorod performance (Kato et al., 2011), changes to striatal NMDA receptors, the main receptor targets of these projections, lead to profound motor learning deficits (Beutler et al., 2011; Dang et al., 2006). Interestingly, thalamostriatal axons have been shown to directly innervate cholinergic interneurons via NMDA receptors (Consolo et al., 1996a), which are reduced in lateral striatum, a region linked to motor learning (Yin et al., 2009), in Ten-m3 KO mice. Hence, the changes in these major components of the normal thalamostriatal pathway may alter rotorod performance. In particular, an adapted version of the rotorod test was use to specifically probe potential motor learning differences in Ten-m3 WT and KO mice (see Methods). A large diameter rod and a gradual acceleration of the rod across the entire trial period (180 s) were used to normalise for minor motor deficits, such as the reduced stride length observed in Ten-m3 KOs, which may confound differences in learning able to be detected using this paradigm. Learning was assessed by measuring the animal's ability to remain on the rotating rod across repeated presentations of the task, that is, multiple sessions per day, across 5 consecutive days.

On day one, WTs showed a significant improvement in performance across sessions 1-5 (Fig. 3.10A; solid line; $n = 11$, $F(4, 51) = 2.58$, $p = 0.048$, multivariate ANOVA). WT performance further improved dramatically across sessions on day 2 ($n = 11$, $F(4,46) =$

2.82, p = 0.035, univariate ANOVA) but plateaued by day 3 and thereafter (Fig. 3.10A). WT performance improved significantly across the 25 sessions, (n = 11, F(24, 226) = 5.574, p < 0.001, univariate ANOVA). In contrast, performance in KOs was similar across sessions within each of the 5 days (p > 0.05, univariate ANOVA). However, like WTs, KOs (Fig. 3.10A; dashed line) showed a significant improvement in performance across the 25 sessions (n = 14, F(24, 301) = 1.93, p = 0.006, univariate ANOVA).

Between genotypes, WTs and KOs showed similar initial performances on day 1, however, this diverged in session 5. (Fig. 3.10A, *; WT: 47.27 ± 3.92s (mean ± SEM), n = 11; KO: 31 ± 4.95s (mean ± SEM), n = 14; F(1,22) = 5.94, p = 0.02, multivariate ANOVA). A divergence was also observed in the latter sessions of day 2, as WTs improved dramatically, while KO performance remained constant (Fig. 3.10A, *; session 8: WT: 64.36 ± 6.29s (mean ± SEM); KO: 39.86 ± 7.78s, F(1,24) = 5.4, p = 0.03; session 9: WT: 79.81 ± 10.27s; KO: 42.43 ± 9.67s, F(1,24) = 6.6, p = 0.02; session 10: WT: 80.91 ± 7.99s; KO: 44.86 ± 9.38s, F(1,24) = 7.78, p = 0.01, multivariate ANOVA). Similarly, performance remained significantly different between genotypes in sessions 11-15 on day 3 (Fig. 3.10A, *; session 11: WT: 79.91 ± 7.19s (mean ± SEM); KO: 43.79 ± 7.26s, F(1,24) = 11.7, p = 0.002; session 12: WT: 84.45 ± 8.5s; KO: 50.21 ± 9.75s, F(1,24) = 6.4, p = 0.02; session 13: WT: 96.64 ± 7.82s; KO: 42.21 ± 9.97s, F(1,24) = 16.5, p < 0.001; session 14: WT: 89.64s ± 7.59; KO: 61.07 ± 10.47s, F(1,24) = 4.3, p = 0.05; session 15: WT: 91.64 ± 8.32s; KO: 57.93 ± 10.75s, F(1,24) = 5.48, p = 0.03, multivariate ANOVA). By day 4, latencies became more comparable between genotypes, with WTs only showing a significantly better performance in session 17 (Fig.

3.10A, *; WT: 72.45 ± 8.03s (mean ± SEM); KO: 44.26 ± 8.26s, F(1,24) = 5.58, p = 0.03, multivariate ANOVA). This convergence in performance continued into day 5, where latencies were similar between genotypes in all sessions except session 25 (WT: 89.81 ± 7.72s (mean ± SEM); KO: 64.93 ± 7.27s, F(1,24) = 5.23, p = 0.032, multivariate ANOVA).

The difference in performance between genotypes was also examined by comparing sum of latencies in each training day (Fig. 3.10B). The sum of latencies was not different between genotypes on day 1 (F(1,23) = 1.52, p = 0.23, multivariate ANOVA), suggesting an equal initial performance. WT animals showed significantly higher total latencies than KOs on day 2 (Fig. 3.10B, *; WT: 330.45 ± 33.93s (mean ± SEM), n = 11; KO: 221.07 ± 32.18s , n = 14; F(1,23) = 5.19, p = 0.032, multivariate ANOVA) and day 3 (Fig. 3.10B, *; WT: 442.27 ± 30.79s (mean ± SEM), n = 11; KO: 255.21 ± 40.00s, n = 14; F(1,23) = 12.24, p = 0.002, multivariate ANOVA). While KOs continued to improve, albeit, at a slow rate, on days 4 and 5, WT performance plateaued. This was such that the sum of latencies began to converge between genotypes on day 4, (WT: 400 ± 35.81s (mean ± SEM), n = 11; KO: 285.5 ± 45.14s (mean ± SEM), n = 14; F(1,23) = 3.54, p = 0.07, multivariate ANOVA) and could no longer be distinguished by day 5 (F(1,23) = 1.61, p = 0.22, multivariate ANOVA). This convergence in performance, along with the comparable initial performances, suggests that the altered gait observed in Ten-m3 KOs did not impede their ability to perform this motor task.

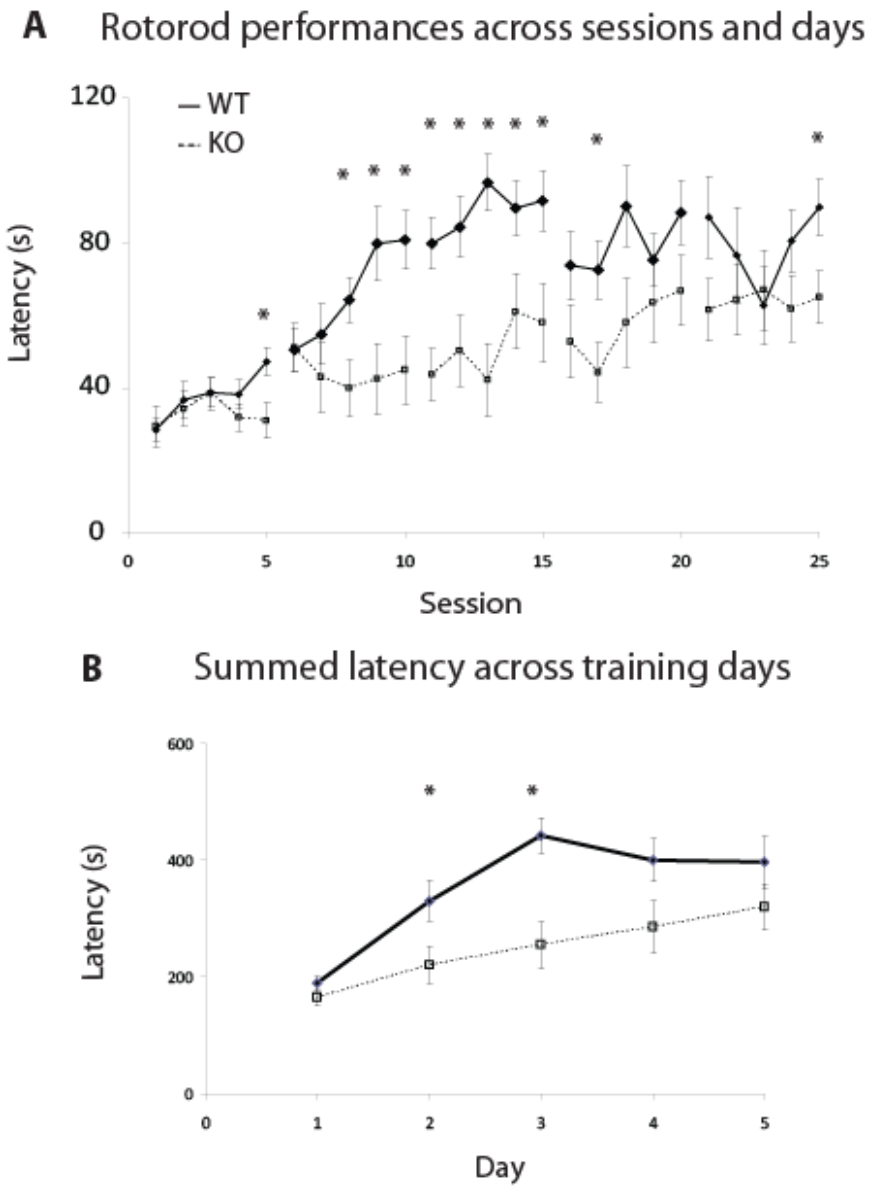
A
Rotorod performances across sessions and days
WT
KO
Latency (s)
120
80
40
0
0
5
10
15
20
25
Session
B
Summed latency across training days
Latency (s)
600
400
200
0
0
1
2
3
4
5
Day

Figure 3.10. Performance in motor learning on an accelerating rotorod

(A) Mice were tested on an accelerating rotorod in 5 sessions per day, across 5 consecutive days. WTs (solid line) showed improved performance across sessions on days 1 and 2 but plateaued by day 3. Overall, WT performance improved significantly across the 25 sessions ($n = 11$, $F(24, 226) = 5.574$, $p << 0.001$, univariate ANOVA). In contrast, KOs (dashed line) did not show significant improvement across sessions within days. However, like WTs, KOs showed a significant improvement in performance across the 25 sessions ($n = 14$, $F(24, 301) = 1.93$, $p = 0.006$, univariate ANOVA). Between genotypes, WTs and KOs showed similar initial performances on day 1, but diverged in session 5. (*; WT: 47.27 ± 3.92s (mean ± SEM), $n = 11$; KO: 31 ± 4.95s (mean ± SEM), $n = 14$; $F(1,22) = 5.94$, $p = 0.02$, multivariate ANOVA). A similar divergence was observed in sessions 8, 9 and 10 on day 2 (*). Performance remained significantly different between genotypes in sessions 11-15 on day 3. By day 4, latencies became more comparable between genotypes, with WTs only showing a significantly better performance in session 17 (*; WT: 72.45 ± 8.03s (mean ± SEM); KO: 44.26 ± 8.26s, $F(1,24) = 5.58$, $p = 0.03$, multivariate ANOVA). By day 5, latencies were similar between genotypes in all sessions except session 25 (*; WT: 89.81 ± 7.72s (mean ± SEM); KO: 64.93 ± 7.27s, $F(1,24) = 5.23$, $p = 0.032$, multivariate ANOVA).

(B) Sum of latencies for performance on each day of training. Performance on day 1 was very similar between genotypes. Across days, both WTs and KOs showed improvements in performance, with WTs plateauing after day 3. The rate at which this improvement occurred differed between genotypes. WT animals showed significantly higher total latencies than KOs on day 2 (WT: 330.45 ± 33.93s (mean ± SEM), $n = 11$; KO: 221.07 ± 32.18s , $n = 14$; $F(1,23) = 5.19$, $p = 0.032$, multivariate ANOVA) and day 3 (WT: 442.27 ± 30.79s (mean ± SEM), $n = 11$; KO: 255.21 ± 40.00s, $n = 14$; $F(1,23) = 12.24$, $p = 0.002$, multivariate ANOVA). KO performance continued to improve on days 4 and 5, while WTs plateaued such that the sum of latencies for WT and KOs converged on day 5.

Discussion

Summary of results

As the first study to explore the *in vivo* roles for Ten-m3 in the formation of thalamostriatal circuits, the current work has uncovered significant anatomical and behavioural deficits associated with this pathway in adult Ten-m3 KO mice. Bulk anterograde tracing experiments suggest that the absence of Ten-m3 does not affect the targeting of the thalamostriatal projection to the ipsilateral striatal matrix, *per se*. Within the matrix, however, evidence of targeting errors were observed. Notably, this projection filled a significantly larger area of the striatal matrix in KOs compared to WTs. This appeared to occur in conjunction with and/or as a result of a loss of the characteristic clustering of thalamostriatal terminals from the PF. Further, in mid-caudal sections, there was a tendency for thalamostriatal terminals to avoid the VL striatum. In dual retrograde focal tracer experiments, Ten-m3 KOs showed a significant reduction in the area and number of PF cells projecting to the mid-caudal striatum (ie. red cells) compared to WTs. One of the major postsynaptic targets of thalamostriatal axons, the cholinergic interneurons, was also significantly reduced at the level of the anterior commissure in Ten-m3 KOs. This was particularly striking in the VL quadrant of the mid-caudal striatum. These changes occurred in the absence of differences to the area and number of cells comprising the PF. Intriguingly, however, the cross-sectional area and number of cells comprising the mid-caudal levels of the striatum were also significantly reduced in KOs compared to WTs. Finally, the behavioural consequences of these anatomical

deficits were investigated using well characterised paradigms for examining two aspects of striatal function: motor function/coordination and motor learning. To test motor function, a footprint analysis was used to show that Ten-m3 KO mice exhibited a slight hopping action in some aspects of their locomotive activity, and a significantly reduced stride length, but not step width, compared to WT mice. This motor deficit did not appear to affect the initial or final performance of KO animals in the motor learning task. However, KOs displayed significantly lower latencies on days 2-4, compared to WTs. WT mice showed improvements in performance between sessions within training days, with improvements observed from day 1, and a plateauing of performance evident by day 3. In contrast, KO performance improved at a slower rate, being most evident across training days, indicating a delay in procedural learning in these animals.

Technical considerations

Anterograde tracer injections made into the PF were of similar size between WT and KO mice, suggesting that the differences in the thalamostriatal pathway were a result of genotypic differences. Although all tracer injections hit the PF, in most cases, tracer was also observed in structures dorsal of the PF, such as the hippocampus, caudal pretectal area and cingulate cortex, along the pipette tract. Control experiments, however, showed very scant to no striatal label in cases where the focus of the injection was too dorsal, that is, in the cortex and/or hippocampus, or too caudal, in pretectal areas (data not shown), in both genotypes, suggesting that the majority of striatal terminals observed in these experiments originated from the PF.

An intriguing and unexpected observation made from anterograde tracing experiments was that, despite the overall increase in the area occupied by thalamic terminals, there appeared to be a tendency for thalamostriatal projections to avoid the VL quadrant of mid-caudal striatum. Due to the small number of cases where the area immediately surrounding this region was intensely labeled, however, a more formal analysis of this was, unfortunately, not possible. Further, since heat maps were only generated from rostral sections, which were reacted for TSA with the original intention to compare the distribution of the thalamostriatal axons with striosomes, which are most numerous rostrally, these maps are not informative with respect to mid-caudal striatum. Moreover, heat maps could not be reliably generated from DAB-reacted sections. Thus, future studies should specifically target the VL region of the PF to examine this in more detail.

Further, since representative rostral sections were reacted for TSA and analysed, only areas were computed and compared between genotypes. It would be of interest to investigate potential volumetric changes in terminal distribution, as well as gross anatomy for the striatum and PF in Ten-m3 KO animals. This type of analysis may magnify the area differences presented here, and/or reveal potential region specific changes within the striatum, which is suggested by the retrograde tracing studies.

Retrograde tracer injections were made into lateral striatum to examine back-labeled cells in the lateral PF (ie. lateral to the fr), according to the topography of thalamostriatal projections, as this is the largest, and, hence, most accessible region of the rodent PF. For this reason, only sagittal sections through lateral PF were analysed. This was also the

reason for investigating potential differences along the RC axis, as medial injections would have led to back-labeled cells in medial regions of the PF, including that medial of the fr, which, in the sagittal plane, constitute very few sections. In the early stages of these experiments, sections medial to the fr were also examined, although labeled cells were often scarce and difficult to distinguish. These regions were, therefore, not analysed. It may be interesting, however, to investigate topography along the ML axis, particularly as the differences observed in anterograde tracing data was analysed along the ML and DV axes in coronal sections.

Another technical consideration associated with retrograde tracing experiments arose during the analysis stage. Firstly, the rostral and caudal boundaries of the PF were less distinct compared to medial and lateral ones. Likewise, the dorsal boundary was not as evident in the sagittal plane. Hence, the perimeter of the PF was ultimately determined using a combination of images from the DAPI, Alexa Fluor-488 and Texas Red channels. The sections of interest were also remounted and processed for a conventional Nissl stain, which provided a better visual location of PF boundaries and was used to further ensure that the boundaries of the PF were determined as accurately as possible. No systematic differences were observed between genotypes, and, thus, changes in KOs can not be attributed to difficulties in determining these borders.

Normal thalamostriatal projections in mice

Previous tracing studies on the thalamostriatal pathway have been examined in rats (Lanciego et al., 2004; Veening et al., 1980; Vercelli et al., 2003), monkeys (Parent and

Parent, 2005b), cats (Herkenham and Pert, 1981) and briefly in mice (Ellender et al., 2013). Here, we extend the analysis of this pathway in mice. Similar to those shown previously in other mammalian species, thalamostriatal projections from the PF were strictly ipsilateral and terminated in the striatal matrix (Gonzalo, 2002; Herkenham and Pert, 1981). Further, these thalamostriatal projections were distributed throughout the matrix in a general topographical manner (Lanciego et al., 2004; Veening et al., 1980; Vercelli et al., 2003). Although a comprehensive analysis of topography was unable to be performed due to the bulk nature of the injections, a 'loose' topography was evident in WT mice. For instance, injections into the lateral PF led to terminal label in dorsal to lateral regions of the striatum and medially labeled PF regions resulted in terminal label in medial striatum, which correlates with the topography of these projections in rats (Lanciego et al., 2004).

Within the matrix, thalamic terminals were arranged into dense patches distributed amongst areas of sparser label and regions completely devoid of label, with the latter corresponding to striosomes. This patchy patterning of terminals from the PF has been described previously in other species, with single cell tracing studies indicating that it arises from the clustering of collaterals from single PF neurons (Deschênes et al., 1996b; Gonzalo, 2002; Lanciego et al., 2004; Parent and Parent, 2005b). This may be reflected by observations that patches of thalamostriatal terminals were more obvious when injection sites were smaller and in regions further away from the focus of the label, particularly in cases of larger injections (current study). Further, experiments examining the overlap of thalamostriatal patches and Ten-m3-positive patches suggest that there

may be two populations of thalamic terminals (see Chapter 4), one of which may confound the patchy distribution of the other. Hence, the characteristic patchy patterning of thalamostriatal terminals is conserved in mice.

As mentioned above, single cell tracing studies indicate that axons from PF cells bifurcate a number of times in the striatum to terminate in multiple clusters along the RC and DV axes (Deschênes et al., 1996b; Parent and Parent, 2005b). In the rat, clusters of terminals originating from a single PF cell appear to extend more than 1 mm across the RC axis (Deschênes et al., 1996b). That dual focal injections into the striatum, made approximately 500 μm apart, along the RC axis, did not result in double-labeled PF cells suggests that this extent of collateralisation of PF axons may not be observed in mice. Further studies, however, are required to resolve this.

Ten-m3 KO mice show abnormally targeted thalamostriatal terminals

Thalamostriatal projections from the PF in Ten-m3 KO mice were found to be strictly ipsilateral and confined to the matrix, as in WT mice. That the compartmentalisation of these projections was unchanged is consistent with previous work (Tran, 2009) showing that the organisation of the striatal compartments, in terms of the number of striosomes and the percentage area occupied by this compartment, was not significantly altered in the absence of Ten-m3. Further, the expression of Ten-m3 in distinct patches within the striatal matrix is suggestive of a more complex role in the patterning of these projections.

The topographical organisation of thalamostriatal terminals was altered in Ten-m3 KOs. Injections into the lateral portion of the PF resulted in subtle differences in the topography of thalamostriatal terminals between genotypes, generally expanding slightly more medial to the equivalent case in WTs. Hence, the overall broad topography appeared to be conserved in these regions in KOs. When the tracer spilled into slightly more medial regions, however, a more dramatic difference was observed, with the resulting terminals located in medial striatum in WTs compared to middle regions in KOs. These data resulted from a small number of cases (1 x WT, 2 x KO), and, hence, further experiments are required to confirm that the differences in medial regions are as dramatic as they appear. Mapping deficits in Ten-m3 KOs have been shown previously in the visual system, where the absence of Ten-m3 leads to the aberrant extension of the ipsilateral retinogeniculate terminal zone from the normal DM region of the dLGN along the entire DM-VL axis (Leamey et al., 2007b) and a caudal shift in retinocollicular terminals during development (Dharmaratne et al., 2012). It is possible that the differences observed in the thalamostriatal pathway are more subtle compared to studies in the visual system, at least in lateral regions.

The expression of Ten-m3 in distinct patches within the striatal matrix strongly resembles the heterogeneous pattern of thalamostriatal terminals in the striatal matrix in WT mice. Intriguingly, the normal clustering of thalamostriatal terminals appears to be abolished in the absence of Ten-m3. Moreover, this loss of the clustering of terminals may, or may not, be linked to the concurrent increased spread of terminals to cover a larger area of the striatal matrix. Further studies will be required to resolve this issue. Interestingly,

although the patchy patterning of thalamostriatal terminals closely resembles the matrisomes formed by corticostriatal terminals in primates and cats (Flaherty and Graybiel, 1993a; Malach and Graybiel, 1986), these have yet to be linked to this compartment. Hence, we propose that thalamostriatal terminals from the PF constitute another set of matrisomes, which may overlap with or be distinct from those formed by corticostriatal projections. Further studies would be required to resolve this. We thus propose that Ten-m3 may demarcate a novel matrisome compartment required for the correct targeting of thalamostriatal axons (Fig. 3.11). This issue will be further explored in Chapter 4.

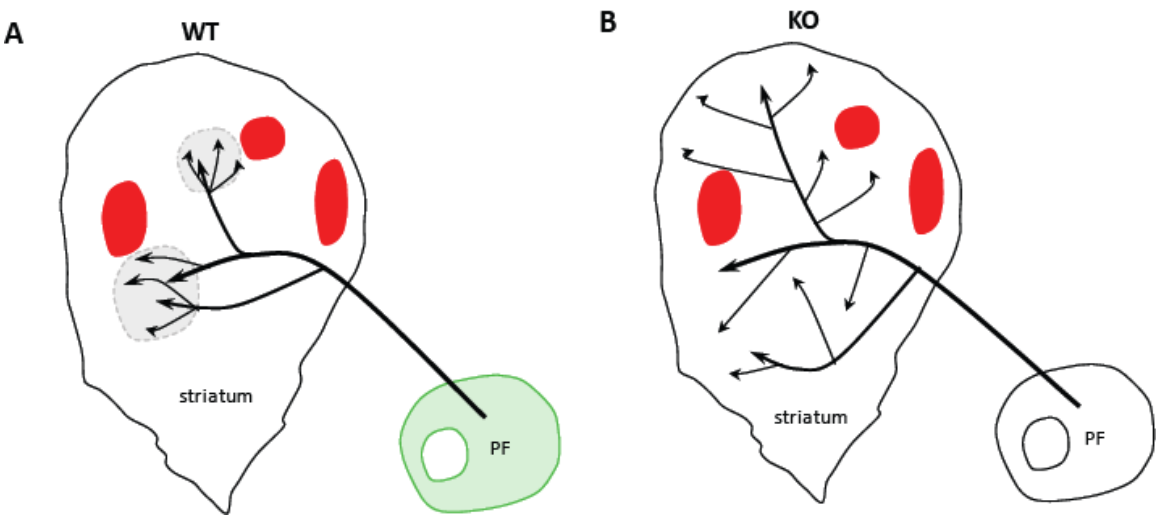

Figure 3.11. The hypothesised role of Ten-m3 in the precise targeting of patchy thalamostriatal terminals from the PF and the changes in Ten-m3 KO mice.

(A) In WTs, Ten-m3 is expressed in the PF (green) and striatum. In the striatum, this expression is distributed in patches (grey). Normally, thalamostriatal axons (arrows) project to the striatal matrix (white), avoiding striosomes (red patches), where they arborise and collateralise to form multiple terminal foci during development. In the matrix, thalamostriatal terminals are hypothesised to target Ten-m3-positive cells (grey), which may constitute a novel matrisome compartment, to form an overall 'patchy' termination pattern in the striatum.

(B) In the absence of Ten-m3 in the striatum and PF in KO mice, thalamostriatal terminals spread out throughout the matrix compartment. We propose that the absence of the adhesive signals normally exhibited by Ten-m3 to attract and confine these projections to distinct regions of the matrix leads to the uniform and increased spread of thalamostriatal terminals observed in KOs.

Interestingly, despite the overall increase in the area occupied by thalamic terminals in KOs, there was some evidence that these tended to avoid the VL quadrant of mid-caudal striatum. This was often evidenced by the presence of what appeared to be an abrupt border in this area. Due to the small number of cases in which this was able to be confirmed, however (see Technical considerations), further studies are required to resolve this. This is particularly intriguing as changes in a number of other parameters measured independently, such as retrograde tracing data, distribution of cholinergic cells and striatal area and cell number, all showed changes that were either specific to or most marked in mid-caudal striatum, suggesting the possibility of region specific changes (see below).

Insights from retrograde tracing studies as to how thalamostriatal projections are altered in Ten-m3 KOs

Anterograde tracing studies revealed that Ten-m3 KO mice exhibit a loss of the characteristic patchy patterning and an increased spread of thalamostriatal terminals from the PF. The organisation of thalamostriatal projections was further analysed using dual focal retrograde tracing studies. Dual focal injections of CTB conjugated to Alexa Fluor-488 and -594 separated by 500 μm along the RC axis did not produce double-labeled PF cells in KOs, suggesting that, in the absence of Ten-m3, PF terminals from individual cells do not terminate in ectopically rostrocaudally-extended zones within the striatum. Further, the number and area of retrogradely-labeled cells projecting to mid-caudal striatum (ie. red cells) were reduced and the topography altered in the KO PF compared

to WTs. Interestingly, this correlated with the region which thalamostriatal terminals appeared to avoid in anterograde tracing experiments, discussed further below.

Although no double-labeled cells were observed in KOs, it is still unclear whether individual axons are also project aberrantly to different regions of the striatum. That there is no compensation for the reduction in number and area of cells projecting to mid-caudal striatum (red cells) in the population projecting to rostral striatum (green cells), suggests that this may not be occurring. However, it is difficult to rule out the possibility that the mid-caudal projecting cells may be altered independently of the rostrally projecting population. This hypothesis may be supported by current data indicating that Ten-m3 may be exerting a region-specific effect at mid-caudal levels of the striatum, with changes in targeting of axons to VL striatum, striatal area and cell number, in particular, in the cholinergic cell population, only observed at these levels. Moreover, previous studies have shown a caudal shift in retinocollicular axons in Ten-m3 KOs during development, which was only observed in a subset of these projections (Dharmaratne et al., 2012). There also appears to be a correlation between the graded expression pattern of Ten-m3 and the region in which its actions are most potent along the RC axis. In the striatum, Ten-m3 is expressed in a high-caudal to low-rostral gradient, which correlates with the changes observed predominantly in the mid-caudal striatum. This region specific effect is consistent with findings in the visual pathway, where retinogeniculate mapping defects are most prominent in rostral dLGN (Leamey et al., 2007b), where Ten-m3 expression is also highest (Leamey, unpublished observations).

The molecular mechanisms by which Ten-m3 acts to control the accurate targeting and patterning of thalamostriatal axons are currently unclear. Available data suggests that the role of Ten-m3 may be multi-faceted. Previous studies implicating Ten-m3 in neurite outgrowth, fasciculation and adhesion (Leamey et al., 2007a; Tucker and Chiquet-Ehrismann, 2006), suggest it may act as an adhesive target for thalamostriatal axons. Further, the existence of multiple cleavage sites on the teneurin molecule suggests some of its actions may also occur via the release of, notably, the ICD and TCAP sequence, both of which have been shown to alter levels of other genes. In particular, changes in Eph/ephrins, also expressed in the striatum, have been observed in visual structures of Ten-m3 KOs (Glendining, 2011). EphA7 is of particular interest to the present study due to the intriguing similarities in expression patterns it shares with Ten-m3 in the striatum. These proposed molecular mechanisms are investigated in Chapter 4.

Ten-m3 affects cholinergic interneuron number and distribution

The number of cholinergic interneurons was significantly reduced in the commissural striatum, in particular, in the VL quadrant of Ten-m3 KO mice. Further, analysis of the density of cholinergic interneurons only showed significant changes in the VL quadrant, suggesting that these were not due to deficits in cell migration. Total striatal cell number was also significantly reduced in caudal striatal regions of Ten-m3 KO mice. There was, however, no obvious depletion of Nissl-labeled cells in the VL quadrant in these sections. Hence, it is possible, that Ten-m3 KOs may exhibit a blockade in the development of cholinergic interneurons. Cholinergic interneurons mature along a lateral-medial and

caudal-rostral gradient in the first and second postnatal week of development (Schlösser et al., 1999; Semba and Fibiger, 1988). The changes in the lateral and caudal cholinergic population suggest that the earliest born population is most affected in Ten-m3 KOs. Interestingly, however, early-born cholinergic interneurons in Gbx2 mutants are located more medially, while the late-born population are mostly missing (Chen et al., 2010). Hence, further studies are required to determine which cholinergic population is affected in Ten-m3 KOs.

In addition to Gbx2, a number of genes have been implicated in the development of cholinergic cells, including Nkx2.1 and LIM homeobox 7 (Lopes et al., 2012; Marin et al., 2000). There is currently no known link between these genes and teneurin molecules. It is further unclear whether Ten-m3 is expressed in cholinergic interneurons. These cells are born as early as E12.5 in the mouse MGE, while expression studies (Chapter 1) suggest that Ten-m3 is expressed in the ventricular zone of the MGE at E15. Hence, further studies are required determine whether Ten-m3 is expressed in the MGE at earlier stages of development, to compare Ten-m3 expression with that of ChAT-positive cells and to determine potential links between teneurins and genes involved in the genesis of cholinergic interneurons.

Normally, cholinergic interneurons are a major target of thalamostriatal axons from the PF. The current study shows that these components may both be altered, with projections from the PF showing a tendency to avoid the VL quadrant of mid-caudal striatum, where cholinergic interneurons are most markedly reduced in number. That there are

observable changes to both these components in Ten-m3 KOs suggests that (a) both are directly affected by Ten-m3 or (b) changes in one have indirectly led to changes in the other. Since there are currently no molecular links between Ten-m3 and the development of cholinergic interneurons, previous evidence implicating Ten-m3 in neural connectivity suggests that its actions on thalamostriatal connectivity may have indirectly led to changes in the cholinergic population. However, it is currently unclear how the two components influence one another during normal development, because although striatal cholinergic interneurons are generated (E12 in rats) before the emergence of thalamostriatal axons (E19), these cells continue to migrate within the striatum into the second postnatal week of development (Van Vulpen and Van Der Kooy, 1996). Interestingly, the migration of cholinergic interneurons from striosomes into the matrix occurs between P3 and P7 in rats (Van Vulpen and Van Der Kooy, 1996), the same period during which thalamostriatal terminals switch from overlapping with striosomes to being confined to the matrix in mice (current study, see Chapter 4). It is unclear, however, whether this postnatal time period is equivalent between mice and rats, and, thus, needs to be confirmed.

Moreover, the overall changes in the distribution of thalamostriatal axons (reduced patchiness, increased spread) may have a wider effect on their interactions with cholinergic neurons in KOs. Hence, it would be of interest to determine whether and how the dense patches of thalamostriatal terminals correlate with the location of cholinergic neurons in WTs, and further, how their innervation and capacity to drive these cells is impacted in KOs. Future studies should also investigate the time course of

the changes in the distribution of the cholinergic neurons in Ten-m3 KOs and how this relates to the changes in the thalamostriatal projection. The multiple changes occurring in the distribution of thalamostriatal projections and their targets may have dramatic consequences for cholinergic transmission within the striatum of Ten-m3 KO mice. This is discussed in the context of the behavioural data below.

Although region-specific changes to a number of independently measured parameters were found, as described above, it is currently unclear why the VL quadrant of mid-caudal striatum is specifically affected in KOs. Although the caudal striatum shows highest levels of Ten-m3, the ventral regions often show the lowest levels of expression (Chapter 2), suggesting the Ten-m3 levels may not necessarily correlate with potency of its action. Further, although the striatum is divided into different functional divisions, in particular, DM and DL, very few studies have specifically examined the functions of the VL region associated with the 'classically' known 'dorsal' striatum, described in the present study. It is likely that VL striatum is an extension of DL striatum, which is associated with roles in sensorimotor function and stimulus-response learning (Yin et al., 2009). The delayed learning deficits observed in Ten-m3 KOs on the rotorod test (discussed further below) support this theory, however, further studies are required to resolve the functions of this region.

Loss of Ten-m3 leads of deficits in motor function and motor learning

The functional impact of the anatomical deficits observed in the thalamostriatal pathway of Ten-m3 KO mice was investigated behaviourally using analysis of gait and motor learning paradigms. Motor function has long been associated with the striatum, being most noted in humans with disorders associated with degeneration of striatal neurons, including Huntington's chorea and Parkinson's disease (see Albin et al., 1989 for a review). The striatum is also implicated in various forms of learning, including procedural and goal-directed learning (Bradfield et al., 2013; Shiflett and Balleine, 2011; Shiflett et al., 2010). These functions are also presumably reliant on other striatal components, such as arousal and motivation (Balleine, 2011; Ostlund et al., 2011), which have also been linked to the PF (Kinomura et al., 1996; Minamimoto and Kimura, 2002). Learning, however, is also associated with other brain structures, in particular, the hippocampus (Good, 2002). Since the hippocampus, like the striatum, also expresses high levels of Ten-m3, along with other teneurin paralogues (Zhou et al., 2003), it was important to design/use behavioural paradigms to best distinguish between the circuits involved. The hippocampus is classically known for encoding declarative and episodic memories and is predominantly associated with place-based learning in rodents (Doeller et al., 2008). The striatum, on the other hand, encodes procedural memory and is associated with response-based learning (Woolley et al., 2013). Hence, spatial components of learning paradigms were avoided in the current study. Further, many goal-directed learning paradigms testing striatal function utilise sensory stimuli as a

salient signal for an upcoming reward. Ten-m3 KO mice exhibit severe sensory impairments, particularly vision (Leamey et al., 2007b).

An initial attempt was made to test Ten-m3 mice in a goal-oriented learning paradigm that excluded spatial learning and sensory stimuli but examined the function of lateral striatum and the thalamostriatal projection (Yin et al., 2009). An operant conditioning task was trialed, where mice were trained to associate an action (lever press) with a reward in a Skinner box, with the plan to eventually reverse this contingency. Despite this seemingly simple task, many problems were encountered. The most significant was that Ten-m3 KO mice were not sustainable at 90-85% of their free feeding body weights, appearing to lack motivation to eat after a period of carefully monitored food restriction. This apparent loss of motivation may be linked to the anatomical changes observed in the thalamostriatal system of these mice, however, for ethical reasons, further investigations into this were not pursued. The food restriction and subsequent weight reduction required of these mice has been shown to be necessary for food-based reward tasks (Makowiecki et al., 2012). Hence, this task was deemed inappropriate for these mice and simpler tasks that assessed motor performance and learning were used.

Gait analysis indicated that Ten-m3 KO mice exhibit a slightly altered locomotive action, reflected by the reduction in stride length, compared to WTs. Although animals were not measured, no gross differences in body length were evident and previous data showed no significant differences in body weights between genotypes (Leamey et al., 2007b). The striatum has long been implicated in motor function (see Gerfen and Wilson, 1996 for a

review), however, it is unclear whether the thalamostriatal deficits observed in Ten-m3 KOs directly result in this behavioural change. A previous study by Lee *et al.* (2012a) found a significant increase in step width and variance in animals from which a subset of PNNs in the striatum were removed, potentially disrupting circuits that may be involved in regulating and/or coordinating this behavior in adult mice. Further, Ten-m3 has been shown to be expressed in the developing limb of mice (Ben-Zur et al., 2000), the absence of which may also be important in the altered gait observed in the current study. Moreover, the hopping action observed in some aspects of the Ten-m3 KO locomotor activity has previously been observed in the EphA4 mutant, where it is hypothesised that the altered wiring of spinal cord connections in these animals results in the subsequent synchronisation of the normally alternating bilateral motor network (Akay, 2006; Kullander, 2003). Since Ten-m3 is also expressed in the spinal cord (Allen Brain Atlas), it is likely that the loss of Ten-m3 from any, or a combination, of these motor-related brain structures has contributed to the altered gait observed in Ten-m3 KO mice.

The subtle locomotor deficits exhibited by Ten-m3 KO mice did not affect their initial performance in the rotorod motor learning task. The first exposure of animals to the task on day 1 provided an essential baseline measurement of motor function, in contrast to the motor learning behaviour assessed across the course of 5 days. The remarkable similarity in performance between WT and KO animals on this first exposure, in addition to that on the fifth day, signified that the differences in performances in the in-between days (discussed below), did not result from a physical inability of KOs to perform the task due to deficits of motor function.

The accelerating rotorod test was used as the chosen paradigm to examine the functional impact of changes observed in the thalamostriatal pathway in Ten-m3 KOs. Previously, the thalamostriatal pathway was shown not to affect performance on an accelerating rotorod test (Kato et al., 2011), however, the current study found deficits in the learning component of this task in Ten-m3 KOs, who exhibit less specific and generally more wide-spread thalamostriatal terminals in the matrix. Kato *et al.* used a paradigm which accelerated the rotorod from 4-40 rpm in 3s, which, in constrast, was done more gradually in the present study, over 180 s. This difference in paradigms may be of significance, particularly since the PF has previously been shown to have roles in strategy switching and attention orienting (Bradfield et al., 2013; Hulme et al., 2010), abilities which may be constantly required as the speed of the rotorod continues to change with a gradual acceleration. In contrast, the task presumably becomes habitual once the rod reaches full speed, and hence, may require the activation of an alternate striatal pathway. Moreover, as mentioned earlier, changes to striatal NMDA receptors, the main receptor targets of these projections, including on cholinergic neurons (Consolo et al., 1996a), have been linked to deficits on rotorod tests (Beutler et al., 2011; Dang et al., 2006). These receptors may be altered in Ten-m3 KOs due to changes in the distribution of thalamic terminals. Hence, future studies should investigate NMDA receptor levels in Ten-m3 KO striatum.

Differences in rotorod performance were observed between genotypes across sessions within training days, and in the sum of latencies across training days. Hence, KOs

appeared to show deficits in the learning aspect of the task. However, the absence of Ten-m3 did not appear to disrupt the animal's ability to learn completely, only to delay it. Delays in procedural learning have been observed in Parkinson's disease patients (Muslimovic et al., 2007) and mutant mice missing the α7-nicotinic ACh receptor (Young et al., 2011). The latter case is particularly interesting given the region-specific reduction of the striatal cholinergic interneuron population in Ten-m3 KOs, the loss of which is also linked to deficits in spatial learning and memory in Nkx2.1 and Lxh7 mutants (Fragkouli et al., 2005; Magno et al., 2011). The levels of other neurotransmitters, notably ACh, however, have yet to be studied in these animals.

Nicotinic ACh receptors are predominantly associated with dopaminergic afferents, where they play significant roles in the modulation of dopamine release via ACh in the striatum (see Exley and Cragg, 2008 for a review). Both ACh and dopamine are required for reward-based learning in the striatum, and although have historically been believed to have antagonistic effects, recent studies indicate that they may, in fact, have synergistic roles, with the release of one often being highly dependent on the other (Ding et al., 2010; Patel et al., 2012; Threlfell et al., 2012). Striatal cholinergic interneurons, the sole source of striatal ACh, receive the largest proportion of their inputs from the PF (Lapper and Bolam, 1992), which are essential for D1-mediated ACh release via NMDA receptors (Consolo et al., 1996a, 1996b, 1999; Ragozzino, 2004). Interestingly, D1 receptors have been linked to the 'early' stage of skill learning on a rotorod (Yin et al., 2009), which is affected in Ten-m3 KOs, and are most highly expressed in VL striatum (Savasta et al., 1986), where the cholinergic population is reduced in these animals.

Hence, future studies should investigate levels of dopaminergic axons and D1 receptors in Ten-m3 KO striatum, as well as more fully characterising the tendency for PF axons to specifically avoid VL striatum in caudal regions. Moreover, the characteristic burst-pause pattern of spiking in cholinergic interneurons, observed during associative learning and is induced by thalamic stimulation, is dependent on the activation of nicotinic ACh receptors and dopamine release (Ding et al., 2010). Further, thalamostriatal axons from the PF, like corticostriatal axons, are proposed to be modulated by dopaminergic terminals (Moss and Bolam, 2008). These apparently cyclic actions of glutamate, dopamine and ACh, summarised in Figure 3.12, indicate the complex nature of the neurotransmitter systems working together to control striatally-mediated functions, presumably including procedural learning, in the striatum.

Hence, the delayed learning observed in Ten-m3 KO mice may be the result of the reduced number of cholinergic interneurons in the VL striatum. The tendency towards the loss of thalamostriatal terminals in this area, if confirmed, would exacerbate this effect. The reduction in cholinergic interneurons suggests a drop in ACh levels, particularly in the VL striatum, which should be confirmed, and may have wide ranging physiological consequences. Reduced levels of ACh acting on nicotinic ACh receptors suggests a decline in dopamine release normally dependent on these receptors. These reduced dopamine levels can still act on D1- and D2-receptors on MSNs, but may affect the balance between the direct and indirect pathways, and motivational aspects of behaviour. Further, reduced dopamine levels suggest a concurrent reduction in the

modulation of thalamostriatal afferents. Hence, the altered levels of ACh may have wide ranging affects on the normal neurotransmitter systems in striatal circuits (Fig. 3.12).

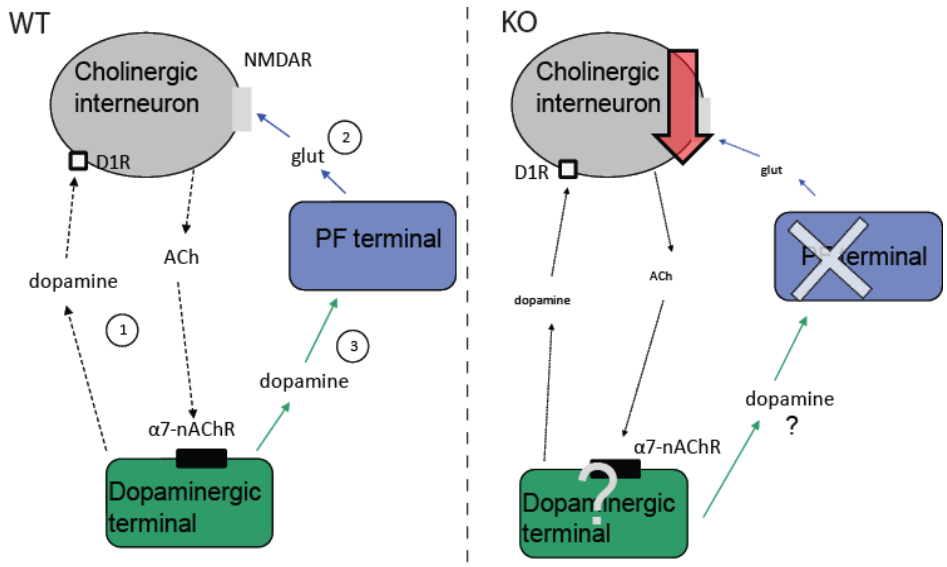

Figure 3.12. The hypothesised cyclic actions of glutamate, dopamine and ACh between thalamostriatal afferents and cholinergic interneurons the mid-caudal VL striatum, and the potential changes in Ten-m3 KO mice.

In WTs, nicotinic ACh receptors (α7-nAChR) are predominantly associated with dopaminergic axons. α7-nAChR modulate dopamine release via ACh, which can affect ACh release via D1 receptors on cholinergic interneurons (1). Glutamatergic thalamostriatal axons from the PF are essential for D1-mediated ACh release via NMDA receptors (2). Moreover, dopaminergic terminals modulate thalamostriatal input (3).

In VL striatum of KOs, the reduction in cholinergic interneurons (arrow), and potentially thalamic afferents from the PF (cross), suggest reduced levels of ACh release, normally mediated through D1 and via NMDA receptors, from these cells. Reduced levels of ACh acting on α7-nAChR suggests a reduction in dopamine release normally dependent on these receptors. Although the precise impact of these changes on dopaminergic terminals and extrinsically-induced dopamine release is unclear, the potentially decreased levels of dopamine, combined with the resulting concurrent reduction in the modulation of thalamostriatal afferents, may contribute to the motor learning deficits observed in the KOs.

Note, for simplicity, interactions between thalamostriatal afferents and MSNs, have not been included in this schematic.

Together, these data suggest that the absence of Ten-m3 leads to changes in the thalamostriatal projection, the cholinergic neuronal population and subsequent deficits in motor coordination and motor learning. Ten-m3 is the first molecular candidate shown to have a role in the formation of thalamostriatal projections. The effects of the absence of Ten-m3 are wide ranging, and it is likely that, within such a intricate and complex system, that the direct changes in one component resulting from the absence of Ten-m3, such as the normal targeting of thalamostriatal axons, may produce a domino effect of changes in a number of other components, including the disruption of the normal neurotransmitter systems within this circuit. This highlights the importance of the role of Ten-m3 in the normal connectivity of striatal circuits. The exact mechanisms by which Ten-m3 is exerting its actions, however, are still unclear. As Ten-m3 is most highly expressed during development, it is likely that its effects will be most significant in younger animals. Further, it is likely that it involves a combination of established functions including adhesion, fasciculation and altering transcription of other genes. With respect to the latter mechanism, a number of axon guidance genes that are altered in Ten-m3 KOs are also expressed in the striatum, namely EphA7. Hence, the next chapter will investigate changes in thalamostriatal projections during development and the potential changes to EphA7 levels in the striatum of Ten-m3 KO mice.

Chapter 4

Mechanisms of Ten-m3 in the developing thalamostriatal pathway

Introduction

The thalamostriatal projection is highly specific in the adult. The normal development of this pathway has been largely neglected by the field. While there are brief reports for cats, opossums and rat (Fisher et al., 1983; Martin et al., 1989; Vercelli et al., 2003), the only detailed study to have examined this did so in rats and the work is available only in the form of a PhD thesis (Srivastava, 1999). This study reported that the compartmentalisation and heterogeneous patterning of these projections within the matrix is first observed at the end of gestation (Srivastava, 1999). The normal development of these projections, including the mechanisms which regulate their patterning and targeting of the striatal matrix compartment, are yet to be described in mice.

Data presented in Chapter 2 showed that Ten-m3 is expressed in intriguing patterns throughout the thalamostriatal pathway during development, suggesting that it may have a role in regulating the formation of this pathway. Further, work presented in Chapter 3 of this thesis revealed that the specific patterning and targeting of thalamostriatal projections in the adult is dependent on the actions of Ten-m3. An analysis of the impact

of Ten-m3 deletion on the development of this pathway therefore, may help reveal the mechanisms by which Ten-m3 is exerting its actions. Additionally, or consequently, it may reveal other developmental processes that are affected in the absence of Ten-m3.

The mechanisms by which Ten-m3 exerts its actions are currently unclear. It has been hypothesised that its ability to form homophilic interactions may regulate the guidance of ingrowing axons to their appropriate cellular targets (Beckmann et al., 2013; Leamey et al., 2007a, 2007b). Further, evidence suggests that expression of other guidance cues, such as EphA7, are altered in visual structures of Ten-m3 KO mice (Glendining, 2011), presumably via cleavage and translocation of the intracellular domain to the cell nucleus. EphA7 is also expressed in patches in the striatal matrix (Janis et al., 1999; Tai et al., 2013), and has a role in the formation of striatofugal projections. The spatial relationship between EphA7 and Ten-m3 is currently unknown. It is possible that Ten-m3 may exert some of its actions upon striatal circuits by altering the expression of EphA7.

The current study will describe the normal development of the thalamostriatal pathway originating from the PF in WT mice. Further, changes to this developmental pattern will be investigated in Ten-m3 KOs to provide additional information as to the potential roles of Ten-m3 during development. Additionally, two of the major mechanisms previously proposed to underlie the actions of teneurins will be investigated. That is, is Ten-m3 acting as a direct attractive target for ingrowing axons? And/or is Ten-m3 acting indirectly to control axon guidance, by altering expression of EphA7 in the striatum?

Methods

DiI tracing

Animals

DiI tracing studies were performed on WT and KO animals at E16, E17, P3, P7, P10 and P15 time points. Littermates were used where possible. Embryonic animals were obtained from timed matings of heterozygous and homozygous mice. Pregnant mothers were anaesthetised using 2-4% isoflurane in oxygen and pups removed by Caesarian section. Pups were decapitated, heads rinsed in 0.1 M PB and postfixed in 4% paraformaldehyde at 4ºC until required. For postnatal animals, pups were euthanised with an overdose of sodium pentibarbitone and transcardially perfused, as described in Chapter 3. Animals were then decapitated, heads rinsed in 0.1 M PB and postfixed in 4% paraformaldehyde at 4ºC until required.

DiI crystal placement

Localisation of the PF at the various developmental age points was determined by assuming that any shrinkage of the tissue due to histological processing is uniform across a given axis. Hence, the ratio of the distance of the PF from the rostral pole of the cortex to the RC length of the cerebral cortex in processed tissue should be equal to the ratio of these same parameters in unprocessed tissue. To determine this ratio in processed tissue, a Nissl stain was performed, as described previously (Chapter 3), on 40 µm-thick coronal

sections spanning the RC length of the cortex for each age point. The RC length of the cortex in processed tissue was determined by multiplying the number of sections spanning this region by 40 µm. Further, the RC length of the cortex was measured in an intact, paraformaldehyde-fixed brain. The ratio obtained from these measurements was then used to calculate PF position in unprocessed tissue:

$$PF_U = \frac{PF_P \text{ x } cerebrum_U}{cerebrum_P}$$

where:

PF_U = distance of PF from rostral pole of cortex in unprocessed tissue

PF_P = distance of PF from rostral pole of cortex in processed tissue

$cortex_U$ = rostral-caudal length of cortex in unprocessed tissue

$cortex_P$ = rostral-caudal length of cortex in processed tissue

The same procedure was used to determine theDV location of the PF in the coronal plane. Table 4.1 shows these measurements for each of the age points analysed. These measurements were marked onto graph paper and used as markers during DiI placement. First, the brain was exposed by removing the skull covering the dorsal surface and a scalpel used to make a coronal cut at the measured RC location of the PF. With the aid of a dissection microscope, a small DiI crystal was placed at the marked DV location, at the lateral edge of the fr, which was often visible. Hence, crystals were placed into DL PF in both hemispheres, as the thalamostriatal projection from the PF is strictly ipsilateral.

Brains were incubated in 1% paraformaldehyde at 37ºC for 3-6 weeks to allow for dye transport.

After the appropriate transport period, brains were embedded in gelatin-albumin hardened with gluteraldehyde, as described previously (Chapter 3), and cut at 80μm in the horizontal, coronal or sagittal plane on the vibratome. Sections were mounted onto glass slides and coverslipped with 50% glycerol in 0.1 M PB containing DAPI. Sections cut in the sagittal plane were used for analysis, as this was better for revealing the fibres and trajectory of thalamic fibres, which run rostral to caudal, particularly in younger animals when these fibers were sparse are were difficult to distinguish from passing fibers within bundles of the internal capsule.

In some cases, immunohistochemistry for TH or μ-OR was performed on DiI labeled sections to determine the development of the compartmentalisation of thalamostriatal terminals. These procedures were described in Chapter 2. Due to the extensive period of incubation that was required for DiI transport, this immunostaining was not always successful. Further, since compartmentalisation of thalamostriatal terminals was not altered in adults, it was not a key focus of the current study to further investigate this during development. Hence, these data were not quantitatively analysed, but are illustrated qualitatively where possible.

Table 4.1: Measurements for DiI placement

Age	**E16**	**E17**	**P3**	**P7**	**P10**	**P15**
RC distance (mm)	2.5	2.5	4.5	4.5	5	5
DV distance (mm)	1.5	1.5	2	2.5	2.5	2.5

Image collection and analysis

Images were taken on a Zeiss deconvolution microscope using filters for DAPI (λ = 360 nm) and Cy3 (λ = 512 nm) and high resolution z-stack images taken on Zeiss Meta Spectral Confocal and Leica SPE-II confocal microscopes to reveal thalamostriatal terminals. Images were exported as tif files using AxioVision Rel. 4.7 and Image J software and low power images merged using the photomerge function in Adobe Photoshop CS3 as described previously.

For analysis of E17 DiI images, 40x confocal images through the dorsal and rostral striatum were taken for each distinct injection. Two images per distinct injection (4 x WT, 4 x KO) for 3 x WT and 3 x KO animals were analysed in Image J. For each image, background was subtracted and images automatically thresholded. Pixels representing obvious confounding artefacts such as blood vessels were selected using the magic wand tool and subtracted prior to analysis. Images were converted to skeleton images and analysed for the number of junctions using the Skeleton plugin. The number of junctions were compared between WT and KO using a t-test.

For postnatal DiI experiments, images were taken throughout the ML extent of the striatum. Two consecutive sections were selected for each of three ML levels through the striatum (medial, middle, lateral) for distinct injections made in WTs and KOs at four developmental age points, P3 (5 x WT, 5 x KO), P7 (6 x WT, 6 x KO), P10 (5 x WT, 5 x KO), P15 (6 x WT, 4 x KO), for analysis. Sections for each level were selected such that lateral sections approximately corresponded to 2.64 mm from the midline and medial sections to 1.2 mm from the midline in the adult mouse brain (Paxinos and Franklin, 2001). Various landmarks were used to determine these levels in early postnatal brains, such as the position of the junction between the dLGN and ventral LGN for medial sections and the appearance of the GP in lateral sections.

Analysis was performed on the DiI channel for each image in Image J. The perimeter of the striatum was traced using the polygon tool and the enclosed area determined. Images were subsequently thresholded at a constant value of 20. Images were processed to produce 100 x100 matrices and heat maps using R, as described in Chapter 3. Heat maps were produced by averaging matrices across all samples separately for each striatal level and age point. Graphs plotting the distribution of label along the RC and DV axes were generated by summing pixels across y and x axes, respectively, in the averaged matrices for each level and age point. Distributions across the x and y axes were analysed using a K-S test. Moreover, areas under the distribution plots were calculated by summing the Y-values in each plot for separate lateral and medial levels for WTs and KOs.

BDA injections at P25-30

Due to the intriguing developmental patterns of the thalamostriatal pathway in KOs, these projections were further investigated at P25-30. Further, since DiI did not completely label this pathway by the end of the second postnatal week, *in vivo* BDA injections were used so that results would be comparable to those shown in adults in Chapter 3. BDA injections were performed as for adults, with coordinates determined to be 1.3 mm rostral of lambda, 0.8 mm lateral of the midline and 3.1 mm deep. The tracer was allowed to transport for 5 days before animals were euthanised, transcardially perfused and the brain processed as described previously for adult BDA injections. Thalamostriatal terminals were detected using DAB and imaged on a Zeiss Deconvolution microscope. For injection sites, one image through the centre of the injection, and for terminal label, two images, one rostral and one at the level of the anterior commissure, were analysed for 3 x WT and 3 x KO cases, using ImageJ, as previously described (Chapter 3).

In situ hybridisation and labeling of thalamostriatal terminals at P10

One possible mechanism by which Ten-m3 may be acting to guide PF terminals is by acting directly as an attractive target. If this is the case, we expect that Ten-m3-positive cells may delineate the thalamostriatal terminal patches originating from the PF. To investigate this, injections of CTB were made into the PF of P10 WT mice, and alternate sections processed for *in situ* hybridisation for Ten-m3 and immunohistochemistry for

CTB. P10 was selected due to the high level of Ten-m3 expression using *in situ* hybridisation at this age point (Chapter 2), whereas expression appears to be dramatically reduced in adults (Allen Brain Atlas). *In vivo* injections to the PF at ages younger than P10 would have been technically very difficult to achieve and would have risked cannibalisation of the pups by the mother.

Pressure injections of CTB (List Labs) were performed as described for BDA injections (Chapter 3). The coordinates of the PF were determined, based on the coordinates used for adult WT mice, to be 0.9 mm rostral of lambda, 0.5 mm lateral of the midline and 3 mm deep. The tracer was allowed to transport for 5 days before the animal was euthanised and the brain removed, frozen and sectioned as for *in situ* hybridisation experiments (Chapter 2). One series of sections was used to detect Ten-m3 using *in situ* hybridisation, as described previously (Chapter 2). An adjacent alternate series was processed for immunohistochemistry for CTB using a protocol adapted from Angelucci et al. (1996). Sections were thawed at RT for 30 min before being fixed in 4% paraformaldehyde for 45 min. After washing 3 x 5 min in 0.1 M PB, sections were blocked using 4% NRS, 2.5% BSA, 0.3% TritonX-100 in 0.1 M PB for 2 hr at RT and subsequently incubated in goat anti-CTB (ListLabs; 1:4000 in 2% NRS, 2.5% BSA, 2% TritonX-100 in 0.1 M PB) overnight at 4°C. Sections were then washed 3 x 15 min in 0.1 M PB and incubated in 2% NRS, 2.5% BSA in 0.1 M PB for 10 min before incubating in rabbit anti-goat-488 secondary antibody (Invitrogen; 1:200 in 2% NRS, 2.5% BSA, 1% TritonX-100 in 0.1 M PB) for 2 hr at RT. Sections were washed 3 x 5 min in 0.1 M PB and coverslipped with 50% glycerol in 0.1 M PB with DAPI.

Images of Ten-m3 *in situ* hybridisation and CTB-labeled sections were taken using the Zeiss Deconvolution microscope as previously described. For two successful cases, alternate sections spanning the RC extent of the striatum were overlayed in Photoshop as previously described for the overlaying of TH and Ten-m3-labeled images, to determine the overlap between Ten-m3-positive cells and thalamostriatal terminals in WT mice.

EphA7 *in situ* hybridisation

A second mechanism by which Ten-m3 may be acting to guide thalamostriatal axons during development is indirectly, by changing the expression patterns of downstream axon guidance molecules. Preliminary data generated by other members of the laboratory, suggests that EphA7 may be one of these candidates, as its expression is downregulated in visual structures of Ten-m3 KO mice (Glendining, 2011). EphA7 is also expressed in patches in the matrix (Janis et al., 1999; Tai et al., 2013) and, hence, could potentially correlate with Ten-m3-positive patches and may also be downregulated in the striatum of Ten-m3 KO mice. Firstly, distribution patterns of Ten-m3 and EphA7 were compared in adjacent sections of P3 WT striatum. *In situ* hybridisation was performed for Ten-m3 as described in Chapter 2, and for EphA7 using the same protocol. Both sense and antisense probes were generated using primers as specified in Table 4.2. The initial construct used to generate EphA7 probes were produced by Kelly Glendining (Glendining, 2011). Images of adjacent sections were processed and overlayed as described for TH and Ten-m3 in Chapter 3.

Table 4.2. Primer sequences used for probe synthesis for in situ hybridization for EphA7.

Gene	Accession number	Primer sequence (5'-3')
EphA7	NM_010141.3	Forward: GCTGTAAATGGAGTTTCGGAC Reverse: GTGTGGCAACATCAAGCCTA

The overlayed images showed a striking partially overlapping but mostly complementary relationship between Ten-m3 and EphA7. To calculate the area of overlap between Ten-m3 and EphA7, images were thresholded in ImageJ and total positive-pixel areas determined for each gene separately, and the image calculator function used to 'add' Ten-m3 and EphA7-positive pixels to determine the overlapping area. This area was reported as a percentage of the total pixel area for each gene separately. Hence, both genes appeared to be expressed within different matrisome compartments. It was then hypothesised that these matrisomes may comprise the entire matrix compartment. Hence, immunohistochemistry for TH was performed on a third, adjacent set of sections to label striosomes (as described in Chapter 2), and images overlayed with those of Ten-m3 and EphA7 expression.

To determine potential changes to the distribution and intensity levels of EphA7 expression in Ten-m3 KO mice, *in situ* hybridisation was also performed on P3 KO tissue. Intensity analysis was performed to compare expression levels between 3 x WT and 3 x KOs at three striatal levels: rostral, medial and caudal. This was performed using ImageJ, as described in Chapter 2. Briefly, images were converted to 8 bit grayscale

files, inverted and background subtracted before being thresholded automatically. The polygon tool was used to trace the perimeter of the striatum and the total pixel count within this contour determined. This was analysed using a repeated measures ANOVA combining all images from all striatal levels, and a one-way ANOVAs were used to compare distinct striatal levels.

Western Blotting

To determine potential changes in EphA7 protein levels in the absence of Ten-m3, Western blotting was performed on pooled striatal tissue from WT and Ten-m3 KO mice. Tissue from the SC was used as a positive control.

P3 mice were euthanised, decapitated and the skull quickly removed. The SC was dissected out. A coronal cut was then made approximately half way along the rostrocaudal length of the cortex, dividing the striatum roughly into rostral and caudal portions. The striatum was scooped out from rostral and caudal portions of both hemispheres. Every attempt was made to obtain striatal tissue from both hemispheres and rostral and caudal regions, however, often tissue from caudal regions were not able to be accurately acquired and were therefore abandoned. Tissue from 8-10 animals of each genotype was collected into tubes on dry ice, and combined to form two pooled samples from separate striatum and SC for WT and KO mice.

Total tissue was weighed and homogenised in 200 µL radio-immunoprecipitation assay (RIPA) buffer containing protease inhibitor cocktail, 10 mM NaF, 1 mM Na_3VO_4 and 1

mM phenylmethylsulfonyl fluoride (PMSF), and solubilised for 2 hr on a rotator at 4°C. Samples were subsequently centrifuged at 12,000g for 15 min at 4°C, and the supernatant collected. Protein samples were quantified using a dilution series against known concentrations of BSA standards using a protein assay concentrate (BioRad) on the POLARgalaxy microplate reader in the Bosch Molecular Biology Facility.

For Western blotting, 40 µg protein samples were diluted in 1 x Laemmli buffer containing 10% SDS, 62.5 mM Tris-HCl, pH 6.8, 0.05% bromophenol blue, 20% glycerol and 10% β-metcaptoethanol. Samples were run on 6% SDS PAGE gels, along with a Kaleidoscope ladder (BioRad), for 80 min at 150V. Gels were subsequently equilibrated in transfer buffer containing 20% methanol before being transferred using a Bio-Rad Trans-Blot Turbo Transfer system for 15 min at 15V. Membranes were subsequently blocked in 1% BSA in 1% Tween, 10 mM Tris buffered saline (TTBS) for 1 hr and then cut below the 75kDa mark into two. The top portion was incubated in rabbit anti-EphA7 (Abcam; 1:100 in 1% BSA, 0.02% sodium azide, 0.0025% phenol red in TTBS), and the bottom in rabbit anti-β-actin monoclonal IgG (cell signaling technology; 1: 1000 in 5% BSA in TTBS) overnight at 4°C. Membranes were washed 3 x 10 min in TTBS before incubating in anti-rabbit HRP (Cell signaling technology; 1:10000 in 2% skim milk in TTBS) for 1 hr at RT. Membranes were washed 3 x 10 min in TTBS and imaged using a BioRad ChemiDoc system (Bosch Molecular Biology Facility). Images of western blots were analysed for relative intensity using ImageLab software (BioRad) and analysed using a multivariate ANOVA.

Results

Normal development of thalamostriatal projections in mice

The normal development of thalamostriatal projections is yet to be described in mice. Hence, DiI tracing in fixed tissue was first used to determine the early development of this pathway in WT mice. Ages used for analysis were chosen based on the reported timing of initial ingrowth of the pathway in the rat, that is, at E17 (Srivastava, 1999), and to match those of the expression studies in Chapter 2. Sagittal sections were used for this analysis as preliminary studies found that early branches, in particular, were most easily distinguishable amongst fibers of the internal capsule in this plane, as these extend rostrally and collaterals appeared to form along an orthogonal axis. This contrasts with the coronal sections that were used for the bulk of the adult studies described in Chapter 3, making it somewhat difficult to make direct comparisons (see Discussion). However, this will be done where possible.

At E16, bundles of axons were observed in the striatum. In the horizontal plane (Fig. 4.1A), fibers were observed to enter through the internal capsule, radiating towards rostral striatum (Fig. 4.1A, dashed line). High resolution, confocal images (Fig. 4.1A') revealed that these fibers were largely unbranched, and, hence, may not form connections with striatal cells at this stage. By E17 (Fig. 4.1B), collateral branches had begun to form, with higher resolution images allowing these to be clearly observed extending at approximately right angles to their parent axon fiber to innervate the striatum (Fig.

4.1B'). At low power, thalamic efferents were also observed extending into the cortex (Fig. 4.1B).

By early postnatal ages, thalamostriatal axons from the PF branched extensively in the striatum. At P3, thalamic terminals were dense and mostly concentrated in rostral and dorsal regions, with some clustering of terminals observed in lateral striatum (Fig. 4.2A, arrowhead). In contrast, at medial levels, sparse thalamostriatal terminals extended out along the axon fiber trajectory, from the striatal-pallidal border to dorsal and rostral striatum (Fig. 4.2B). Distinct holes within densely labeled regions, as observed in adults, were not obvious at this age. Double labeling with TH (Fig. 4.2C, green) confirmed this, with close up images showing that thalamostriatal terminals (Fig. 4.2D') and striosomes (Fig. 4.2D'') overlap considerably (Fig. 4.2D) at this stage. It thus appears that thalamic afferents are not confined to the striatal matrix in early development.

By P7, thalamostriatal terminals were more extensive in the striatum. Laterally, terminals densely innervated rostral and dorsal striatum (Fig. 4.2E). Medially, diffuse terminals covered the rostral and dorsal two thirds of the striatum (Fig. 4.2F). Dense clustering of terminals was further evident in lateral striatum at this age (Fig. 4.2E, arrowhead), with regions of sparser label, as well as distinct 'holes' present within otherwise labeled regions, observed at both levels (Fig. 4.2E, F; arrows). This was somewhat reminiscent of the patchy pattern observed in adults. Double labeling with TH (Fig. 4.2G, green) showed that the 'holes' correlated with striosomes. Higher power confocal images showed thalamostriatal terminals (Fig. 4.2H') forming at the boundaries

of striosomes (Fig. 4.2H’’), with only a few fibers overlapping with TH-positive regions (Fig. 4.2H).

By P10 (Fig. 4.2I) and P15 (Fig. 4.2J), thalamostriatal terminals covered the majority of the striatum. At P10, the patchy patterning of terminals was more evident than at P7 (Fig. 4.2I, arrowheads). In addition, distinct holes with sharp boundaries were also evident suggesting a high level of compartmentalisation (Fig. 4.2I, arrow). At P15, much of the high resolution detail of the terminal patterning was less evident, presumably due to the nature of the uptake and transport of DiI at this age, with terminals generally appearing diffuse. Some evidence of patchiness was still present as at younger ages, and compartmentalisation was well defined, with ‘holes’ with sharp boundaries evident within the thalamic label (Fig. 4.2I, J; arrows).

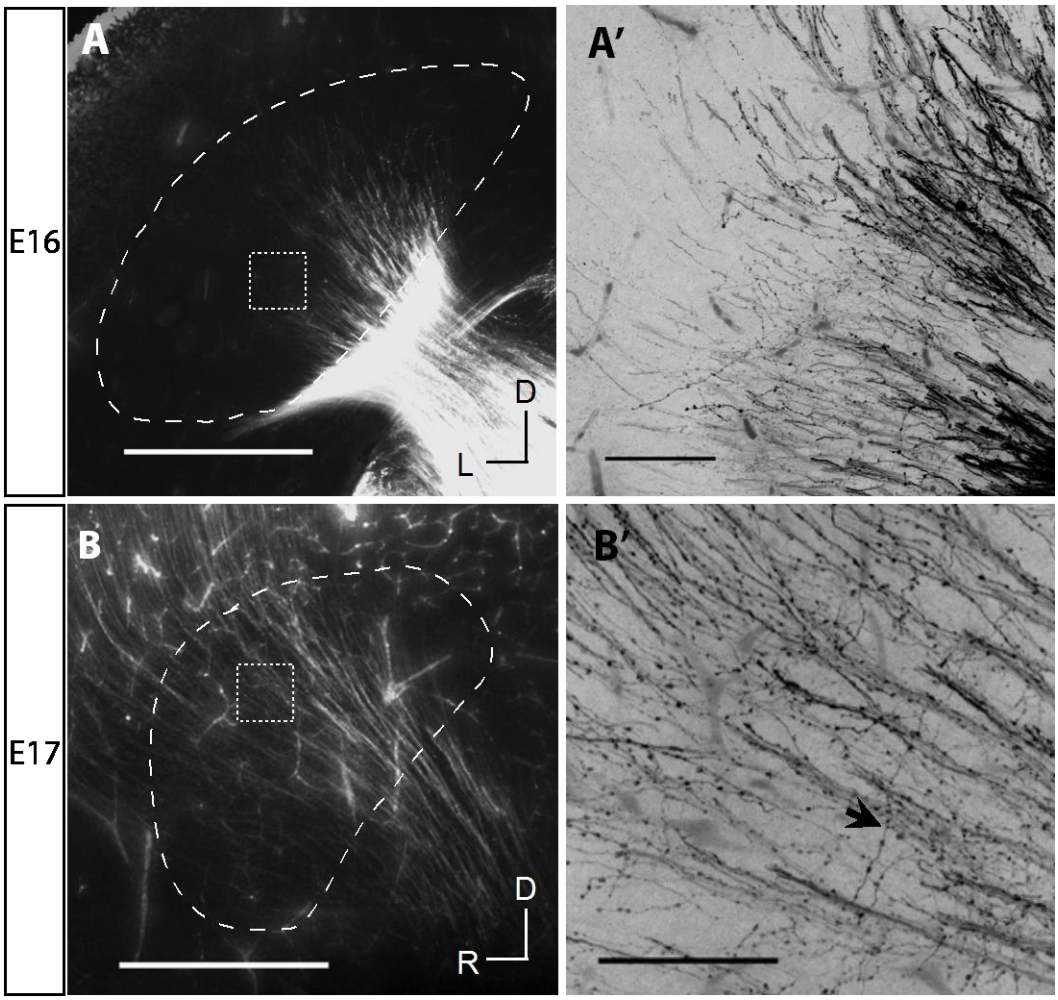

Figure 4.1. Embryonic development of thalamostriatal projections in WT mice.
(A) A horizontal section through the striatum (dashed line) at E16 showing bundles of thalamostriatal axons radiating towards rostral regions of the nucleus. (A') Higher power confocal image of the boxed region indicated in (A) showed that these fibers were predominantly unbranched at this age.
(B) A sagittal section through E17 striatum (dashed line) showing DiI-labeled thalamostriatal axons. Some fibers were observed extending into the cortex. (B') Higher power confocal image of the boxed region indicated in (B) showed collateral branches extending out at approximately right angles to their primary axon (arrow).
Scale bars in A and B indicate 500 μm, Scale bars in A' and B' indicate 100 μm. D is dorsal, R is rostral, L is lateral. For A and A', rostral is up, lateral is left. For B and B', dorsal is up, rostral is left.

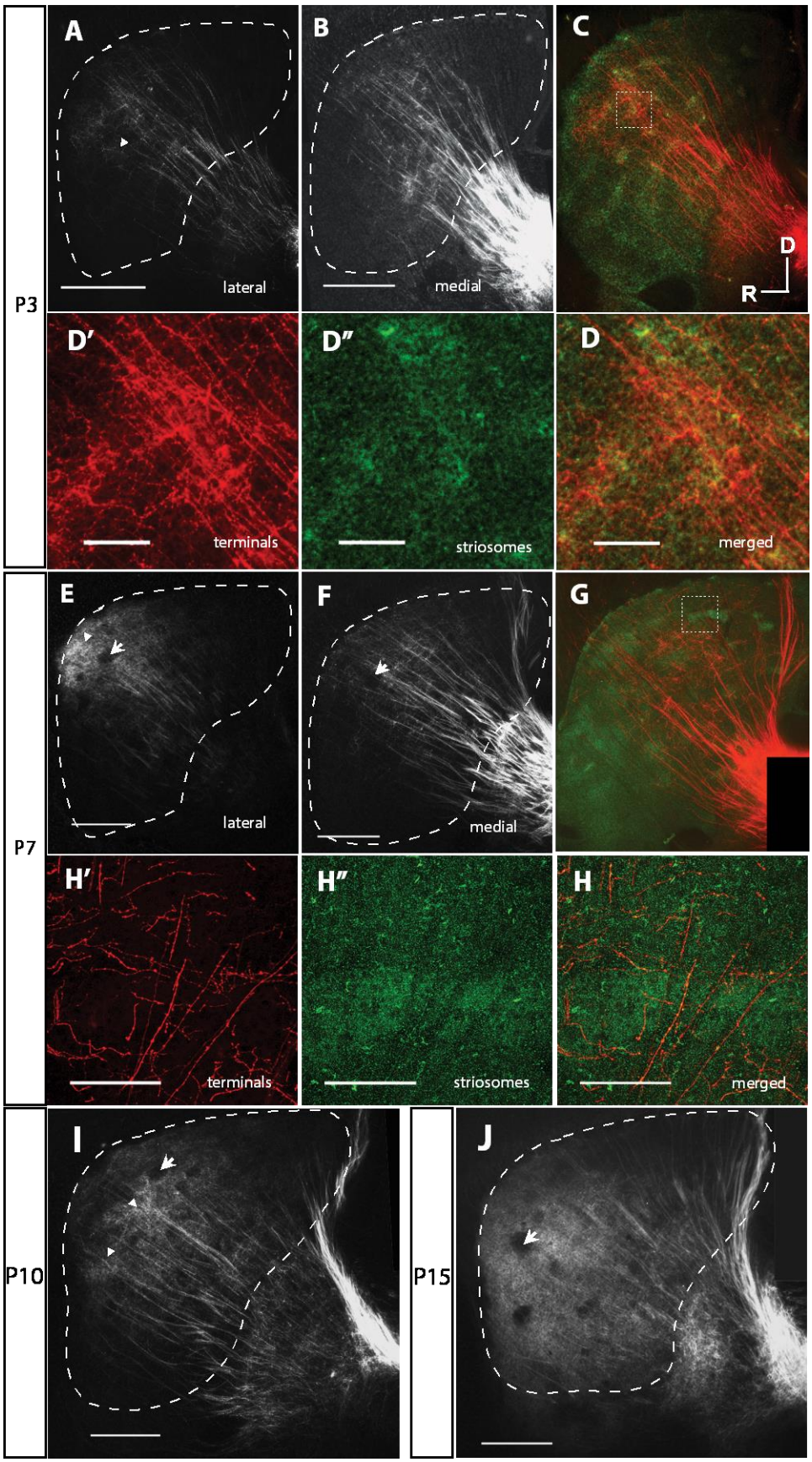
P3
A
lateral
B
medial
C
D
R
D′
terminals
D″
striosomes
D
merged
P7
E
lateral
F
medial
G
H′
terminals
H″
striosomes
H
merged
P10
I
P15
J

Figure 4.2. Postnatal development of thalamostriatal projections in WT mice.

(A-B) Sagittal sections through the striatum (dashed line), showing thalamostriatal terminals at P3. (A) In lateral striatum, thalamostriatal terminals were dense and mostly concentrated in rostral and dorsal regions. Some evidence of clustering of terminals was observed (arrowhead) although regions of dense versus sparse label were not obvious (B) At medial levels, sparse thalamostriatal terminals extended out along the axon trajectory, from the striatal-pallidal junction to dorsal and rostral striatum.

(C-D) Double labeling sections with TH (green) suggested that comparmentalisation was not yet complete at this age. Close up images of the boxed region indicated in (C) showed that thalamostriatal terminals (D') and striosomes (D'') overlapped considerably, with processes often extending across striosome boundaries (D).

(E-F) Sagittal sections through the striatum (dashed line) at P7. (E) At lateral levels, thalamostriatal terminals were more numerous and dense within rostral and dorsal striatum. Both dense patches of terminals (arrowhead), as well as more sparsely labeled regions could now be observed. Within the otherwise labeled area, distinct 'holes' could also be seen (arrow). (F) At medial levels, diffuse terminals covered the rostral and dorsal two thirds of the striatum. 'Holes' within labeled regions were also observed (arrow).

(G-H) Double labeling sections for TH revealed more distinct boundaries between terminals and striosomes at this age than at P3. High resolution confocal images of the boxed region indicated in (G) showed thalamostriatal terminals (H') forming at the boundaries of striosomes (H''), with only a few overlapping fibers evident (H). These correspond to the 'holes' in the thalamic label.

(I) A sagittal section through the striatum (dashed line) showing thalamostriatal terminals at P10. Thalamostriatal terminals covered the majority of the striatum, again, with dense patches of terminals evident (arrowheads) interspersed by regions with sparser label. Distinct 'holes' were also observed in the striatal label, presumably correlating with striosomes (arrow).

(J) A sagittal section through the striatum (dashed line) showing thalamostriatal terminals at P15. Thalamostriatal terminals appeared diffuse, and high resolution detail was not visible at this age point, suggesting that DiI tracing may no longer accurately label these fibers. A hint of patchiness, along with distinct 'holes' (arrow), which presumably correlate with striosomes were, however, still evident.

Scale bar in A applies to C. Scale bar in E applies to G. Scale bars in A-C, E-G, I-J indicate 500 μm. Scale bars in D', D'', D, H', H'', H indicate 100 μm. For all images, D is dorsal, R is rostral.

Development of thalamostriatal projections in Ten-m3 KO mice

To determine whether Ten-m3 may be involved in the development of the thalamostriatal pathway, these projections were also traced in Ten-m3 KO mice at corresponding time points to those in WTs; that is, E16, E17, P3, P7, P10 and P15.

Similar to WTs, bundles of axons originating from the PF were observed to enter the striatum at E16 (Fig. 4.3A, dashed line). High resolution confocal images (Fig. 4.3A') showed that, as in WTs, these fibers did not send branches into the striatum at this age. The first collateral branches were observed at E17 (Fig. 4.3B), extending at approximately right angles to their parent axon fiber into various regions of the striatum (Fig. 4.3B', arrow). Compared to WTs, however, these branches appeared to be less abundant (see Fig. 4.3B' and Fig. 4.5 for quantification). At low power, some thalamostriatal fibers were also observed extending into the cortex (Fig. 4.3B).

At early postnatal ages, the distribution of thalamostriatal terminals appeared to differ from WTs in the first postnatal week. At P3, terminals in lateral striatum were dense and concentrated along the majority of the axon fiber trajectory (Fig. 4.4A) and appeared to cover a larger area compared to WTs. Medially, sparse thalamostriatal terminals extended out along the axon fiber trajectory, from the striatal-pallidal border to dorsal and rostral striatum (Fig. 4.4B). Similar to WTs, however, distinct holes within labeled regions, as observed in adults, were not obvious at this age. This was confirmed by double labeling sections with TH (Fig. 4.4C, green), with close up images indicating that

thalamostriatal terminals (Fig. 4.4D') and striosomes (Fig. 4.4D'') overlapped considerably, such that terminals often abutted striosome boundaries (Fig. 4.4D).

By the end of the first postnatal week, terminal label was dense, and predominantly concentrated in rostral and dorsal regions of lateral striatum (Fig. 4.4E), similar to that observed in WTs. At medial levels, thalamostriatal terminals were diffuse and appeared to cover more of the striatum compared to WTs (Fig. 4.4F). At both striatal levels, distinct 'holes' were observed within the labeled region (Fig. 4.4E, F; arrows). Double labeling for TH (Fig. 4.4G, green) showed that these 'holes' correlated with striosomes, with high power confocal images confirming that thalamostriatal terminals (Fig. 4.4H') surrounded striosomes (Fig. 4.4H'') with only a few fibers overlapping TH-positive regions (Fig. 4.4H). Hence, it appears that compartmentalisation of thalamostriatal terminals is complete in KOs by P7, as in WTs. A notable difference between WT and KO at this age, however, was the absence of a patchy appearance of the terminals within the matrix. Instead, terminal label was more uniform, being generally bright near the centre and declining more peripherally. This distribution was interrupted only by the distinct 'holes' in the label, which correlate with striosomes.

By P10 (Fig. 4.4I) and P15 (Fig. 4.4J), thalamostriatal terminals covered the majority of the striatum although the patchy pattern was less obvious than in WTs. Likewise, terminal label at P15 was often diffuse and lacked the detail observed at younger ages, and fiber bundles were particularly highly labeled. Despite this, compartmentalisation of

terminals was apparent and more defined, with ‘holes’ within densely labeled regions evident at both later age points (Fig. 4.4I, J; arrows).

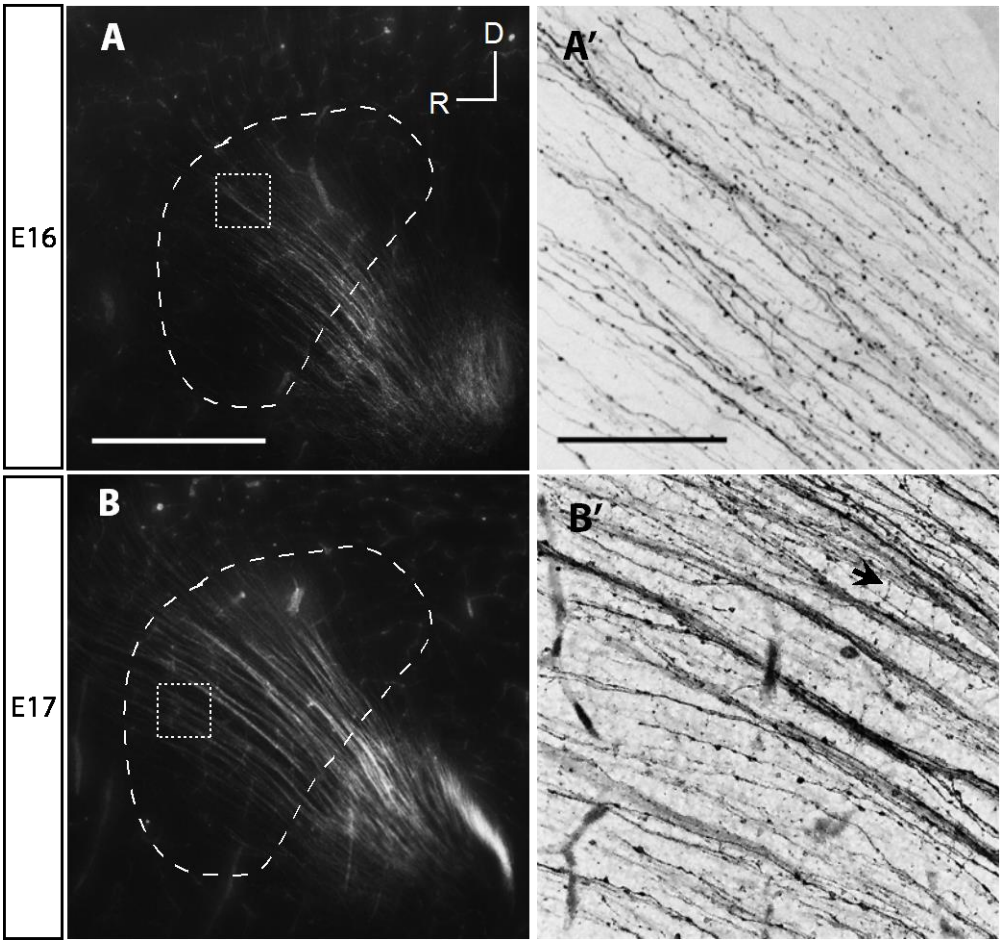

Figure 4.3. Embryonic development of thalamostriatal projections in Ten-m3 KO mice.
(A) A sagittal section through the striatum (dashed line) at E16, showing bundles of axons originating from the PF entering the nucleus. (A’) High power confocal image of the boxed region indicated in (A) suggests that these fibers remained mostly unbranched at this age.
(B) A sagittal section at E17, showing thalamostriatal axons in the striatum (dashed line). Some of these fibers extended into the cortex. (B’) Confocal image of the boxed region indicated in (B) showed collateral branches forming at approximately right angles to their parent axon (arrow). These branches appeared less abundant compared to WTs (see Fig. 4.5).
Scale bar in A applies to B. Scale bar in A’ applies to B’. Scale bar in A indicates 500 μm. Scale bars in A’ indicatea 100 μm. D is dorsal, R is rostral. For all images, dorsal is up, rostral is left.

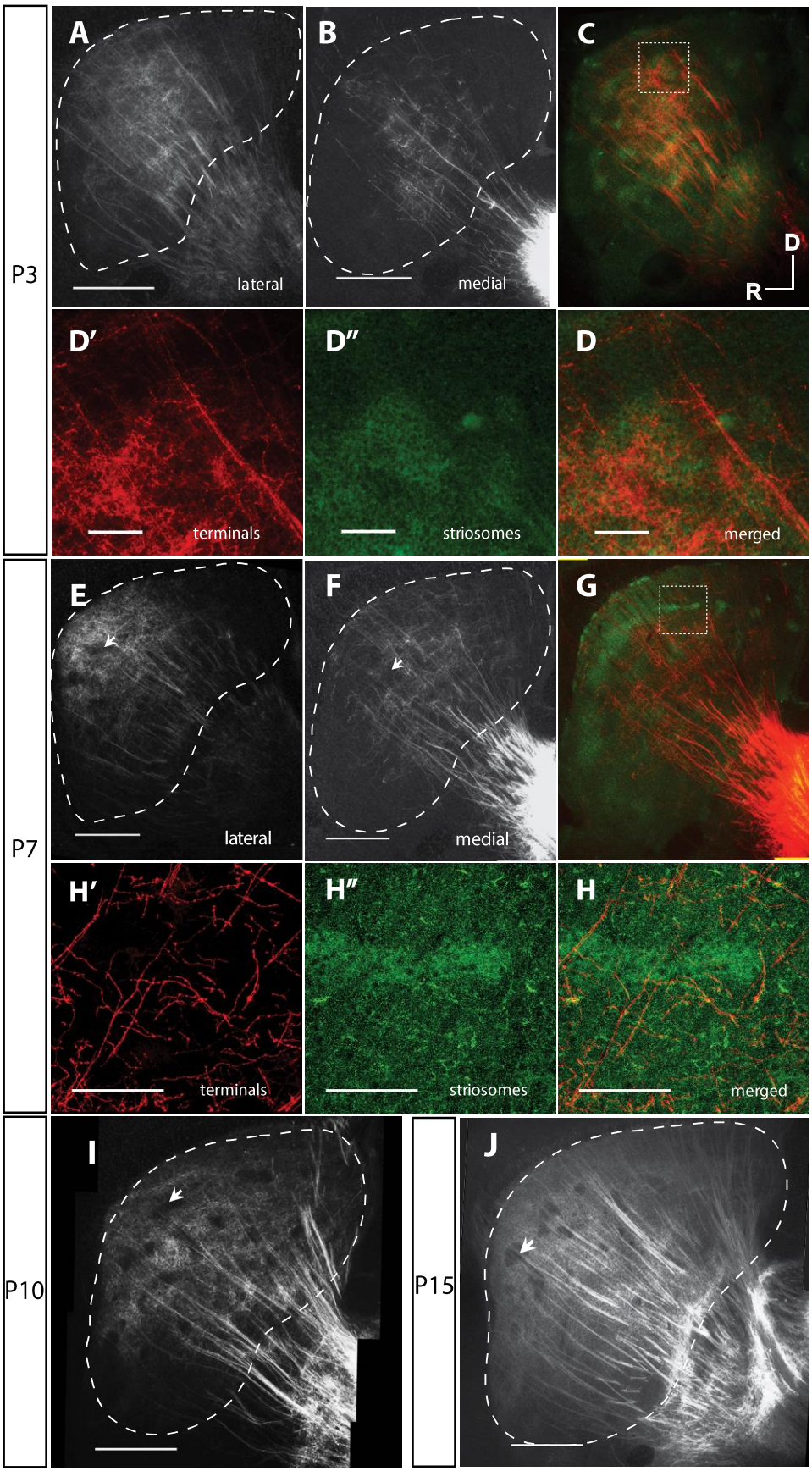
P3
A
lateral
B
medial
C
D
R
D′
terminals
D″
striosomes
D
merged
P7
E
lateral
F
medial
G
H′
terminals
H″
striosomes
H
merged
P10
I
P15
J

Figure 4.4. Postnatal development of thalamostriatal projections in Ten-m3 KO mice.
(A-B) Sagittal sections through the striatum (dashed line) at P3. (A) In lateral striatum, thalamostriatal terminals were dense and concentrated along the majority of the extent of the axon trajectory. These appeared to cover a larger area compared to WTs. (B) Medially, sparse thalamostriatal terminals extended out along the axon fiber trajectory, from the striatal-pallidal junction to dorsal and rostral striatum.
(C-D) Double labeled sections for TH (green) showed that, like WTs, boundaries around striosomes were not distinct at this age, with a close up of the boxed region indicated in (C) showing thalamostriatal terminals (D') and striosomes (D'') often overlapping and abutting striosome boundaries (D).
(E-F) Sagittal sections through the striatum (dashed line) at P7. (E) At lateral levels, terminal label was dense and predominantly concentrated in rostral and dorsal striatum, similar to WTs. (F) At medial levels, thalamostriatal terminals diffusely covered the entire striatum and appeared to be more extensive compared to WTs. At both striatal levels, holes were observed within the labeled region (arrows), however, there was no evidence of clustering of terminals as in WTs.
(G-H) Sections double labeled for TH (green) confirmed a more mature compartmental organisation. High power confocal image through the region indicated in (G) showed terminals (H') forming strict boundaries surrounding striosomes (H''), such that only a few fibers abutted patch boundaries (H).
(I) A sagittal section through the striatum (dashed line) showing thalamostriatal terminals at P10. Thalamostriatal terminals covered the majority of the striatum in a mostly diffuse manner, with distinct holes evident in the striatal label, presumably correlating with striosomes (arrow).
(J) A sagittal section through the striatum (dashed line) showing thalamostriatal terminals at P15. Thalamostriatal terminals, similar to WTs, were mostly diffuse and lacked the detail observed at younger ages, with fiber bundles being particularly highly labeled. Distinct holes were still observed within the labeled region (arrow), presumably correlate with striosomes.
Scale bar in A applies to C. Scale bar in E applies to G. Scale bars in A-C, E-G, I-J indicate 500 μm. Scale bars in D', D'', D, H', H'', H indicate 100 μm. For all images, D is dorsal, R is rostral.

Ten-m3 KOs have fewer thalamostriatal collateral branches at E17

Thalamostriatal collaterals were first observed in the striatum in at E17 in both WT and Ten-m3 KO mice. In WT, these branches were numerous and extended out at right angles to their parent axon (Fig. 4.5A). These branches were similarly observed in KOs (Fig. 4.5B), however, they appeared much less numerous compared to WTs. Indeed, quantitative analysis confirmed that WTs exhibited a significantly higher number of branch junctions compared to KOs (Fig. 4.5C, *; WT: 1478.8 ± 346.87, n = 3; KO: 684.4 ± 325.1, n = 3, p = 0.04, t-test).

The development of thalamostriatal projections is altered in Ten-m3 KO mice

The postnatal development of thalamostriatal projections were compared between genotypes by examining potential differences in their topographic distribution using a semi-quantitative analysis. Individual images through the striatum were processed and used to produce heat maps representing the average distribution of terminals across distinct injection sites for separate medial and lateral levels for each of three postnatal age points, P3, P7 and P10. Sections from P15 were not included due to the unreliability of DiI labeling at this time point. Potential differences in the average distribution of thalamostriatal terminals were compared between genotypes.

At P3, thalamostriatal terminals were sparse at both lateral and medial levels in WTs. These terminals were predominantly localised to the dorsal and rostral regions of lateral

striatum (Fig. 4.6A) and along axons in the mid-dorsal regions of medial striatum (Fig. 4.6B). In KOs, thalamostriatal terminals were comparably denser in dorsal striatum at lateral levels (Fig. 4.6A'), where they also expanded much more ventrally compared to WTs in the rostral half of striatum. At medial levels, however, terminals were similarly sparse in both genotypes and largely targeted mid striatum, but tended to be located slightly more ventral compared to WTs (Fig. 4.6B'). These differences were reflected quantitatively, with the average distribution of terminal label along the RC (Fig. 4.6C, ***) and DV axes (Fig. 4.6C', ***) at lateral levels being significantly different between genotypes ($p < 0.001$, K-S test). In medial striatum, thalamostriatal terminals were similarly distributed along the RC axis (Fig. 4.6D; $p = 0.37$, K-S test) but were significantly different along the DV axis (Fig. 4.6D'; $p = 0.002$, K-S test). Further, the area under these plots (Fig. 4.6E) showed increased terminal label in KOs laterally, but were similar between genotypes in medial striatum.

At P7, thalamostriatal terminals were more extensive in both genotypes. In WTs, terminals covered the entire dorsal half of lateral striatum, being most dense in dorsal and rostral regions (Fig. 4.6F). Medially, thalamostriatal terminals were still focused in the middle striatal regions, spreading into more ventral regions compared to P3 (Fig. 4.6G). In KOs, thalamostriatal terminals covered the majority of the dorsal half of the lateral striatum (Fig. 4.6F'), similar to WTs, although they also showed a tendency to invade slightly more ventral regions in the rostral half of the striatum. Medially, these terminals were localised to middle striatal regions (Fig. 4.6G'), where they appeared to cover a smaller area and were less dense compared to WTs. The average distribution of terminal

label at P7 was not significantly different along either the RC (Fig. 4.6H) or DV axes (Fig. 4.6H') in lateral sections (DV: $p = 0.47$; RC: $p = 0.11$, K-S test) between genotypes. In contrast, distribution of terminals was significantly different along both the RC (Fig. 4.6I, **) and DV axes (Fig. 4.6I', **) in medial sections between WT and KOs ($p = 0.004$, K-S test). These changes were reflected in area under the curve calculations (Fig. 4.6J), which, in contrast to P3, indicated a small difference in lateral striatum but a more obvious reduction in terminal label in KOs in medial striatum, compared to WTs.

At P10, thalamostriatal terminals continued to spread out to fill different regions of the striatum. In WTs, terminals remained confined and densely localised to the dorsal half of lateral striatum (Fig. 4.6K). At medial levels, terminals covered the entire caudal two-thirds of the nucleus (Fig. 4.6L). In KOs, thalamostriatal terminals were strikingly different compared to WTs, occupying much more ventral regions of rostral striatum at lateral levels (Fig. 4.6K'), though they appeared to avoid the caudal VL region. Further, terminals covered almost the entire medial striatum (Fig. 4.6L'). Quantitatively, the average distribution of terminal label at P10 was significantly different along the RC (Fig. 4.6M, ***) and DV axes (Fig. 4.6M', ***) in lateral striatum between genotypes ($p < 0.001$, K-S test). Medially, this distribution of terminals was similar along the RC axis (Fig. 4.6N) but was significantly different along the DV axis (Fig. 4.6N', *; $p = 0.024$, K-S test). Moreover, area under the curve calculations (Fig. 4.6O) indicated similar differences to those observed at P3, with KOs showing increased terminal label in lateral striatum, but were more similar to WTs medially.

The differences in terminal distribution were observed in the absence of changes to striatal area, with that of lateral and medial striatum appearing to develop similarly, with no significant differences found between genotypes (data not shown).

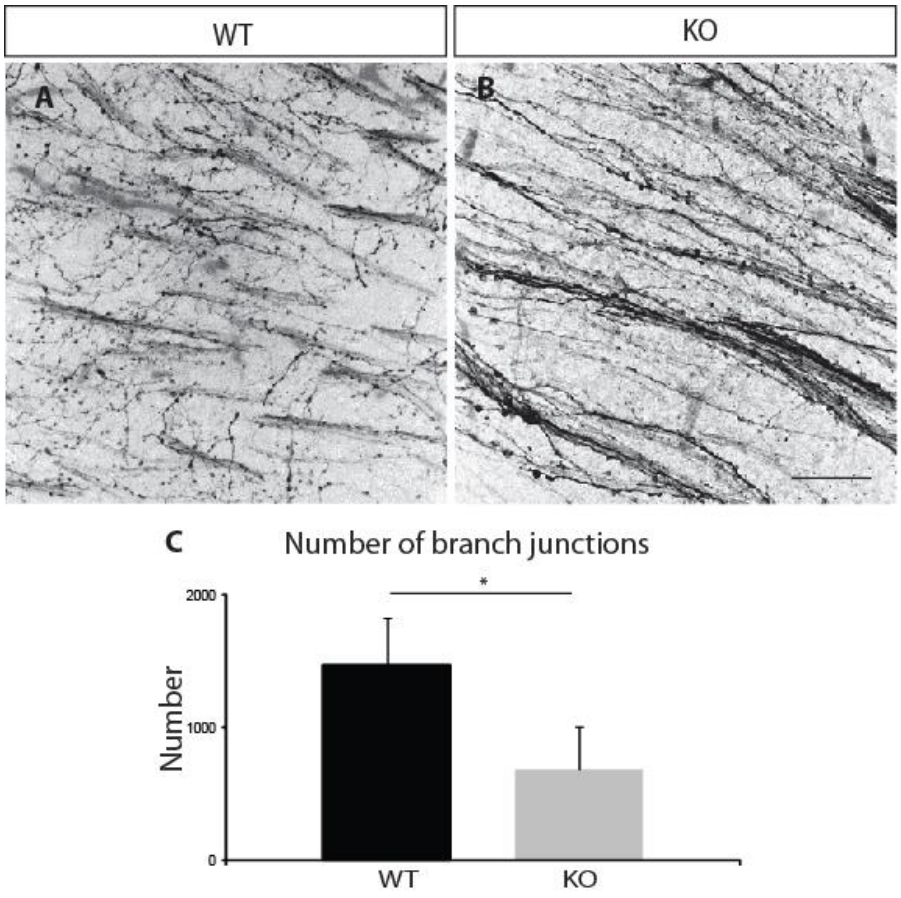

Figure 4.5. Thalamostriatal axons first extend branches into the striatum at E17 in mice.
(A) In WTs, numerous thalamic branches extended out at right angles to their parent axon.
(B) In KOs, thalamostriatal branches also extended at right angles to the parent axon, but were sparse, compared to WTs.
(C) Quantitatively, WTs showed a significantly higher number of branch junctions compared to KOs (WT: 1478.8 ± 346.87, n = 3; KO: 684.4 ± 325.1, n = 3, p = 0.04, t-test).
Scale bar in B applies to A. Scale bar indicates 100 μm. For all images, dorsal is up, rostral is left. Values in graph indicate mean ± SEM.

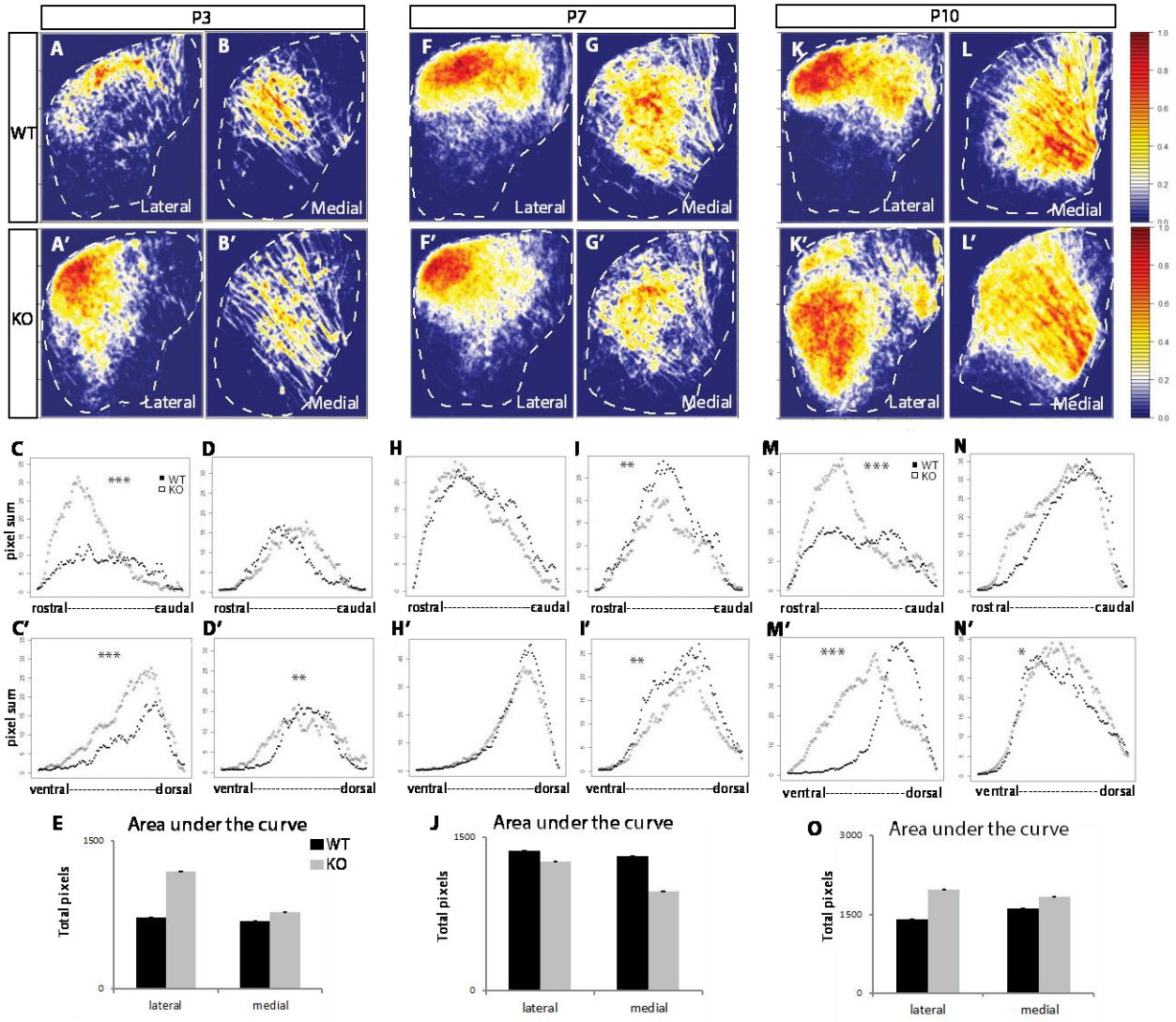
P3
P7
P10
WT
KO
A
B
F
G
K
L
A′
B′
F′
G′
K′
L′
Lateral
Medial
C
D
H
I
M
N
C′
D′
H′
I′
M′
N′
pixel sum
WT
KO
***
**
*
rostral
caudal
ventral
dorsal
E
J
O
Area under the curve
Total pixels
lateral
medial

Figure 4.6. Thalamostriatal projections are altered in KOs at P3, P7 and P10.

(A-B) Heat maps indicating thalamostriatal terminals in WTs at P3. (A) Laterally, terminals were found in dorsal and rostral striatum. (B) Terminals were sparser medially and localised along axons in mid-dorsal striatum.

(A'-B') Heat maps indicating thalamostriatal terminals in KOs at P3 (A') Laterally, terminals were dense dorsorostrally, but also expanded more ventrally in the rostral half of striatum. (B') Medially, terminals were sparse and mainly localised along axons in mid-striatum.

(C-D) The average distribution of terminals along the RC axis. These were significantly different laterally (C) but were similar between genotypes medially (D).

(C'-D') The average distribution of terminal label along the DV axis. Terminals were significantly different between genotypes in lateral (C') and medial striatum (D').

(E) Area under the curves in (C/C') and (D/D'). KOs showed a dramatic increase in terminal label in lateral striatum, but were more similar to WTs medially.

(F-G) As for (A-B) at P7. (F) Laterally, terminals covered the dorsal half of the striatum, being most dense dorsorostrally. (G) Medially, terminals covered a larger area of middle striatal regions, compared to that at P3.

(F'-G') As for (A'-B') at P7. (F') In lateral striatum, thalamostriatal terminals were similar to WTs, but expanded slightly more ventrally in the rostral half of striatum. (G') Likewise, medially, terminals were similarly distributed to those in WTs but appeared to cover a smaller area.

(H-I) As for (C-D) at P7. (H) Laterally, terminal label was similar along the RC axis between genotypes but was significantly different between genotypes medially (I).

(H'-I') As for (C'-D') at P7. Distribution of terminals was significantly different between genotypes in lateral (H') and medial striatum (I').

(J) Area under the curves in (H/H') and (I/I'). In contrast to (E), terminal label was similar in lateral striatum but reduced in KOs in medial striatum compared to WTs.

(K-L) As for (A-B) at P10. (K) In lateral striatum, terminals were similar to previous ages. (L) Medially, terminals spread out to cover the entire caudal two-thirds of the nucleus.

(K'-L') As for (A'-B') in P10 KOs. (K') Laterally, terminals were dense across much of the DV axis of rostral striatum, but avoided the VL region caudally . (L') Medially, terminals covered the majority of the striatum.

(M-N) As for (C-D) at P10. Distribution of terminals was significantly different along the RC axis laterally (M), but were comparable between genotypes medially (N).

(M'-N') As for (C'-D') at P10. Distribution of terminals was significantly different laterally (M') and medially (N').

(O) Areas under the curves in (M/M') and (N/N'). Similar to (E), KOs showed increased terminal label in lateral striatum but were similar to WTs medially.
* indicates $p < 0.05$. ** indicates $p < 0.01$. *** indicates $p < 0.001$. See text for statistics. Values in graphs indicate means ± SEM. For all heat maps, dorsal is up, rostral is left.

Thalamostriatal terminals showed a similar phenotype to adults by the fourth postnatal week of development

DiI tracing studies were useful for revealing differences in terminal distribution between genotypes, but were not reliable for quantification of terminal spread due to the nature of the injections and transport (see Discussion). Since thalamostriatal terminals were significantly expanded in adult KOs, compared to WTs, this projection was examined at one final developmental age point, P25-30, using *in vivo* tracing with BDA. BDA injections into lateral PF of WTs resulted in thalamostriatal terminals in dorsal and lateral regions of the striatum (Fig. 4.7A), as in adults. In KOs, terminals also resembled patterns observed in adults, being more widely distributed and invading more ventral regions, although mostly avoided the VL segment (Fig. 4.7B). Compared to WTs, thalamostriatal terminals covered a slightly increased area of the striatum (Fig. 4.7C), however, this did not reach significance, possibly due to the smaller numbers of animals used here (n = 3) compared to adult data reported in Chapter 3 (n = 8).

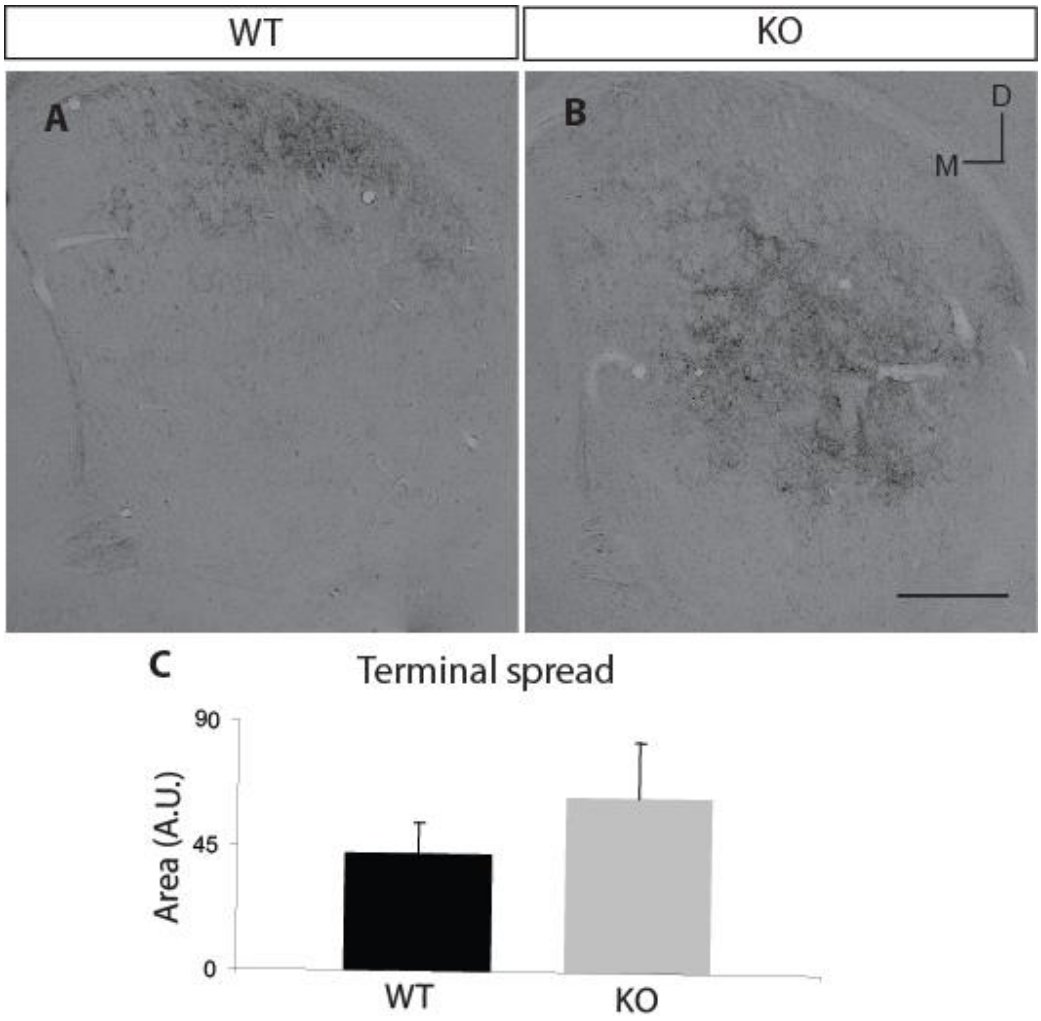

Figure 4.7. Thalamostriatal projections in WTs and KOs at P25-30.

Striatal terminal label resulting from BDA injections into lateral PF.

(A) A coronal section through WT striatum showing thalamostriatal terminals covering dorsal and lateral regions of the nucleus.

(B) In KOs, terminals were distributed in more mid-lateral regions in the striatum and generally appeared to cover a larger area of the striatum compared to WTs.

(C) Compared to WTs, thalamostriatal terminals covered a slightly increased area of the striatum, however, this is difference is not statistically significant.

Scale bar in B applies to A. Scale bar represents 1 mm. D is dorsal, M is medial. For all images, dorsal is up, medial is left. Values in graph indicate mean ± SEM.

Ten-m3 is an adhesive cue for a subset of thalamostriatal axons

One of the potential mechanisms by which Ten-m3 may be acting to control the guidance and targeting of thalamostriatal axons from the PF during development is by acting as a direct attractive cue. This was investigated by examining the overlap of Ten-m3 expression with thalamostriatal terminal label in adjacent sections of P10 WT mice. As observed previously, Ten-m3 was expressed in patches throughout the striatum (Fig. 4.8A). In addition, thalamostriatal terminals were dense at the focus of the label (Fig. 4.8, *) but were also distributed in a patchy pattern in the matrix, which was most evident away from this epicentre (Fig. 4.8B), where regions of both dense (Fig. 4.8B, arrows) and sparser label were present. Small regions completely devoid of terminals shown previously to correspond to striosomes were also evident. The overlay of Ten-m3 and thalamostriatal terminals showed numerous regions of overlap (Fig. 4.8C, arrows). Interestingly, these regions were most evident in areas away from the focus of the label, where the patchy distribution of terminals was also clearer. Closer to the focus of the label (Fig. 4.8C, *), regions of overlap and no overlap were both observed. Patches were also less obvious in this region, presumably due to the density of labeled terminals near the focus of the label, which could potentially act to obscure patches. It is, therefore, possible that there are two populations of thalamostriatal projections from the PF, those which form patchy, dense terminations on Ten-m3 positive regions and those that form less dense terminations on Ten-m3 negative cells.

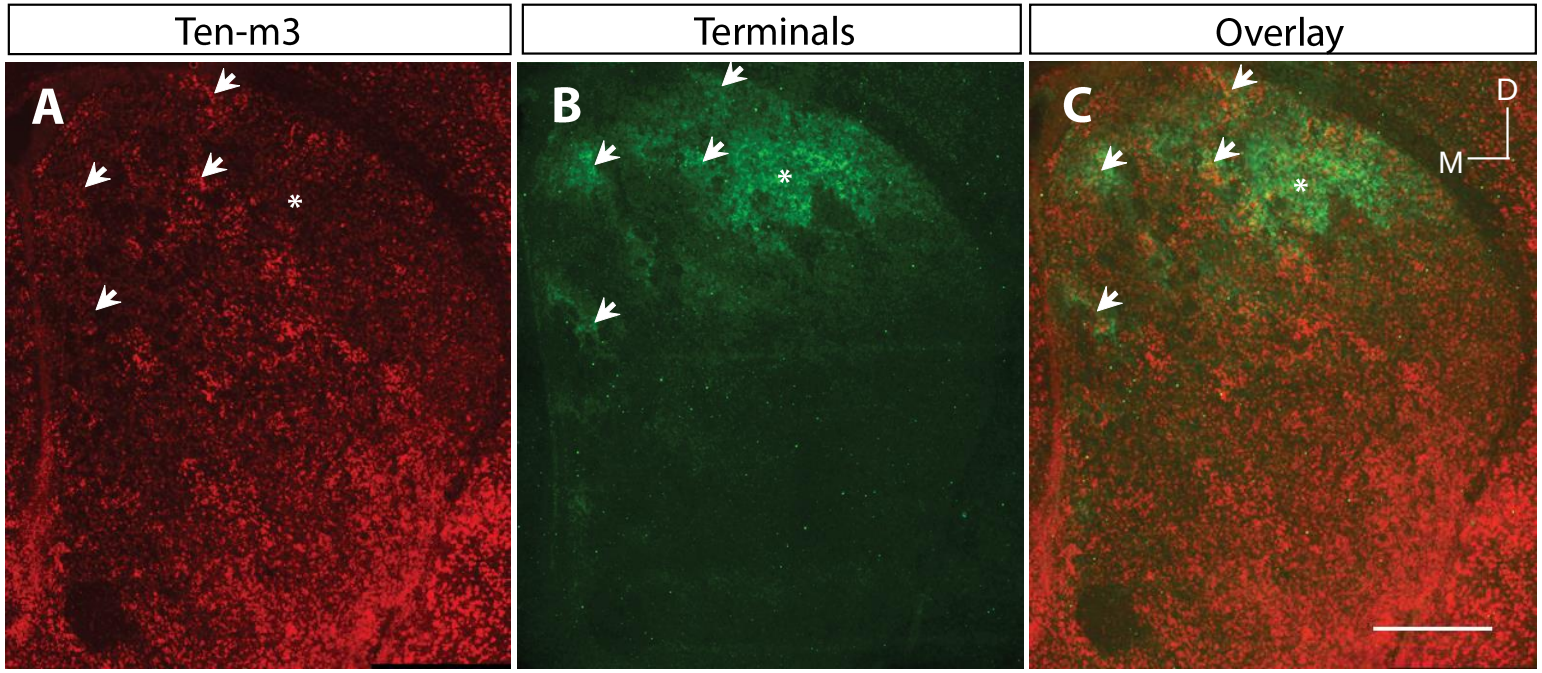

Figure 4.8. Ten-m3 acts as an adhesive guidance cue for a subset of thalamostriatal axons.

(A) A coronal section showing *in situ* hybridisation for Ten-m3 expressed in patches throughout the striatum.

(B) An adjacent section showing thalamostriatal terminals localised to dorsal striatum, in a patchy pattern of terminations (arrows). Patches were less obvious closer to the focus of the label (*). Distinct holes within labeled regions were evident, presumably corresponding to striosomes.

(C) Overlay of (A) and (B). Ten-m3 and thalamostriatal terminals showed regions of overlap (arrows), being most apparent further away from the focus of the injection (*). Near the focus of the injection, thalamostriatal terminals also overlapped with regions devoid of Ten-m3 expression. Hence, a subset of thalamostriatal axons target Ten-m3-positive cells.

Scale bar in C applies to A and B. Scale bar in C indicates 500 µmm. D is dorsal, M is medial. For all images, dorsal is up, medial is left.

Ten-m3 may alter EphA7 expression in the striatum

Based on previous studies indicating that EphA7 expression was reduced in visual structures of Ten-m3 KOs (Glendining, 2011), striatal EphA7 expression was examine in KOs. First, EphA7 and Ten-m3 mRNA distributions were examined in adjacent sections of P3 WT mice using *in situ* hybridisation (Fig. 4.9). Ten-m3, as shown previously, was expressed in bands/patches throughout the striatum (Fig. 4.9A). Interestingly, EphA7 was also expressed in a highly organised arrangement of bands in the striatum (Fig. 4.9B), described in more detail below. The overlay of Ten-m3 and EphA7 showed a complex relationship between the two genes (Fig. 4.9C). EphA7 levels were highest in regions of moderate Ten-m3 expression (Fig.4.9A-E, arrows), such that the high Ten-m3- and EphA7-positive bands appeared exactly adjacent to one another. Quantitatively, the overlap represented 22.4 ± 1.6% (mean ± SEM) and 20.1 ± 3.1% (mean ± SEM) of Ten-m3 and EphA7 expression, respectively (Fig. 4.9F). Further, areas of Ten-m3 expression overlapped with regions devoid of EphA7 (Fig. 4.9A-C, arrowheads). Hence, there was a partially complementary relationship between these genes. Moreover, since these genes are currently the only known markers of matrisomes (current study, Tai et al., 2013), it was of interest to determine whether EphA7 and Ten-m3-positive matrisomes occupy the entire matrix. Hence, immunohistochemistry for TH performed on an adjacent set of sections (Fig. 4.9D) revealed striosomes overlapping with areas showing low levels of the two genes (Fig. 4.9A-E, *). However, areas of low TH, that is, those comprising the matrix, also overlapped with regions showing low levels of Ten-m3 and EphA7 (Fig. 4.9A-E, #). Hence, these partially distinct matrisomes together only occupy a subregion of the striatal matrix.

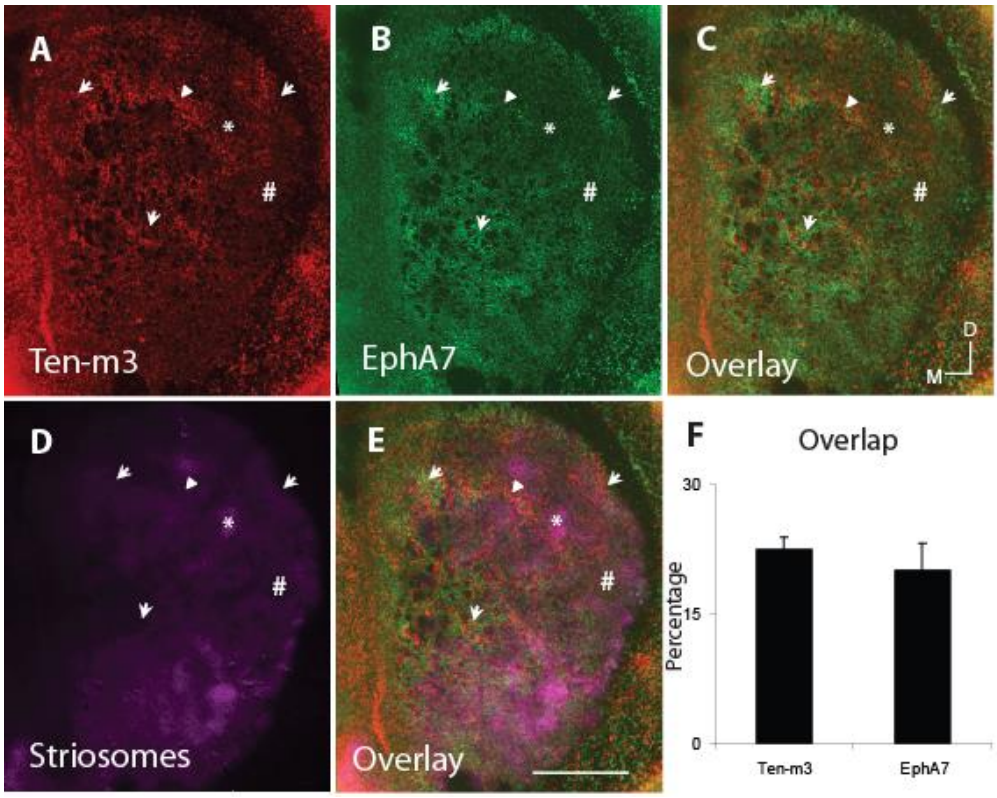

Figure 4.9. Comparison of Ten-m3 and EphA7 expression in the striatal matrix at P3.

(A) A coronal section through the striatum showing *in situ* hybridisation for Ten-m3. Ten-m3 was expressed in bands/patches throughout the striatum, as described previously.

(B) An adjacent section showing *in situ* hybridisation for EphA7. Like Ten-m3, EphA7 was expressed in a highly organised arrangement of bands in the striatum (see Fig. 4.10).

(C) An overlay of (A) and (B). EphA7 was predominantly expressed in regions of moderate Ten-m3 levels (arrows), such that Ten-m3 and EphA7-positive bands were exactly adjacent to one another. Ten-m3 expression also overlapped with regions devoid of EphA7 (arrowheads).

(D) An adjacent section labeled with immunohistochemistry for TH to label striosomes, showing patches located mostly in lateral striatum.

(E) Overlay of (A), (B) and (D). Striosomes overlapped with areas showing low levels of the two genes (*). Areas of low TH, that is, those comprising the matrix, also overlapped with regions showing low levels of Ten-m3 and EphA7 (#).

(F) Graph showing overlap of Ten-m3 and EphA7 as a percentage of the total area occupied by these genes, respectively. The overlap represented 22.4 ± 1.6% (mean ± SEM) and 20.1 ± 3.1% (mean ± SEM) of Ten-m3 and EphA7 expression, respectively.

Scale bar in E applies to A-D. Scale bar indicates 1 mm. D is dorsal, M is medial. For all images, dorsal is up, medial is left. Data in graph indicates mean ± SEM.

Although only partially overlapping in distribution, the possibility that Ten-m3 may act in part by regulating EphA7 expression nevertheless remains. EphA7 expression was subsequently compared in WT and Ten-m3 KO striatum. *In situ* hybridisation for EphA7 in WTs showed expression in bands/patches in rostral (Fig. 4.10A), middle (Fig. 4.10B) and caudal striatum (Fig. 4.10C). A prominent EphA7-positive band along the dorsal and lateral border of the striatum, approximately correlating with the subcallosal streak, was observed at all levels through the striatum. Ventrally, a number of EphA7-positive bands were oriented approximately parallel, along the DM-VL axis, separated by unlabeled regions. EphA7-positive bands in the middle of the striatum were most numerous at rostral levels, becoming less numerous in progressively more caudal regions. In Ten-m3 KOs, EphA7 was similarly expressed in bands/patches in rostral (Fig. 4.10A'), middle (Fig. 4.10B') and caudal striatal levels (Fig. 4.10C'). The distribution of EphA7 in Ten-m3 KOs was comparable to that in WTs, with a prominent band observed along the striatal border at all RC levels. A number of parallel bands were, likewise, distributed throughout the remainder of the striatum, decreasing in number at progressively more caudal levels.

The intensity of EphA7 expression, however, often appeared lower in the striatum of Ten-m3 KOs, particularly in middle and caudal sections. Quantitatively, EphA7 expression the striatum as a whole was not significantly reduced in KOs (Fig. 4.10D; $F(1,4) = 1.3$, $p = 0.32$, repeated measures ANOVA). When striatal sections were analysed at separate rostral, middle and caudal levels (Fig. 4.10E), EphA7 expression was only significantly reduced at middle striatal levels (WT: 8990.3 ± 68.2 (mean ± SEM), n

= 3; KO: 6852.3 ± 511.7, n = 3, F(1,4) = 17.15, p = 0.01, one-way ANOVA). In KOs, EphA7 expression was significantly reduced in caudal striatum compared to middle levels (middle: 6852 ± 511.7, n = 3; caudal: 4220 ± 602.7, n = 3, F(1,4) = 11.08, p = 0.03, one-way ANOVA).

EphA7 protein levels were also analysed by performing Western blotting on striatal tissue from WT and Ten-m3 KOs (Fig. 4.10F). Tissue from the SC was analysed as a positive control. An EphA7 band was visible at approximately 100 kDA in all samples, as was β-actin at 42 kDA, which was used as a loading control. This is close to the manufacture's predicted molecular weight of 112 kDa. Qualitatively, EphA7 was high in WT striatum and SC, and was still evident in KO striatum and SC. Quantitatively, EphA7 protein levels in KOs were 73.3 ± 12.6% (mean ± SEM) of that in WT striatum (Fig. 4.10G), however, this was not significantly different (p = 0.15, paired t-test). Similarly, EphA7 levels in KO SC were 70.6 ± 14.5% (mean ± SEM) of that in WTs (Fig. 4.10G; p = 0.26, paired t-test).

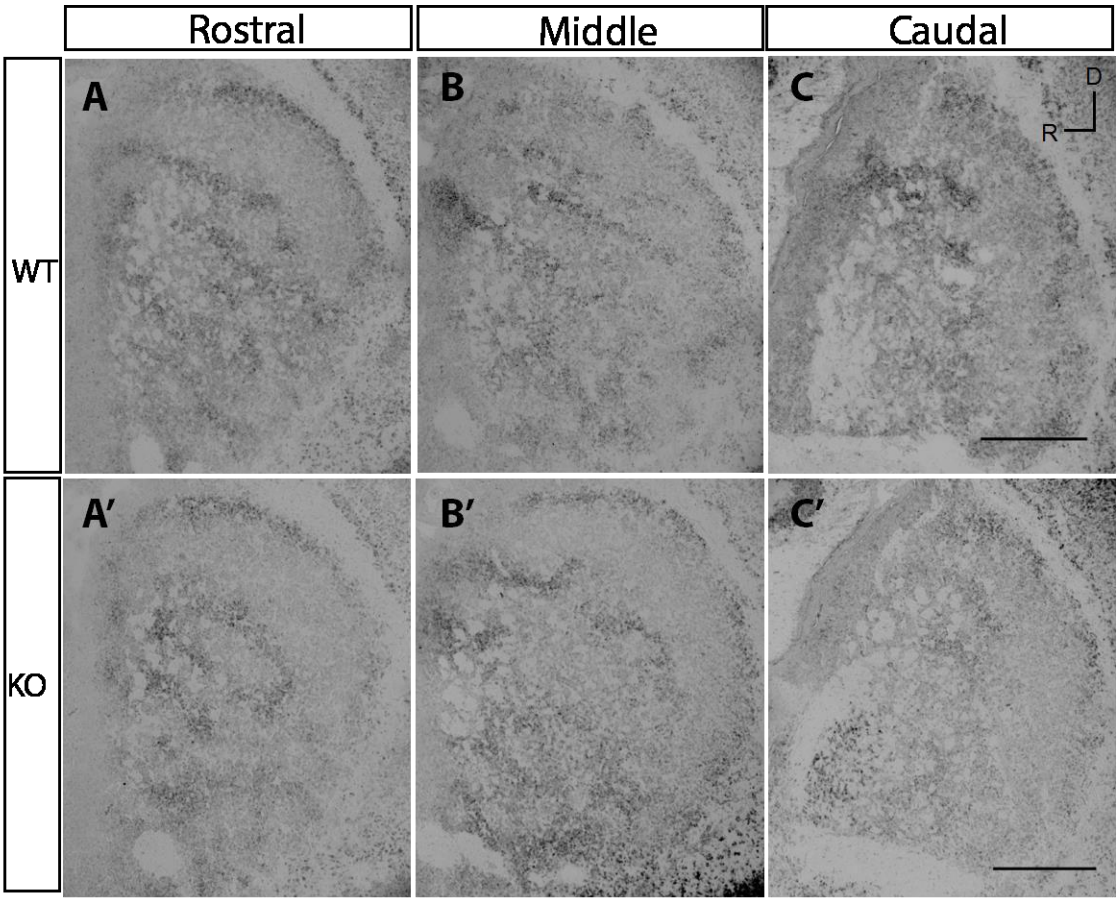
Rostral
Middle
Caudal
A
B
C
D
R
WT
A′
B′
C′
KO

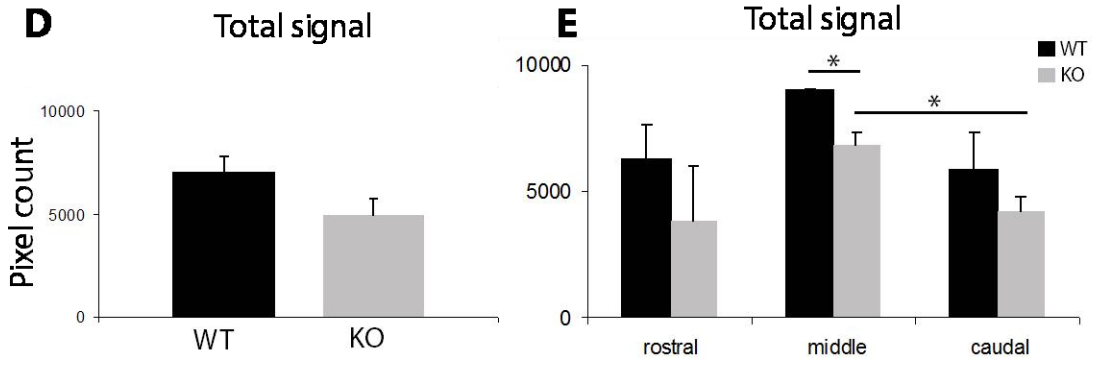
D
Total signal
Pixel count
10000
5000
0
WT
KO
E
Total signal
10000
5000
0
WT
KO
*
*
rostral
middle
caudal

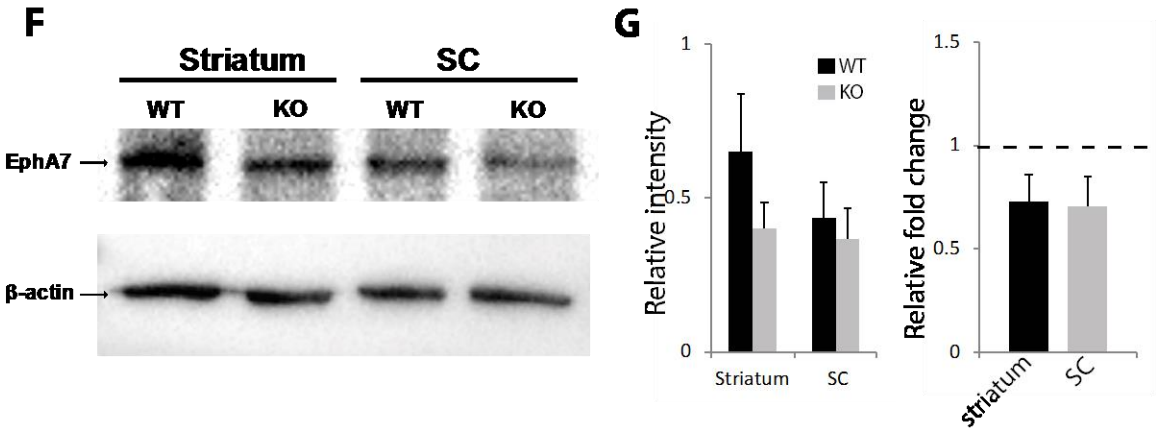
F
Striatum
SC
WT
KO
WT
KO
EphA7
β-actin
G
Relative intensity
1
0.5
0
WT
KO
Striatum
SC
Relative fold change
1.5
1
0.5
0
striatum
SC

Figure 4.10. EphA7 levels are reduced in Ten-m3 KO striatum.

(A-C) Coronal sections through the striatum in P3 WT mice showing EphA7 expression. EphA7 was expressed in bands/patches throughout the striatum. A prominent EphA7-positive band lined the dorsal and lateral border of the striatum. Ventrally, a number of parallel bands, oriented along the DM-VL axis, were evident, separated by unlabeled regions. These patterns were present at rostral (A), middle (B) and caudal levels (C). EphA7-positive bands in the middle of the striatum were generally reduced at caudal levels.

(A'-C') As for (A-C) in P3 KO mice. Similar to WTs, EphA7 was expressed in bands/patches along the striatal border and as parallel bands ventrally at rostral (A'), middle (B') and caudal levels (C'). Likewise, EphA7-positive bands decreased in number at progressively more caudal levels. The intensity of EphA7 expression, however, appeared lower compared to WTs.

(D-E) Quantitative analysis of EphA7 expression in the striatum. (D) In the striatum as a whole, EphA7 expression was reduced in KOs compared to WTs ($p = 0.32$, repeated measures ANOVA). (E) In separate rostral, middle and caudal levels, EphA7 expression was reduced at all levels in KOs, however, was only significantly reduced at middle striatal levels compared to WT mice (WT: 8990.3 ± 68.2 (mean ± SEM), $n = 3$; KO: 6852.3 ± 511.7, $n = 3$, $p = 0.01$, one-way ANOVA). In KOs, EphA7 expression was significantly reduced in caudal striatum compared to middle levels (middle: 6852 ± 511.7, $n = 3$; caudal: 4220 ± 602.7, $n = 3$, $p = 0.03$, one-way ANOVA).

(F-G) Western blotting for EphA7 on tissue from the striatum and SC of WT and Ten-m3 KOs. Tissue from the SC was analysed as a positive control. (F) An EphA7 band was observed at approximately 100 kDA in all samples; β-actin was used as a loading control. EphA7 was high in WT striatum and SC, and appeared to be reduced in KO tissue. (G) EphA7 protein levels in KO striatum were $73.3 \pm 12.6\%$ of that in WT striatum, however, this reduction was not significantly different between genotypes. Similarly, EphA7 levels in KO SC were $70.6 \pm 14.5\%$ of that in WT SC, however, this difference was not statistically significant (p -0.26, paired t-test).

Scale bar in C applies to A and B. Scale bar in C' applies to A' and B'. Scale bars in C and C' indicate 500 μm. D is dorsal, M is medial. For all images, dorsal is up, medial is left. Data in graphs indicate mean ± SEM.

Discussion

Summary of results

This study constitutes the first investigation into the development of thalamostriatal projections originating from the PF in mice. Using DiI tracing in fixed tissue, this study is the first to show that while thalamic axons pass through the striatum at E16, they do not form collateral branches until E17. Ten-m3 KOs, similarly, first formed thalamostriatal collateral branches at E17, however, these were fewer in number compared to WTs. Throughout postnatal ages, differences in the distribution and location of terminals were evident between genotypes. Interestingly, terminal label filled larger areas of lateral striatum in KOs at P3 and P10, however, were reduced in medial striatum at P7, compared to WTs. Thalamostriatal terminals were further investigated using *in vivo* BDA injections at P25-30, which showed a generally similar pattern to that observed in adults.

The mechanisms by which Ten-m3 may be exerting its roles in the guidance of thalamostriatal projections were also investigated. Firstly, the hypothesis that Ten-m3 may be acting as a direct attractive guidance cue was examined by comparing Ten-m3 and terminal distribution in adjacent sections at P10. A partial overlap of terminals with Ten-m3-positive cells suggests that Ten-m3 may be acting directly as a guide for and/or to promote the arborisation of a subset of thalamostriatal terminals at Ten-m3 positive patches during development. A second hypothesis that Ten-m3 may act indirectly by

altering transcription of other guidance genes was examined by investigating EphA7 in the striatum. Comparison of EphA7 and Ten-m3 mRNA using *in situ* hybridisation indicated a partially complementary pattern of expression. Further, immunohistochemistry for TH on adjacent sections suggested that EphA7- and Ten-m3-positive matrisomes only comprise a subregion of the matrix compartment. Additionally, *in situ* hybridisation for EphA7 in Ten-m3 KOs showed similar distribution of EphA7 in bands to WTs. The levels, however, were reduced in KO striatum, particularly at middle striatal levels. Western blot analysis for EphA7 protein further suggests that this may also be reduced in striatum of Ten-m3 KOs.

Technical considerations

Developmental tracing studies were performed using DiI crystal placement into the PF from E17 to P15 in fixed tissue. This method was adopted due to the small size and inaccessibility of the PF in young animals, particularly in embryonic and early postnatal-aged animals. Further, this method has previously been used to trace projections in this circuit (Srivastava, 1999; Vercelli et al., 2003). Although every precaution was taken to ensure that these injections were as similar as possible, some considerations should be noted. Firstly, since crystals of DiI were used, the volume of dye placed in individual injection sites was not easily controlled for. Similar sized crystals were used as much a possible, however, exact size and volume were not easily measured. Secondly, although the placement of these crystals almost certainly targeted the PF, as only cases where there was evidence of placement at just lateral to the fr were included for analysis, the amount of spread of DiI was difficult to account for. DiI, as a lipophilic dye, is believed to be

transported via lateral diffusion through the plasma membrane. These properties also suggest that the dye is readily taken up by neurons of adjacent cells or processes (Godement et al., 1987; Honig and Hume, 1989), such as those of adjacent thalamic structures, some of which also project to the striatum. However, the rate and extent of diffusion is believed to be reduced in fixed tissue. Nevertheless, differences in the spread or uptake of dye at the injection site may account for some of the variability present in this data. For these reasons, formal quantitative measures of the area and density of terminals were not performed, and analysis was confined to comparing distributions of labeled terminals.

The first thalamostriatal branches were observed at E17 in both genotypes, however, KOs appeared to exhibit a reduced number of branch junctions compared to WTs. Since WT and KO cases were obtained from different litters, it would be useful to confirm these results using littermates. This may not be an easy task as the number of KOs can be low within a single litter. Alternatively, a larger number of samples can be used to correct for the use of animals from multiple litters.

In addition, at later postnatal ages, particularly P15, fiber bundles of the internal capsule became particularly intensely labeled by DiI, especially at medial levels, whereas staining within the striatum itself became fainter and more diffuse compared to younger ages. It is possible that the dye was not efficiently transported into terminals in these cases, and hence, may not be an accurate reflection of their distribution at later age points. Hence,

the data from this age group was not analysed, and experiments at one additional age point, P25-30, was examined using *in vivo* injections of BDA.

As mentioned briefly above, the developmental DiI tracing experiments were analysed in the sagittal plane, in contrast to those performed in adults, which used coronal sections (Chapter 3). This was done as it allowed thalamostriatal fibers to be more readily distinguished from those passing through within the internal capsule, particularly at younger ages. This difference in methodologies makes it difficult for a direct comparison to be made on phenotypes between developing and adult cases, particularly the caudal specific changes. Material was, however, analysed separately for lateral and medial regions in developing animals, and, hence, changes in the VL region of caudal striatum were noted where obvious. In particular, changes in area specific to caudal striatum, as found in adults, may have been present in this material but were obscured by the axis of measurement. Hence, it would be prudent to confirm these with coronal sections in the future.

The hypothesis that Ten-m3 may be acting as a direct guidance cue for thalamostriatal axons was examined by comparing Ten-m3 mRNA distribution, using *in situ* hybridisation, with thalamostriatal terminals. Initially, a number of commercial Ten-m3 antibodies were trialed, using a combination of fixation, antigen retrieval, and detection techniques, however, to no avail. An extended period of time was spent on this as it is known that the correlation between mRNA and protein is often variable (Maier et al., 2009). Further, although Ten-m3 protein has been shown on axons in the visual pathway,

it is unknown whether this is also the case for thalamostriatal axons. Moreover, direct protein-protein correlation between Ten-m3-positive thalamostriatal axons and striatal cells and compartments would have provided better evidence of their relationships. Unfortunately, examination of protein distribution proved impossible within the time-constraints of this thesis, and hence, an attempt to spatially correlate thalamostriatal terminals, striosomes and Ten-m3 mRNA in adjacent thin sections proved to be the only available option. Further, as mentioned in Chapter 2, given the diameter of the striatal components whose distribution were being compared (typically greater than 100 μm) as opposed to the thickness of cryostat sections (15 μm) and alignment methods used, this approach allowed a sufficient level of accuracy to determine the relationship between Ten-m3, EphA7 mRNA and thalamostriatal patches, at least for the qualitative approach used here. Importantly, a consistent relationship was observed in all examples analysed suggesting the efficacy of this approach.

Western blotting for EphA7 detected multiple bands following antibody labelling. A band at approximately 100 kDa, close to the predicted molecular weight for EphA7 (112kDa), was the highest in intensity, and consistently present in all blots, and was therefore determined to correspond to EphA7. In all blots, high levels of β-actin were observed, compared to relatively low levels of EphA7. It is reasonable that, due to the low sensitivity of Western blot analysis as a quantitative technique, small differences may not have been accurately detected. This may also explain the lack of differences in protein compared to RNA levels in the positive control, ie. the SC in Ten-m3 KOs (discussed below). Additional studies using a more quantitative approach, such as

ELIZA or protein mass spectroscopy, would be useful to confirm the results presented here.

Normal development of the thalamostriatal projection in mice

In the first study to investigate the development of thalamostriatal projections originating from the PF in mice, thalamostriatal axons were found in the striatum by E16, however, collateral branches did not arise until E17. This is in general agreement with studies performed in rats, where the first thalamostriatal fibers are observed in the striatum embryonically at E19, approximately two-three days before birth (Srivastava, 1999; Vercelli et al., 2003). Further, in rats, the clustering of these terminals into patches was reported to be present as early as E19.5 (Srivastava, 1999). While there was some evidence of clustering of terminals by P3 in the current study, an obviously patchy distribution was not observed until P7. Hence, there may be a slightly later appearance of patches in mice compared to rats. Alternatively, the previous study performed on rats may have used a different definition of clustering than used here. In particular, it may refer to the increased density of thalamostriatal axons in the matrix versus the striosomes, rather than the formation of dense patches compared to more sparsely labeled regions in the matrix, which were observed in addition to regions devoid of label corresponding with striosomes in the present study. Interestingly, the timing of the clustering of thalamic terminals into patches, observed here in mice between P3 and P7, correlated well with the period when Ten-m3-positive patches became more defined bands, compared to those seen earlier at E17 (Chapter 2). This temporal correlation is consistent with the hypothesis that interactions between Ten-m3 expressing PF projections and

subregions of the matrix play critical roles in the patterning of thalamic terminals, discussed in detail later.

The development of the compartmentalisation of thalamostriatal terminals was also observed from P3. At this age, thalamostriatal terminals showed a reduced innervation of striosomes compared to the matrix, but did not completely avoid striosomes as at later ages. This pattern was more refined by P7, where terminals formed strict boundaries enclosing striosomes, with only a small number of overlapping terminals observed. Hence, as for the clustering of terminals into patches, compartmentalisation of these fibers appears to develop slightly later in mice compared to rats, where it was first observed at birth (Srivastava, 1999). Further, these data suggest that thalamostriatal processes may initially exhibit broad terminal zones, which become refined towards the end of the first postnatal week of development. To our knowledge, this is the first study to describe the refinement of thalamostriatal terminals and, hence, the mechanisms involved have yet to be characterised.

The spatiotemporal development of thalamostriatal terminals was also investigated in the current study in postnatal ages. Although there were no differences in the size of the striatum between lateral and medial levels at each developmental time point, there were some signs of a developmental gradient in thalamostriatal targeting along the ML and RC axes. The initial targeting of terminals to dorsal and rostral striatum at P3 and progressively more caudal regions in later development was particularly obvious at lateral levels. This is consistent with previous studies in rats, which show that

thalamostriatal terminals first project to rostral, and are densest in lateral striatum (Srivastava, 1999; Vercelli et al., 2003). Further, a number of striatal features display a general lateral to medial spatiotemporal developmental gradient, including striatal neurogenesis, clustering of cells to form striosomes and the development of nigrostriatal projections (Bayer, 1984; Graybiel and Hickey, 1982; Specht et al., 1981; Voorn et al., 1988). These spatiotemporal gradients were described for embryonic ages. Hence, higher resolution analysis of these projections at smaller age intervals would be required to properly determine the existence of a lateral to medial gradient in mice. Further, striatal neurogenesis has been described in a caudal to rostral gradient, the opposite to that observed in the current study, and previously in rats (Srivastava, 1999; Vercelli et al., 2003). It is currently unclear how the development of other afferent projections proceeds along this axis. Hence, knowledge of the development of other afferent projections would reveal whether this gradient is a feature of thalamostriatal projections, or whether it is more widely observed.

Thalamostriatal terminals are altered in Ten-m3 KOs during development

The development of thalamostriatal projections is initially delayed in KOs compared to WTs. Although thalamostriatal terminals were first observed in KO striatum at the same age as in WTs, ie. at E17, there was a significantly lower number of branches in KOs. This suggests that Ten-m3 may have a role in the formation of these collaterals. Collateral branching is believed to arise from actin filament-based protrusions (Gallo, 2011). Teneurins have previously been linked to the actin cytoskeleton in various ways.

Teneurins are believed to regulate actin organisation via the cytoskeleton adaptor protein, CAP/ponsin (Nunes et al., 2005). In addition, Ten-m2 expression in the cytoplasm has been shown to enhance neurite elongation, enlarge growth cones and filopodia formation, and is further colocalised with actin (Rubin et al., 1999, 2002). Similarly, Ten-m3 has been shown to enhance neurite outgrowth (Leamey et al., 2007a), presumably using similar mechanisms. Further, TCAP-1 has been shown to increase actin and β-tubulin expression in primary hippocampal cells (Al Chawaf et al., 2007b). Moreover, the family of Eph receptors and ephrin ligands have also been shown to regulate axon branching (see Gibson and Ma, 2010 for a review). It is possible that Ten-m3 may also be indirectly controlling collateral branching by altering Eph/ephrin levels, as preliminary data suggests that various members of this family of guidance cues are altered in Ten-m3 KO mice (current study, Glendining, 2011). Hence, the reduction in collateral branching in the absence of Ten-m3 can occur via a number of mechanisms.

Subsequent to the initial delay in thalamostriatal collateral branching, thalamostriatal terminals appear to exhibit path-finding deficits along the ML axis in the first postnatal week of development in KOs. Analysis of separate lateral and medial striatal levels revealed that terminals were significantly different in terms of distribution and intensity in lateral striatum at P3 and in medial striatum at P7, compared to WTs. Similar path-finding deficits have been observed in the visual pathway of Ten-m3 KO mice previously (Dharmaratne et al., 2012; Leamey et al., 2007b). The apparent difference in the targeting of thalamostriatal terminals along the ML axis with time also suggests additional changes in the spatiotemporal gradient of development of this pathway in Ten-

m3 KOs. Although the direction of development appears to be normal, that is, lateral to medial, the temporal aspect appears to be altered. Alternatively, or in conjunction, this could also be reflective of developmental changes within the striatum itself, possibly to the cholinergic population, which is altered in adults (Chapter 3). Hence, further studies are required to investigate striatal morphology during development and higher resolution studies to further investigate the spatiotemporal gradient of the thalamostriatal projection in KOs.

Intriguingly, the initial delay in thalamostriatal development recovers at later stages of development, so much so that these projections covered an increased area of lateral striatum by P3. Surprisingly, there was little evidence of this at P7, where there was actually a slight reduction in the area covered in medial striatum, but by P10, the terminals covered a broader area as in adults. These projections were analysed at one further age point, P25-30 where a similar pattern of projections to that in adults was observed, however, the slight increase in terminal area in KOs was not significant. The mechanisms associated with these changes are unclear, however, the current data suggests that mechanisms involved in refinement and pruning of axons may be altered in the absence of Ten-m3, leading to increased projections in KO adults. It is unclear, however, when these mechanisms of refinement and pruning occur, as they have yet to be studied in the striatum. Our data indicate some evidence of refinement of thalamostriatal projections between P3 and P7, during which the overlap of terminals with striosomes was clearly reduced. At the same time, the clustering of thalamostriatal axons into dense patches was also occurring. In addition, the striatum undergoes a wide period of

postnatal development up until the end of the fourth postnatal week, with the second to fourth postnatal weeks believed to the be most critical, encompassing the major period of corticostriatal synaptogenesis and MSN maturation (Hattori and McGeer, 1973; Lee and Sawatari, 2011; Tepper et al., 1998). Hence, a number of developmental mechanisms may be influencing the normal development of thalamostriatal projections, which may be altered in Ten-m3 KOs. Further studies are required to investigate which processes are altered and how these may be occuring.

It was interesting to note that even though thalamostriatal terminals expanded ventrally to fill a larger area of the matrix in Ten-m3 KOs versus WTs, they nevertheless appeared to avoid the caudal VL segment of the nucleus. Although this data cannot be taken as definitive given that axons in WTs were not seen in this area either, it is worth noting as it is consistent with the adult KO data where thalamostriatal terminals seemed to also avoid this region. The mechanisms that would prevent these axons from targeting this specific region despite a marked expansion right to its borders are currently unclear. This data, together with that reported in Chapter 3 strongly suggests that the caudal VL segment of the striatum may be a significant area. Notably, it is this location where the effects of Ten-m3 deletion are most marked, evidence by changes in striatal area and the number of cholinergic neurons. Hence, it would be of interest to examine the time course of changes in the distribution of cholinergic neurons in relation to the formation of the thalamostriatal projection. This issue will be taken up in further in Chapter 5.

In addition to the above differences, the patchy terminal patterning of thalalmostriatal terminals observed in WTs by P7, was abolished throughout development, as in adult KOs. This is hypothesised to be a direct result of the loss of Ten-m3-positive patches in the striatum, discussed in more detail below.

Ten-m3 is a direct attractive cue to a subset of thalamostriatal axons

Ten-m3 has been shown to have important roles in path finding, previously in the visual system (Dharmaratne et al., 2012; Leamey et al., 2007b), and in the thalamostriatal circuit in the current study, where it also appears to have roles in the unique patterning of these terminals into clusters. The mechanisms by which Ten-m3 exerts these roles are currently unclear. One of the main hypotheses proposes that Ten-m3 may be acting directly as an attractive guidance cue. This stems from established adhesive properties of Ten-m3, along with evidence that they form homophilic interactions with adjacent cells (Beckmann et al., 2013; Feng et al., 2002; Leamey et al., 2007a). The temporal and spatial expression of Ten-m3 patches in the striatum and in PF cells suggest that it may demarcate interconnected cells of this circuit. Previous studies indicate that Ten-m3 is localised to the cell membrane and along afferent axons in the visual pathway (Leamey et al., 2007a, 2007b), suggesting that it may also be localised to thalamostriatal axons and the membrane of a subset of striatal neurons to form direct adhesive contacts. Attempts to investigate this using commercial Ten-m3 antibodies, however, were unsuccessful (see Technical considerations). Hence, future studies should confirm that Ten-m3 is present within thalamostriatal axons.

Nevertheless, the distribution of Ten-m3 mRNA in the striatum was compared with thalamostriatal terminals to reveal a partial overlap, suggesting that a subset of thalamostriatal terminals contact Ten-m3-positive striatal neurons. This partial overlap suggests that the hypothesis that Ten-m3-positive matrisomes demarcate the target cells of thalamostriatal axons may only be true for a subset of PF axons. This is somewhat to be expected as Ten-m3 is only expressed in a subregion of the matrix (Chapter 1), while thalamostriatal projections from the PF have been shown to innervate the entire striatal matrix compartment (Lanciego et al., 2004). Nevertheless, the data presented is consistent with the possibility that Ten-m3 may exert an attractive signal to promote targeting and/or branching of thalamic axons to specific subregions of the matrix for a subpopulation of PF cells, to result in the formation of the characteristic patchy distribution of this projection. This is consistent with evidence that teneurins can act as homophilic attractive guidance molecules (Hong et al., 2012; Mosca et al., 2012). Further, it has been postulated that binding of the ECDs on afferents and targets both expressing a given teneurin may be the cue to trigger cleavage of the ICDs and, thus the intracellular cascade that triggers terminal arborisation and branching (Bagutti, 2003). This therefore would argue for a direct role for Ten-m3 in the guidance of the thalamostriatal projection.

It is also possible that other molecular cues may also be involved in the specific targeting of these projections, including those whose expression may be regulated by Ten-m3. Other teneurin paralogs, Ten-m1, 2 and 4, are also expressed in the striatum (Allen Brain

Atlas), however, the compartmentalisation of these is yet to be characterised. Further, all teneurins appear to be expressed in the PF (Allen Brain Atlas). Recent studies indicate that Ten-m2 and Ten-m4, like Ten-m3, have roles in the connectivity of the ipsilateral visual pathway (Young, 2011; Young et al., 2013). Hence, these molecules may have complementary and/or overlapping roles in thalamostriatal circuits. In addition, a number of Eph receptors and their ephrin ligands are also expressed in the striatum (Janis et al., 1999; Tai et al., 2013). Of particular note is EphA7, which is expressed in bands that are often exactly adjacent to Ten-m3-positive patches in the striatal matrix. Hence, the inhibitory actions of Eph molecules (McLaughlin et al., 2003) may act in conjunction with Ten-m3 to control the specific targeting of thalamostriatal axons. Further studies, however, are required to confirm this.

Ten-m3 may be acting indirectly by altering EphA7 expression

A second proposed mechanism of action for Ten-m3 is that it may be indirectly controlling the targeting of thalamostriatal axons by altering expression of downstream guidance cues. The main downstream molecular candidate is EphA7, as levels of this gene are significantly reduced in visual structures in Ten-m3 KO mice (Glendining, 2011). As mentioned above, comparison of Ten-m3 and EphA7 mRNA expression indicates a close, partially complementary spatial relationship within the striatal matrix. Further, although EphA7 distribution appears to be conserved in Ten-m3 KOs, quantitative analysis of intensity levels indicates that EphA7 is significantly reduced in the striatum. Further, Western blot analysis for EphA7 protein levels in striatum and SC of Ten-m3 KO animals suggest a slight, but non-significant reduction of EphA7

compared to WTs for both neural structures. However, given the high levels of β-actin in the cells, a more quantitative technique may allow for improved quantification of EphA7 protein levels. Previous studies showing a significant reduction of EphA7 levels in the SC of Ten-m3 KOs used real-time quantitative PCR. These experiments were attempted for striatal tissue, using tissue taken from the SC as a positive control. However, due to the student's inexperience with the technique, a number of inconsistent results were obtained, with those previously found but also within replicate trials. Hence, due to time constraints, these experiments were abandoned. Nevertheless, the similar magnitude of the decrease in EphA7 protein levels found here for the SC and striatum suggest that this decrease is real, and thus, future studies should investigate the changes in EphA7 levels the striatum of Ten-m3 KOs using real-time PCR.

The data presented here therefore support the hypothesis that Ten-m3 may exert some of its roles by altering EphA7 gene expression. This is believed to occur via the cleavage of the ICD and its translocation to the cell nucleus. Preliminary studies, however, indicate no direct interaction between Ten-m3 and EphA7 (Glendining, 2011), suggesting that Ten-m3 may be upstream of EphA7 within the same molecular pathway. Direct nuclear detection of the ICD has been shown for Ten-m1 and Ten-m2, along with their interaction with CAP/ponsin and Zic1, respectively (Bagutti, 2003; Drabikowski et al., 2005; Kenzelmann et al., 2008; Nunes et al., 2005). Additionally, another cleaved region of the teneurin protein, TCAP, from the distal region of the C-terminal of the molecule, may also influence expression levels of other genes. Recent studies indicate that TCAP-3 can influence levels of Ten-m1 *in vitro* (Qian et al., 2004) and TCAP-1 and TCAP-3 can

increase cAMP levels (Qian et al., 2004; Wang et al., 2005). The cellular mechanisms by which these changes occur *in vivo*, however, are currently unknown.

In conclusion, the current study proposes that Ten-m3 is important in the formation of thalamostriatal collaterals at the very initial stages of their development. The delay in collateral branching is accompanied by changes in their distribution. The demonstration that dense patches of thalamostriatal terminals express Ten-m3, and that loss of Ten-m3 disrupts the initial formation of these patches argues strongly for a direct role in targeting thalamostriatal axons to these patches, and/or in promoting their branching within these regions. In the absence of Ten-m3, thalamostriatal axon arborisation is initially delayed and then recovers but occurs with reduced specificity. The reduced levels of EphA7 as well as other yet to be identified candidates may contribute to this by acting as potential inhibitory cues. In addition to the loss of patches, axons are distributed over an abnormally large part of the striatum throughout much of development, arguing for an additional role for Ten-m3 in establishing topography.

Chapter 5

General discussion

Conclusions and implications

The highly complex nature of striatal circuitry is reflective of its contribution to a wide range of important roles, from simpler actions such as motor control and volition, to higher order cognitive functions such as motivation and emotion. Although the striatum and its circuits have been the subject of many studies within the past decade, the cellular and molecular mechanisms involved in their formation are still poorly understood. In particular, the development of one of the main striatal circuits, the thalamostriatal pathway originating from the PF, has received remarkably little attention. This thesis provides the first investigation into this pathway in both adult and developing mice. In addition, the first molecular candidate involved in the formation, guidance and targeting of the thalamostriatal projection is proposed here in Ten-m3. Further, Ten-m3 is proposed as one of the first molecular markers of a matrisome compartment that partially overlaps with thalamostriatal terminals, for which it is believed to be acting both as an attractive guidance/branching cue and indirectly by altering gene transcription, in particular of EphA7. Moreover, Ten-m3 appears to have a region-specific affect in the mid-caudal striatum, where striatal structure and the cholinergic cell population are affected. Hence, these findings will add substantially to our currently limited knowledge

of matrisome compartments, the patterning and development of thalamostriatal circuitry and the roles of Ten-m3. These conclusions will be expanded upon below.

In Chapter 1, the expression patterns of Ten-m3 in the developing striatum were characterised. Here, Ten-m3 was first observed at late embryonic ages, where it continued to be highly expressed into the middle of the second postnatal week of development. Intriguingly, expression was observed in two distinct but overlapping patterns. The most obvious was a pattern of patches, evident from E17, which matured into oblique bands oriented predominantly along the DM-VL axis of the striatum in postnatal animals. This is the first study to describe teneurins expressed in a patchy pattern, however, is consistent with the intrinsic structure of the striatum, where a number of genes, proteins and enzymes have previously been shown to be expressed in patches (Desban et al., 1993; Graybiel and Ragsdale, 1978; Herkenham and Pert, 1981; van der Kooy, 1984; Lança et al., 1986; Murrin and Ferrer, 1984; Ragsdale and Graybiel, 1990). Localisation of Ten-m3-positive patches to the striatal matrix suggests that it marks a subset of matrisomes. This little known compartment has previously only been characterised by the clustering of afferent terminals (Flaherty and Graybiel, 1993a; Malach and Graybiel, 1986) and efferent neurons (Desban et al., 1993; Flaherty and Graybiel, 1993b; Jiménez-Castellanos and Graybiel, 1989; Tai et al., 2013), and more recently, marked by the expression of EphA7 receptors (Tai et al., 2013). Hence, we propose that Ten-m3 is one of the first molecular markers of matrisomes.

Further, the partially complementary spatial relationship between Ten-m3 and EphA7-positive patches shown in Chapter 4 indicates that these genes mostly mark distinct matrisomes. Hence, we propose that, unlike striosomes, a number of distinct matrisomes exist, and that these can be distinguished molecularly by expression of Ten-m3 and EphA7. Interestingly, Ten-m3 and EphA7-positive matrisomes only occupy a proportion of the matrix, suggesting the existence of others. It is unclear how corticostriatal and striatofugal matrisomes correlate with those marked by Ten-m3 and EphA7. However, experiments in Chapters 3 and 4 suggest that Ten-m3-positive matrisomes correlate with the clustered thalamostriatal terminals originating from the PF. Although Ten-m3 has previously been proposed to act homophilically to directly guide axons, this is first evidence of its capacity to direct the clustering of axons *in vivo*. Moreover, its close spatial relationship with EphA7-positive bands suggests that they may be working together to tightly control the branching and specific clustering of thalamic terminals. Thus, it is likely that other matrisome markers may also be involved in striatal connectivity.

The patchy pattern of Ten-m3 expression in the striatum was superimposed on a high-dorsocaudal to low-ventrorostral gradient. This graded pattern is consistent with that shown for Ten-m3 in structures of the visual system, and corresponds with the chemoaffinity hypothesis suggesting that they indicate roles in topographic mapping of interconnected structures (Sperry, 1963). This was used to survey afferent/efferent structures for Ten-m3 to identify the PF as a key locus of action. Ten-m3 was subsequently shown to have a similar temporal profile and high-dorsal to low-ventral

gradient in the PF to that found for the striatum, and correlates with the development and topographic arrangement of thalamostriatal branches shown in Chapters 3 and 4. Hence, these patterns of expression were subsequently shown to be important for the topography of thalamostriatal projections from the PF, as they were for retinogeniculate and retinocollicular projections, suggesting conserved roles for Ten-m3 in neural circuits.

In addition, Chapter 4 proposed novel roles for Ten-m3 in neural connectivity. In addition to the demonstration of targeting deficits, these developmental studies revealed a novel role for Ten-m3 in the formation of collateral branches of thalamostriatal axons, with apparent delays observed early on in KOs, suggesting that the anchorage of teneurin molecules to the actin cytoskeleton may be important in the formation of collateral branches in early development. Similar roles described previously, such as neurite outgrowth, presumably also utilise similar mechanisms.

In addition to assessing the functions of Ten-m3 during development, Chapter 4 presented the first investigation into the normal development of the mouse thalamostriatal pathway. Here, the thalamostriatal projection first reached the striatum at E16, with collateral branches observed at E17. At later postnatal ages, thalamostriatal terminals appeared to first fill rostral and dorsal regions, particularly in lateral striatum. These were consistent with studies in rats (Srivastava, 1999). This spatiotemporal gradient of development is partially consistent with that of the majority of other striatal events, such as neurogenesis and the clustering of striosome neurons, which occur along a lateral to medial gradient (Bayer, 1984; Krushel et al., 1995). However, these events also form

along a caudal to rostral gradient, which conflicts with the densest regions of thalamostriatal terminals in rostral striatum in mice and rats. Interestingly, these are the first studies to describe the development of striatal afferent/efferent projections along this axis.

In addition, the study of the development of normal thalamostriatal projections presented in Chapter 4, revealed that these projections initially show considerable overlap with striosomes at P3, but become refined with age such that terminals mostly occupy the striatal matrix by P7. This is the first study to describe a period refinement for striatal afferents. Moreover, this refinement period also appears to correlate with the migration of cholinergic interneurons from striosomes to the intermediate zone in the matrix of rats (Van Vulpen and Van Der Kooy, 1996). Further studies would be required to confirm this temporal correlation in mice, however, these studies may suggest that the refinement of thalamostriatal axons may influence the final positions of cholinergic interneurons.

One of the most surprising findings in the work presented in this thesis was the apparent reversal of the initial delay in thalamostriatal branching shown in Chapter 4 to result in increased occupancy of terminals in the matrix of adult Ten-m3 KO animals shown in Chapter 3. The most parsimonious interpretation of this data is that mechanisms underlying the refinement of these projections in later stages of development may be lacking in the absence of Ten-m3, thereby implicating the gene in these processes. This is the first study to implicate teneurins in these roles. Further, the timing and molecular mechanisms involved in these processes have yet to be described for striatal circuits. As

mentioned above, developmental experiments in Chapter 4, however, indicate that these refinement processes are occurring between P3 and P7 in mouse striatum, and are concurrent with the refinement of thalamostriatal terminals. Interesting, the latter, but not the former, process is maintained in Ten-m3 KOs. Hence, these studies constitute one of the first investigations showing refinement of thalamostriatal axons in the striatum and is the first to implicate a molecular candidate, in Ten-m3, in these processes.

In Chapter 3, the changes observed in the thalamostriatal pathway in the absence of Ten-m3 were reflected behaviourally by altered gait and delayed learning in KO animals. The former behavioural deficit may also be linked to Ten-m3 expression in the spinal cord (Allen Brain Atlas). Further, they suggest that the PF may indeed have a role in motor learning on an accelerated rotorod test, in contrast to previous studies (Kato et al., 2011). These behavioural deficits indicate the importance of the specificity of neural projections, and hence, the importance of axon guidance cues such as the family of teneurin molecules, during normal brain development. This is further reflected by the number of human genetic disorders associated with axon guidance deficits (Engle, 2010). In addition, teneurins have been linked to a number of cancers (see Ziegler et al., 2012 for a review), presumably due to their control of normal proliferation and cell survivial (Kinel-Tahan et al., 2007). Moreover, other teneurins have also been linked to mentral retardation (Minet and Chiquet-Ehrismann, 2000) and bipolar disease (Craddock and Sklar, 2013). Hence, the roles of teneurins in the normal patterning and connectivity of neural circuits has important implications for human health. Since these genes are conserved and expressed across all vertebrates, it is of vital importance that our limited

knowledge of their functions and mechanisms continue to be studied. Hence, the studies comprising this thesis are an important addition to our current knowledge of teneurins.

In addition to controlling axon branching and axon guidance of afferent thalamostriatal projections, loss of Ten-m3 also appeared to influence a subpopulation of the striatal neuronal population, most notably the cholinergic interneurons in a subregion of the striatum. Concurrent reductions in striatal cell number at this level suggest that Ten-m3 may play a role in the genesis of the earliest population of cholinergic interneurons, which normally occupy the VL quadrant. Currently, there are no known links between genes implicated in the development of cholinergic interneurons, such as Gbx2 and Lhx7 (Chen et al., 2010; Lopes et al., 2012; Marin et al., 2000), and teneurins, hence, suggesting further potential pathways with which Ten-m3 may be associated. Alternatively, these changes may be defects in migration and/or an indirect effect of changes to the thalamostriatal pathway in these mice.

The mechanisms underlying the diverse roles shown by Ten-m3 in the adult and developing thalamostriatal pathway in Chapters 3 and 4, respectively, were investigated in latter part of Chapter 4. These studies confirm previous evidence that Ten-m3 may act via multiple mechanisms. It was shown to work as a direct adhesive guidance cue for ingrowing thalamostriatal axons, and indirectly by altering the expression levels of other guidance genes, particularly EphA7, in the striatum. The partial spatial overlap of Ten-m3 expression with thalamostriatal terminals at P10 suggests that Ten-m3 may act to guide a subpopulation of thalamostriatal projections to Ten-m3-positive cells, presumably

through its adhesive properties and subsequent cell-cell contact. Additionally, it may act to promote branching in these regions, leading to the clustering of thalamic projections to produce dense patches of terminals in the matrix. It is proposed that the loss of patchiness observed is almost certainly a direct result of the deletion of Ten-m3.

In addition to the loss of thalamostriatal patches, there was also a marked increase in the spread of terminals within the matrix. While the topographically corresponding gradients of Ten-m3 in the PF and striatum may play a direct role in this, it is also likely that other axonal guidance molecules may be involved. In particular, the interesting pattern of EphA7 expression exactly adjacent to Ten-m3 in the striatum suggests that these, and possibly other similar guidance cues, may be working with Ten-m3 to control this specific patterning, possibly via inhibitory mechanisms previously attributed to these molecules (McLaughlin et al., 2003). The reduction in EphA7 expression levels in the striatum of Ten-m3 KOs, as has been noted for the visual pathway, supports the theory that they may belong to the same molecular pathway and have overlapping functions in these circuits. The actions of Ten-m3 on thalamostriatal axons are summarised in Fig. 5.1. Hence, these data suggest that the molecular pathways in which Ten-m3 may be associated with in the visual pathway may be conserved in the striatum. That is, Ten-m3 and EphA7 may belong to the same molecular pathway, with Ten-m3 located upstream of EphA7.

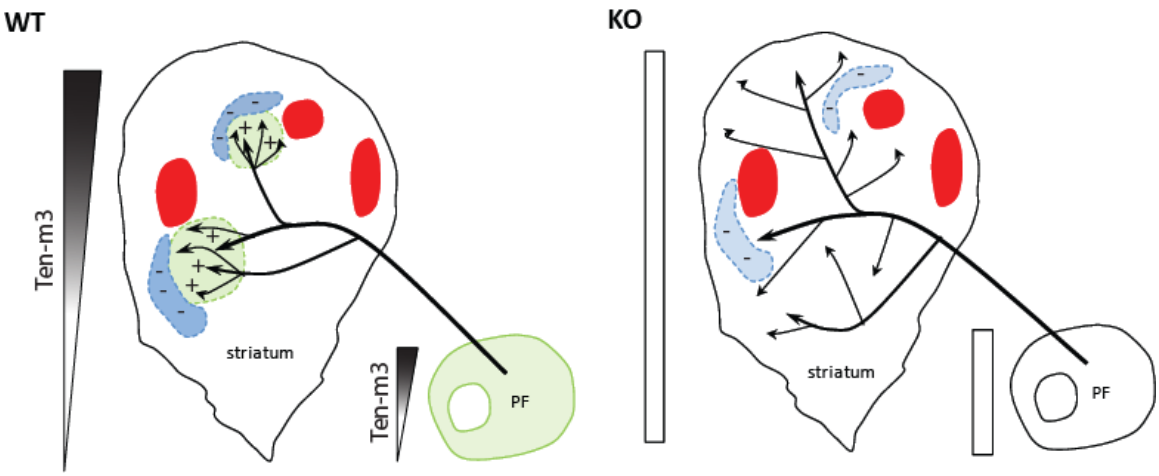

Figure 5.1. A summary of the role of Ten-m3-positive patches in the precise targeting of patchy thalamostriatal terminals from the PF and the changes in Ten-m3 KO mice.

In WTs, both the PF and striatum express Ten-m3 (green) in a high-dorsal to low-ventral gradient. In the striatum, this expression is also distributed in patches (green). The present data show that thalamostriatal axons (arrows) project to the striatal matrix, avoiding striosomes (red), where they arborise and collateralise to form multiple terminal foci correlating with Ten-m3-positive cells to form an overall 'patchy' termination pattern in the striatum. Hence, Ten-m3 appears to be acting as an attractive cue (+) for targeting thalamostriatal axons to these patches, and/or in promoting their branching within these regions. The close spatial expression of EphA7 (blue) suggests that these normally inhibitory cues (-) may work with Ten-m3 to control this specific targeting.

In the absence of Ten-m3 in the striatum and PF in KO mice, thalamostriatal terminals are diffuse and spread out to target the matrix (white) in a homogeneous fashion, but still avoid striosomes (red). The reduced specificity of the thalamic projection in the matrix is proposed to be a direct result of the absence of the patchy expression of Ten-m3. In addition, the loss of its expression in topographically corresponding gradients in the striatum and PF, along with the reduced expression of EphA7 in the striatum in KOs, and possibly other similar guidance cues, may also exacerbate this reduced specificity of thalamostriatal targeting.

Future directions

This thesis constitutes the first investigation of the adult and developing mouse thalamostriatal pathway as well as the roles of Ten-m3 in this circuit. The discovery that Ten-m3 has key roles roles in regulating the distribution of thalamostriatal projections and the cholinergic cell population has raised a number of questions that could not be addressed within the time constraints of the PhD candidature. Some of the more notable issues which should be addressed by subsequent workers are raised below.

The results of anatomical tracing studies suggest that Ten-m3 has roles in a number of developmental processes, including collateralisation, fasciculation, and patterning of terminals. These roles should be investigated at higher resolution to confirm and examine the extent and cellular details of these changes. This was not possible using the current tracing studies as all axons of interest, and more so, were labeled due to the small size of the PF, particularly at the age at which the first collateral branches arose, that is E17. Instead, cell culture studies may allow for the closer analysis of the growth of axons lacking Ten-m3. Hence, dissociated primary cultures or co-culturing organotypic slices from developing PF and striatum from WT and Ten-m3 KO mice may allow for single axons to be analysed for branching and differences in fasciculation. Further, the apparent abolishment of the clustered patterning of thalamostriatal terminals in KOs requires further investigation. Some aspects may be revealed by changes to collateral branching. However, small changes in the clustering of these terminals may be best examined using single-cell tracing studies *in vivo*, similar to those described by Deschenes et al. (1996a).

Dual retrograde tracer injections into the striatum revealed interesting changes to the subpopulation of PF cells projecting to mid-caudal striatum. They, however, were unable to reveal whether these cells exhibit increased terminal zones, caudally-shifted terminal zones or both, in the absence of Ten-m3. These would, likewise, require focal injections or single cell tracing injections into the PF. These experiments may also reveal the extent to which terminals target the VL striatum, which appeared by be avoided in KOs more so than WTs, however, was not clear from the present study.

The finding that a subpopulation of striatal cholinergic interneurons was altered in the absence of Ten-m3 was surprising, but intriguing, due to the changes observed in their main afferent input, the thalamostriatal pathway, and the consequent behavioural deficits. Firstly, it is currently unclear whether Ten-m3-positive cells correlate to striatal cholinergic interneurons. Considering that changes to this population are altered in the absence of Ten-m3, it would be prudent to investigate this. Preliminary studies suggest that immunohistochemistry for ChAT is not highly informative in sections processed for *in situ* hybridisation protocols required to reveal Ten-m3 expression. Hence, dual immunohistochemistry would be required, which necessitates access to a Ten-m3 antibody. Alternatively, thicker sections may be trialed for *in situ* hybridisation.

In addition, further studies are required to examine the striatal cholinergic population in Ten-m3 KOs. In particular, the development of these cells would be of particular interest as they exhibit a lateral to medial and rostral to caudal spatiotemporal developmental gradient, arising from E12 in rats (Schlösser et al., 1999; Semba and Fibiger, 1988).

Since the deficits observed are localised to caudal and VL striatum, the earliest born population may be the most affected in Ten-m3 KO mice. Interestingly, Chen et al.(2010) found that early-born cholinergic cells in Gbx2 mutants occupy abnormally medial regions of the striatum, while late-born cells were missing. Since it is unclear whether there is a link between Gbx2 and Ten-m3, it may be prudent in investigate the cholinergic population across a wide developmental window. This can done using immunohistochemistry for ChAT beginning at E12, and at small time intervals up until birth to pick up potential differences in the number and/or distribution of the early and late-born population.

The relationship between the thalamostriatal axons and cholinergic interneurons, particularly in the VL quadrant of mid-caudal striatum, needs to be further addressed. Future studies should investigate the colocalisation of these two components, using double labeling of thalamostriatal terminals and immunohistochemistry for ChAT in Ten-m3 KO mice, particularly in the VL quadrant. It would be of interest to examine this in adults and during development, as one the issues raised from these results is that it is currently unclear which of these components comes first to influence the final organisation of the other. During development, it would be particularly interestingly to look at this correlation between P3 and P7, as cholinergic interneurons have been shown to migrate from striosomes to the matrix by P7 in rats (Van Vulpen and Van Der Kooy, 1996), and there appears to be a corresponding refinement of thalamostriatal terminals between P3 and P7 in mice. It may first be necessary to determine the timing of this migration in mice. These experiments may reveal whether the retraction of thalamic

terminals away from striosomes is responsible for the migration of cholinergic interneurons into the matrix.

The loss of cholinergic interneurons to the VL quadrant of the striatum suggests changes to a number of neurotransmitters in this region. Firstly, ACh, normally released by cholinergic cells may be reduced, and, hence, ACh release should be measured in Ten-m3 KOs, possibly using voltammetry, such as that performed by Threlfell et al. (2012). Further, the activity of cholinergic interneurons can also be examined using antibodies to p-Ser240-244-S6rp, which has recently been shown to be a reliable estimate of activity in these cells (Bertran-Gonzalez et al., 2012). Moreover, the delay in learning observed in Ten-m3 KO mice is similarly observed in mutants lacking the α7-nicotinic ACh receptor, suggesting that these may altered in Ten-m3 KOs. In addition, these receptors are linked to D1-dopamine and NMDA receptors. In particular, D1 receptors are associated with the 'early' stage of skill learning on a rotorod (Yin et al., 2009) and are most highly expressed in VL striatum (Savasta et al., 1986), both of which are altered in Ten-m3 KO mice. Hence, D1 receptors should also be investigated. Furthermore, the proposed reduction in ACh and D1 receptors also suggests altered levels of dopamine, particularly in VL striatum. Hence, immunohistochemistry for TH would reveal any changes to dopaminergic innervations in KOs.

The impact of the altered patterning of thalamostriatal projections outside the VL quadrant on cholinergic drive would also be of interest. In order to investigate this, it would be prudent to first look at the relationship between the cholinergic cells and the

thalamostriatal patches in WT animals. If there is a strong correlation, the more diffuse terminals in KOs suggests there may be decreased activation or less-specific drive of cholinergic cells by thalamostriatal terminals. This can be investigated using *in vitro* brain slices preserving the thalamostriatal projection and recording cholinergic response to thalamic activation, such as shown by Ding et al. (2010).

The partial overlap of Ten-m3 mRNA and labeled terminals suggests that Ten-m3 is acting as a direct attractive cue for ingrowing PF axons. It is unclear whether Ten-m3 protein is expressed along thalamostriatal axons and on the surface of these striatal cells with which they contact. Hence, immunohistochemistry for Ten-m3 is required to reveal direct Ten-m3 protein-protein interactions. Further, it is currently unclear which striatal cell types express Ten-m3. Literature suggests that these most likely correspond to both direct and indirect pathway MSNs and cholinergic interneurons (see Smith et al., 2009 for a review). Hence, it would be interesting to determine which, if all of these cell types, express Ten-m3. As mentioned above, immunohistochemistry for ChAT would label cholinergic cells, or DARPP-32 would reveal MSNs. This may provide more information as to which efferent pathways may be affected by the absence of Ten-m3.

The partial overlap between Ten-m3 and thalamostriatal terminals suggests that other cues are also involved in the guidance of these projections. It is likely that EphA7-positive matrisomes, previously shown to correlate with efferent striatofugal axons, may also govern the positioning of thalamostriatal projections. Hence, the spatial correlation between EphA7 and these terminals should be examined. Further, the reduction of

EphA7 in the striatum of Ten-m3 KO mice provides support for the hypothesis that it may have a role in the thalamostriatal pathway. It would be of interest to determine whether EphA7 is responsible for the phenotypes observed in Ten-m3 KO mice, which would reveal more about the potential interactions between the two genes. Therefore, the thalamostriatal pathway should be investigated in EphA7 KO mice. Similar anterograde tracing experiments as those performed in the present study would reveal whether these animals show similar gross changes to the specificity of the targeting of thalamostriatal axons.

Finally, it is unclear from our studies whether developing and/or adult expression of Ten-m3 is responsible for the adult phenotype in KO mice. Since Ten-m3 is most highly expressed in neural structures in early postnatal development (Leamey et al., 2007a, 2007b; Ben-Zur et al., 2000), it is likely that changes to circuitry and behaviour in adults is a direct consequence of changes observed in young animals. However, the apparently multimodal nature of Ten-m3 may reflect differing roles at different developmental stages; for instance branching, fasciculation and pathfinding roles may be important at perinatal ages, while synaptic organisation and function (Hong et al., 2012; Mosca et al., 2012; Silva et al., 2011) would be important later in development and into adulthood. Therefore, the altered phenotype may also be the result of expression in adults. To resolve the temporal roles of Ten-m3, the timing of expression would need to be controlled, for instance, using the Cre-loxP recombination system. This combined with optogenetic approaches to probe changes in behaviour and circuitry would be ideal approaches to study these questions.

References

Akay, T. (2006). Behavioral and Electromyographic Characterization of Mice Lacking EphA4 Receptors. J. Neurophysiol. *96*, 642–651.

Albin, R.L., Young, A.B., and Penney, J.B. (1989). The functional anatomy of basal ganglia disorders. Trends Neurosci. *12*, 366–375.

Anderson, J.J., Chase, T.N., and Engber, T.M. (1993). Substance P increases release of acetylcholine in the dorsal striatum of freely moving rats. Brain Res. *623*, 189–194.

Anderson, S.A., Qiu, M., Bulfone, A., Eisenstat, D.D., Meneses, J., Pedersen, R., and Rubenstein, J.L. (1997). Mutations of the homeobox genes Dlx-1 and Dlx-2 disrupt the striatal subventricular zone and differentiation of late born striatal neurons. Neuron *19*, 27–37.

Angelucci, A., Clascá, F., and Sur, M. (1996). Anterograde axonal tracing with the subunit B of cholera toxin: a highly sensitive immunohistochemical protocol for revealing fine axonal morphology in adult and neonatal brains. J. Neurosci. Methods *65*, 101–112.

Angevine, J.B., Jr (1970). Time of neuron origin in the diencephalon of the mouse. An autoradiographic study. J. Comp. Neurol. *139*, 129–187.

Angevine, J.B., Jr, and McConnell, J. (1974). Time of origin of striatal neurons in the mouse: an autoradiographic study. Anat. Rec. *178*, 300.

Aosaki, T., Graybiel, A.M., and Kimura, M. (1994). Effect of the nigrostriatal dopamine system on acquired neural responses in the striatum of behaving monkeys. Science *265*, 412–415.

Apicella, P. (2007). Leading tonically active neurons of the striatum from reward detection to context recognition. Trends Neurosci. *30*, 299–306.

Arenas, E., Alberch, J., Perez-Navarro, E., Solsona, C., and Marsal, J. (1991). Neurokinin receptors differentially mediate endogenous acetylcholine release evoked by tachykinins in the neostriatum. J. Neurosci. Off. J. Soc. Neurosci. *11*, 2332–2338.

Arlotta, P., Molyneaux, B.J., Jabaudon, D., Yoshida, Y., and Macklis, J.D. (2008). Ctip2 Controls the Differentiation of Medium Spiny Neurons and the Establishment of the Cellular Architecture of the Striatum. J. Neurosci. *28*, 622–632.

Bacci, J.-J., Kachidian, P., Kerkerian-Le Goff, L., and Salin, P. (2004). Intralaminar thalamic nuclei lesions: widespread impact on dopamine denervation-mediated cellular defects in the rat basal ganglia. J. Neuropathol. Exp. Neurol. *63*, 20–31.

Bagutti, C. (2003). The intracellular domain of teneurin-2 has a nuclear function and represses zic-1-mediated transcription. J. Cell Sci. *116*, 2957–2966.

Balleine, B.W. (2011). Sensation, Incentive Learning, and the Motivational Control of Goal-Directed Action. In Neurobiology of Sensation and Reward, J.A. Gottfried, ed. (Boca Raton (FL): CRC Press),.

Bamford, N.S., Zhang, H., Schmitz, Y., Wu, N.-P., Cepeda, C., Levine, M.S., Schmauss, C., Zakharenko, S.S., Zablow, L., and Sulzer, D. (2004). Heterosynaptic dopamine neurotransmission selects sets of corticostriatal terminals. Neuron *42*, 653–663.

Barral, J., Galarraga, E., and Bargas, J. (1999). Muscarinic presynaptic inhibition of neostriatal glutamatergic afferents is mediated by Q-type Ca2+ channels. Brain Res. Bull. *49*, 285–289.

Barroso-Chinea, P., Castle, M., Aymerich, M.S., Pérez-Manso, M., Erro, E., Tuñon, T., and Lanciego, J.L. (2007). Expression of the mRNAs encoding for the vesicular glutamate transporters 1 and 2 in the rat thalamus. J. Comp. Neurol. *501*, 703–715.

Barroso-Chinea, P., Castle, M., Aymerich, M.S., and Lanciego, J.L. (2008). Expression of vesicular glutamate transporters 1 and 2 in the cells of origin of the rat thalamostriatal pathway. J. Chem. Neuroanat. *35*, 101–107.

Baumgartner, S., Martin, D., Hagios, C., and Chiquet-Ehrismann, R. (1994). Tenm, a Drosophila gene related to tenascin, is a new pair-rule gene. EMBO J. *13*, 3728–3740.

Bayer, S.A. (1984). Neurogenesis in the rat neostriatum. Int. J. Dev. Neurosci. *2*, 163–175.

Beckmann, J., Vitobello, A., Ferralli, J., Brož, D., Rijli, F.M., and Chiquet-Ehrismann, R. (2011). Human teneurin-1 is a direct target of the homeobox transcription factor EMX2 at a novel alternate promoter. BMC Dev. Biol. *11*, 35.

Beckmann, J., Schubert, R., Chiquet-Ehrismann, R., and Müller, D.J. (2013). Deciphering Teneurin Domains That Facilitate Cellular Recognition, Cell–Cell Adhesion, and Neurite Outgrowth Using Atomic Force Microscopy-Based Single-Cell Force Spectroscopy. Nano Lett. *13*, 2937–2946.

Beckstead, R.M. (1984). The thalamostriatal projection in the cat. J. Comp. Neurol. *223*, 313–346.

Bennett, B.D., and Bolam, J.P. (1994). Synaptic input and output of parvalbumin-immunoreactive neurons in the neostriatum of the rat. Neuroscience *62*, 707–719.

Berendse, H.W., and Groenewegen, H.J. (1990). Organization of the thalamostriatal projections in the rat, with special emphasis on the ventral striatum. J. Comp. Neurol. *299*, 187–228.

Berendse, H.W., Galis-de Graaf, Y., and Groenewegen, H.J. (1992). Topographical organization and relationship with ventral striatal compartments of prefrontal corticostriatal projections in the rat. J. Comp. Neurol. *316*, 314–347.

Bernácer, J., Prensa, L., and Giménez-Amaya, J.M. (2007). Cholinergic Interneurons Are Differentially Distributed in the Human Striatum. PLoS ONE *2*, e1174.

Bertran-Gonzalez, J., Chieng, B.C., Laurent, V., Valjent, E., and Balleine, B.W. (2012). Striatal Cholinergic Interneurons Display Activity-Related Phosphorylation of Ribosomal Protein S6. PLoS ONE *7*, e53195.

Beutler, L.R., Eldred, K.C., Quintana, A., Keene, C.D., Rose, S.E., Postupna, N., Montine, T.J., and Palmiter, R.D. (2011). Severely Impaired Learning and Altered Neuronal Morphology in Mice Lacking NMDA Receptors in Medium Spiny Neurons. PLoS ONE *6*, e28168.

Bicknese, A.R., Sheppard, A.M., O'Leary, D.D., and Pearlman, A.L. (1994). Thalamocortical axons extend along a chondroitin sulfate proteoglycan-enriched pathway coincident with the neocortical subplate and distinct from the efferent path. J. Neurosci. Off. J. Soc. Neurosci. *14*, 3500–3510.

Bohus, B., and de Wied, D. (1967). Avoidance and escape behavior following medial thalamic lesions in rats. J. Comp. Physiol. Psychol. *64*, 26–29.

Bolam, J.P., Wainer, B.H., and Smith, A.D. (1984). Characterization of cholinergic neurons in the rat neostriatum. A combination of choline acetyltransferase immunocytochemistry, Golgi-impregnation and electron microscopy. Neuroscience *12*, 711–718.

Bolam, J.P., Ingham, C.A., Izzo, P.N., Levey, A.I., Rye, D.B., Smith, A.D., and Wainer, B.H. (1986). Substance P-containing terminals in synaptic contact with cholinergic neurons in the neostriatum and basal forebrain: a double immunocytochemical study in the rat. Brain Res. *397*, 279–289.

Bolam, J.P., Izzo, P.N., and Graybiel, A.M. (1988). Cellular substrate of the histochemically defined striosome/matrix system of the caudate nucleus: a combined Golgi and immunocytochemical study in cat and ferret. Neuroscience *24*, 853–875.

Bradfield, L.A., Bertran-Gonzalez, J., Chieng, B., and Balleine, B.W. (2013). The Thalamostriatal Pathway and Cholinergic Control of Goal-Directed Action: Interlacing New with Existing Learning in the Striatum. Neuron.

Brand, S., and Rakic, P. (1979). Genesis of the primate neostriatum: [3H]thymidine autoradiographic analysis of the time of neuron origin in the rhesus monkey. Neuroscience *4*, 767–778.

Brauth, S.E., Kitt, C.A., and Gerfen, C.R. (1988). Calcium binding protein in the basal ganglia system of a non-mammalian vertebrate: an immunohistochemical study in the reptile Caiman crocodilus. Brain Res. *452*, 367–372.

Brown, L.L., Smith, D.M., and Goldbloom, L.M. (1998). Organizing principles of cortical integration in the rat neostriatum: corticostriate map of the body surface is an ordered lattice of curved laminae and radial points. J. Comp. Neurol. *392*, 468–488.

Brown, M.S., Ye, J., Rawson, R.B., and Goldstein, J.L. (2000). Regulated intramembrane proteolysis: a control mechanism conserved from bacteria to humans. Cell *100*, 391–398.

Carman, J.B., Cowan, W.M., Powell, T.P., and Webster, K.E. (1965). A bilateral cortico-striatal projection. J. Neurol. Neurosurg. Psychiatry *28*, 71–77.

Carr, O.P., Glendining, K.A., Leamey, C.A., and Marotte, L.R. (2013). Overexpression of Ten-m3 in the retina alters ipsilateral retinocollicular projections in the wallaby (Macropus eugenii). Int. J. Dev. Neurosci. Off. J. Int. Soc. Dev. Neurosci.

Castiblanco-Piñeros, E., Quiroz-Padilla, M.F., Cardenas-Palacio, C.A., and Cardenas, F.P. (2011). Contribution of the parafascicular nucleus in the spontaneous object recognition task. Neurobiol. Learn. Mem. *96*, 272–279.

Castle, M., Aymerich, M.S., Sanchez-Escobar, C., Gonzalo, N., Obeso, J.A., and Lanciego, J.L. (2005). Thalamic innervation of the direct and indirect basal ganglia pathways in the rat: Ipsi- and contralateral projections. J. Comp. Neurol. *483*, 143–153.

Chang, H.T., and Kita, H. (1992). Interneurons in the rat striatum: relationships between parvalbumin neurons and cholinergic neurons. Brain Res. *574*, 307–311.

Al Chawaf, A., St. Amant, K., Belsham, D., and Lovejoy, D.A. (2007a). Regulation of neurite growth in immortalized mouse hypothalamic neurons and rat hippocampal primary cultures by teneurin C-terminal-associated peptide-1. Neuroscience *144*, 1241–1254.

Al Chawaf, A., St Amant, K., Belsham, D., and Lovejoy, D.A. (2007b). Regulation of neurite growth in immortalized mouse hypothalamic neurons and rat hippocampal primary cultures by teneurin C-terminal-associated peptide-1. Neuroscience *144*, 1241–1254.

Chen, L., Chatterjee, M., and Li, J.Y.H. (2010). The mouse homeobox gene Gbx2 is required for the development of cholinergic interneurons in the striatum. J. Neurosci. Off. J. Soc. Neurosci. *30*, 14824–14834.

Christensen, J., Sørensen, J.C., Ostergaard, K., and Zimmer, J. (1999). Early postnatal development of the rat corticostriatal pathway: an anterograde axonal tracing study using biocytin pellets. Anat. Embryol. (Berl.) *200*, 73–80.

Chronister, R.B., Farnell, K.E., Marco, L.A., and White, L.E., Jr (1976). The rodent neostriatum: a Golgi analysis. Brain Res. *108*, 37–46.

Consolo, S., Baldi, G., Giorgi, S., and Nannini, L. (1996a). The cerebral cortex and parafascicular thalamic nucleus facilitate in vivo acetylcholine release in the rat striatum through distinct glutamate receptor subtypes. Eur. J. Neurosci. *8*, 2702–2710.

Consolo, S., Baronio, P., Guidi, G., and Di Chiara, G. (1996b). Role of the parafascicular thalamic nucleus and N-methyl-D-aspartate transmission in the D1-dependent control of in vivo acetylcholine release in rat striatum. Neuroscience *71*, 157–165.

Consolo, S., Cassetti, A., and Uboldi, M.C. (1999). The parafascicular thalamic nucleus but not the prefrontal cortex facilitates the nitric oxide/cyclic GMP pathway in rat striatum. Neuroscience *91*, 51–58.

Cowan, W.M., and Powell, T.P. (1956). A study of thalamo-striate relations in the monkey. Brain J. Neurol. *79*, 364–390.

Craddock, N., and Sklar, P. (2013). Genetics of bipolar disorder. Lancet *381*, 1654–1662.

Dang, M.T., Yokoi, F., Yin, H.H., Lovinger, D.M., Wang, Y., and Li, Y. (2006). From the Cover: Disrupted motor learning and long-term synaptic plasticity in mice lacking NMDAR1 in the striatum. Proc. Natl. Acad. Sci. *103*, 15254–15259.

Danik, M., Cassoly, E., Manseau, F., Sotty, F., Mouginot, D., and Williams, S. (2005). Frequent coexpression of the vesicular glutamate transporter 1 and 2 genes, as well as coexpression with genes for choline acetyltransferase or glutamic acid decarboxylase in neurons of rat brain. J. Neurosci. Res. *81*, 506–521.

DeLong, M.R. (1990). Primate models of movement disorders of basal ganglia origin. Trends Neurosci. *13*, 281–285.

Deng, J., and Elberger, A.J. (2003). Corticothalamic and thalamocortical pathfinding in the mouse: dependence on intermediate targets and guidance axis. Anat. Embryol. (Berl.) *207*, 177–192.

Desban, M., Gauchy, C., Kemel, M.L., Besson, M.J., and Glowinski, J. (1989). Three-dimensional organization of the striosomal compartment and patchy distribution of striatonigral projections in the matrix of the cat caudate nucleus. Neuroscience *29*, 551–566.

Desban, M., Kemel, M.L., Glowinski, J., and Gauchy, C. (1993). Spatial organization of patch and matrix compartments in the rat striatum. Neuroscience *57*, 661–671.

Deschamps, C., Faideau, M., Jaber, M., Gaillard, A., and Prestoz, L. (2009). Expression of ephrinA5 during development and potential involvement in the guidance of the mesostriatal pathway. Exp. Neurol. *219*, 466–480.

Deschamps, C., Morel, M., Janet, T., Page, G., Jaber, M., Gaillard, A., and Prestoz, L. (2010). EphrinA5 protein distribution in the developing mouse brain. BMC Neurosci. *11*, 105.

Deschênes, M., Bourassa, J., and Parent, A. (1995). Two different types of thalamic fibers innervate the rat striatum. Brain Res. *701*, 288–292.

Deschênes, M., Bourassa, J., Doan, V.D., and Parent, A. (1996a). A single-cell study of the axonal projections arising from the posterior intralaminar thalamic nuclei in the rat. Eur. J. Neurosci. *8*, 329–343.

Deschênes, M., Bourassa, J., Doan, V.D., and Parent, A. (1996b). A single-cell study of the axonal projections arising from the posterior intralaminar thalamic nuclei in the rat. Eur. J. Neurosci. *8*, 329–343.

Dharmaratne, N., Glendining, K.A., Young, T.R., Tran, H., Sawatari, A., and Leamey, C.A. (2012). Ten-m3 is required for the development of topography in the ipsilateral retinocollicular pathway. PloS One *7*, e43083.

Ding, J.B., Guzman, J.N., Peterson, J.D., Goldberg, J.A., and Surmeier, D.J. (2010). Thalamic Gating of Corticostriatal Signaling by Cholinergic Interneurons. Neuron *67*, 294–307.

Ding, J.B., Oh, W.-J., Sabatini, B.L., and Gu, C. (2011). Semaphorin 3E–Plexin-D1 signaling controls pathway-specific synapse formation in the striatum. Nat. Neurosci. *15*, 215–223.

Doeller, C.F., King, J.A., and Burgess, N. (2008). Parallel striatal and hippocampal systems for landmarks and boundaries in spatial memory. Proc. Natl. Acad. Sci. U. S. A. *105*, 5915–5920.

Donoghue, J.P., and Herkenham, M. (1986). Neostriatal projections from individual cortical fields conform to histochemically distinct striatal compartments in the rat. Brain Res. *365*, 397–403.

Drabikowski, K., Trzebiatowska, A., and Chiquet-Ehrismann, R. (2005). ten-1, an essential gene for germ cell development, epidermal morphogenesis, gonad migration, and neuronal pathfinding in Caenorhabditis elegans. Dev. Biol. *282*, 27–38.

Dubé, L., Smith, A.D., and Bolam, J.P. (1988). Identification of synaptic terminals of thalamic or cortical origin in contact with distinct medium-size spiny neurons in the rat neostriatum. J. Comp. Neurol. *267*, 455–471.

Ebihara, K., Yamamoto, K., Ueda, K., Koshikawa, N., and Kobayashi, M. (2013). Cholinergic interneurons suppress action potential initiation of medium spiny neurons in rat nucleus accumbens shell. Neuroscience *236*, 332–344.

Eblen, F., and Graybiel, A.M. (1995). Highly restricted origin of prefrontal cortical inputs to striosomes in the macaque monkey. J. Neurosci. Off. J. Soc. Neurosci. *15*, 5999–6013.

Elena Erro, M., Lanciego, J.L., and Gimenez-Amaya, J.M. (2002). Re-examination of the thalamostriatal projections in the rat with retrograde tracers. Neurosci. Res. *42*, 45–55.

Ellender, T.J., Harwood, J., Kosillo, P., Capogna, M., and Bolam, J.P. (2013). Heterogeneous properties of central lateral and parafascicular thalamic synapses in the striatum. J. Physiol. *591*, 257–272.

Encha-Razavi, F., and Sonigo, P. (2003). Features of the developing brain. Childs Nerv. Syst. ChNS Off. J. Int. Soc. Pediatr. Neurosurg. *19*, 426–428.

Engle, E.C. (2010). Human genetic disorders of axon guidance. Cold Spring Harb. Perspect. Biol. *2*, a001784.

Evans, A.E., Kelly, C.M., Precious, S.V., and Rosser, A.E. (2012). Molecular Regulation of Striatal Development: A Review. Anat. Res. Int. *2012*, 1–14.

Exley, R., and Cragg, S.J. (2008). Presynaptic nicotinic receptors: a dynamic and diverse cholinergic filter of striatal dopamine neurotransmission. Br. J. Pharmacol. *153 Suppl 1*, S283–297.

Féger, J., Bevan, M., and Crossman, A.R. (1994). The projections from the parafascicular thalamic nucleus to the subthalamic nucleus and the striatum arise from separate neuronal populations: a comparison with the corticostriatal and corticosubthalamic efferents in a retrograde fluorescent double-labelling study. Neuroscience *60*, 125–132.

Feng, K., Zhou, X.-H., Oohashi, T., Mörgelin, M., Lustig, A., Hirakawa, S., Ninomiya, Y., Engel, J., Rauch, U., and Fässler, R. (2002). All four members of the Ten-m/Odz family of transmembrane proteins form dimers. J. Biol. Chem. *277*, 26128–26135.

Fentress, J.C., Stanfield, B.B., and Cowan, W.M. (1981). Observation on the development of the striatum in mice and rats. Anat. Embryol. (Berl.) *163*, 275–298.

Fishell, G., and van der Kooy, D. (1987). Pattern formation in the striatum: developmental changes in the distribution of striatonigral neurons. J. Neurosci. Off. J. Soc. Neurosci. *7*, 1969–1978.

Fishell, G., and van der Kooy, D. (1991). Pattern formation in the striatum: neurons with early projections to the substantia nigra survive the cell death period. J. Comp. Neurol. *312*, 33–42.

Fisher, R.S., Levine, M.S., Gazzara, R.A., Hull, C.D., and Buchwald, N.A. (1983). Postnatal development of caudate input neurons in the cat. J. Comp. Neurol. *219*, 51–69.

Flaherty, A.W., and Graybiel, A.M. (1993a). Two input systems for body representations in the primate striatal matrix: experimental evidence in the squirrel monkey. J. Neurosci. Off. J. Soc. Neurosci. *13*, 1120–1137.

Flaherty, A.W., and Graybiel, A.M. (1993b). Output architecture of the primate putamen. J. Neurosci. Off. J. Soc. Neurosci. *13*, 3222–3237.

Floeter, M.K., and Jones, E.G. (1985). Transplantation of fetal postmitotic neurons to rat cortex: survival, early pathway choices and long-term projections of outgrowing axons. Brain Res. *354*, 19–38.

Fragkouli, A., Hearn, C., Errington, M., Cooke, S., Grigoriou, M., Bliss, T., Stylianopoulou, F., and Pachnis, V. (2005). Loss of forebrain cholinergic neurons and impairment in spatial learning and memory in LHX7-deficient mice. Eur. J. Neurosci. *21*, 2923–2938.

François, C., Percheron, G., Yelnik, J., and Tandé, D. (1988). A topographic study of the course of nigral axons and of the distribution of pallidal axonal endings in the centre médian-parafascicular complex of macaques. Brain Res. *473*, 181–186.

François, C., Percheron, G., Parent, A., Sadikot, A.F., Fenelon, G., and Yelnik, J. (1991). Topography of the projection from the central complex of the thalamus to the sensorimotor striatal territory in monkeys. J. Comp. Neurol. *305*, 17–34.

Fremeau, R.T. (2002). The identification of vesicular glutamate transporter 3 suggests novel modes of signaling by glutamate. Proc. Natl. Acad. Sci. *99*, 14488–14493.

Fremeau, R.T., Jr, Troyer, M.D., Pahner, I., Nygaard, G.O., Tran, C.H., Reimer, R.J., Bellocchio, E.E., Fortin, D., Storm-Mathisen, J., and Edwards, R.H. (2001). The expression of vesicular glutamate transporters defines two classes of excitatory synapse. Neuron *31*, 247–260.

Gallo, G. (2011). The cytoskeletal and signaling mechanisms of axon collateral branching. Dev. Neurobiol. *71*, 201–220.

Galvan, A., and Smith, Y. (2011). The primate thalamostriatal systems: Anatomical organization, functional roles and possible involvement in Parkinson's disease. Basal Ganglia *1*, 179–189.

Gerfen, C.R. (1984). The neostriatal mosaic: compartmentalization of corticostriatal input and striatonigral output systems. Nature *311*, 461–464.

Gerfen, C.R. (1985). The neostriatal mosaic. I. Compartmental organization of projections from the striatum to the substantia nigra in the rat. J. Comp. Neurol. *236*, 454–476.

Gerfen, C.R. (1989). The neostriatal mosaic: striatal patch-matrix organization is related to cortical lamination. Science *246*, 385–388.

Gerfen, C.R. (1992). The neostriatal mosaic: multiple levels of compartmental organization in the basal ganglia. Annu. Rev. Neurosci. *15*, 285–320.

Gerfen, C.R., and Surmeier, D.J. (2011). Modulation of striatal projection systems by dopamine. Annu. Rev. Neurosci. *34*, 441–466.

Gerfen, C.R., and Wilson, C. (1996). The basal ganglia. In Handbook of Chemical Neuroanatomy, (Elsevier),.

Gerfen, C.R., Herkenham, M., and Thibault, J. (1987). The neostriatal mosaic: II. Patch- and matrix-directed mesostriatal dopaminergic and non-dopaminergic systems. J. Neurosci. Off. J. Soc. Neurosci. *7*, 3915–3934.

Gibson, D.A., and Ma, L. (2010). Developmental regulation of axon branching in the vertebrate nervous system. Development *138*, 183–195.

Giménez-Amaya, J.M., and Graybiel, A.M. (1991). Modular organization of projection neurons in the matrix compartment of the primate striatum. J. Neurosci. *11*, 779–791.

Glendining, K.A. (2011). Molecular mechanisms underlying Ten-m3 mediated guidance of the ipsilateral visual pathway. University of Sydney.

Godement, P., Vanselow, J., Thanos, S., and Bonhoeffer, F. (1987). A study in developing visual systems with a new method of staining neurones and their processes in fixed tissue. Dev. Camb. Engl. *101*, 697–713.

Goldman, P.S., and Nauta, W.J. (1977). An intricately patterned prefronto-caudate projection in the rhesus monkey. J. Comp. Neurol. *72*, 369–386.

Gonzalo, N. (2002). The parafascicular thalamic complex and basal ganglia circuitry: further complexity to the basal ganglia model. Thalamus Relat. Syst. *1*, 341–348.

Good, M.A. (2002). Spatial memory and hippocampal function: Where are we now? Psicologica *23*, 109–138.

Gras, C., Herzog, E., Bellenchi, G.C., Bernard, V., Ravassard, P., Pohl, M., Gasnier, B., Giros, B., and El Mestikawy, S. (2002). A third vesicular glutamate transporter expressed by cholinergic and serotoninergic neurons. J. Neurosci. Off. J. Soc. Neurosci. *22*, 5442–5451.

Gras, C., Amilhon, B., Lepicard, E.M., Poirel, O., Vinatier, J., Herbin, M., Dumas, S., Tzavara, E.T., Wade, M.R., Nomikos, G.G., et al. (2008). The vesicular glutamate transporter VGLUT3 synergizes striatal acetylcholine tone. Nat. Neurosci. *11*, 292–300.

Graybiel, A.M. (1984). Correspondence between the dopamine islands and striosomes of the mammalian striatum. Neuroscience *13*, 1157–1187.

Graybiel, A.M. (1990). Neurotransmitters and neuromodulators in the basal ganglia. Trends Neurosci. *13*, 244–254.

Graybiel, A.M., and Hickey, T.L. (1982). Chemospecificity of ontogenetic units in the striatum: demonstration by combining [3H]thymidine neuronography and histochemical staining. Proc. Natl. Acad. Sci. U. S. A. *79*, 198–202.

Graybiel, A.M., and Ragsdale, C.W., Jr (1978). Histochemically distinct compartments in the striatum of human, monkeys, and cat demonstrated by acetylthiocholinesterase staining. Proc. Natl. Acad. Sci. U. S. A. *75*, 5723–5726.

Graybiel, A.M., Ragsdale, C.W., Jr, Yoneoka, E.S., and Elde, R.P. (1981). An immunohistochemical study of enkephalins and other neuropeptides in the striatum of the cat with evidence that the opiate peptides are arranged to form mosaic patterns in register with the striosomal compartments visible by acetylcholinesterase staining. Neuroscience *6*, 377–397.

Graybiel, A.M., Baughman, R.W., and Eckenstein, F. (1986). Cholinergic neuropil of the striatum observes striosomal boundaries. Nature *323*, 625–627.

Groenewegen, H.J., and Berendse, H.W. (1994). The specificity of the "nonspecific" midline and intralaminar thalamic nuclei. Trends Neurosci. *17*, 52–57.

Groenewegen, H.J., Vermeulen-Van der Zee, E., te Kortschot, A., and Witter, M.P. (1987). Organization of the projections from the subiculum to the ventral striatum in the rat. A study using anterograde transport of Phaseolus vulgaris leucoagglutinin. Neuroscience *23*, 103–120.

Halladay, A.K., Yue, Y., Michna, L., Widmer, D.A., Wagner, G.C., and Zhou, R. (2000). Regulation of EphB1 expression by dopamine signaling. Brain Res. Mol. Brain Res. *85*, 171–178.

Hattori, T., and McGeer, P.L. (1973). Synaptogenesis in the corpus striatum of infant rat. Exp. Neurol. *38*, 70–79.

Hattori, T., Takada, M., Moriizumi, T., and Campbell, K.J. (1990). Direct striatothalamic projections in the neonatal rat. Brain Res. Dev. Brain Res. *54*, 137–141.

Hazrati, L.N., and Parent, A. (1992). Convergence of subthalamic and striatal efferents at pallidal level in primates: an anterograde double-labeling study with biocytin and PHA-L. Brain Res. *569*, 336–340.

Hensch, T.K. (2005). Critical period plasticity in local cortical circuits. Nat. Rev. Neurosci. *6*, 877–888.

Herkenham, M., and Pert, C.B. (1981). Mosaic distribution of opiate receptors, parafascicular projections and acetylcholinesterase in rat striatum. Nature *291*, 415–418.

Heyers, D., Kovjanic, D., and Redies, C. (2003). Cadherin expression coincides with birth dating patterns in patchy compartments of the developing chicken telencephalon. J. Comp. Neurol. *460*, 155–166.

Higley, M.J., Gittis, A.H., Oldenburg, I.A., Balthasar, N., Seal, R.P., Edwards, R.H., Lowell, B.B., Kreitzer, A.C., and Sabatini, B.L. (2011). Cholinergic Interneurons Mediate Fast VGluT3-Dependent Glutamatergic Transmission in the Striatum. PLoS ONE *6*, e19155.

Hong, W., Mosca, T.J., and Luo, L. (2012). Teneurins instruct synaptic partner matching in an olfactory map. Nature *484*, 201–207.

Honig, M.G., and Hume, R.I. (1989). Dil and diO: versatile fluorescent dyes for neuronal labelling and pathway tracing. Trends Neurosci. *12*, 333–335, 340–341.

Hulme, O.J., Whiteley, L., and Shipp, S. (2010). Spatially Distributed Encoding of Covert Attentional Shifts in Human Thalamus. J. Neurophysiol. *104*, 3644–3656.

Ince, E., Ciliax, B.J., and Levey, A.I. (1997). Differential expression of D1 and D2 dopamine and m4 muscarinic acetylcholine receptor proteins in identified striatonigral neurons. Synap. N. Y. N *27*, 357–366.

Iñiguez, C., De Juan, J., al-Majdalawi, A., and Gayoso, M.J. (1990). Postnatal development of striatal connections in the rat: a transport study with wheat germ agglutinin-horseradish peroxidase. Brain Res. Dev. Brain Res. *57*, 43–53.

Inokawa, H., Yamada, H., Matsumoto, N., Muranishi, M., and Kimura, M. (2010). Juxtacellular labeling of tonically active neurons and phasically active neurons in the rat striatum. Neuroscience *168*, 395–404.

Izzo, P.N., and Bolam, J.P. (1988). Cholinergic synaptic input to different parts of spiny striatonigral neurons in the rat. J. Comp. Neurol. *269*, 219–234.

Jain, M., Armstrong, R.J., Barker, R.A., and Rosser, A.E. (2001). Cellular and molecular aspects of striatal development. Brain Res. Bull. *55*, 533–540.

Janis, L.S., Cassidy, R.M., and Kromer, L.F. (1999). Ephrin-A binding and EphA receptor expression delineate the matrix compartment of the striatum. J. Neurosci. *19*, 4962–4971.

Jankovic, J. (2008). Parkinson's disease: clinical features and diagnosis. J. Neurol. Neurosurg. Psychiatry *79*, 368–376.

Jiménez-Castellanos, J., and Graybiel, A.M. (1989). Compartmental origins of striatal efferent projections in the cat. Neuroscience *32*, 297–321.

Johnston, J.B. (1923). Further contributions to the study of the evolution of the forebrain. J. Comp. Neurol. *35*, 337–481.

Johnston, J.G., Boyd, S.R., and van der Kooy, D. (1987). Compartmentalization of the embryonic striatum after intraocular transplantation. Brain Res. *430*, 310–314.

Johnston, J.G., Gerfen, C.R., Haber, S.N., and van der Kooy, D. (1990). Mechanisms of striatal pattern formation: conservation of mammalian compartmentalization. Brain Res. Dev. Brain Res. *57*, 93–102.

Kachidian, P., Vuillet, J., Nieoullon, A., Lafaille, G., and Kerkerian-Le Goff, L. (1996). Striatal neuropeptide Y neurones are not a target for thalamic afferent fibres. Neuroreport *7*, 1665–1669.

Kaneko, T., Fujiyama, F., and Hioki, H. (2002). Immunohistochemical localization of candidates for vesicular glutamate transporters in the rat brain. J. Comp. Neurol. *444*, 39–62.

Kato, S., Kuramochi, M., Kobayashi, K., Fukabori, R., Okada, K., Uchigashima, M., Watanabe, M., Tsutsui, Y., and Kobayashi, K. (2011). Selective Neural Pathway Targeting Reveals Key Roles of Thalamostriatal Projection in the Control of Visual Discrimination. J. Neurosci. *31*, 17169–17179.

Kawaguchi, Y. (1997). Neostriatal cell subtypes and their functional roles. Neurosci. Res. *27*, 1–8.

Kawaguchi, Y., Wilson, C.J., and Emson, P.C. (1989). Intracellular recording of identified neostriatal patch and matrix spiny cells in a slice preparation preserving cortical inputs. J. Neurophysiol. *62*, 1052–1068.

Kemp, J.M. (1968). Observations on the caudate nucleus of the cat impregnated with the Golgi method. Brain Res. *11*, 467–470.

Kemp, J.M., and Powell, T.P. (1970). The cortico-striate projection in the monkey. Brain J. Neurol. *93*, 525–546.

Kemp, J.M., and Powell, T.P. (1971). The structure of the caudate nucleus of the cat: light and electron microscopy. Philos. Trans. R. Soc. Lond. B. Biol. Sci. *262*, 383–401.

Kenzelmann, D., Chiquet-Ehrismann, R., Leachman, N.T., and Tucker, R.P. (2008). Teneurin-1 is expressed in interconnected regions of the developing brain and is processed in vivo. BMC Dev. Biol. *8*, 30.

Kenzelmann-Broz, D., Tucker, R.P., Leachman, N.T., and Chiquet-Ehrismann, R. (2010). The expression of teneurin-4 in the avian embryo: potential roles in patterning of the limb and nervous system. Int. J. Dev. Biol. *54*, 1509–1516.

Kimura, M., Rajkowski, J., and Evarts, E. (1984). Tonically discharging putamen neurons exhibit set-dependent responses. Proc. Natl. Acad. Sci. U. S. A. *81*, 4998–5001.

Kinel-Tahan, Y., Weiss, H., Dgany, O., Levine, A., and Wides, R. (2007). Drosophila odz gene is required for multiple cell types in the compound retina. Dev. Dyn. Off. Publ. Am. Assoc. Anat. *236*, 2541–2554.

Kinomura, S., Larsson, J., Gulyás, B., and Roland, P.E. (1996). Activation by attention of the human reticular formation and thalamic intralaminar nuclei. Science *271*, 512–515.

Kita, H. (1993). Chapter 4 GABAergic circuits of the striatum. In Progress in Brain Research, (Elsevier), pp. 51–72.

Kita, H., and Kitai, S.T. (1988). Glutamate decarboxylase immunoreactive neurons in rat neostriatum: their morphological types and populations. Brain Res. *447*, 346–352.

Kitai, S.T., Kocsis, J.D., Preston, R.J., and Sugimori, M. (1976). Monosynaptic inputs to caudate neurons identified by intracellular injection of horseradish peroxidase. Brain Res. *109*, 601–606.

Kocsis, J.D., Sugimori, M., and Kitai, S.T. (1977). Convergence of excitatory synaptic inputs to caudate spiny neurons. Brain Res. *124*, 403–413.

Koerts, J., Leenders, K.L., and Brouwer, W.H. (2009). Cognitive dysfunction in non-demented Parkinson's disease patients: Controlled and automatic behavior. Cortex *45*, 922–929.

Koós, T., and Tepper, J.M. (1999). Inhibitory control of neostriatal projection neurons by GABAergic interneurons. Nat. Neurosci. *2*, 467–472.

Van der Kooy, D. (1984). Developmental relationships between opiate receptors and dopamine in the formation of caudate-putamen patches. Brain Res. *316*, 300–303.

Van der Kooy, D. (1996). Early postnatal lesions of the substantia nigra produce massive shrinkage of the rat striatum, disruption of patch neuron distribution, but no loss of patch neurons. Brain Res. Dev. Brain Res. *94*, 242–245.

Van der Kooy, D., and Fishell, G. (1987). Neuronal birthdate underlies the development of striatal compartments. Brain Res. *401*, 155–161.

Van der Kooy, D., and Fishell, G. (1992). Embryonic lesions of the substantia nigra prevent the patchy expression of opiate receptors, but not the segregation of patch and matrix compartment neurons, in the developing rat striatum. Brain Res. Dev. Brain Res. *66*, 141–145.

Korematsu, K., Goto, S., Okamura, A., and Ushio, Y. (1998). Heterogeneity of cadherin-8 expression in the neonatal rat striatum: comparison with striatal compartments. Exp. Neurol. *154*, 531–536.

Kozorovitskiy, Y., Saunders, A., Johnson, C.A., Lowell, B.B., and Sabatini, B.L. (2012). Recurrent network activity drives striatal synaptogenesis. Nature *485*, 646–650.

Kreitzer, A.C. (2009). Physiology and pharmacology of striatal neurons. Annu. Rev. Neurosci. *32*, 127–147.

Krushel, L.A., and van der Kooy, D. (1993). Pattern formation in the developing mammalian forebrain: selective adhesion of early but not late postmitotic cortical and striatal neurons within forebrain reaggregate cultures. Dev. Biol. *158*, 145–162.

Krushel, L.A., Johnston, J.G., Fishell, G., Tibshirani, R., and van der Kooy, D. (1993). Spatially localized neuronal cell lineages in the developing mammalian forebrain. Neuroscience *53*, 1035–1047.

Krushel, L.A., Fishell, G., and van der Kooy, D. (1995). Pattern formation in the mammalian forebrain: striatal patch and matrix neurons intermix prior to compartment formation. Eur. J. Neurosci. *7*, 1210–1219.

Kubota, Y., and Kawaguchi, Y. (1993). Spatial distributions of chemically identified intrinsic neurons in relation to patch and matrix compartments of rat neostriatum. J. Comp. Neurol. *332*, 499–513.

Kubota, Y., Inagaki, S., Shimada, S., Kito, S., Eckenstein, F., and Tohyama, M. (1987). Neostriatal cholinergic neurons receive direct synaptic inputs from dopaminergic axons. Brain Res. *413*, 179–184.

Kullander, K. (2003). Role of EphA4 and EphrinB3 in Local Neuronal Circuits That Control Walking. Science *299*, 1889–1892.

Kusnoor, S.V., Parris, J., Muly, E.C., Morgan, J.I., and Deutch, A.Y. (2010). An extra-cerebellar role for Cerebellin1: Modulation of dendritic spine density and synapses in striatal medium spiny neurons. J. Comp. Neurol. NA–NA.

Lacey, C.J., Bolam, J.P., and Magill, P.J. (2007). Novel and Distinct Operational Principles of Intralaminar Thalamic Neurons and Their Striatal Projections. J. Neurosci. *27*, 4374–4384.

Lança, A.J., Boyd, S., Kolb, B.E., and van der Kooy, D. (1986). The development of a patchy organization of the rat striatum. Brain Res. *392*, 1–10.

Lanciego, J.L., Gonzalo, N., Castle, M., Sanchez-Escobar, C., Aymerich, M.S., and Obeso, J.A. (2004). Thalamic innervation of striatal and subthalamic neurons projecting to the rat entopeduncular nucleus. Eur. J. Neurosci. *19*, 1267–1277.

Lapper, S.R., and Bolam, J.P. (1992). Input from the frontal cortex and the parafascicular nucleus to cholinergic interneurons in the dorsal striatum of the rat. Neuroscience *51*, 533–545.

Leamey, C.A., Glendining, K.A., Kreiman, G., Kang, N.-D., Wang, K.H., Fassler, R., Sawatari, A., Tonegawa, S., and Sur, M. (2007a). Differential Gene Expression between Sensory Neocortical Areas: Potential Roles for Ten_m3 and Bcl6 in Patterning Visual and Somatosensory Pathways. Cereb. Cortex *18*, 53–66.

Leamey, C.A., Merlin, S., Lattouf, P., Sawatari, A., Zhou, X., Demel, N., Glendining, K.A., Oohashi, T., Sur, M., and Fässler, R. (2007b). Ten_m3 regulates eye-specific patterning in the mammalian visual pathway and is required for binocular vision. PLoS Biol. *5*, e241.

Lee, H., and Sawatari, A. (2011). Medium spiny neurons of the neostriatal matrix exhibit specific, stereotyped changes in dendritic arborization during a critical developmental period in mice. Eur. J. Neurosci. *34*, 1345–1354.

Lee, H., Leamey, C.A., and Sawatari, A. (2012a). Perineuronal nets play a role in regulating striatal function in the mouse. *In press*.

Lee, H., Leamey, C.A., and Sawatari, A. (2012b). Perineuronal Nets Play a Role in Regulating Striatal Function in the Mouse. PLoS ONE *7*, e32747.

Lee, I.H., Seitz, A.R., and Assad, J.A. (2006). Activity of tonically active neurons in the monkey putamen during initiation and withholding of movement. J. Neurophysiol. *95*, 2391–2403.

Levine, A., Bashan-Ahrend, A., Budai-Hadrian, O., Gartenberg, D., Menasherow, S., and Wides, R. (1994). Odd Oz: a novel Drosophila pair rule gene. Cell *77*, 587–598.

Li, H., Bishop, K.M., and O'Leary, D.D.M. (2006). Potential target genes of EMX2 include Odz/Ten-M and other gene families with implications for cortical patterning. Mol. Cell. Neurosci. *33*, 136–149.

Lopes, R., Verhey van Wijk, N., Neves, G., and Pachnis, V. (2012). Transcription factor LIM homeobox 7 (Lhx7) maintains subtype identity of cholinergic interneurons in the mammalian striatum. Proc. Natl. Acad. Sci. *109*, 3119–3124.

Lovejoy, D.A., Al Chawaf, A., and Cadinouche, M.Z.A. (2006). Teneurin C-terminal associated peptides: an enigmatic family of neuropeptides with structural similarity to the corticotropin-releasing factor and calcitonin families of peptides. Gen. Comp. Endocrinol. *148*, 299–305.

Magno, L., Kretz, O., Bert, B., Ersözlü, S., Vogt, J., Fink, H., Kimura, S., Vogt, A., Monyer, H., Nitsch, R., et al. (2011). The integrity of cholinergic basal forebrain neurons depends on expression of Nkx2-1: Impairment of cholinergic neurons following Nkx2-1 deletion. Eur. J. Neurosci. *34*, 1767–1782.

Magrassi, L., Ehrlich, M.E., Butti, G., Pezzotta, S., Govoni, S., and Cattaneo, E. (1998). Basal ganglia precursors found in aggregates following embryonic transplantation adopt a striatal phenotype in heterotopic locations. Dev. Camb. Engl. *125*, 2847–2855.

Maier, T., Güell, M., and Serrano, L. (2009). Correlation of mRNA and protein in complex biological samples. FEBS Lett. *583*, 3966–3973.

Makowiecki, K., Hammond, G., and Rodger, J. (2012). Different Levels of Food Restriction Reveal Genotype-Specific Differences in Learning a Visual Discrimination Task. PLoS ONE *7*, e48703.

Malach, R., and Graybiel, A.M. (1986). Mosaic architecture of the somatic sensory-recipient sector of the cat's striatum. J. Neurosci. *6*, 3436–3458.

Mallet, N., Le Moine, C., Charpier, S., and Gonon, F. (2005). Feedforward inhibition of projection neurons by fast-spiking GABA interneurons in the rat striatum in vivo. J. Neurosci. Off. J. Soc. Neurosci. *25*, 3857–3869.

Marin, O., Anderson, S.A., and Rubenstein, J.L. (2000). Origin and molecular specification of striatal interneurons. J. Neurosci. Off. J. Soc. Neurosci. *20*, 6063–6076.

Marín, O., Yaron, A., Bagri, A., Tessier-Lavigne, M., and Rubenstein, J.L. (2001). Sorting of striatal and cortical interneurons regulated by semaphorin-neuropilin interactions. Science *293*, 872–875.

Martin, G.F., Ho, R.H., and Hazlett, J.C. (1989). The early development of major projections to the dorsal striatum in the North American opossum. Brain Res. Dev. Brain Res. *47*, 161–170.

Matsumoto, N., Minamimoto, T., Graybiel, A.M., and Kimura, M. (2001). Neurons in the thalamic CM-Pf complex supply striatal neurons with information about behaviorally significant sensory events. J. Neurophysiol. *85*, 960–976.

McFarland, N.R., and Haber, S.N. (2001). Organization of thalamostriatal terminals from the ventral motor nuclei in the macaque. J. Comp. Neurol. *429*, 321–336.

McGeorge, A.J., and Faull, R.L.M. (1989). The organization of the projection from the cerebral cortex to the striatum in the rat. Neuroscience *29*, 503–537.

McLaughlin, T., and O'Leary, D.D.M. (2005). Molecular gradients and development of retinotopic maps. Annu. Rev. Neurosci. *28*, 327–355.

McLaughlin, T., Hindges, R., and O'Leary, D.D.M. (2003). Regulation of axial patterning of the retina and its topographic mapping in the brain. Curr. Opin. Neurobiol. *13*, 57–69.

Mengual, E., de las Heras, S., Erro, E., Lanciego, J.L., and Giménez-Amaya, J.M. (1999). Thalamic interaction between the input and the output systems of the basal ganglia. J. Chem. Neuroanat. *16*, 187–200.

Merlin, S., Horng, S., Marotte, L.R., Sur, M., Sawatari, A., and Leamey, C.A. (2012). Deletion of Ten-m3 Induces the Formation of Eye Dominance Domains in Mouse Visual Cortex. Cereb. Cortex *In press*.

Messier, B., and Leblond, C.P. (1960). Cell proliferation and migration as revealed by radioautography after injection of thymidine-H3 into male rats and mice. Am. J. Anat. *106*, 247–285.

Mieda, M., Kikuchi, Y., Hirate, Y., Aoki, M., and Okamoto, H. (1999). Compartmentalized expression of zebrafish ten-m3 and ten-m4, homologues of the Drosophila ten(m)/odd Oz gene, in the central nervous system. Mech. Dev. *87*, 223–227.

Miller, M.W., and Nowakowski, R.S. (1988). Use of bromodeoxyuridine-immunohistochemistry to examine the proliferation, migration and time of origin of cells in the central nervous system. Brain Res. *457*, 44–52.

Minamimoto, T., and Kimura, M. (2002). Participation of the thalamic CM-Pf complex in attentional orienting. J. Neurophysiol. *87*, 3090–3101.

Minamimoto, T., Hori, Y., and Kimura, M. (2009). Roles of the thalamic CM–PF complex—Basal ganglia circuit in externally driven rebias of action. Brain Res. Bull. *78*, 75–79.

Minet, A.D., and Chiquet-Ehrismann, R. (2000). Phylogenetic analysis of teneurin genes and comparison to the rearrangement hot spot elements of E. coli. Gene *257*, 87–97.

Minet, A.D., Rubin, B.P., Tucker, R.P., Baumgartner, S., and Chiquet-Ehrismann, R. (1999). Teneurin-1, a vertebrate homologue of the Drosophila pair-rule gene ten-m, is a neuronal protein with a novel type of heparin-binding domain. J. Cell Sci. *112 (Pt 12)*, 2019–2032.

Mink, J.W., and Thach, W.T. (1993). Basal ganglia intrinsic circuits and their role in behavior. Curr. Opin. Neurobiol. *3*, 950–957.

Molenaar, J.J., Koster, J., Zwijnenburg, D.A., van Sluis, P., Valentijn, L.J., van der Ploeg, I., Hamdi, M., van Nes, J., Westerman, B.A., van Arkel, J., et al. (2012). Sequencing of neuroblastoma identifies chromothripsis and defects in neuritogenesis genes. Nature *483*, 589–593.

Moon Edley, S., and Herkenham, M. (1984). Comparative development of striatal opiate receptors and dopamine revealed by autoradiography and histofluorescence. Brain Res. *305*, 27–42.

Morris, G., Arkadir, D., Nevet, A., Vaadia, E., and Bergman, H. (2004). Coincident but distinct messages of midbrain dopamine and striatal tonically active neurons. Neuron *43*, 133–143.

Mosca, T.J., Hong, W., Dani, V.S., Favaloro, V., and Luo, L. (2012). Trans-synaptic Teneurin signalling in neuromuscular synapse organization and target choice. Nature *484*, 237–241.

Moss, J., and Bolam, J.P. (2008). A Dopaminergic Axon Lattice in the Striatum and Its Relationship with Cortical and Thalamic Terminals. J. Neurosci. *28*, 11221–11230.

Moss, J., Ungless, M.A., and Bolam, J.P. (2011). Dopaminergic axons in different divisions of the adult rat striatal complex do not express vesicular glutamate transporters. Eur. J. Neurosci. *33*, 1205–1211.

Murrin, L.C., and Ferrer, J.R. (1984). Ontogeny of the rat striatum: correspondence of dopamine terminals, opiate receptors and acetylcholinesterase. Neurosci. Lett. *47*, 155–160.

Muslimovic, D., Post, B., Speelman, J.D., and Schmand, B. (2007). Motor procedural learning in Parkinson's disease. Brain *130*, 2887–2897.

Ng, T., Chand, D., Song, L., Al Chawaf, A., Watson, J.D., Boutros, P.C., Belsham, D.D., and Lovejoy, D.A. (2012). Identification of a novel brain derived neurotrophic factor (BDNF)-inhibitory factor: regulation of BDNF by teneurin C-terminal associated peptide (TCAP)-1 in immortalized embryonic mouse hypothalamic cells. Regul. Pept. *174*, 79–89.

Nieoullon, A., and Kerkerian-Le Goff, L. (1992). Cellular interactions in the striatum involving neuronal systems using "classical" neurotransmitters: possible functional implications. Mov. Disord. Off. J. Mov. Disord. Soc. *7*, 311–325.

Nieoullon, A., Scarfone, E., Kerkerian, L., Errami, M., and Dusticier, N. (1985). Changes in choline acetyltransferase, glutamic acid decarboxylase, high-affinity glutamate uptake and dopaminergic activity induced by kainic acid lesion of the thalamostriatal neurons. Neurosci. Lett. *58*, 299–304.

Nisenbaum, L.K., Webster, S.M., Chang, S.L., McQueeney, K.D., and LoTurco, J.J. (1998). Early patterning of prelimbic cortical axons to the striatal patch compartment in the neonatal mouse. Dev. Neurosci. *20*, 113–124.

Nishikawa, S., Goto, S., Hamasaki, T., Ogawa, M., and Ushio, Y. (1999). Transient and compartmental expression of the reeler gene product reelin in the developing rat striatum. Brain Res. *850*, 244–248.

Nunes, S.M., Ferralli, J., Choi, K., Brown-Luedi, M., Minet, A.D., and Chiquet-Ehrismann, R. (2005). The intracellular domain of teneurin-1 interacts with MBD1 and CAP/ponsin resulting in subcellular codistribution and translocation to the nuclear matrix. Exp. Cell Res. *305*, 122–132.

O'Leary, D.D., and Koester, S.E. (1993). Development of projection neuron types, axon pathways, and patterned connections of the mammalian cortex. Neuron *10*, 991–1006.

O'Rahilly, R., and Muller, F. (1994). The embryonic human brain: an atlas of developmental stages (New York: Wiley-Liss).

Olson, L., Seiger, A., and Fuxe, K. (1972). Heterogeneity of striatal and limbic dopamine innervation: highly fluorescent islands in developing and adult rats. Brain Res. *44*, 283–288.

Olsson, M., Campbell, K., Wictorin, K., and Björklund, A. (1995). Projection neurons in fetal striatal transplants are predominantly derived from the lateral ganglionic eminence. Neuroscience *69*, 1169–1182.

Olsson, M., Björklund, A., and Campbell, K. (1998). Early specification of striatal projection neurons and interneuronal subtypes in the lateral and medial ganglionic eminence. Neuroscience *84*, 867–876.

Oohashi, T., Zhou, X.H., Feng, K., Richter, B., Mörgelin, M., Perez, M.T., Su, W.D., Chiquet-Ehrismann, R., Rauch, U., and Fässler, R. (1999). Mouse ten-m/Odz is a new family of dimeric type II transmembrane proteins expressed in many tissues. J. Cell Biol. *145*, 563–577.

Ostlund, S.B., Wassum, K.M., Murphy, N.P., Balleine, B.W., and Maidment, N.T. (2011). Extracellular dopamine levels in striatal subregions track shifts in motivation and response cost during instrumental conditioning. J. Neurosci. Off. J. Soc. Neurosci. *31*, 200–207.

Parent, A., and Hazrati, L.N. (1995). Functional anatomy of the basal ganglia. I. The cortico-basal ganglia-thalamo-cortical loop. Brain Res. Brain Res. Rev. *20*, 91–127.

Parent, M., and Parent, A. (2005a). Single-axon tracing and three-dimensional reconstruction of centre median-parafascicular thalamic neurons in primates. J. Comp. Neurol. *481*, 127–144.

Parent, M., and Parent, A. (2005b). Single-axon tracing and three-dimensional reconstruction of centre median-parafascicular thalamic neurons in primates. J. Comp. Neurol. *481*, 127–144.

Parent, A., Mackey, A., and De Bellefeuille, L. (1983). The subcortical afferents to caudate nucleus and putamen in primate: a fluorescence retrograde double labeling study. Neuroscience *10*, 1137–1150.

Passante, L., Gaspard, N., Degraeve, M., Frisen, J., Kullander, K., De Maertelaer, V., and Vanderhaeghen, P. (2008). Temporal regulation of ephrin/Eph signalling is required for the spatial patterning of the mammalian striatum. Development *135*, 3281–3290.

Patel, J.C., Rossignol, E., Rice, M.E., and Machold, R.P. (2012). Opposing regulation of dopaminergic activity and exploratory motor behavior by forebrain and brainstem cholinergic circuits. Nat. Commun. *3*, 1172.

Paxinos, G., and Franklin, K. (2001). The mouse brain in stereotaxic coordinates (Sydney: Academic Press).

Perreault, M.L., Fan, T., Alijaniaram, M., O'Dowd, B.F., and George, S.R. (2012). Dopamine D1–D2 Receptor Heteromer in Dual Phenotype GABA/Glutamate-Coexpressing Striatal Medium Spiny Neurons: Regulation of BDNF, GAD67 and VGLUT1/2. PLoS ONE *7*, e33348.

Phelps, P.E., Brady, D.R., and Vaughn, J.E. (1989). The generation and differentiation of cholinergic neurons in rat caudate-putamen. Brain Res. Dev. Brain Res. *46*, 47–60.

Powell, T.P., and Cowan, W.M. (1954). The connexions of the midline and intralaminar nuclei of the thalamus of the rat. J. Anat. *88*, 307–319.

Qian, X., Barsyte-Lovejoy, D., Wang, L., Chewpoy, B., Gautam, N., Al Chawaf, A., and Lovejoy, D.A. (2004). Cloning and characterization of teneurin C-terminus associated peptide (TCAP)-3 from the hypothalamus of an adult rainbow trout (Oncorhynchus mykiss). Gen. Comp. Endocrinol. *137*, 205–216.

Quirozpadilla, M., Guillazoblanch, G., Valemartinez, A., and Martinicolovius, M. (2006). Excitotoxic lesions of the parafascicular nucleus produce deficits in a socially transmitted food preference. Neurobiol. Learn. Mem. *86*, 256–263.

Quiroz-Padilla, M.F., Guillazo-Blanch, G., Vale-Martínez, A., Torras-García, M., and Martí-Nicolovius, M. (2007). Effects of parafascicular excitotoxic lesions on two-way active avoidance and odor-discrimination. Neurobiol. Learn. Mem. *88*, 198–207.

Ragozzino, M.E. (2004). Dynamic Changes in Acetylcholine Output in the Medial Striatum During Place Reversal Learning. Learn. Mem. *11*, 70–77.

Ragsdale, C.W., Jr, and Graybiel, A.M. (1990). A simple ordering of neocortical areas established by the compartmental organization of their striatal projections. Proc. Natl. Acad. Sci. U. S. A. *87*, 6196–6199.

Ragsdale, C.W., Jr, and Graybiel, A.M. (1991). Compartmental organization of the thalamostriatal connection in the cat. J. Comp. Neurol. *311*, 134–167.

Raju, D.V., Shah, D.J., Wright, T.M., Hall, R.A., and Smith, Y. (2006). Differential synaptology of vGluT2-containing thalamostriatal afferents between the patch and matrix compartments in rats. J. Comp. Neurol. *499*, 231–243.

Rakic, P., and Caviness, V.S., Jr (1995). Cortical development: view from neurological mutants two decades later. Neuron *14*, 1101–1104.

Ramanathan, S., Hanley, J.J., Deniau, J.-M., and Bolam, J.P. (2002). Synaptic convergence of motor and somatosensory cortical afferents onto GABAergic interneurons in the rat striatum. J. Neurosci. Off. J. Soc. Neurosci. *22*, 8158–8169.

Rice, M.W., Roberts, R.C., Melendez-Ferro, M., and Perez-Costas, E. (2011). Neurochemical characterization of the tree shrew dorsal striatum. Front. Neuroanat. *5*, 53.

Richards, A.B., Scheel, T.A., Wang, K., Henkemeyer, M., and Kromer, L.F. (2007). EphB1 null mice exhibit neuronal loss in substantia nigra pars reticulata and spontaneous locomotor hyperactivity. Eur. J. Neurosci. *25*, 2619–2628.

Richards, L.J., Koester, S.E., Tuttle, R., and O'Leary, D.D. (1997). Directed growth of early cortical axons is influenced by a chemoattractant released from an intermediate target. J. Neurosci. Off. J. Soc. Neurosci. *17*, 2445–2458.

Royce, G.J. (1983). Single thalamic neurons which project to both the rostral cortex and caudate nucleus studied with the fluorescent double labeling method. Exp. Neurol. *79*, 773–784.

Rubin, B.P., Tucker, R.P., Martin, D., and Chiquet-Ehrismann, R. (1999). Teneurins: a novel family of neuronal cell surface proteins in vertebrates, homologous to the Drosophila pair-rule gene product Ten-m. Dev. Biol. *216*, 195–209.

Rubin, B.P., Tucker, R.P., Brown-Luedi, M., Martin, D., and Chiquet-Ehrismann, R. (2002). Teneurin 2 is expressed by the neurons of the thalamofugal visual system in situ and promotes homophilic cell-cell adhesion in vitro. Dev. Camb. Engl. *129*, 4697–4705.

Rudkin, T.M., and Sadikot, A.F. (1999). Thalamic input to parvalbumin-immunoreactive GABAergic interneurons: organization in normal striatum and effect of neonatal decortication. Neuroscience *88*, 1165–1175.

Russchen, F.T., Smeets, W.J., and Hoogland, P.V. (1987). Histochemical identification of pallidal and striatal structures in the lizard Gekko gecko: evidence for compartmentalization. J. Comp. Neurol. *256*, 329–341.

Sadikot, A.F., Parent, A., Smith, Y., and Bolam, J.P. (1992a). Efferent connections of the centromedian and parafascicular thalamic nuclei in the squirrel monkey: a light and electron microscopic study of the thalamostriatal projection in relation to striatal heterogeneity. J. Comp. Neurol. *320*, 228–242.

Sadikot, A.F., Parent, A., and François, C. (1992b). Efferent connections of the centromedian and parafascicular thalamic nuclei in the squirrel monkey: a PHA-L study of subcortical projections. J. Comp. Neurol. *315*, 137–159.

Samuel, D., Kerkerian-Le Goff, L., Kumar, U., Errami, M., Scarfone, E., and Nieoullon, A. (1990). Changes in striatal cholinergic, gabaergic, dopaminergic and serotoninergic biochemical markers after kainic acid-induced thalamic lesions in the rat. J. Neural Transm. Park. Dis. Dement. Sect. *2*, 193–203.

Savasta, M., Dubois, A., and Scatton, B. (1986). Autoradiographic localization of D1 dopamine receptors in the rat brain with [3H]SCH 23390. Brain Res. *375*, 291–301.

Schiffmann, S.N., Libert, F., Vassart, G., and Vanderhaeghen, J.J. (1991). Distribution of adenosine A2 receptor mRNA in the human brain. Neurosci. Lett. *130*, 177–181.

Schilman, E.A., Uylings, H.B.M., Galis-de Graaf, Y., Joel, D., and Groenewegen, H.J. (2008). The orbital cortex in rats topographically projects to central parts of the caudate-putamen complex. Neurosci. Lett. *432*, 40–45.

Schlösser, B., Klausa, G., Prime, G., and Ten Bruggencate, G. (1999). Postnatal development of calretinin- and parvalbumin-positive interneurons in the rat neostriatum: an immunohistochemical study. J. Comp. Neurol. *405*, 185–198.

Selemon, L.D., and Goldman-Rakic, P.S. (1985). Longitudinal topography and interdigitation of corticostriatal projections in the rhesus monkey. J. Neurosci. Off. J. Soc. Neurosci. *5*, 776–794.

Semba, K., and Fibiger, H.C. (1988). Time of origin of cholinergic neurons in the rat basal forebrain. J. Comp. Neurol. *269*, 87–95.

Semba, K., Vincent, S.R., and Fibiger, H.C. (1988). Different times of origin of choline acetyltransferase- and somatostatin-immunoreactive neurons in the rat striatum. J. Neurosci. Off. J. Soc. Neurosci. *8*, 3937–3944.

Sheleg, M., Yochum, C.L., Wagner, G.C., Zhou, R., and Richardson, J.R. (2013). Ephrin-A5 deficiency alters sensorimotor and monoaminergic development. Behav. Brain Res. *236*, 139–147.

Sheth, A.N., McKee, M.L., and Bhide, P.G. (1998). The sequence of formation and development of corticostriate connections in mice. Dev. Neurosci. *20*, 98–112.

Shiflett, M.W., and Balleine, B.W. (2011). Contributions of ERK signaling in the striatum to instrumental learning and performance. Behav. Brain Res. *218*, 240–247.

Shiflett, M.W., Brown, R.A., and Balleine, B.W. (2010). Acquisition and performance of goal-directed instrumental actions depends on ERK signaling in distinct regions of dorsal striatum in rats. J. Neurosci. Off. J. Soc. Neurosci. *30*, 2951–2959.

Shink, E., Bevan, M.D., Bolam, J.P., and Smith, Y. (1996). The subthalamic nucleus and the external pallidum: two tightly interconnected structures that control the output of the basal ganglia in the monkey. Neuroscience *73*, 335–357.

Sidibé, M., and Smith, Y. (1996). Differential synaptic innervation of striatofugal neurones projecting to the internal or external segments of the globus pallidus by thalamic afferents in the squirrel monkey. J. Comp. Neurol. *365*, 445–465.

Sidibé, M., and Smith, Y. (1999). Thalamic inputs to striatal interneurons in monkeys: synaptic organization and co-localization of calcium binding proteins. Neuroscience *89*, 1189–1208.

Sidibé, M., Paré, J.-F., and Smith, Y. (2002). Nigral and pallidal inputs to functionally segregated thalamostriatal neurons in the centromedian/parafascicular intralaminar nuclear complex in monkey. J. Comp. Neurol. *447*, 286–299.

Sieber, B.-A., Kuzmin, A., Canals, J.M., Danielsson, A., Paratcha, G., Arenas, E., Alberch, J., Ögren, S.O., and Ibáñez, C.F. (2004). Disruption of EphA/ephrin-A signaling in the nigrostriatal system reduces dopaminergic innervation and dissociates behavioral responses to amphetamine and cocaine. Mol. Cell. Neurosci. *26*, 418–428.

Silva, J.-P., Lelianova, V.G., Ermolyuk, Y.S., Vysokov, N., Hitchen, P.G., Berninghausen, O., Rahman, M.A., Zangrandi, A., Fidalgo, S., Tonevitsky, A.G., et al. (2011). Latrophilin 1 and its endogenous ligand Lasso/teneurin-2 form a high-affinity transsynaptic receptor pair with signaling capabilities. Proc. Natl. Acad. Sci. U. S. A. *108*, 12113–12118.

Simonetti, T., Lee, H., Bourke, M., Leamey, C.A., and Sawatari, A. (2009). Enrichment from birth accelerates the functional and cellular development of a motor control area in the mouse. PloS One *4*, e6780.

Simpson, T.I., Pratt, T., Mason, J.O., and Price, D.J. (2009). Normal ventral telencephalic expression of Pax6 is required for normal development of thalamocortical axons in embryonic mice. Neural Develop. *4*, 19.

Smart, I., and Sturrock, R.R. (1979). Ontogeny of the neostriatum. In The Neostriatum, (New York: Pergmon), pp. 127–146.

Smith, Y., and Parent, A. (1986). Differential connections of caudate nucleus and putamen in the squirrel monkey (Saimiri sciureus). Neuroscience *18*, 347–371.

Smith, Y., Raju, D.V., Pare, J.-F., and Sidibe, M. (2004). The thalamostriatal system: a highly specific network of the basal ganglia circuitry. Trends Neurosci. *27*, 520–527.

Smith, Y., Raju, D., Nanda, B., Pare, J.-F., Galvan, A., and Wichmann, T. (2009). The thalamostriatal systems: Anatomical and functional organization in normal and parkinsonian states. Brain Res. Bull. *78*, 60–68.

Snyder-Keller, A., Costantini, L.C., and Graber, D.J. (2001). Development of striatal patch/matrix organization in organotypic co-cultures of perinatal striatum, cortex and substantia nigra. Neuroscience *103*, 97–109.

Sohur, U.S., Padmanabhan, H.K., Kotchetkov, I.S., Menezes, J.R.L., and Macklis, J.D. (2012). Anatomic and Molecular Development of Corticostriatal Projection Neurons in Mice. Cereb. Cortex N. Y. N 1991.

Somogyi, P., Bolam, J.P., and Smith, A.D. (1981). Monosynaptic cortical input and local axon collaterals of identified striatonigral neurons. A light and electron microscopic study using the Golgi-peroxidase transport-degeneration procedure. J. Comp. Neurol. *195*, 567–584.

Song, D.D., and Harlan, R.E. (1994). Genesis and migration patterns of neurons forming the patch and matrix compartments of the rat striatum. Brain Res. Dev. Brain Res. *83*, 233–245.

Sorimachi, M., and Kataoka, K. (1975). High affinity choline uptake: an early index of cholinergic innervation in rat brain. Brain Res. *94*, 325–336.

Specht, L.A., Pickel, V.M., Joh, T.H., and Reis, D.J. (1981). Light-microscopic immunocytochemical localization of tyrosine hydroxylase in prenatal rat brain. I. Early ontogeny. J. Comp. Neurol. *199*, 233–253.

Spencer, H.J. (1976). Antagonism of cortical excitation of striatal neurons by glutamic acid diethyl ester: evidence for glutamic acid as an excitatory transmitter in the rat striatum. Brain Res. *102*, 91–101.

Sperry, R.W. (1963). Chemoaffinity in the orderly growth of nerve fiber patterns and connections. Proc. Natl. Acad. Sci. U. S. A. *50*, 703–710.

Srivastava, V. (1999). Pattern formation in the mammalian striatum: The development of the thalamostriatal projection in the rodent.

Sturrock, R.R. (1980). A developmental study of the mouse neostriatum. J. Anat. *130*, 243–261.

Sun, J.H., Gao, Q., Zhang, J., Bao, L.H., Dong, H.M., Liang, N., Li, G.B., Li, Z.H., and Gao, Y.M. (2010). Ephrinb3 induces mesostriatal dopaminergic projection to the striatum. Biochem. Biophys. Res. Commun. *400*, 194–199.

Tai, A.X., Cassidy, R.M., and Kromer, L.F. (2013). EphA7 expression identifies a unique neuronal compartment in the rat striatum. J. Comp. Neurol.

Tandé, D., Féger, J., Hirsch, E.C., and François, C. (2006). Parafascicular nucleus projection to the extrastriatal basal ganglia in monkeys. Neuroreport *17*, 277–280.

Tepper, J.M., and Bolam, J.P. (2004). Functional diversity and specificity of neostriatal interneurons. Curr. Opin. Neurobiol. *14*, 685–692.

Tepper, J.M., Sharpe, N.A., Koós, T.Z., and Trent, F. (1998). Postnatal development of the rat neostriatum: electrophysiological, light- and electron-microscopic studies. Dev. Neurosci. *20*, 125–145.

Thompson, R., and Yang, S. (1982). Retention of individual spatial reversal problems in rats with nigral, caudoputamenal, and reticular formation lesions. Behav. Neural Biol. *34*, 98–103.

Thompson, R., Kao, L., and Yang, S. (1981). Rapid forgetting of individual spatial reversal problems in rats with parafascicular lesions. Behav. Neural Biol. *33*, 1–16.

Threlfell, S., Lalic, T., Platt, N.J., Jennings, K.A., Deisseroth, K., and Cragg, S.J. (2012). Striatal dopamine release is triggered by synchronized activity in cholinergic interneurons. Neuron *75*, 58–64.

Tikhonravov, D.L. (1998). Effects of lesioning of the parafascicular nucleus of the thalamus on an operant food-procuring reflex in rats. Neurosci. Behav. Physiol. *28*, 423–425.

Tran, H. (2009). The Development of the Rodent Striatum: Roles for Ten-m3. Honours. University of Sydney.

Trzebiatowska, A., Topf, U., Sauder, U., Drabikowski, K., and Chiquet-Ehrismann, R. (2008). Caenorhabditis elegans teneurin, ten-1, is required for gonadal and pharyngeal basement membrane integrity and acts redundantly with integrin ina-1 and dystroglycan dgn-1. Mol. Biol. Cell *19*, 3898–3908.

Tucker, R.P., and Chiquet-Ehrismann, R. (2006). Teneurins: a conserved family of transmembrane proteins involved in intercellular signaling during development. Dev. Biol. *290*, 237–245.

Tucker, R.P., Chiquet-Ehrismann, R., Chevron, M.P., Martin, D., Hall, R.J., and Rubin, B.P. (2001). Teneurin-2 is expressed in tissues that regulate limb and somite pattern formation and is induced in vitro and in situ by FGF8. Dev. Dyn. Off. Publ. Am. Assoc. Anat. *220*, 27–39.

Tucker, R.P., Kenzelmann, D., Trzebiatowska, A., and Chiquet-Ehrismann, R. (2007). Teneurins: transmembrane proteins with fundamental roles in development. Int. J. Biochem. Cell Biol. *39*, 292–297.

Tucker, R.P., Beckmann, J., Leachman, N.T., Schöler, J., and Chiquet-Ehrismann, R. (2012). Phylogenetic analysis of the teneurins: conserved features and premetazoan ancestry. Mol. Biol. Evol. *29*, 1019–1029.

Veening, J.G., Cornelissen, F.M., and Lieven, P.A. (1980). The topical organization of the afferents to the caudatoputamen of the rat. A horseradish peroxidase study. Neuroscience *5*, 1253–1268.

Vercelli, A., Marini, G., and Tredici, G. (2003). Anatomical organization of the telencephalic connections of the parafascicular nucleus in adult and developing rats. Eur. J. Neurosci. *18*, 275–289.

Vogt, C., and Vogt, O. (1941). Thalamusstudien I-III. I. Zur Einfurung, II. Homogenitat und Grenzgestaldung der Grisea des Thalamus, III. Griseum centrale (centrum medianum Luys). J Physiol Neurol Lpz *50*, 30–154.

Voorn, P., Kalsbeek, A., Jorritsma-Byham, B., and Groenewegen, H.J. (1988). The pre- and postnatal development of the dopaminergic cell groups in the ventral mesencephalon and the dopaminergic innervation of the striatum of the rat. Neuroscience *25*, 857–887.

Van Vulpen, E.H., and Van Der Kooy, D. (1996). Differential maturation of cholinergic interneurons in the striatal patch versus matrix compartments. J. Comp. Neurol. *365*, 683–691.

Walker, R.H., and Graybiel, A.M. (1993). Dendritic arbors of spiny neurons in the primate striatum are directionally polarized. J. Comp. Neurol. *337*, 629–639.

Wang, L., Rotzinger, S., Al Chawaf, A., Elias, C.F., Baršytė-Lovejoy, D., Qian, X., Wang, N.-C., De Cristofaro, A., Belsham, D., Bittencourt, J.C., et al. (2005). Teneurin proteins possess a carboxy terminal sequence with neuromodulatory activity. Mol. Brain Res. *133*, 253–265.

Webster, K.E. (1965). The cortico-striatal projection in the cat. J. Anat. *99*, 329–337.

Wichterle, H., Turnbull, D.H., Nery, S., Fishell, G., and Alvarez-Buylla, A. (2001). In utero fate mapping reveals distinct migratory pathways and fates of neurons born in the mammalian basal forebrain. Dev. Camb. Engl. *128*, 3759–3771.

Wilson, C.J. (1993). The generation of natural firing patterns in neostriatal neurons. Prog. Brain Res. *99*, 277–297.

Woolley, D.G., Laeremans, A., Gantois, I., Mantini, D., Vermaercke, B., Op de Beeck, H.P., Swinnen, S.P., Wenderoth, N., Arckens, L., and D'Hooge, R. (2013). Homologous involvement of striatum and prefrontal cortex in rodent and human water maze learning. Proc. Natl. Acad. Sci. U. S. A. *110*, 3131–3136.

Wu, Y., and Parent, A. (2000). Striatal interneurons expressing calretinin, parvalbumin or NADPH-diaphorase: a comparative study in the rat, monkey and human. Brain Res. *863*, 182–191.

Wu, Y., Richard, S., and Parent, A. (2000). The organization of the striatal output system: a single-cell juxtacellular labeling study in the rat. Neurosci. Res. *38*, 49–62.

Xu, Z.C., Wilson, C.J., and Emson, P.C. (1991). Restoration of thalamostriatal projections in rat neostriatal grafts: an electron microscopic analysis. J. Comp. Neurol. *303*, 22–34.

Yin, H.H. (2004). Contributions of Striatal Subregions to Place and Response Learning. Learn. Mem. *11*, 459–463.

Yin, H.H., and Knowlton, B.J. (2006). The role of the basal ganglia in habit formation. Nat. Rev. Neurosci. *7*, 464–476.

Yin, H.H., Mulcare, S.P., Hilário, M.R.F., Clouse, E., Holloway, T., Davis, M.I., Hansson, A.C., Lovinger, D.M., and Costa, R.M. (2009). Dynamic reorganization of striatal circuits during the acquisition and consolidation of a skill. Nat. Neurosci. *12*, 333–341.

Young, T.R. (2011). Distinct roles for Ten-m2 and Ten-m4 in the development of the mouse visual system. University of Sydney.

Young, T.R., and Leamey, C.A. (2009). Teneurins: Important regulators of neural circuitry. Int. J. Biochem. Cell Biol. *41*, 990–993.

Young, J.W., Meves, J.M., Tarantino, I.S., Caldwell, S., and Geyer, M.A. (2011). Delayed procedural learning in α7-nicotinic acetylcholine receptor knockout mice. Genes Brain Behav. *10*, 720–733.

Young, T.R., Bourke, M., Zhou, X., Oohashi, T., Sawatari, A., Fässler, R., and Leamey, C.A. (2013). Ten-m2 Is Required for the Generation of Binocular Visual Circuits. J. Neurosci. *33*, 12490–12509.

Yue, Y., Widmer, D.A., Halladay, A.K., Cerretti, D.P., Wagner, G.C., Dreyer, J.L., and Zhou, R. (1999). Specification of distinct dopaminergic neural pathways: roles of the Eph family receptor EphB1 and ligand ephrin-B2. J. Neurosci. *19*, 2090–2101.

Zheng, L., Michelson, Y., Freger, V., Avraham, Z., Venken, K.J.T., Bellen, H.J., Justice, M.J., and Wides, R. (2011). Drosophila Ten-m and filamin affect motor neuron growth cone guidance. PloS One *6*, e22956.

Zhou, X.-H., Brandau, O., Feng, K., Oohashi, T., Ninomiya, Y., Rauch, U., and Fässler, R. (2003). The murine Ten-m/Odz genes show distinct but overlapping expression patterns during development and in adult brain. Gene Expr. Patterns GEP *3*, 397–405.

Ziegler, A., Corvalán, A., Roa, I., Brañes, J.A., and Wollscheid, B. (2012). Teneurin protein family: an emerging role in human tumorigenesis and drug resistance. Cancer Lett. *326*, 1–7.

Ben-Zur, T., Feige, E., Motro, B., and Wides, R. (2000). The Mammalian Odz Gene Family: Homologs of a Drosophila Pair-Rule Gene with Expression Implying Distinct yet Overlapping Developmental Roles. Dev. Biol. *217*, 107–120.